AN INVESTIGATION OF THE USE OF MIXED PHASE ELECTRODES IN ALL-SOLID-STATE CELLS

A Thesis presented for the
Degree of Doctor of Philosophy
in the Faculty of Science
of the University of St. Andrews
(1989)

DEDICATION

TO MY PARENTS - THANK YOU

DECLARATION

a) I, Michael D. Rogers, hereby certify that this thesis has been composed by myself, that it is a record of my own work, and that it has not been accepted in partial or complete fulfilment of any other degree of professional qualification.

Signed Date 8|6|89

(Michael D. Rogers)

b) I was admitted to the Faculty of Science of the University of St. Andrews under Ordinance No. 12 on 1st October 1984 and as a candidate for the degree of Ph.D. on 1st October 1985.

Signed Date 8|6|89

(Michael D. Rogers)

c) I hereby certify that the candidate has fulfilled the condition of the Resolution and Regulations appropriate to the degree of Ph.D.

Signature of Supervisor Date 8.6.89

(Colin. A. Vincent)

ACKNOWLEDGEMENTS

I would like to thank Dr. Colin Vincent for his much needed encouragement and advice throughout the time I was working with him and for his patience in awaiting the finished thesis.

I also owe a great deal of gratitude to the University of St. Andrews for providing a Research Scholarship, travel grants and research facilities.

Thanks are also due to various members of the Chemistry Department, in particular to Jim Bews for frequent advice on the computing facilities and to the staff of the electronic and mechanical workshops for their help with equipment.

In the Geology Department I would like to thank Angus Calder and Alastair Reid for running the XRD analyses, to Andrew Mackie for initial help with the EPMA sample preparation and to Donald Herd for tuition and help in operating the electron microprobe.

Thanks to Mr. C.D. Sinclair of the Statistics Department for information concerning the geometric distribution and random number generation using Minitab.

Lastly my thanks to Helen for helping with the last stages of putting together this thesis.

ABSTRACT

A 'mixed phase' or 'composite' electrode is frequently used to enhance the power output from an all-solid-state cell by increasing the contact area between the electrode and electrolyte regions of the cell. Situated between the bulk electrolyte and current collector a composite electrode consists of a finely ground mixture of the two components, its properties being dependent on its thickness, the component ratio, their relative conductivities and the particle size. The work presented in this thesis reports an experimental and computer investigation of the properties of such electrodes.

Experimentally a three electrode cell was used with the working electrode comprising a composite of niobium disulphide insertion material and a glassy silver ion-conducting electrolyte. The component ratio, the thickness, the electrolyte conductivity and the particle size of the composite were all varied and the effect on the apparent chemical diffusion coefficient of silver ions measured using a galvanostatic pulse technique.

A computer simulation of composite electrodes was modified to investigate similar parameters. Six, eight and twelve coordination lattices were used to represent the mixed phase electrode, and the effect of the coordination, the component ratio, and the particle size on the contact area between the two phases was examined. Effects of particle orientation and size distribution was also studied.

Electron probe microanalysis experiments were carried out in order to study the silver ion concentration distribution within the composite electrode to see if it functioned efficiently in transporting ions throughout its depth. This efficiency was compared for high and low conductivity electrolytes and with an electrode consisting of the pure insertion material.

An attempt was also made to improve the conductivity of the glass electrolytes by using small amounts of metallic silver to produce pseudo-ionic conductance.

TABLE OF CONTENTS

Chapter 3. COMPUTER MODEL

Chapter 4. PROGRAMMES

Chapter 5. DIFFUSION STUDY

Chapter 6. EPMA STUDIES

Chapter 7. P.I.C. STUDY

Chapter 8. SUMMARY

Appendix 1. DATA ANALYSIS

Appendix 2. PERCOLATION THEORY

1 INTRODUCTION

A battery or electrochemical power source is a device which converts chemically stored energy directly into electrical energy without the intermediate, and energetically wasteful, forms of thermal and mechanical energy usually involved in the generation of electricity. Compared with conventional power sources batteries offer the advantages of portability and of being able to store energy conveniently and efficiently. In addition they are modular and therefore the power source can easily be enlarged or reduced in size. [1]

This enables batteries to be used in a diverse range of applications largely dependent on their large range of size and properties. Table 1 roughly categorises batteries according to the energy available from them and illustrates some of the prerequisites for common applications of that type of cell (after Vincent [2]).

Battery type	Energy	Examples	Applications	Requirements
Miniature	100 mWh-2 Wh	Li/I_2	Calculators, Pacemakers	1,2,3
Batteries for portable devices	2 Wh-100 Wh	Zn/MnO_2	Toys, Torches, Personal Hi-fi	4,5
Starting, lighting, ignition	100-600 Wh	Lead-Acid	Cars, buses, lawnmowers	6,7
Vehicle traction	20-630 kWh (2 MWh)	Lead-Acid	Forklifts, Milk Floats (Submarines)	1,7,8 5
Stationary batteries	250 Wh-5 MWh	Ni/Cd	Emergency/remote power sources	3,7
Load levelling batteries.	5-100 MWh	Lead-Acid	Load levelling	6,7,9,10

Table 1
Common battery types and applications.
Requirements: 1 - High Energy Density, 2 - Small Size, 3 - Long Lifetime, 4 - Cheap, 5 - Safe, 6 - Large Currents and Capacity, 7 - Rechargeable, 8 - Lightness, 9 - Modular, 10 - Good Efficiency.

This diversity of utilisation and breadth of application has lead to a great deal of research effort into developing novel, improved batteries and in extending the performance of existing systems.

The work described in this thesis examines factors affecting the performance of batteries composed solely of solid materials which use a 'mixed phase' electrode to improve their properties. This chapter considers the advantages offered by all-solid-state batteries and describes some of the materials more commonly used in such systems.

2 FACTORS LIMITING BATTERY PERFORMANCE

A number of parameters are important in determining the performance of operational batteries. The more important of these are defined in Table 2.

Parameter	Definition
Theoretical capacity	The theoretical number of coulombs of charge available (Ah)
Practical Capacity	The actual charge delivered during discharge. (Ah)
Specific Capacity	The capacity per unit weight or volume (Ah/kg)
Rated Capacity	The practical capacity measured under rigidly defined discharge conditions terminating at a prespecified cut-off voltage.
Theoretical Energy	The total amount of energy available from a cell assuming total discharge.
Specific Energy	The energy per unit weight or volume (Wh/kg).
Practical Available Energy	The actual energy delivered during cell discharge.
Rated Power	The power delivered under stated discharge conditions.
Cycle Life	The number of times a cell can be charged and discharged before a certain proportion of its capacity is lost.

Table 2.
Some important battery operating parameters.

During the operation of a battery a number of factors reduce performance levels from the optimum theoretical values.

Firstly the driving force behind each of the current carrying processes (in the electrodes, the electrolytes and at the interfaces) results in a reduction of the cell potential from the thermodynamic equilibrium value predicted by the Nernst equation. (On recharging the voltage required to drive the same current is higher than the equilibrium value for the same reason.) The difference between the actual cell voltage and the equilibrium value is known as the *polarisation voltage* or, more commonly, the *overpotential.*

The two prime causes of overpotential are Ohmic losses (or iR drop) and electrode losses. The former is associated with the internal resistance of the electrolyte phase and other components in the cell, and is generally dependent upon such factors as the cell geometry and the characteristics of the electrode and electrolyte materials. In systems where the electrode material is closely intermingled with the electrolyte the close intermeshing of the two components and tortuosity factors make it difficult to separate iR effects from electrode losses. Examples of such systems are porous electrodes and all-solid-state systems where mixed phase electrodes or conducting diluents are in use.

Under normal operating conditions iR drop is the predominant cause of polarisation losses in most modern battery systems and therefore battery design incorporates a number of considerations aimed at minimising such losses eg high conductivity components and optimal cell geometry.

Electrode losses can be subdivided into mass and charge transfer processes the slower of which can be the current limiting electrode process. Transport limited processes occur when the active species is not available for reaction at the electrode surface due to transportation rates to the electrode being too slow. Mass transport can be brought about by a concentration gradient (diffusion), an electric field gradient (migration) and a density gradient (convection). The work described in this thesis concentrates on diffusion limited cells where the effects of migration and convection are negligible.

In charge transfer control the limitation to the current arises because of the difficulty of ion or electron transfer across the electrode interface. The rate is controlled by the potential difference across the double layer formed at the electrode and hence by the potential of that electrode. The overall rate is made up of the rates of a number of contributory processes including changes in the solvation number and bond breaking and reforming stages which occur as the ionic species reacts at the interface.

For a simple charge transfer limited process the overall current density is related to the over-potential by the Butler-Volmer equation:-

$$i = i_o[\exp\{-\alpha\eta F/RT\} - \exp\{(1-\alpha)F\eta/RT\}]$$

where i_o is the exchange current which exists when the electrode is at equilibrium, α is a symmetry factor, T is the temperature, η is the overpotential and R the gas constant.

Other factors can also prevent the actual performance of a battery system attaining its theoretical capacity. For example in real systems all the available reactants may not be used in the cell reaction. This may be because the reactants lie off a conducting path through the cell and therefore cannot participate in reaction. Alternatively they may undergo secondary reactions or be lost through leakage.

3 SOLID STATE BATTERIES

An ideal electrolyte must meet a number of criteria.[3] It must be chemically and physically stable in terms of structure and composition during the lifetime of the battery. It should possess a high decomposition potential thus allowing the use of electrodes with a large potential difference and consequently yielding a high energy density. It must have a high ionic conductivity and a negligible electronic conductivity in order to maximise current drawing capability and minimise self discharge and so boost the shelf life.

The use of solid electrolytes meets some of the above requirements and also provides additional attributes of interest, limiting some of the problems associated with liquid electrolytes. Their utilisation allows cells to be constructed without the necessity for immobilisers and separators thus improving energy densities. There is no possibility of the emission of dangerous fluids so consequently an all-solid-state cell is safer and can have a longer shelf life than conventional cells. There is also greater opportunity for miniaturisation and optimising cell design.[2]

The major disadvantage in using solid electrolytes is the generally low ionic conductivity of the materials - typically two or three orders of magnitude lower than common liquid electrolyte systems. There are exceptions and these will be mentioned below.

Other problems are associated with the interface between the electrolyte and electrode material. Figure 1 illustrates the difference between a liquid/solid (or gas/solid) interface and a solid/solid boundary. In the former case the fluid wets the whole surface of the electrode, even filling pores and other surface structures. The surface area is therefore maximised and such porous electrodes are well described in theory.[4] At the solid/solid interface contact is restricted to point contacts between the two materials so the area at which charge transfer can occur is limited.

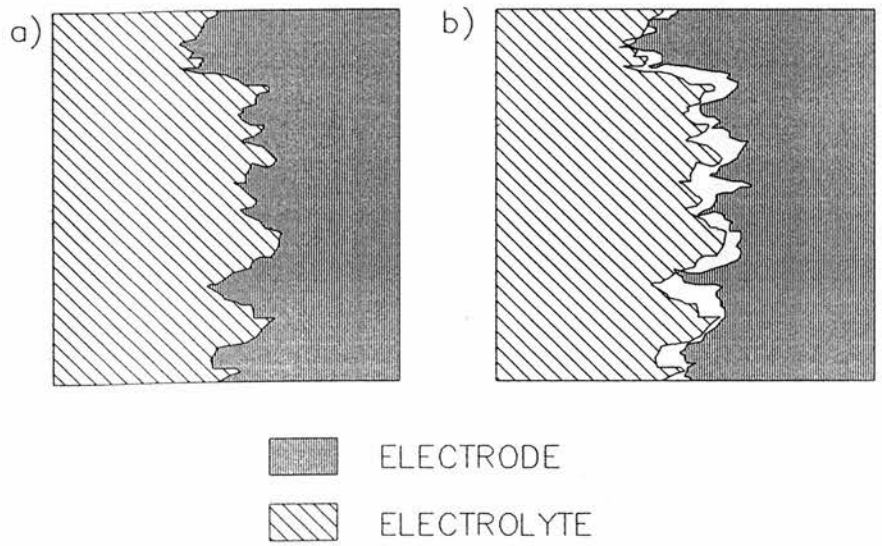

Figure 1.
a) Liquid electrolyte/solid electrode and b) solid electrolyte/solid electrode interfaces illustrating the different contact areas.

In cells the rate of charge transfer across the interface between electrode and electrolyte is given by the normal heterogeneous rate equation:-

$$Rate = kc_o A$$

where k is a potential dependent rate constant, c_o is the surface concentration and A is the operational interfacial area. The current and hence the power output are both determined by the rate of charge transfer so optimising the area of contact between electrode and electrolyte is exceedingly important in all-solid-state cells.

This limitation can affect secondary cell efficiency. With conventional electrode systems electrode reaction usually involves a destruction of the crystalline lattice and a subsequent rebuilding during charge/discharge cycles. This causes a number of problems when only point contacts are involved in the reconstruction phase. Figure 2 depicts the effects which can occur. The points concentrate the electric field at their tips so preferential deposition and lattice build up can occur at these points. This may initiate a gradual pushing apart of the two solid components and slow loss of contact over a number of cycles (Figure 2a). Alternatively dendrites can form and slowly stretch between the electrodes causing short circuit. (Figure 2b)

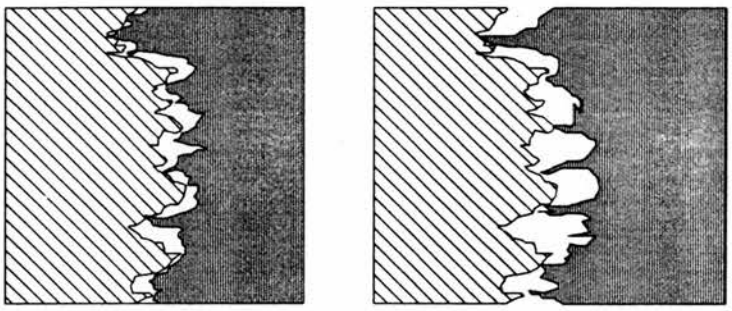

Figure 2a.
Dendrites causing loss of contact between electrode and electrolyte.

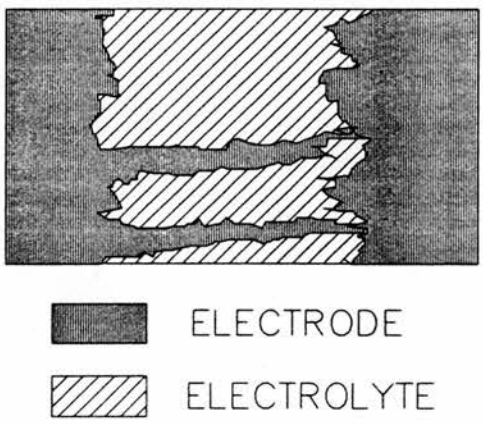

Figure 2b.
Dendrite growth causing short circuiting.

4 SOLID ELECTROLYTES

Historically solid electrolytes have been recognised for most of this century. In particular Schottky and Frenkel defect conduction mechanisms have been well described for ionic transport in crystalline lattices. The magnitude of such conductivity is however generally low except at temperatures approaching the melting point of the material. The first "fast ionic conductor" to be described was silver iodide (AgI) which shows a transition at 146^{o}C to a more highly conducting phase.[5] In the early 1960's two crystalline materials with ionic conductivities comparable to salt solutions were characterised.

The first of these was silver rubidium iodide ($RbAg_4I_5$)[6] and it was found to have a silver ion conductivity approaching 0.1 Scm.$^{-1}$ The other material sodium-β-alumina is a particularly stable

material with a high sodium ion conductivity. Since then the number and type of ion-conducting solids has expanded and includes crystalline materials, amorphous glasses and polymers, and heterogeneous systems.

Figure 3 illustrates some specific examples of the more common electrolytes and depicts their conductivity range as a function of temperature (from Vincent[2]). This work does not undertake to give an exhaustive examination of the structures, properties and scope of these materials, though references are given which discuss the materials more fully. Instead the materials will be examined with reference to the useful properties they possess for incorporation into all-solid-state battery systems.

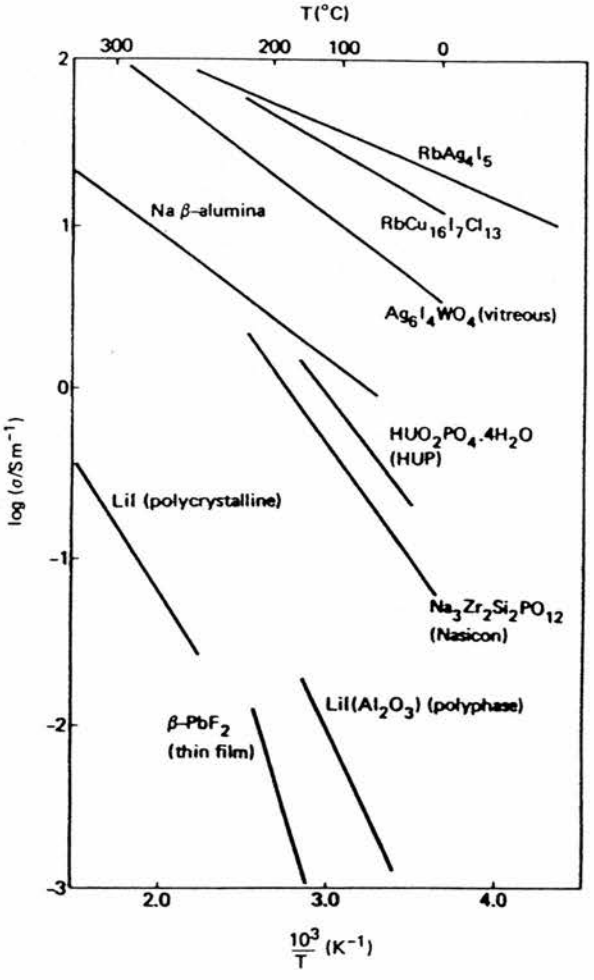

Figure 3.
Examples and conductivities of some solid electrolytes.

Crystalline materials offer the highest ionic conductivities of all the solid electrolytes as depicted above in figure 3. They have well defined structures and their conductivities can be explained well theoretically and are easily examined using well known experimental techniques. They are physically strong (but often very brittle), are very stable to high temperatures and generally have high ionic transport numbers - transporting predominantly one type of ion.[6] On the negative side their physical nature makes them expensive and difficult to fabricate in useful forms. For example β-alumina is frequently used as a ceramic. Their hardness also limits the interfacial contact and restricts their ability to absorb stresses and strains.

An alternative to pure crystalline materials are the composite electrolyte systems[7] in which a defect conductor is mixed with an insulating material such as alumina. This is thought to modify the surface of the defect conductor[8,9] enhancing surface conduction and frequently resulting in a conductivity enhancement of two or three orders of magnitude, compared with the pure defect conductor.

As well as an enhanced conductivity composite electrolytes are softer and more easy to manufacture than pure crystalline electrolytes. Again only one ion is transported. They are however poorly understood theoretically and their conductivities are relatively low.

Polymer electrolytes[10,11] generally consist of an ionic salt dissolved in a polar polymer - most commonly poly(ethylene oxide) (PEO). Such materials are very easy to prepare by solvent casting and hot pressing. They are extremely flexible leading to good interfacial contact over large surface areas, even during solid state reaction processes. They can be formed into very thin sheets and are extremely lightweight giving rise to potentially large energy densities despite low conductivities at room temperature (though recent innovations are pushing this upward for example by the addition of crystalline materials[12] or crosslinking the polymer[13]). They are however somewhat unstable at high temperatures and in the presence of oxidants and are physically very weak. They show appreciable anionic transport thus reducing their overall efficiency for battery usage.[14]

Glasses are even more easily prepared simply by liquefying their components and quenching.[15,16] They can frequently be formed over a wide composition range and their properties are less susceptible than crystalline materials to small changes in stoichiometry. Conductivities approach those of the crystalline conductors and they generally only have cationic mobility. However they are hard materials, although this is very much a function of composition. They are also somewhat unstable and frequently require annealing to optimise properties and limit fall off with usage.[17]

5 ELECTRODE MATERIALS

Traditionally for high energy batteries lithium electrodes have been commonly utilised but these have problems associated with poor stripping/plating efficiency. This has pointed towards the use of metal alloys such as Li_3Bi[18] or other sources of lithium which are more stable and effective but pay a penalty of reduced cell potential.

Two new classes of electrode materials have shown promise in high energy battery systems. The first of these, though more recent in terms of development, are the electronically conducting polymers.[19] These are generally unsaturated, conjugated systems typified by polyacaetylene. When reacted with nucleophiles or electrophiles they yield "doped" systems which can act as anodes or cathodes depending on the dopant. The electrode potential is related to the degree and type of doping. These electrodes suffer from a number of problems and in particular are generally unstable in the presence of oxygen, have a low cycle life and cycle efficiency.[20] Investigation is continuing and more recent materials or processes[21] are beginning to overcome some of the disadvantages. The prospect of an extremely light, high energy density all-polymer battery available in a wide range of configurations continues to provide the impetus for further work.

However the most promising materials for use in high energy density cells both with liquid[22] and solid electrolytes[23] are the so-called insertion electrode materials. These electrodes operate by a topochemical reaction in which metal ions (or other species) are incorporated reversibly into gaps in the host crystal lattice. These materials are examples of solid solution electrodes.[24] For a mixed conducting, non-stoichiometric electrode A_xMX_y incorporating the electroactive species A by an insertion reaction :-

$$nA + A_xMX_y \quad \text{-->} \quad A_{x+n}MX_y$$

Armand[25] showed that the electrode criteria important in high energy secondary cells are :-

a) MX_y must have a high electronic conductivity and a high ionic conductivity of A in the lattice.

b) MX_y must have a high capacity for incorporating A in its structure.

c) The electrode reaction must be reversible.

d) The interfaces with the electrolyte must be stable and afford good contact and fast charge transfer.

e) No phase or major structural changes must take place during the insertion process.

f) The free energy of reaction should be high, constant over the intercalation range in order to give high energy densities and a constant cell potential.

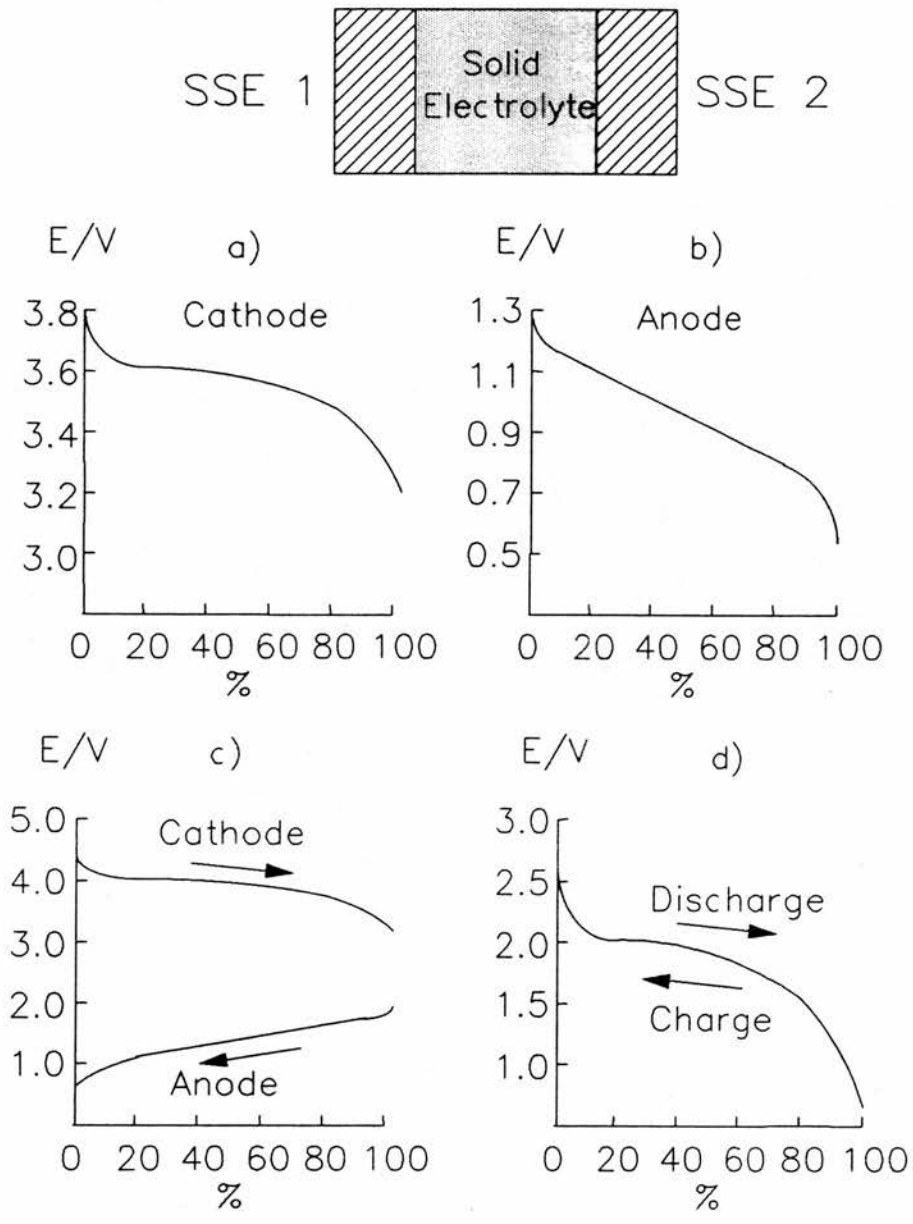

Figure 4.
Example of a rocking chair cell.
Cell potential of a) SSE 1 and b) SSE 2 as a function of intercalation level. c) Individual cell potentials during discharge. d) Overall cell potential during cycling.

A combination of two different solid solution electrodes, which can both incorporate the same guest species leads to the concept of a "rocking chair" cell in which the mobile species rocks back and forth between the two electrodes. Of course the electrodes must have different potentials and Figure 4 shows how the individual electrode potentials change with the intercalation level and how the overall cell potential changes on cycling. This form of cell has been successfully investigated recently.[26,27]

The most promising solid solution electrodes have either layered structures or open tunnel (framework) crystal lattices. It is the former "intercalation" electrodes which have been more thoroughly investigated though more recently some of the framework structures have proved equally interesting.

5.1 TRANSITION METAL DICHALCOGENIDES

The phenomenon of intercalation (two-dimensional insertion) is widespread ranging from the intercalation compounds of graphite[28] to the intercalation of amorphous polymer between semi-crystalline lamellae in polymer blends. A common feature of all these materials is a change in the interlammelar distance or configuration upon intercalation.

The best described materials for use as electrodes are the transition metal dichalcogenides (TCh_2 - where T is a transition metal and Ch is sulphur or selenium). Initial interest centred on their properties as superconductors[29] since they have a relatively high transition temperature of around 10K. Figure 5 illustrates which of the transition metals chalcogenides take up layered structures.

5.1.1 Structure of the Materials TCH_2

The general structure of these compounds consists of a layer of metal atoms sandwiched between two sheets of chalcogen atoms.[30] Depending on the relative positions of these sheets the metal atoms can be in either octahedral or trigonal prismatic sites (both 6:3 coordinations) between the chalcogen atoms.

The overall host structure is composed of stacks of such layers held together by weak van der Waals forces. A full description of the crystal structure of the materials is exceedingly complex since there are many permutations of the relative layer positions in each stack and of the coordination of the atoms within each layer. Thus a number of polymorphs or more strictly polytypes can exist for many of these structures.

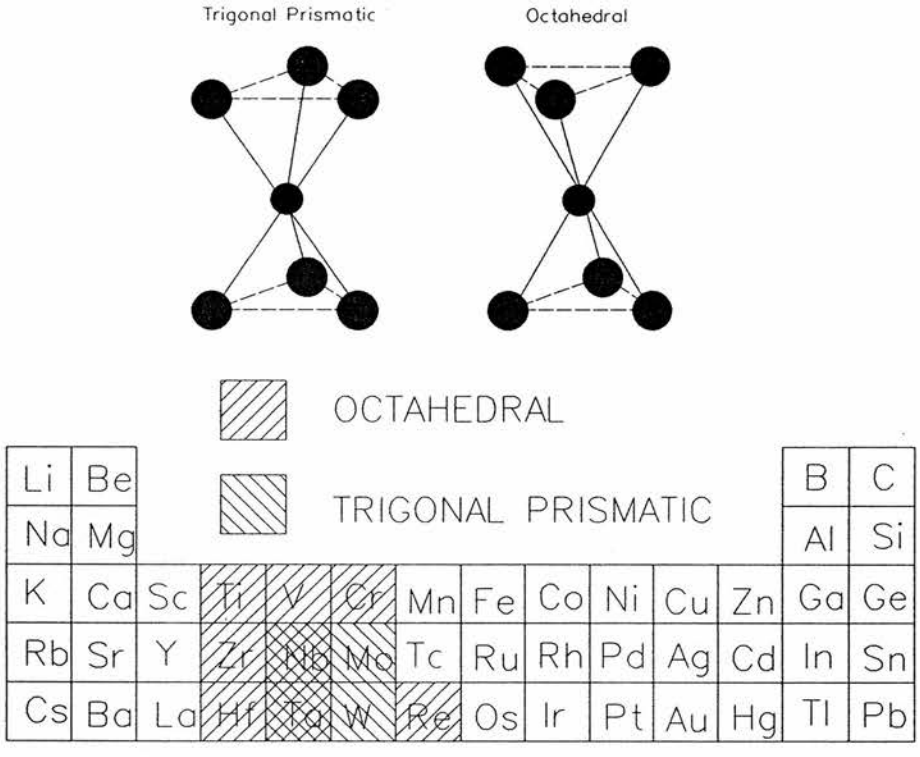

Figure 5.
Transition metals which form dichalcogenides and the trigonal prismatic and octahedral structures.

The structures of the host materials and the intercalated compounds can be described by a number of different representations and notations.[30] One of these describes the relative positions of all the atoms present with reference to the three different sites (designated A,B,C) present in a hexagonally close packed lattice. The anion positions are designated A,B and C using upper case letters, the transition metal atoms using lower case letters a,b and c. Inserted species are represented as [a], [b] and [c].

The number of layers present in repeat units of the c-direction of the crystal structure can be used as an indication of the layer disposition. The coordination of the transition metal in the TCh_2 layers is given by the first letter of the symmetry, H for hexagonal, R for rhombohedral and T for trigonal prismatic. Individual polytypes are subscripted in the order of discovery e.g. $4H_aTaS_2$.

It is common not to attempt to depict the three-dimensional structures of these compounds but to show a single section through the crystal lattice (usually the $1\,1\,\bar{2}\,0$ section). This illustrates the relative positions of the ions present. Some examples of the different types of structure and nomenclature are given in Figure 6.[31]

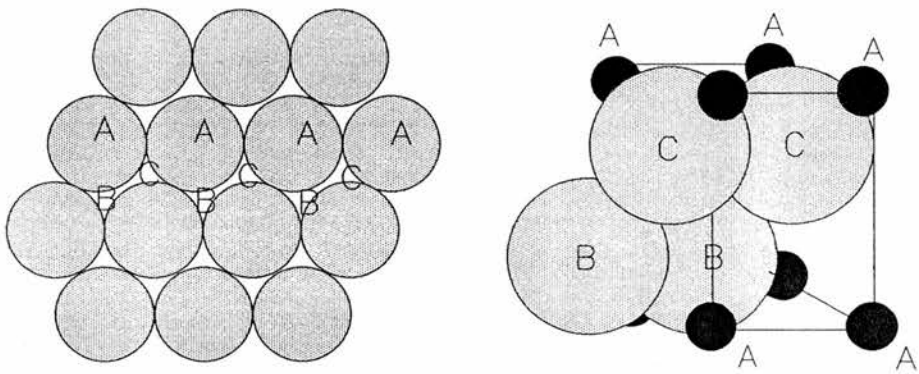

Figure 6a).
Three different sites in a hexagonally close packed lattice.

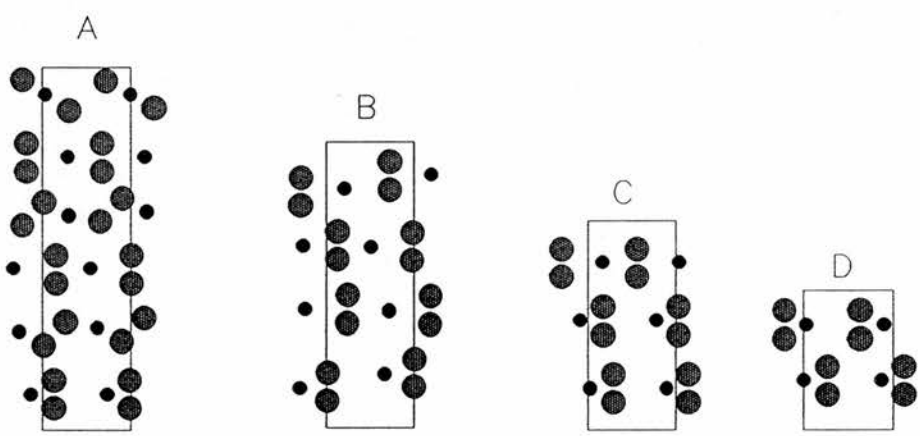

Figure 6b).
Some examples of 1 1 $\bar{2}$ 0 sections through typical transition metal dichalcogenide lattice structures. A - 6R TaS_2, 6R $TaSe_2$; B - $4H_a TaSe_2$; C - 3R NbS_2, 3R TaS_2, 3R MoS_2; D - 2H NbS_2, 2H TaS_2

5.1.2 Synthesis of the transition metal dichalcogenides

The most common synthetic route to the TCh_2 compounds is direct combination of the elements at elevated temperatures.[30] The exact polytype formed is dependent on the exact molar ratio of raw materials, the reaction time and temperature and the cooling method as exemplified by NbS_2[32].

Chemical transport techniques can be used to make single crystals of the more common members of the group of transition metal dichalcogenides and such materials are invaluable in X-ray diffraction studies and are also being used in measurements of diffusion rates of ions in different crystal planes.

Other techniques have been used for specific compounds. Examples are reduction of metal oxides with carbon disulphide or reaction of metal chlorides with hydrogen sulphide at elevated temperatures. More recently plasma-enhanced chemical vapour deposition has been used to make films of titanium disulphide in a thin layer solid-state battery configuration.[33]

5.1.3 Synthesis of the Intercalated Materials A_xTCh_2

The reactions available to make intercalates of the transition metal dichalcogenides are generally similar to those used to prepare the host structures though there are some differences.[30] The first method successfully used was the reaction of the disulphides with a solution of an alkali metal in ammonia. However, ammonia is co-intercalated and must be driven out thermally or using vacuum techniques. Also structural disruption which occurs during the cointercalation may be permanent and the TCh_2 may be reduced by the ammonia. It is one of the few methods available for inserting divalent cations.

Other solvents such as THF or hexamethyl phosphotriamide have been used in conjunction with various lithium derivatives (e.g. lithium naphthalides) the most successful reagent being n-butyl lithium. Such non-polar solvents reduce cointercalation and reduction problems because conditions are much milder.

Direct combination of the elements is also a possibility and the thermal history determines the phase structure of the product. Impurity phases are often a problem and the intercalation level must usually be high, especially for production of regular single crystals.[34]

The commonest method is to use the TCh_2 compound as the cathode in an electrochemical cell usually with the anode as the source of the intercalant species. With this technique the exact intercalation level can be defined by controlling the current passed. The rate of reaction is determined by the current and the intercalation level correlates with the cell potential. The process is easily reversible by changes in the direction of the applied current or potential. The use of solid electrolytes reduces the possibility of cointercalation.

5.1.4 Structure of the intercalates A_xTCh_2

A large number of species are able to be intercalated into the layered transition metal dichalcogenides. Many of the elements are able to react directly or indirectly to form well defined com-

pounds. In general only monovalent ions are easily introduced into the structure, though divalent cations have been reported for some hosts. The other main intercalants are small polar molecules such as amides, nitrogen heterocycles, water, amines and various oxides.

On intercalation the layered structure must adjust to allow inclusion of the guest species. The layers either undergo an expansion along the crystallographic c-axis or move laterally to form a different polytype. Both are shown schematically in Figure 7. The intercalated species have a choice of octahedral/tetrahedral or trigonal prismatic sites to enter. This is dependent on the nature and size of the intercalant, its polarity and the original host structure.[30]

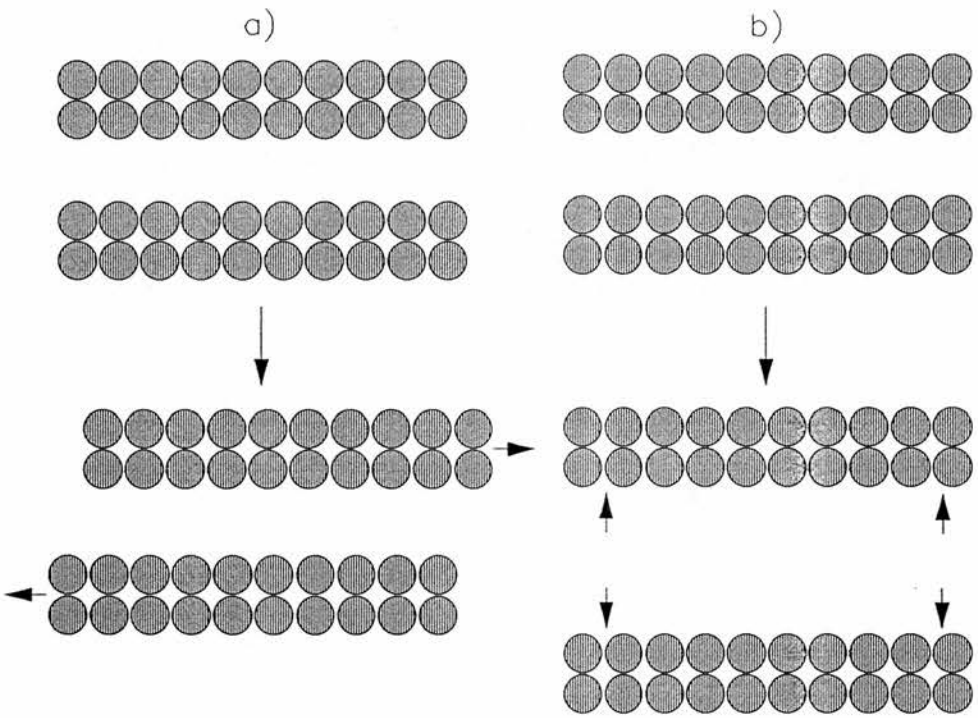

Figure 7.
a) Lateral movement and b) expansion of transition metal dichalcogenide layers during the intercalation process.

Metal rich phases $A_xT_{1+y}Ch_2$ can be formed if the initial molar ratios of reactants are inaccurate or by reduction of the host lattice. The excess metal ions are resident between the TCh_2 layers, bonding these layers more strongly together. This can limit the intercalation level by blocking diffusion paths and also reduce the diffusion rate. In addition it can inhibit the c-axis expansion on intercalation, forcing the production of other polytypes.[32]

The phenomenon of staging has been observed for some of the dichalcogenides. As with graphite this occurs when the intercalated species only lie between every nth layer in the crystal structure (giving an n-stage compound). More recently for silver intercalation into some disulphides it has been shown that the island domain model of Daumas and Herold[35] more appropriately describes the intercalation procedure.[36] That is the intercalation occurs between all layers and the staging arises due to localised rearrangement of the structure.

5.2 ALTERNATIVE SOLID SOLUTION ELECTRODES

Although the transition metal dichalcogenides are the most studied solid solution electrodes a large number of alternative systems are available.

Alternative layered structures include the intercalation compounds of carbon which have long been examined for a variety of purposes but are now under consideration as electrodes.[28] FeOCl is another layered compound which has shown some promise because of its cost. It is capable of reversibly incorporating 0.5 moles of lithium per mole of FeOCl and exhibits no change in the lattice parameters as the insertion proceeds.[37]

Initial results on $NiPS_3$, which also forms a layered structure, suggested a maximum capacity of up to 3 lithium atoms per mole of host material. However later results indicated that the actual capacity is half of this. A range of these compounds (formula MPX_3 where M is a transition metal and X is S or Se) have been investigated by Rouxel[38]. The results indicate that certain members of this series could perform satisfactorily over a limited range of guest concentrations.

Other compounds based on Li_xVS_2 are $Li_xM_yV_{1-y}S_2$ where vanadium atoms are replaced by either chromium or iron (M = Cr or Fe) have been investigated in liquid electrolyte systems.[39] When chromium is substituted the maximum lithium capacity is extended to 0.6 moles per mole of host, when it is iron this is further enhanced to 0.8 moles per mole of host.

As well as layered structures compounds with three-dimensional framework lattices are also under investigation. Many transition metal oxides form such structures and the tunnels provide sites for the incorporation of alkali metal ions. These materials exhibit a wide range of behaviour (with respect to electronic conductivity, charge/discharge behaviour and diffusion rates of guest species) important in usage as solid solution electrodes.

For example the tungsten and vanadium bronzes[40] have well characterised linear tunnel structures but have very low diffusion rates of alkali metal ions in the structure to be of practical importance in secondary batteries. Slightly different structures such as V_6O_{13} have much higher diffusion coefficients[41] and this material in particular is showing considerable promise in high energy battery systems.[42]

6 MIXED PHASE ELECTRODES

Some of the problems discussed above associated with all-solid-state cells can be overcome by the introduction of a mixed phase electrode (MPE). Such an electrode (also known as a composite electrode) is illustrated schematically in Figure 8. It consists of finely interpenetrating networks of electrode and electrolyte particles located between the pure electrolyte and electrode components of the cell.[43] (It should be noted that the pure electrode component may simply be a current collector incorporated directly into the MPE.) The structure of the composite bears close resemblance to the use of carbon black to enhance the electronic conductivity of a poorly conductive electrode material.

The composite is formed by finely mixing and compressing the two components or by sintering of the mixture between the two bulk phases. This is carried out to optimise the contact area between the components minimising the number of voids or isolated particles which cannot participate in the cell mechanism.

The properties of the composite rely on ionic current passage through chains of electrolyte particles, mass and charge transfer across the electrolyte interface with the electrode particles and subsequent electronic transport through chains of electrode particles to the current collector.

Thus the thickness of the MPE is important in determining the ohmic polarisation losses. The electronic and ionic conductivities of the components also contribute to this. The interfacial area can be altered by adjustment of the particle sizes and the relative ratios of the two components. Lastly the physical characteristics of the two components, e.g their hardness, can affect the number of voids etc. in the structure and play an important role in optimising the operative area. The use of an MPE also reduces the likelihood of dendrite formation and interfacial separations occurring.

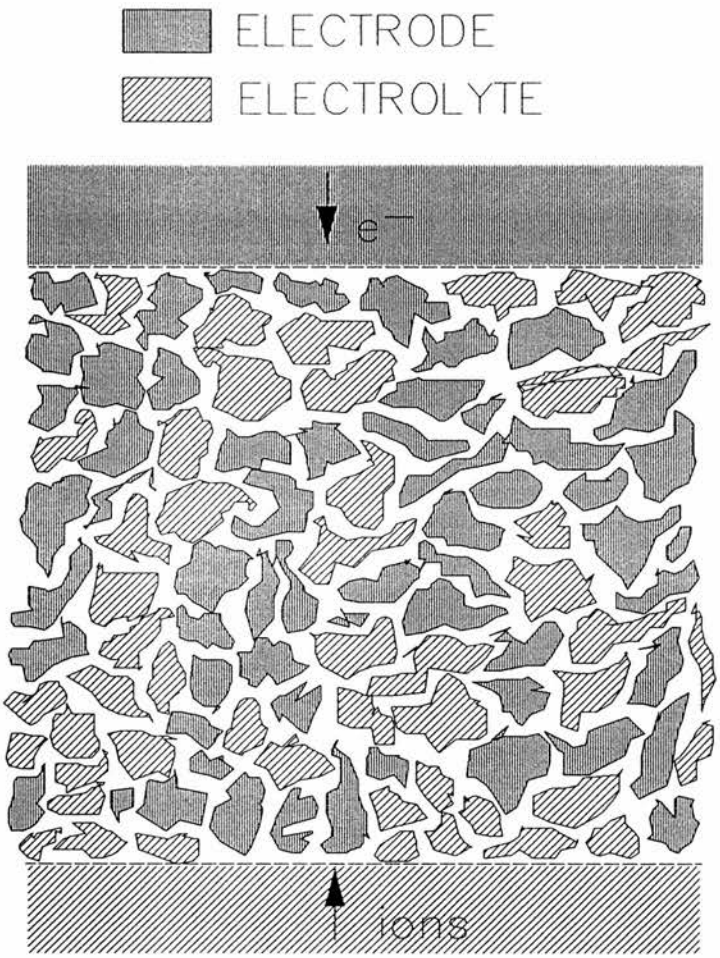

Figure 8.
Diagrammatic representation of a mixed phase electrode.

6.1 THE OPTIMUM MIXED PHASE ELECTRODE

The properties of the materials outlined above give a guide to the best materials for the construction of a good mixed phase electrode. Insertion materials are indicated as the best electrode materials, since their structural changes are minimised and can be controlled if the degree of insertion is limited. Also since the reaction occurs in the host structure rather than at the boundary with the electrolyte then dendrite formation and the interface loss of contact can be minimised. This allows good reversibility. Appropriate materials also fulfil the requirements of stability, high degrees of intercalation for high energy densities etc. In conjunction with the insertion material a soft electrolyte should be used. This gives good interfacial contact and retains this during cycling.

The work described in this thesis investigates means of optimising the performance of mixed phase electrodes and examines factors which should be crucial in determining the properties of the composite electrodes.

Firstly a computer model is used to ascertain the effect on the interfacial contact area between electrode and electrolyte particles of changing such properties as the particle coordination, the particle size and alignment, and varying the lattice parameters. Galvanostatic pulse measurements are then performed on real systems to determine how similar parameters (particle size, ionic conductivity and electrode/electrolyte ratio) change the apparent chemical diffusion coefficient for the mixed phase electrode. Lastly electron microprobe analyses are made of sectioned electrodes to determine how efficient the electrode is, under different conditions, in transporting metal ions throughout its depth.

In this work niobium disulphide is used with glassy silver electrolytes because it provides an easily accessible system for study. Unlike the lithium systems few special conditions are necessary; the diffusion coefficient is high and the material is fairly representative of the layered intercalation materials. There is also a considerable variety of glassy silver electrolytes to work with.

7 REFERENCES

1 Hopkinson J. "The New Batteries", EPRI Journal 6 (1981) 7

2 Vincent C.A., Bonino F., Lazzari M., Scrosati B. "Modern Batteries : An Introduction To Electrochemical Power Sources", Publ. Edward Arnold (1984)

3 Hagenmuller P. "Solid Electrolytes. General Principles, Characterisation, Materials, Applications" Ed. Van Gool W., Publ. Academic Press (1978)

4 De Levie R. "Electrochemical Response Of Porous And Rough Electrodes", Adv. In Electrochem. And Electrochem. Engineering 6 (1967) 329

5 Takahashi T., Kuwabara K., Yamamoto O., "The Electrical Conductivity And The Crystal Structure Of Silver Iodide", J. Electrochem. Soc. 116 (1969) 357

6 Ingram M.D., Vincent C.A. "Solid Electrolytes", Annual Reports A (J. Chem. Soc.) (1977)

7 Liang C.C., "Conduction Characteristics Of The Lithium Iodide-Aluminium Oxide Solid Electrolytes" J. Electrochem. Soc. 120 (1973) 1289

8 Poulsen F.W. "Composite Electrolytes" Transport-Structure Relations In Fast Ion And Mixed Conductors - 6th Riso International Symposium 37, Eds. Poulsen F.W. Et Al., Publ. Riso International Laboratory

9 Wagner J.B. "Composite Electrolytes", Solid State Batteries (Nato Asi Series. Series E: Applied Sciences No. 101), Eds. Sequeira C.A.C., Hooper A., Publ. Martinus Nijhoff Publishers (1985)

10 Armand M.B. "Polymer Solid Electrolytes - An Overview", Solid State Ionics 9 & 10 (1983) 745

11 Vincent C.A. "Polymer Electrolytes", Chemistry in Britain 25 (1989) 391

12 Skaarup S., West K., Zachau-Christiansen B. "Mixed Phase Solid Electrolytes", Solid State Ionics 28-30 (1989) 975

13 Gauthier M., Fauteux D., Vassort G., Belanger A., Duval M., Ricoux P., Chabagno J.-M., Muller D., Rigaud P., Armand M.B., Deroo D. "Assessment Of Polymer-Electrolyte Batteries For EV And Ambient Temperature Applications", J. Electrochem. Soc. 132 (1985) 1332

14 Shriver D.F., Clancy S., Blonsky P.M., Hardy L.C. "Ion Transport Numbers For New Polymer Electrolytes", Transport-Structure Relations In Fast Ion And Mixed Conductors - 6th Riso International Symposium 353, Eds. Poulsen F.W. Et Al., Publ. Riso International Laboratory

15 Owen J.R. "Ionically Conducting Glasses", Solid State Batteries (Nato Asi Series. Series E: Applied Sciences No. 101)p 49, Eds. Sequeira C.A.C., Hooper A., Publ. Martinus Nijhoff Publishers (1985)

16 Magistris A., Chiodelli G., Schiraldi A. "Formation Of High Conductivity Glasses In The System AgI-Ag_2O-B_2O_3", Electrochim. Acta 24 (1979) 203

17 Ingram M.D., Vincent C.A., Wandless A.R. "Temperature Dependence Of Ionic Conductivity In Glass: Non-Arrhenius Behaviour In The $Ag_7I_4AsO_4$ System", J. Non-Cryst. Solids 53 (1982) 73

18 Weppner W., Huggins R.A. "Electrochemical Investigation Of The Chemical Diffusion, Partial Ionic Conductivities And Other Kinetic Parameters In Li_3Sb And Li_3Bi", Journal Of Solid State Chemistry 22 (1977) 297

19 Pethrick R.A. "Conductivity in Polymeric Materials", Solid State Batteries (Nato Asi Series. Series E: Applied Sciences No. 101). p197, Eds. Sequeira C.A.C., Hooper A., Publ. Martinus Nijhoff Publishers (1985)

20 Farrington G.C., Huq R. "Polyacetylene Electrodes For Non-Aqueous Lithium Batteries" Journal Of Power Sources 14 (1985) 3

21 Hirooka M. "Development Of Conductive Polymers", New Materials & New Processes 3 (1985) 52

22 West K., Jacobsen T., Atlung S."Modeling Of Porous Insertion Electrodes With Liquid Electrolyte", J. Electrochem. Soc. 129 (1982) 1480

23 Padula A., Patriarca M., Scrosati B., Croce F. "Titanium And Niobium Disulphides As Intercalation Electrodes In Copper And Silver Solid-State Cells", Solid State Ionics 9 & 10 (1983) 365

24 Steele B.C.H. "Chemical Diffusion", Fast Ion Transport In Solids. Solid State Batteries And Devices p103, Ed. Van Gool W., Publ. North-Holland Publishing Company (1973)

25 Armand M.B. "Intercalation Electrodes", Materials For Advanced Batteries p45, Eds. Murphy D.W., Broadhead J., Steele B.C.H., Publ. Plenum Press (1980)

26 Scrosati B., Di Pietro B., Residori L. "Li_xWO_2/Li_yWO_3 Organic Electrolyte Cyclable Cell", Nature Preprint

27 Lazzari M., Scrosati B. "A Cyclable Lithium Organic Electrolyte Cell Based On Two Intercalation Electrodes", J. Electrochem. Soc. 127 (1980) 773

28 Touzain Ph. "Graphite Intercalation Compounds For Primary And Secondary Batteries Electrodes", Annales De Physique Supplement. French Japanese Colloquium On Insertion Compounds Of Graphite. 11 (1985) 23

29 Van Maaren M.H., Schaeffer G.M. "Superconductivity In Group Va Dichalcogenides", Phys. Lett. 20 (1966) 131

30 Whittingham M.S. "Chemistry Of Intercalation Compounds: Metal Guests In Chalcogenide Hosts", Prog. Solid St. Chem. 12 (1978) 41

31 Leith R.M.A., Terhell J.C.J.M. "Transition Metal Dichalcogenides", Preparation And Crystal Growth Of Materials With Layered Structures p143, Ed. Leith R.M.A., Publ. D. Riedel Publishing Co. (1977)

32 Jellinek F., Brauer G., Muller H. "Molybdenum And Niobium Sulphides" Nature 185 (1960) 376

33 Kanehori K., Ito Y., Kirino F., Miyauchi K., Kudo T. "Titanium Disulfide Films Fabricated By Plasma CVD", Solid State Ionics 18&19 (1986) 818

34 Bouwmeester H.J.M. "The Thermodynamic And Kinetic Properties Of Silver Intercalated Niobium Disulfide", Solid State Ionics 16 (1985) 163

35 Daumas N., Herold A. "Sur Les Relations Entre La Notion De Stade Et Les Mecanismes Reactionnels Dans Les Composes D'Insertion Du Graphite", C.R. Acad. Sci. Ser. C. 269 (1969) 373

36 Scholz G.A., Frindt R.F. "Structure And Staging Of Intercalated Ag_xTaS_2 And Ag_xTiS_2", Mat. Res. Bull. 15 (1980) 1703

37 Palvdeau P., Coic L., Rouxel J., Portier J. "The Lithium And Molecular Intercalates Of FeOCl", Mat. Res. Bull. 13 (1978) 221

38 Brec R., Rouxel J. "Lithium Intercalation In Layered Transition Metal Chalcogenophosphates", Comm. Eur. Communities [Rep.] Eur 1979 Eur 6350 Proc. Meet. On Prospects Battery Appl. Subsequent R&D Requir. p237

39 Murphy D.W., Di Salvo F.J., Carides J.N. "Vanadium Disulphide: Metal Substitution And Lithium Intercalation", Journal Of Solid State Chemistry 29 (1979) 339

40 Dickens P.G., Whittingham M.S. "The Tungsten Bronzes And Related Compounds", Quart. Rev. 22 (1968) 30

41 Jacobsen T., West K., Zachau-Christiansen B., Atlung S. "A.C. Impedance Studies On Li Insertion In V_6O_{13} Single Crystals", Electrochim. Acta 30 (1985) 1205

42 Hooper A. "Solid-state Rechargeable Batteries", Solid State Batteries (Nato Asi Series. Series E: Applied Sciences No. 101). p399, Eds. Sequeira C.A.C., Hooper A., Publ. Martinus Nijhoff Publishers (1985)

43 Atlung S., Zachau-Christiansen B., West K., Jacobsen T. "The Composite Insertion Electrode Theoretical Part. Equilibrium In The Insertion Compound And Linear Potential Dependence", J. Electrochem. Soc. 131 (1984) 1200

1 PREPARATION OF MATERIALS

1.1 PREPARATION OF NIOBIUM DISULPHIDE

Previous work [1, 2, 3] has demonstrated that the hexagonal (2H) phase of niobium disulphide is the predominantly formed phase when reaction of elemental niobium and sulphur occurs at between 850 °C and 1000 °C. The product is a mixture of hexagonal and rhombohedral (3R) phases but the proportion of the hexagonal phase can be maximised by quenching rapidly. [4]

Powdered niobium and sulphur were thoroughly ground and mixed in the required molar ratio (3.7164 g Nb: 2.5648g S). The mixture was sealed into an evacuated quartz ampoule, ensuring that the free volume of the ampoule was minimised, and placed into an oven. The oven was raised slowly in temperature to 900 °C at a rate of no more than 50 °C per hour to reduce the possibility of explosion of the ampoule as the components vaporise. The temperature was monitored using a Comark digital thermometer connected to a NiAl/NiCr thermocouple which was protected with ceramic tubing and placed adjacent to the ampoule. The reaction vessel was maintained at 900 °C for 10 days and the ampoule then quenched into liquid nitrogen.

X-ray powder diffraction (Co Kα or Cu Kα radiation) showed that, as expected, all samples containing hexagonal NbS_2 also contained some proportion of the rhombohedral form. The lines at d-spacings of 2.80 Å, 2.59 Å, 2.33 Å, 2.07 Å, and 1.63 Å were indicative of the hexagonal form, and those at 2.74 Å, 2.42 Å, 2.24 Å, 1.91 Å, and 1.76 Å characterised the rhombohedral phase. Other lines in the diffraction pattern were common to both forms, the strongest of these being at 5.95 Å, 2.84 Å, 1.98 Å, 1.66 Å, 1.60 Å and 1.50 Å. The hexagonal phase was also characterised by a metallic sheen and a higher open circuit potential with respect to a pure silver reference electrode when formed into an electrochemical cell (approximately 0.4 V compared with approximately 0.2 V for the rhombohedral phase). Since a good open circuit potential was the main requirement for the experiments described later the same sample of hexagonal NbS_2 was used in all subsequent diffusion experiments, after being ground and sieved (see below).

A series of experiments showed that even when as similar conditions as possible were used in the preparation (i.e. the same Nb:S mixture, equally sized and filled ampoules and identical heat treatment of the samples), in some cases the predominant form found was the hexagonal phase and in others the rhombohedral. This may be attributable to inhomogeneity in the Nb:S mixture leading to non-stoichiometric material or to a "seeding" effect depending on which crystal phase was produced

first. However, three features were apparent. Firstly a temperature of 900 °C to 925 °C gave the hexagonal form more consistently than temperatures approaching 1000 °C. The usage of full ampoules gave better results than using partially full ampoules, although more care had to be taken during the sealing procedure to keep the heat away from the powdered materials. (This may explain the failure to produce the hexagonal phase sometimes - the heating causing some reaction or loss of materials through vaporisation.) Lastly it was not found to be possible to convert the rhombohedral phase to the hexagonal form by further heating to 900 °C for prolonged periods of time.

$Ag_{0.05}NbS_2$ was also synthesised from the appropriate molar quantities of the elements (0.2156g Ag, 3.7164g Nb, 2.5648g S) in an identical manner, heating the ampoules to 1000 °C for 10 days. The product had a very shiny metallic appearance and an open circuit potential of approximately 0.35 V relative to pure silver, this being significantly lower than that for $Ag_{0.05}NbS_2$ produced electrochemically. The X-ray diffraction pattern showed broad peaks centred approximately at d-spacings of 5.99 Å, 3.00 Å, 2.83 Å, 2.42 Å, 2.14 Å, 1.98 Å, 1.66 Å, and 1.49 Å, the strongest of these corresponding to the lines common to both hexagonal and rhombohedral phases.

1.2 PREPARATION OF SILVER SALTS

The three silver salts prepared (γ-AgI, Ag_2WO_4 and Ag_3AsO_4) decompose in the presence of light and moisture. All the reactions described below were therefore carried out in a darkened laboratory with the reaction vessels wrapped in aluminium foil until the dry product was isolated. The products were always stored over phosphorus pentoxide desiccant in an evacuated desiccator, with individual containers wrapped in aluminium foil to ensure darkness. They were only removed when required and returned to the desiccator as soon as was possible.

1.3 PREPARATION OF γ-SILVER IODIDE

An approximately 0.5 molar solution of potassium iodide was added dropwise to a slight excess of equimolar silver nitrate solution acidified with a small amount of dilute nitric acid. The solution was stirred constantly throughout the addition and then allowed to stand for 30 minutes. The yellow precipitate of silver iodide (AgI) was filtered off through a sintered glass funnel, washed very thoroughly with distilled water and subsequently with analar grade acetone. The silver iodide was then dried in an evacuated desiccator over phosphorus pentoxide before being finely ground (in order to produce the γ-phase [5]) and stored as described above.

1.4 PREPARATION OF SILVER TUNGSTATE

Silver tungstate (Ag_2WO_4) was prepared by the dropwise addition of an excess of 0.5 molar silver nitrate solution to a stirred 0.5 molar solution of silver tungstate. The reaction mixture was heated to approximately 80 °C throughout this addition and maintained at a pH of between 9 and 10 by the addition, as necessary, of dilute sodium hydroxide solution. This was required to produce the correct phase of silver tungstate. [6] The white product was then filtered off, washed dried and stored in the same manner as the silver iodide.

1.5 PREPARATION OF SILVER ARSENATE

Silver arsenate (Ag_3AsO_4) was prepared by precipitation from a 0.5 molar solution of silver nitrate on the dropwise addition to it of an equal amount of 0.167 molar sodium hydrogen arsenate solution, with continual stirring. The brown precipitate of silver arsenate was collected, dried and stored in the previously described manner.

2 PREPARATION AND CHARACTERISATION OF GLASSY ELECTROLYTES

Silver ion conducting glasses from five different chemical systems based on silver iodide were synthesised. Two of these were binary, consisting of two components in different ratios, one was pseudo-binary, where the proportion of one component varied against a constant ratio of the two other constituents, and the remaining two systems were ternary, comprising three components in different ratios. The systems examined were a) AgI-Ag_2WO_4, [7] b) AgI-Ag_3AsO_4, [8] c) AgI-(Ag_2O:B_2O_3), [9] d) AgI-Ag_3AsO_4-$AgPO_3$ [10] and e) AgI-Ag_2WO_4-$AgPO_3$. The latter system has not been reported before but two glasses were produced analogous to those found in the ternary arsenate system d. In all cases precautions were taken to exclude light and moisture on storage of the glasses as discussed in the previous section.

2.1 PREPARATION OF BINARY GLASSES

Two binary glasses were prepared from the silver iodide:silver tungstate system, the first containing 80 mole per cent AgI ($4AgI:Ag_2WO_4 \rightarrow Ag_6I_4WO_4$ - silver iodotungstate) and the second 30 mole per cent AgI ($3AgI:7Ag_2WO_4$). A glass corresponding to the 80 mole per cent tungstate glass was also prepared in the silver iodide:silver arsenate system ($4AgI:Ag_3AsO_4 \rightarrow Ag_7I_4AsO_4$ - silver iodoarsenate). An identical synthetic technique was employed in each case.

The two constituents, in the required molar proportions, were thoroughly mixed and ground together. The mixture was then transferred to a specially designed Pyrex tube with a small-bore outlet at one end to facilitate pouring. The tube was heated under a continuous nitrogen flow until fusion of the materials was complete. The tube was then tilted, allowing small droplets of the melt to fall into a large dewar of liquid nitrogen. Excess liquid nitrogen was poured off and the glass electrolyte thawed and dried over phosphorus pentoxide in a desiccator which was under continuous evacuation. The glass was then ground and stored until required.

2.2 PREPARATION OF TERNARY GLASSES

The two ternary glasses were prepared from an intimate mixture of the appropriate molar amounts of silver iodide, silver arsenate (or silver tungstate), silver nitrate and ammonium dihydrogen phosphate, the latter components generating the silver phosphate in situ as they decomposed on heating (essentially $AgNO_3 + (NH_4)H_2PO_4 \rightarrow AgPO_3$ plus gaseous products). The mixture was heated in an open platinum crucible until 15 minutes after gas evolution from the melt had ceased. The molten liquid was rapidly quenched by pouring into liquid nitrogen and the glass collected and stored in the normal manner.

The pseudo-binary glasses from the system $AgI\text{-}Ag_2O\text{-}B_2O_3$ were produced by a similar method from a mixture of silver iodide, silver nitrate and boric acid, the latter two constituents always present in the same predetermined ratio yielding a 1:1 molar ratio of Ag_2O and B_2O_3 as they decomposed ($2\,AgNO_3 + 2\,B(OH)_3 \rightarrow Ag_2O + B_2O_3$ and gaseous products). The platinum crucible was maintained at 700 °C until gas evolution was complete and the melt then quenched into liquid nitrogen. The glass was collected, ground and stored in the usual fashion.

2.3 CHARACTERISATION OF GLASSES

The conductivities of all the glasses were measured using frequency response analysis (as detailed in Section 9 below) on 13 mm two-electrode cells. Table 1 below lists these conductivities along with the mole fraction of silver iodide, $x(AgI)$, the colour and the hardness of the important glasses. These latter two properties are related to the silver iodide content of the glass. [9] The measured conductivities compare favourably with values cited in the appropriate references, differences being attributable to the different preparation technique used, to the use of particulate materials and to deviations in stoichiometry. The glass transition temperature of some of the glasses was measured using differential scanning calorimetry and these again correlated well with literature values.

System	Glass	x(AgI)	$\log_{10}$(conductivity)	Colour	Hardness
1	B1	0.80	-2.01 Scm^{-1}	Red	Soft
1	B2	0.65	-2.60 Scm^{-1}	Green/Brown	
1	B3	0.50	-3.46 Scm^{-1}	Brown/Yellow	
1	B4	0.30	-4.46 Scm^{-1}	Brown	
1	B5	0.10	-5.58 Scm^{-1}	Dark Brown	Hard
2	G1	0.96	-3.15 Scm^{-1}	Red/Brown	Soft
2	G2	0.90	-2.11 Scm^{-1}	Red/Brown	
2	G3	0.88	-2.57 Scm^{-1}	Brown	
2	G4	0.70	-4.08 Scm^{-1}	Green/Yellow	
2	G5	0.00	-6.28 Scm^{-1}	Pink	Hard
3		0.80	-1.83 Scm^{-1}	Yellow/Green	Soft
4		0.80	-2.00 Scm^{-1}	Bright Red	Soft

Table 1.
Details of the major glass electrolytes prepared.
In system 1 x(AgI) is the pseudo-binary mole fraction of AgI, in system 2 it is the mole fraction of AgI in the ternary system and in systems 3 and 4 it is the normal binary mole fraction.

System 1 - AgI-(Ag_2O:B_2O_3), System 2 - AgI-Ag_3AsO_4-$AgPO_3$,
System 3 - AgI-Ag_2WO_4, System 4 - AgI-Ag_3AsO_4.

Conductivities at 25 °C except system 1 at 50 °C

X-ray diffraction analyses of all the glasses were also carried out and in general revealed the glasses to completely amorphous, a totally flat trace with no evidence of crystallinity being obtained. In a minority of cases a few small peaks were seen to be present at positions corresponding to those of silver iodide, indicating the presence of traces of free silver iodide. This is commonly found in such systems. [10]

When using the glasses in the working electrode of a three-electrode cell, as described below, it was found that the cell potential did not stabilise for the arsenate-based or ternary tungstate-based glasses. All three electrode cells were therefore fabricated using either $Ag_6I_4WO_4$ or the borate glasses. The ternary arsenate glasses were used in the pseudo-ionic conductance experiments, and silver iodotungstate as the main electrolyte in all the three-electrode cells.

3 SIEVING OF PARTICULATE MATERIALS

A set of six sieves were prepared to allow restriction of the particle sizes of the electrolyte and electrode materials used in cell construction, and to permit selection of specific size ranges of these particles. These sieves were made from transparent perspex tubing shaped so that each piece would fit inside the others (Figure 1), and utilising nylon sheeting of various mesh sizes as the separating agent. This sheeting was glued to the bottom of the perspex rings.

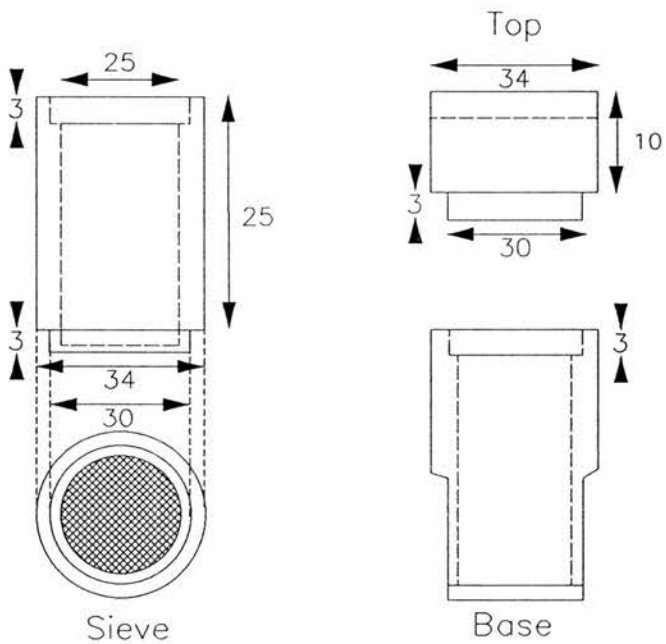

Figure 1.
Details of sieves.

The powdered material was placed in the uppermost sieve. The set of sieves, together with the top and base, were taped together and inserted into a brass holder which was screwed shut to compress the sieves tightly and hence prevent particle escape. This holder was vibrated gently for an hour with an automatic shaker and then the sieves were extracted and the separated particle sizes individually collected and stored. The particle size ranges resulting are shown in Table 2 below.

Sieve	Particle Size	Maximum Particle size	Conductivity (x 10^2)
Sieve 1	> 350 μm	350 μm	1.61 Scm^{-1}
Sieve 2	212 - 350 μm	212 μm	1.80 Scm^{-1}
Sieve 3	150 - 212 μm	150 μm	2.33 Scm^{-1}
Sieve 4	125 - 150 μm	125 μm	2.35 Scm^{-1}
		125 μm	2.38 Scm^{-1}
Sieve 5	75 - 125 μm	75 μm	2.76 Scm^{-1}
Sieve 6	45 - 75 μm	45 μm	3.18 Scm^{-1}
Sieve 7	< 45 μm	25 μm (*)	3.70 Scm^{-1}
Unsieved		175 μm (*)	2.09 Scm^{-1}

Table 2
Particle size ranges collected in each sieve and variation of conductivity with particle size for silver iodotungstate electrolyte. (* = Median particle size)

Since it has been reported [11] that glasses in the silver iodide/silver orthophosphate system showed an increase in conductivity with a decrease in the particle size this effect was investigated for the silver iodotungstate glass. The results obtained showed a similar trend and are also summarised in Table 2.

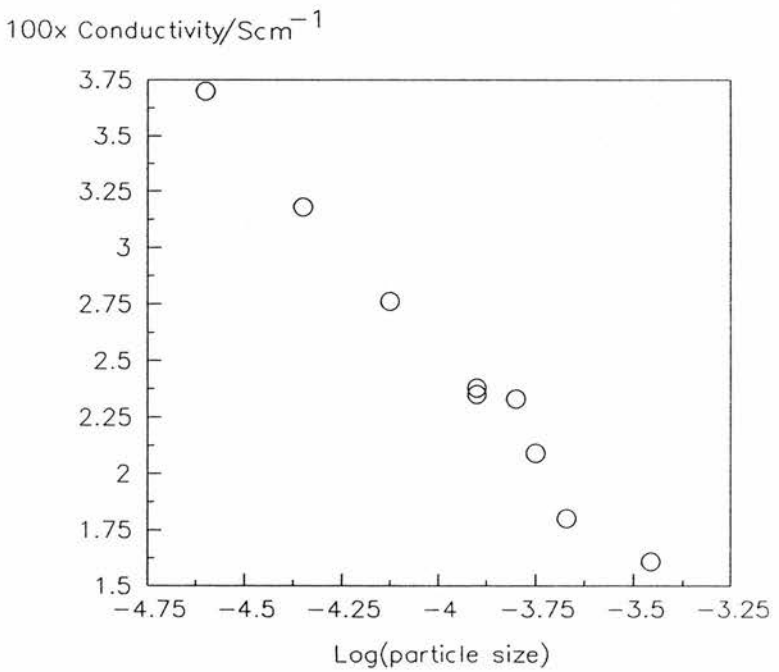

Figure 2.
Effect of particle size on the conductivity of silver iodotungstate electrolyte.

Figure 2 shows a plot of the conductivity versus the logarithm of the minimum particle size in each range. This shows very good linearity and the enhancement in conductivity with the reduction in particle size is probably due to improved contact and packing between the smaller particles. Also shown is the conductivity of the unsieved material which lies on the line at the position corresponding to the median of the whole particle size range. Experimentally this necessitated the use of the same size range (or mixture of size ranges) of particles in the preparation of all the cells described below.

4 PREPARATION OF ELECTROCHEMICAL CELLS

4.1 TWO-ELECTRODE CELLS

Two-electrode cells were employed in two different sets of experiments. Firstly they were used to measure the conductivity of the glasses prepared and, secondly, in the series of experiments to investigate pseudo-ionic conductance as described in Chapter 7.

The fundamental cell configuration was identical in both cases (Figure 3) and consists essentially of two non-blocking electrodes sandwiching the central electrolyte region. The electrode mixture was comprised of a 2:1 mixture by weight of silver metal powder and powdered silver iodotungstate electrolyte, thoroughly ground and mixed together with an agate mortar and pestle. When the cells were to be used to determine the conductivity of the glass the electrolyte region was simply the pure glass used without further grinding. In the pseudo-ionic conductance experiments the electrolyte section was a mixture of the glass and the dopant being added.

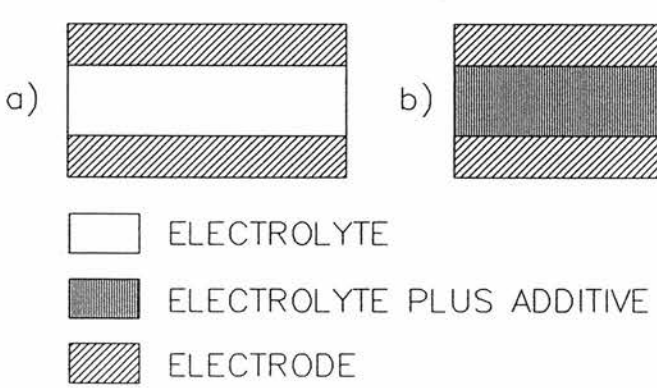

Figure 3.
Schematic representation of two-electrode cell.
a) Conductivity cell b) Pseudo-ionic conductance cell.

Cells were fabricated in both 5 mm and 13 mm diameter sizes using the appropriate Specac dies and anvils, the preparation conditions being dependent on the diameter of the cell. To fabricate the former size approximately 0.05 g of the electrode mixture was pressed onto the lower polished anvil to a pressure of 0.5 tonnes for one minute using a Specac 15000 press. A 0.1 g layer of the electrolyte material was then formed onto this employing a pressure of 1 tonne for two minutes. The upper electrode was added by pressing a further 0.05 g of material to 1.5 tonnes for five minutes, using the other polished anvil to yield a clean upper surface and complete the cell. Finally the base was removed, the dies inverted and the cell gently pushed clear before storage.

The 13 mm cells were prepared in a similar fashion but applying pressures of 0.5 tonnes for one minute, 2 tonnes for two minutes and lastly 3 tonnes for five minutes, utilising 0.6 g of the required material for each section.

4.2 THREE-ELECTRODE CELLS

The configuration and construction of the three-electrode cells used here were described by Razzini [12] and are illustrated in detail in Figure 4.

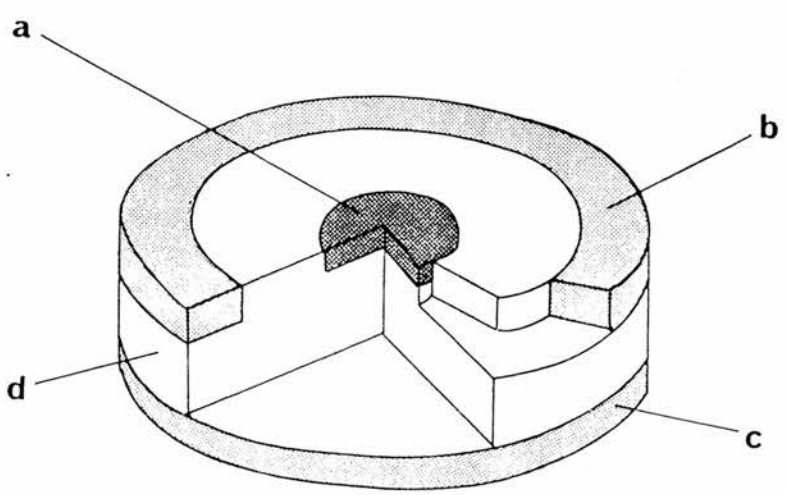

Figure 4.
Schematic representation of three-electrode cell. a) Working electrode, b) Reference electrode, c) Counter electrode, d) Pure electrolyte.

The cells are essentially a cylindrical layered structure, the lowermost layer being the counter electrode comprising a 2:1 mixture by weight of silver powder and silver iodotungstate electrolyte. The central layer is composed of a pure glass electrolyte, usually the high conductivity silver iodotungstate. The upper layer consists of three concentric circular regions, the outermost being the reference electrode ring, corresponding identically in composition to the counter electrode. The middle ring is again pure electrolyte, acting as separator between the reference and working electrodes. The innermost region is the working mixed phase electrode itself, consisting of an intimate mixture of the niobium disulphide solid solution electrode material and one of the silver ion conducting glasses. The relative proportions, sizes and conductivities of the two materials were varied in the different experiments undertaken.

Details of the dimensions of the dies used to manufacture these cells are given in Figure 5 and their usage in the cell pressing procedure is illustrated in Figure 6.

The same pressures, quantities of materials, particle sizes and preparation conditions were employed in every case, except where modification of one of these parameters was being investigated. In general it is probably necessary to optimise the quantities and conditions where different electrode materials or electrolytes are used, especially where the physical properties differ markedly. The conditions described in detail here were found to be suitable by Nairn [4] for niobium disulphide and silver iodotungstate.

The first step of the cell construction involved forming the outer reference ring. Approximately 0.19 g of the 2:1 mixture by weight of silver and silver iodotungstate was pressed at 0.5 tonnes pressure for one minute using the dies as depicted in Figure 6a. The internal former was then pushed clear through the alternative base plate as shown in Figure 6b and the next die arrangement prepared (Figure 6c). This was used to form the central electrolyte separating ring, 0.15 g of the pure electrolyte being compressed at 1 tonne for one minute. Again the internal former utilised was slowly forced clear through one of the holes in the alternative base (Figure 6d).

The working electrode mixture was then prepared from the ground and sieved electrode and electrolyte materials. Typically 0.02 g of material was used, the appropriate quantities of the individual components being weighed and then thoroughly mixed in an agate mortar *without further grinding* to avoid alteration of the size distribution of materials.

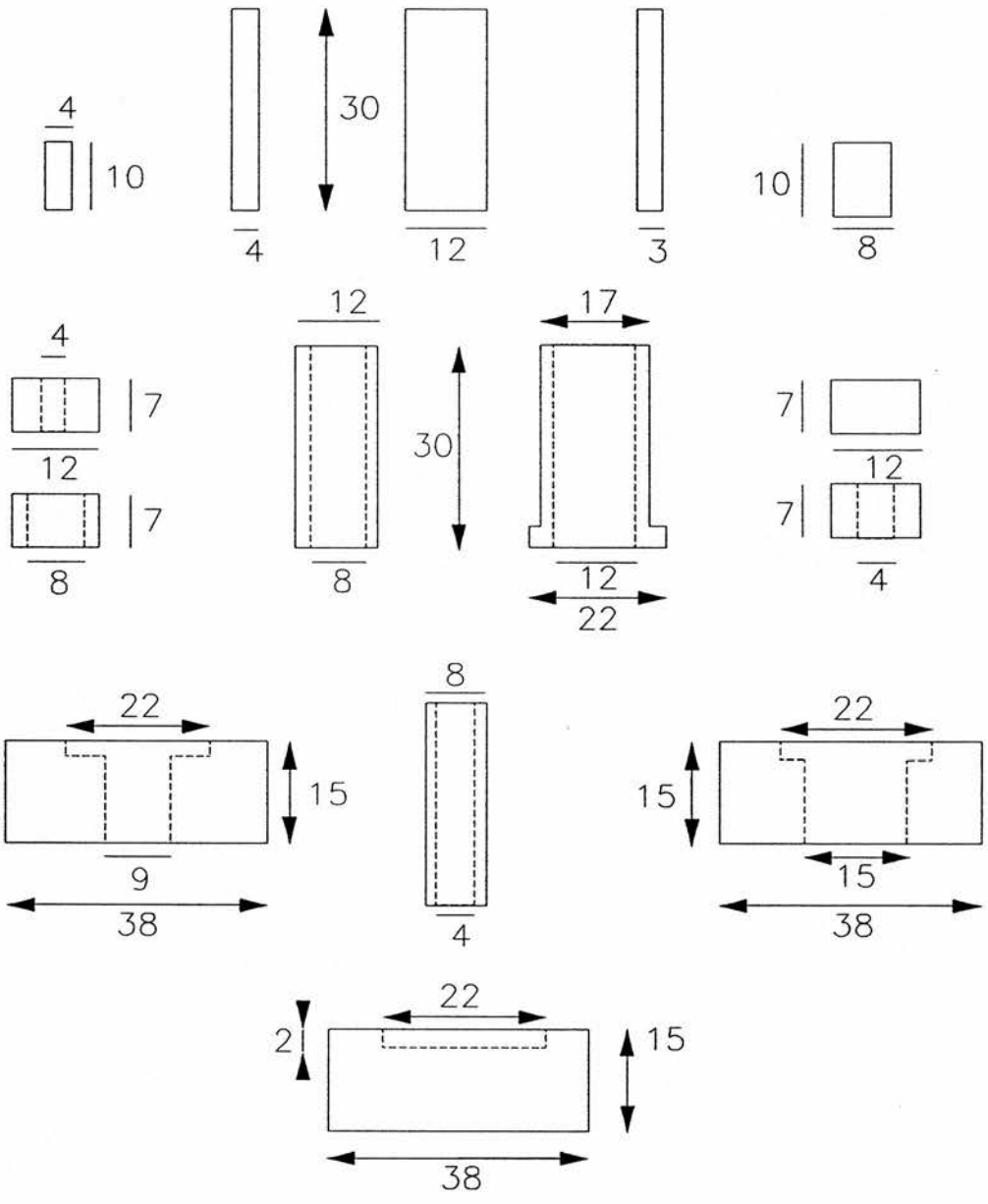

Figure 5.
Dimensions (in mm) of dies used in three-electrode cell construction.

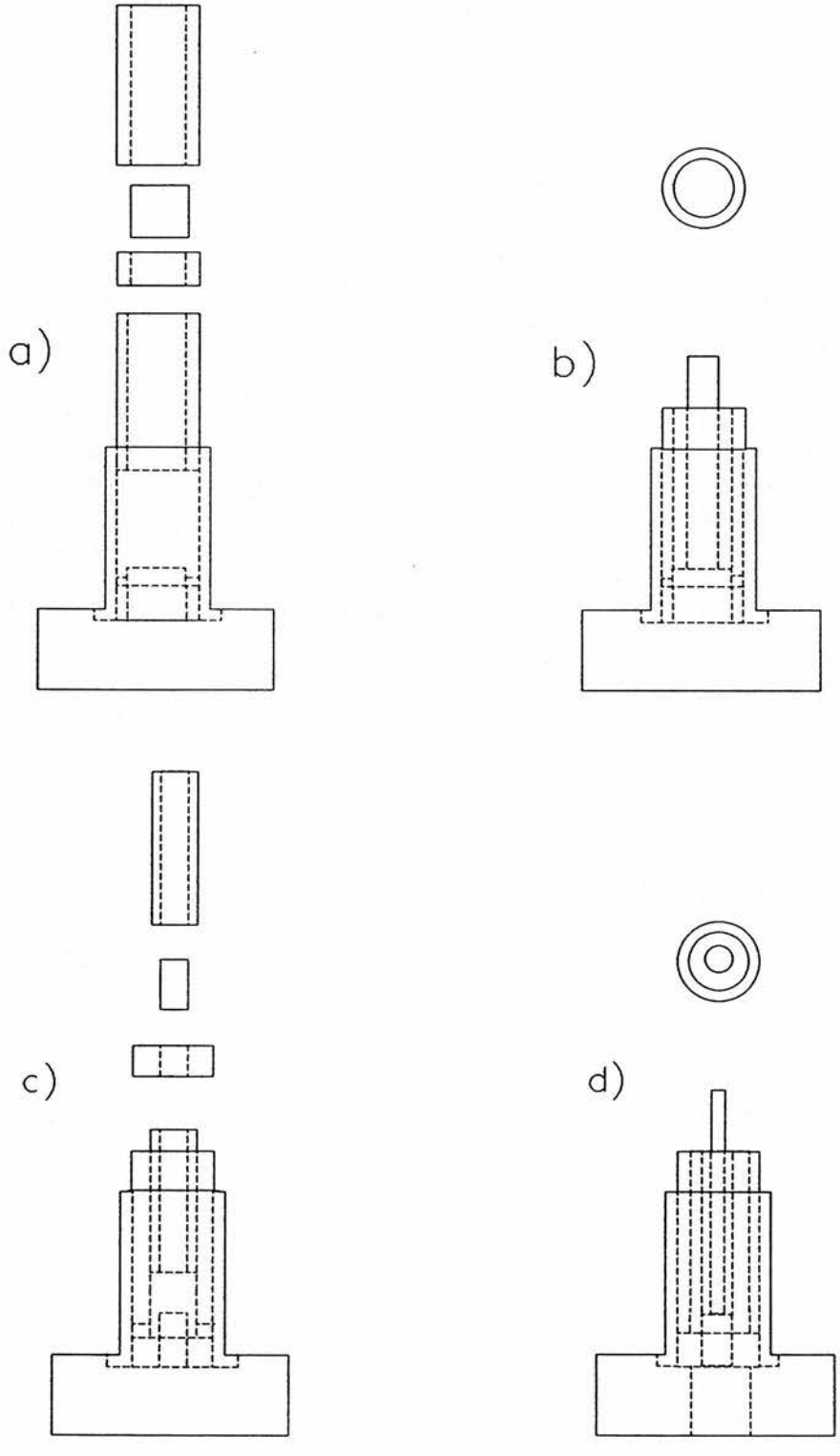

Figure 6a - 6d.
Three-electrode cell construction procedure.

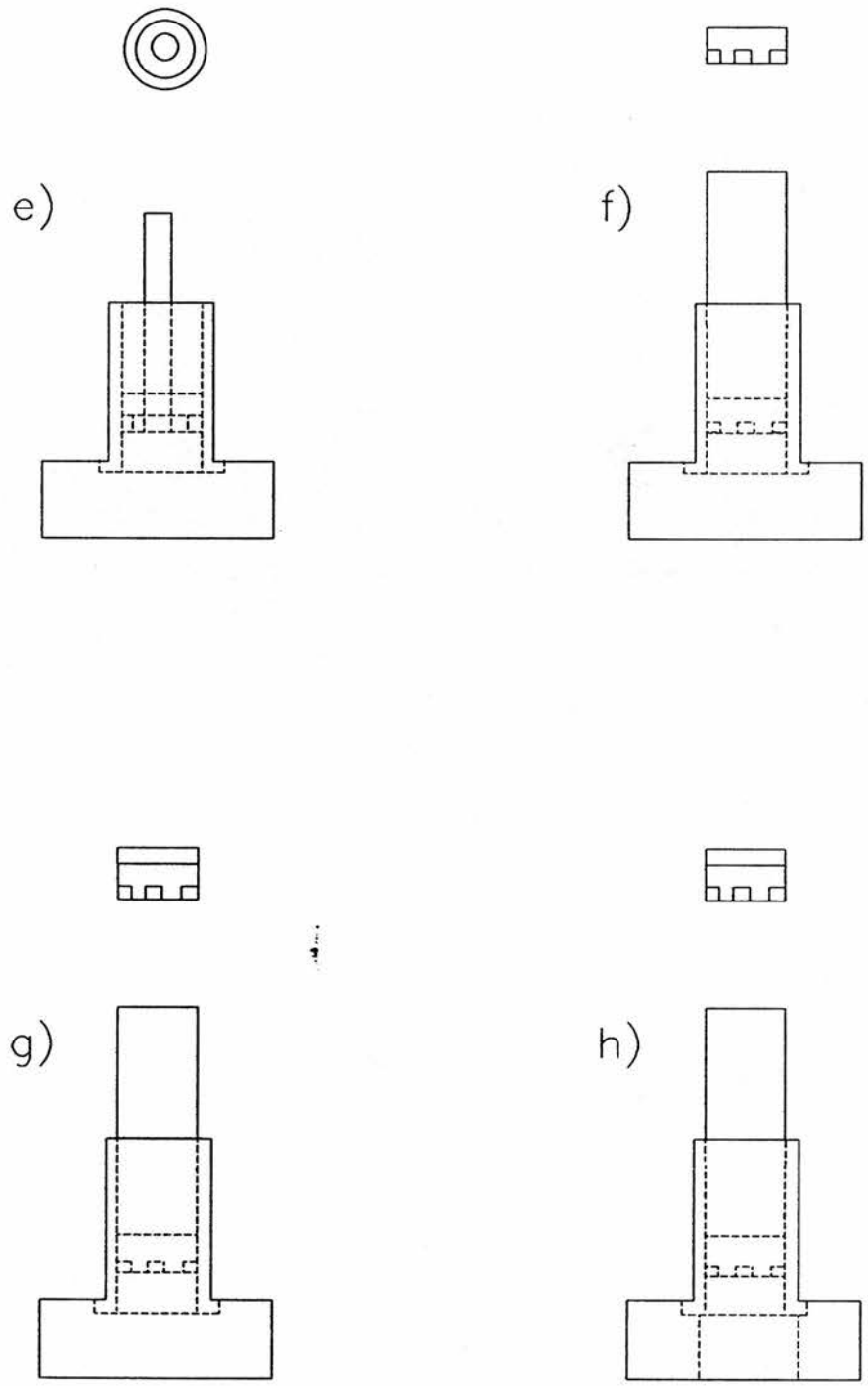

Figure 6e - 6h.
Three-electrode cell construction procedure.

The die arrangement illustrated (Figure 6e) was set up, with a Teflon insulating disc placed between the cell and lower anvil to prevent short circuiting of the working and reference electrodes of the cell during this and later stages of the cell fabrication. The working electrode mixture was pressed into the required position using finger pressure through a plunger guide again made of Teflon to prevent short circuit.

0.3 g of pure electrolyte was then pressed at 2 tonnes for two minutes on top of this layer using the configuration of pieces shown in Figure 6f. An identical set up was used to form the final counter electrode layer from 0.3 g of the 2:1 silver:silver iodotungstate electrode mixture, 3 tonnes of pressure being applied for five minutes.

Finally the completed cell was gently pushed clear through the remaining base plate as shown in Figure 6h. It was then inspected under a microscope for any obvious cracks or defects and its open circuit potential was measured to ensure there were no internal short circuits. The finished cells were stored under vacuum, in darkness over phosphorus pentoxide dessicant before use. At all times the cells were handled with plastic tongs to prevent contamination, and the time outside the cell holder or desiccator was kept to a minimum.

4.3 MEASUREMENT OF CELL THICKNESS

After completion of any experiments all cells were sliced in two to enable the cell thickness to be measured. The thickness required was that of the electrolyte region in the case of the two-electrode cells used for conductivity measurements or the pseudo-ionic conductance experiments. In the case of the three electrode cells it was the thickness of the working electrode that was required in order to calculate the diffusion coefficient. The sectioned cell was mounted on the deck of a travelling microscope and the thickness measured at ten equally spaced intervals perpendicularly across the required region. The average of these readings was taken to be the cell thickness (d). This value was used to calculate the cell constant (K) for the two-electrode cells from the formula $K = d/A$ where A is the area of the cell.

5 CELL HOLDERS AND ENVELOPES

5.1 TWO-ELECTRODE CELL HOLDER

Detailed drawings of the two-electrode cell holders and the modified Pyrex tube and head used as the cell envelope are given in Figure 7. The cell holder was constructed from Teflon with terminals

made from stainless steel. Electrical connections were soldered directly to these terminals and a minimum length of wire was used before connections were made to screened electrical cable. The cable outlets through 7 mm sockets in the tube head, the outlets being sealed with epoxy resin, and then connected to the external circuitry via BNC plugs. A NiAl/NiCr thermocouple was inlet through another socket in the jacket head and positioned next to the cell holder at all times.

All experiments were carried out under a continuous nitrogen flow and a constant temperature was maintained by immersion of the cell holder envelope in a Haake water bath. The temperature was monitored via the internal thermocouple connected to a Comark 2001 digital thermometer. All pseudo-ionic conductance measurements were carried out at 25 °C and the conductivity measurements at either 25 °C or 50 °C.

5.2 THREE-ELECTRODE CELL HOLDER

Details of the three-electrode cell holder and the connections to the cell are depicted in Figure 8a. The cell holder was fabricated from Teflon and the terminals from gold. Electrical connections are made directly to these terminals then through sealed outlets in the Pyrex cell envelope head to the external cabling (Figure 8b). A NiAl/NiCr thermocouple is also sealed into the jacket head, with the tip positioned adjacent to the cell holder allowing the temperature to be monitored via the external Comark thermometer.

The cell holder environment was controlled by placement of the envelope in a Townson and Mercer oil bath maintained at 50 °C. A continuous stream of nitrogen was dried using an AEI-Birlec adsorbing column, then thermostatted by passage through coils of tubing immersed in the oil bath, before being allowed to flow through the cell envelope.

6 CELL STANDARDISATION AND INTERCALATION

All diffusion coefficient measurements in this work were carried out from an initially fixed silver level of 5 % ($Ag_{0.05}NbS_2$). This level was chosen as being in a linear region of the niobium disulphide discharge, and hence avoiding phase changes at higher levels. [13] It is also a high enough intercalation level to avoid rapid changes in diffusion coefficient with small changes in the intercalation level. [14] All pulses were of a small enough current and duration to retain the intercalation level within this region.

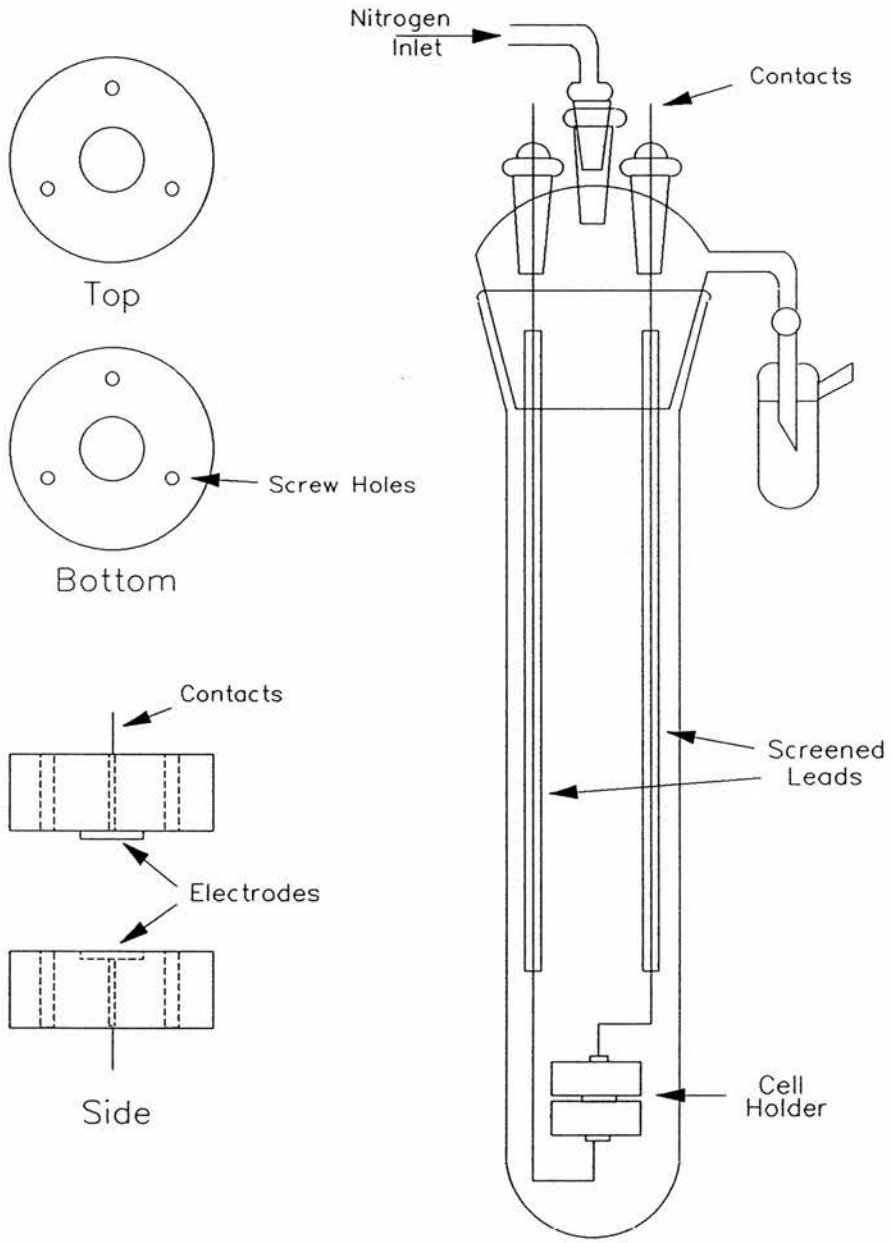

Figure 7.
Two-electrode cell holder and cell envelope.

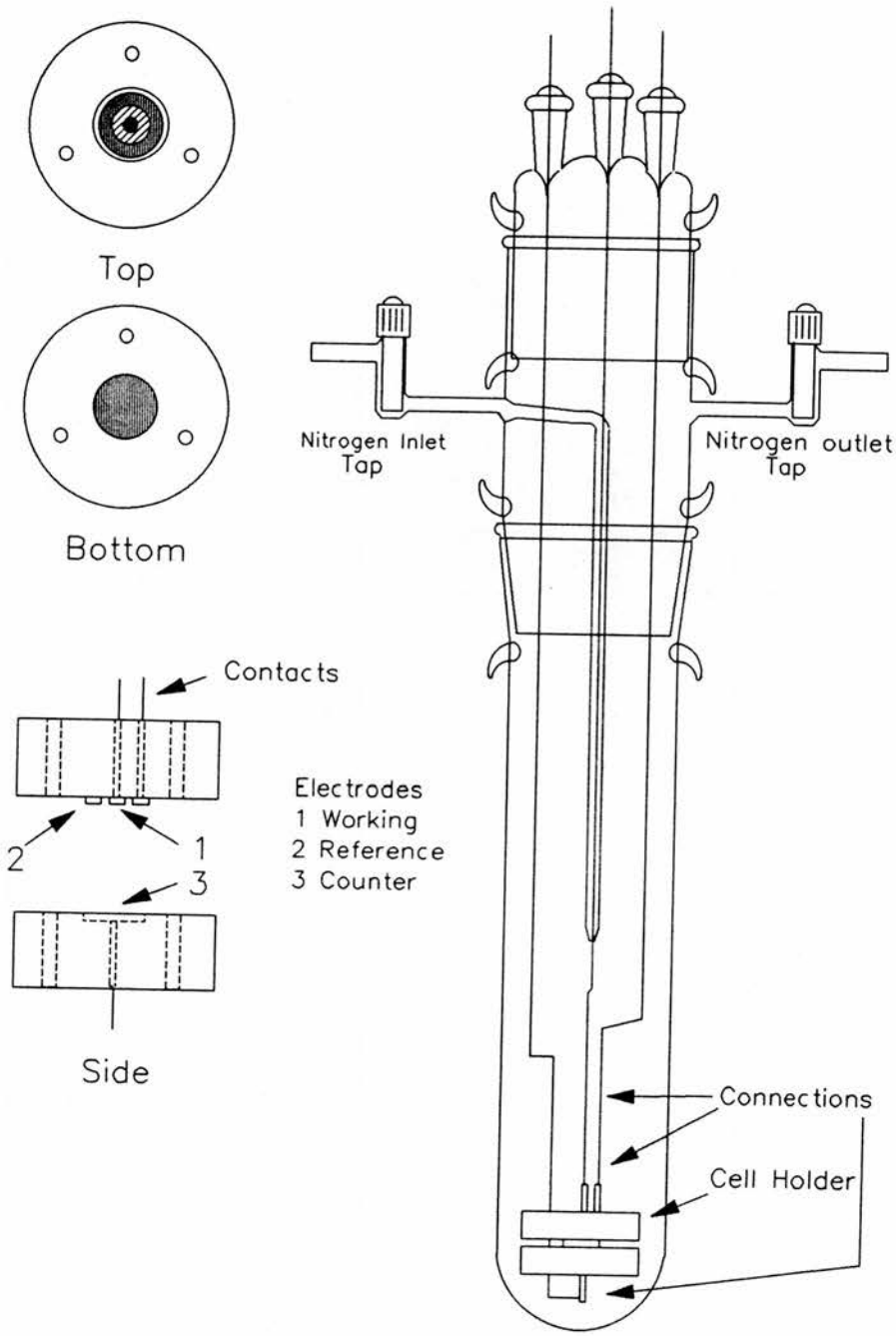

Figure 8.
Three-electrode cell holder and cell envelope.

After insertion into the cell holder and equilibration to 50 °C the cell was maintained at a constant potential of 0.42 V, just above the open circuit potential of the cell, to ensure that the niobium disulphide was completely deintercalated. The cell was then allowed to equilibrate until its potential was constant to within 0.1 mV over a 24 hour period. The intercalation to the 5 % silver level was then carried out galvanostatically and the cell potential was again permitted to equilibrate until it was constant to within 0.1 mV for a day.

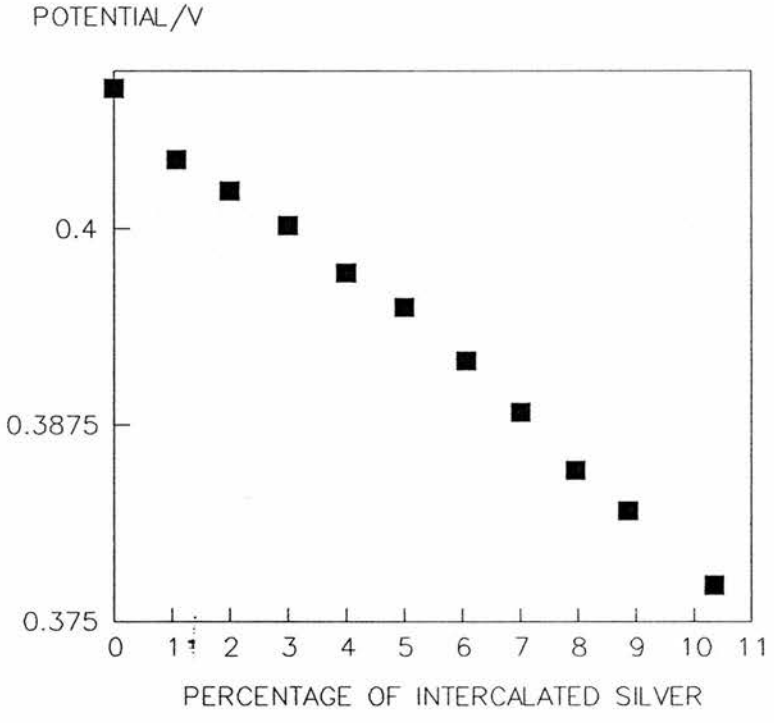

Figure 9.
EMF/intercalation level curve for Ag_xNbS_2.

The discharge curve (i.e. the open cell potential versus degree of intercalation curve) over the range of interest (0 - 10 % Ag) was determined for the sample of hexagonal niobium disulphide prepared above. This was done using a three-electrode cell, prepared under identical conditions to Nairn [4] using a series of 10 μA pulses, each of approximately 1 hours duration. This gave the cell potential at 1 % intervals and the graph obtained (Figure 9) is in good agreement with previously reported curves. [4, 15]

7 INSTRUMENTATION AND PULSE MEASUREMENTS

The experimental configuration used for applying and recording constant currents is illustrated in Figure 10. Basically the cell potential between working and reference electrodes was monitored by a microcomputer-controlled voltmeter while the galvanostat, utilising an external voltage source if necessary, applied a constant current between the working and counter electrodes of the cell.

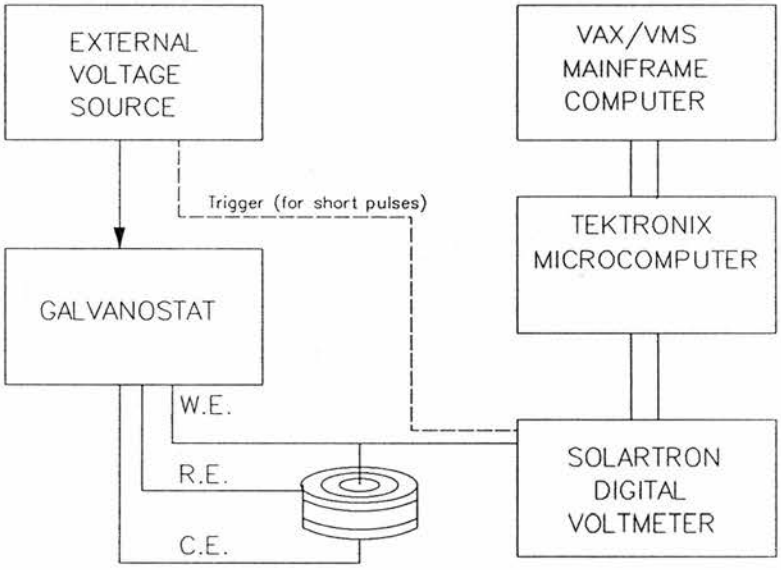

Figure 10.
Block diagram of apparatus used to apply and monitor galvanostatic pulses.

7.1 MICROCOMPUTER AND VOLTMETER

A programmable Solartron 7065 microprocessor digital voltmeter (DVM), accurate to $1\mu V$ in its most sensitive range, was controlled using a Tektronix 4052 microcomputer. The Tektronix was programmed to instruct the DVM to initiate voltage recording and to measure the cell potential at programmed time intervals. The time was monitored by the internal digital clock of the DVM (accurate to within 2.5 ms) and the potentials recorded were transferred via an IEEE interface back to the Tektronix to be stored on magnetic tape.

The Tektronix could be connected to the VAX/VMS mainframe computer and data was transferred from the magnetic tape to permanent storage on the mainframe. Here also the data was

analysed using various programs and statistical packages as detailed in Appendix 1. Graphs were either plotted using a graphics package available on the mainframe or using a plotting program written for the Tektronix.

7.2 GALVANOSTAT/POTENTIOSTAT

The galvanostat/potentiostat used throughout the described experiments was designed and manufactured in the departmental electronic workshop. As it was used predominantly in galvanostatic mode only this will be described in detail with reference to the outline circuit diagram given in Figure 11.

The reference potential circuit and LH00Z010K amplifier are used in a standard constant current generating configuration to supply currents as chosen by the current range selector. In general an external constant voltage source, also designed and built in the department, was used to apply a potential across the summing point (A) of the amplifier via the auxiliary inputs. The standing current within the galvanostat was set to zero and thus the current applied to the cell was controlled by the external input. A switch on the external potentiostat was also employed to start and stop the current flow.

The remainder of the circuit shown illustrates the different options available with the galvanostat, the choice of two or three electrode cells, the choice of galvanostatic or potentiostatic modes, the choice of voltage or current display on the meter etc. A cell voltage offset feature (not shown) was also used which enabled the most sensitive recording range of the DVM to be used for measurement of the cell potential.

7.3 PULSE MEASUREMENT

Before any measurement several checks were carried out on the galvanostat and associated instrumentation. Firstly a dummy cell (a resistor of appropriate value) was attached across the cell connection terminals and the zero standing current in the galvanostat monitored by connection of the current outputs at the rear of the galvanostat to a Solartron 4552 multimeter. The standing current was brought as close to zero as possible by fine rotation of the current setting potentiometer on the front panel. The current measuring device was then connected in series with the dummy cell and the standing current reduced to zero using the fine zero adjustment screw.

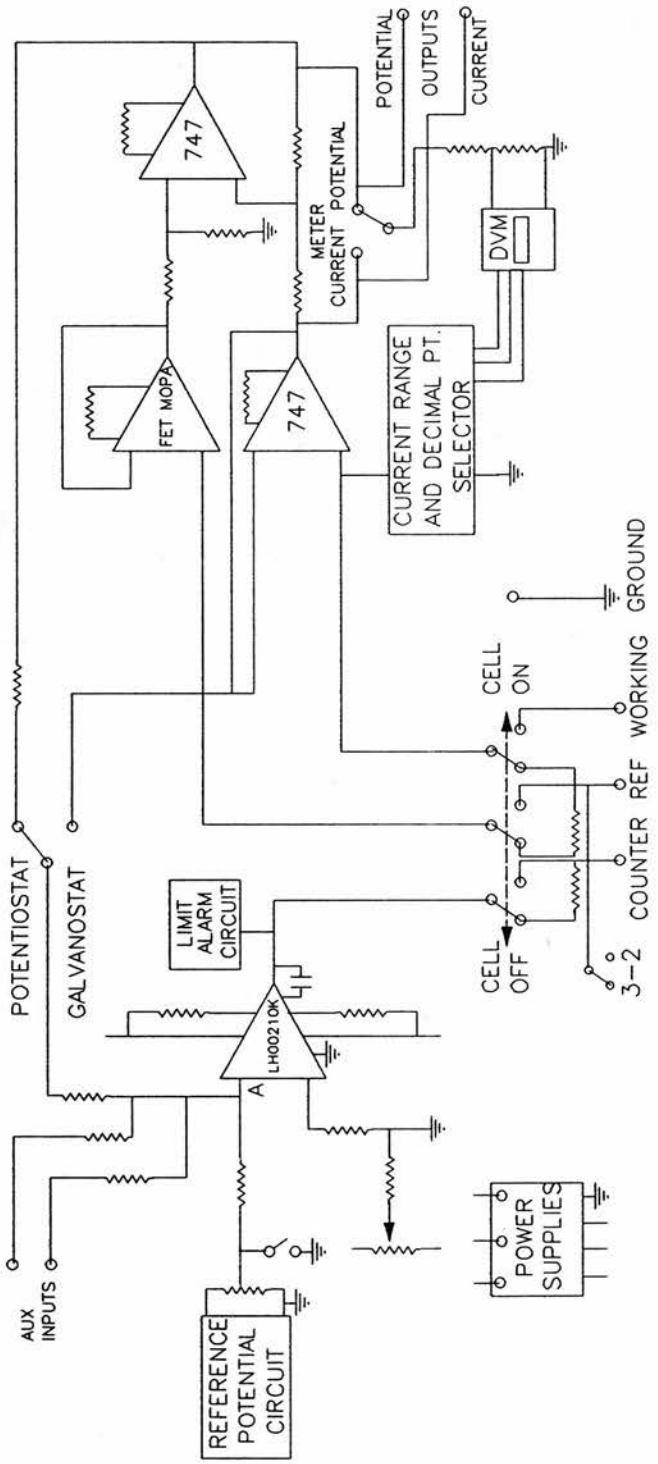

Figure 11.
Outline circuit diagram of galvanostat.

The cell was then connected to the galvanostat and the Solartron DVM attached to the voltage outputs at the rear of the galvanostat. The cell was switched on and the potential offset adjusted to produce a reading on the DVM corresponding to the open circuit potential of the cell. The cell temperature was also checked at this stage by connecting the Comark digital thermometer to the appropriate thermocouple.

The appropriate pulse height and direction was selected on the external potentiostat and the current range selector. The computer program was then initiated and details of the measurements to be taken inserted. Firstly the cell potential was monitored for a few minutes to ensure that it was constant. The current was then switched on manually and the cell potential monitored during the pulse. After the required pulse time the current was stopped and the subsequent voltage relaxation recorded until there was no significant change in the potential between successive measurements.

After each pulse the cell was allowed to relax totally until the cell potential was constant (to 0.1 mV) over a 24 hour period. From this new potential and the duration and size of the current dE/dQ and dE/dx could be calculated for the pulse, where dE is the change in open circuit potential of the cell upon passage of a charge dQ during the pulse and dx is the change in intercalation level of silver in the niobium disulphide.

8 FREQUENCY RESPONSE ANALYSIS AND CONDUCTIVITY MEASUREMENT

All measurements of conductivity were carried out using the technique of frequency response analysis (or AC impedance spectroscopy). Such FRA measurements provide access to a number of important characteristics of solid electrolytes or of solid-state battery systems. Some of these applications will be discussed in more detail in later chapters. In the present instance the technique has simply been used to determine the bulk resistance of a solid electrolyte which is accessible from the high frequency data range. [16,17] A diagrammatic representation of the experimental layout employed is given in Figure 12. AC impedance spectroscopy works by the measurement of the response of a sample to the application of a range of sinusoidal AC frequencies. [18] The sample is usually in series with a standard or measuring resistor whose resistance is of the same order of magnitude as the impedance of the sample. This yields more accurate results. [19] The voltage ratio across the standard resistance and the cell is measured as a function of the applied frequency and the parameters a and b corresponding to the real and imaginary components of this ratio are calculated for each frequency.

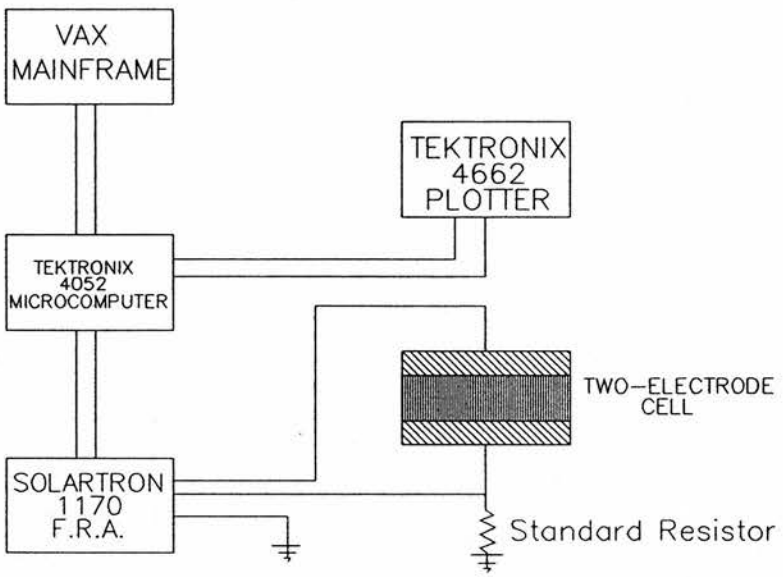

Figure 12.
Block diagram of apparatus used for frequency response analysis.

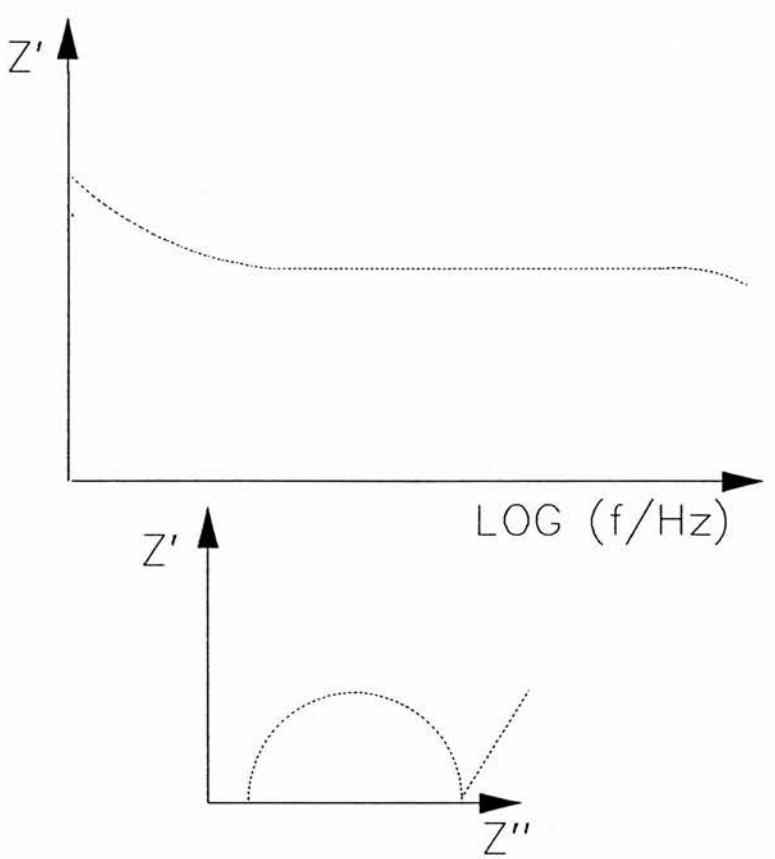

Figure 13. Sample output of impedance spectra.

Here the Solartron 1170 frequency response analyser (FRA) is controlled by program from the Tektronix 4052 computer. The program allows the experimental conditions to be defined in advance and, in particular, the amplitude of the applied AC signal and the frequency range could be limited. The FRA carries out the programmed instructions on a 5 mm or 13 mm two-electrode cell of the configuration outlined above. After a measurement the FRA sends the values of frequency and of a and b to the Tektronix where they are processed to yield values of impedance, which are displayed on the screen.

After completion of a full frequency scan impedance spectra are produced using another program and output to the attached plotter. Sample data is illustrated in Figure 13. The resistance of the electrolyte is obtained from the frequency independent region as shown. Further data analysis for the pseudo-ionic conductance measurements was carried out on the VAX as described in Appendix 1.

9 REFERENCES

1 Morosin B. "Structure Refinement On Nbs_2", Acta Cryst. B30 (1974) 551

2 Jellinek F., Brauer G., Muller H. "Molybdenum And Niobium Sulphides", Nature 185 (1960) 376

3 Kadijk K., Jellinek F. "The System Niobium-Sulphur", Journal Of The Less-Common Metals 19 (1969) 421

4 Nairn I.A. "The Study Of Mixed Phase Electrodes In Solid State Cells", Ph.D. Thesis, University Of St. Andrews (1984)

5 Takahashi T., Kuwabara K., Yamamoto O. "The Electrical Conductivity And The Crystal Structure Of Silver Iodide", J. Electrochem. Soc. 116 (1969) 357

6 Mckechnie J.S., Turner L.D.S, Vincent C.A., Bonino F., Lazzari M., Rivolta B. "Silver Mono-, Di- And Tetra Tungstates", J. Inorg. Nucl. Chem. 41 (1979) 177

7 Takahashi T., Ikeda S., Yamamoto O. "Solid State Ionics: A New High Conductivity Solid Electrolyte $Ag_6I_4WO_4$ And Use Of This Compound In A Solid-Electrolyte Cell", J. Electrochem. Soc. 120 (1973) 647

8 Lazzari M., Scrosati B., Vincent C.A. "An Investigation Of Some Modified Solid Electrolytes Containing AgI", Electrochimica Acta 22 (1977) 51

9 Magistris A., Chiodelli G., Schiraldi A. "Formation Of High Conductivity Glasses In The System AgI-Ag_2O-B_2O_3", Electrochim. Acta 24 (1979) 203

10 Martin S.W., Schiraldi A. "Glass Formation And High Conductivity In The Ternary System AgI + Ag_3AsO_4 + $AgPO_3$: Host To Glassy AgI?", J. Phys. Chem. 89 (1985) 2070

11 Dube D.C., Saraswat A.K. "Study Of Particle Size Effect Of Conductivity And Permittivity In Fast Ion Compacts", Materials For Solid State Batteries 319, Eds. Chowdari B.V.R., Radhakrishna S., Publ. World Scientific Publ. Co. Singapore (1986)

12 Razzini G. "Preparation Techniques Of A New Three-Electrode Electrochemical Solid State Cell", J. Phys. E. Sci. Instrum. 14 (1981) 289

13 Bouwmeester H.J.M. "The Thermodynamic And Kinetic Properties Of Silver Intercalated Niobium Disulfide", Solid State Ionics 16 (1985) 163

14 Smith M.J., Vincent C.A. "Relative Diffusion Coefficients Of Silver In Nbs_2 And Tis_2 Host Materials", Electrochim. Acta 30 (1985) 931

15 Patriarca M., Voso M.A., Scrosati B., Bonino F., Lazzari M. "Behaviour Of Transition-Metal Disulphides As Intercalation Electrodes In Solid-State Cells", Solid State Ionics 6 (1982) 15

16 Archer W.I., Armstrong R.D. "The Application Of A.C. Impedance Methods To Solid Electrolytes", R.S.C. Specialist Periodical Reports. Electrochemistry Vol. 7 p1

17 Schouler E.J.L. "Impedance Spectroscopy In Solid State Electrochemistry", Solid State Protonic Conductors III For Fuel Cells And Sensors p17, Eds. Goodenough J.B., Jensen J., Potler A. Publ. Odense University Press (1985)

18 "Basics Of AC Impedance Measurements", Application Note AC 1 (EG&G Princeton Applied Research)

19 Mougenel J.C., Kessler H. "Optimisation Of A Computerised Complex Impedance Measurement System", Solid State Protonic Conductors III For Fuel Cells And Sensors. p69, Eds. Goodenough J.B., Jensen J., Potler A., Publ. Odense University Press (1985)

1 INTRODUCTION

As described in more detail in Chapter 1, the interface between the solid electrolyte and the electrode material is an important feature in determining the performance characteristics of all-solid-state cells. The incorporation of a mixed phase electrode to increase the contact area between the two solid components and hence enhance the power output was also discussed.

A basic statistical computer model of such a composite electrode was developed by Nairn [1, 2] in order to investigate the effect of composition and configuration changes on the contact area between the two phases forming the MPE. This basic simulation was modified by Harris [3] to improve its operation and to allow consideration of percolation situations which, as described in Appendix 2, bear certain similarities to mixed phase electrodes.

In this investigation the results obtainable from the existing computer model have been extended to demonstrate further the applicability of some concepts of percolation theory. [4] Subsequently the model itself has been reformulated to simulate higher lattice coordinations of the particles composing the mixed phase electrode, and also to permit consideration of particle size variation and different distributions of particle sizes. Other factors such as the effect of a concentration gradient across the composite were also investigated. The actual programs which construct and analyse the mixed phase electrode and percolation simulations, and the alterations made to them to produce all the different variations are discussed in Chapter 4. This chapter outlines the derivation of the computer model and describes the important results produced from the original formulation and its subsequent variants.

2 THE MIXED PHASE ELECTRODE COMPUTER MODEL

The simplest representation of a mixed phase electrode considers it to consist of two different types of particle of identical size and shape, distributed randomly in a simple cubic lattice configuration. An average contact area is assumed between adjacent particles in the lattice. Figure 1 depicts a two dimensional section through this idealised MPE, assuming that the particles are spherical, and illustrates some of the important parameters involved.

This is modelled on the computer as a three dimensional cuboidal array of the two types of particle, situated between two bases, one considered as the pure ionic conductor (component 1) and

the other as the pure electronic conductor (component 2). This means that a particle at position (x,y,z) in the array has six nearest neighbours [(x+1,y,z), (x-1,y,z), (x,y+1,z), (x,y-1,z), (x,y,z+1), (x,y,z-1)] in a simple cubic packing arrangement around it.

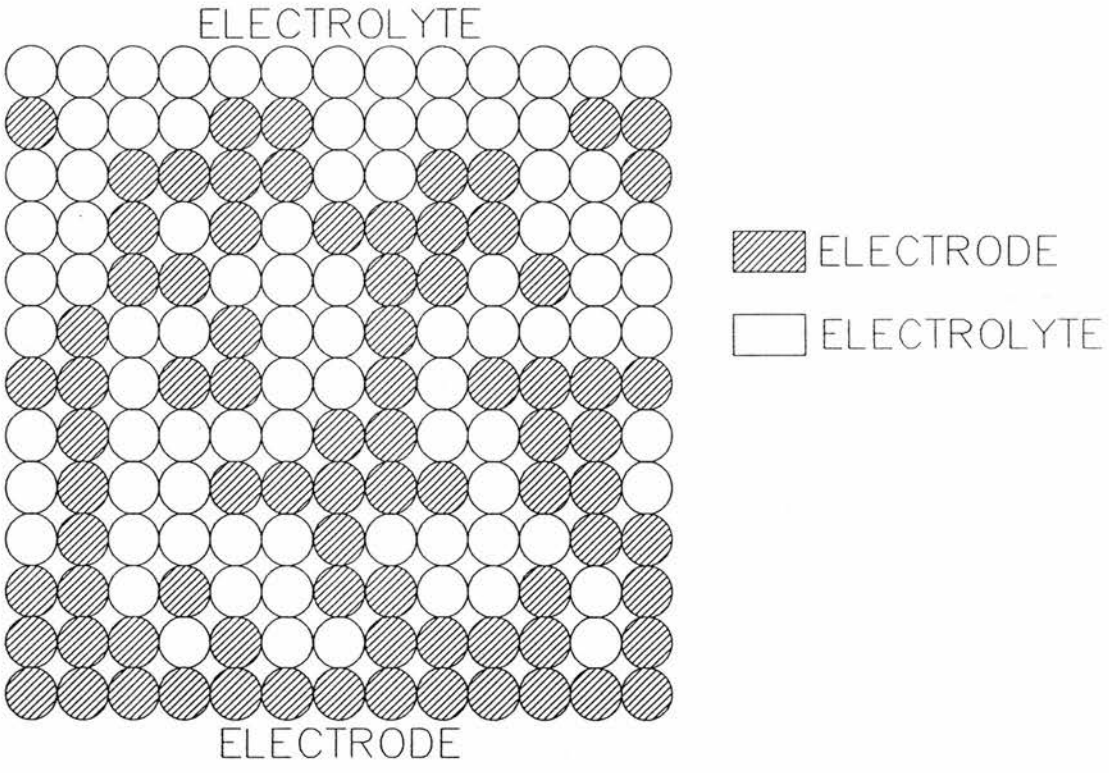

Figure 1.
Representation in two dimensions of an ideal mixed phase electrode.

The two particle types are assigned to the lattice sites (i.e. the array positions) by a random number generator, each particle being assumed to fill one site in the lattice. By examination of the environment of each particle, the array is processed to determine whether a particular particle lies on a chain of particles of its own type connected back to the respective pure component base. Such particles are said to be ***singly connected***. Particles which are not singly connected are not involved in the charge transfer process within the MPE and are thus ***isolated***. The effective contact area is then estimated by counting the number of ***links*** between the two components, where a link is defined as a contact between a singly connected particle of the ionic conductor and a singly connected particle of the electronic conductor.

In order to compare the effective contact areas of arrays of different dimensions the normalised link number (N_L) is defined as [the number of links counted minus the number of particles in the base of the array] / [the total number of particles in the array].

Thus N_L essentially represents the average number of links to a particle when a mixed phase electrode is introduced. When no composite is present N_L is undefined. However the only contact between the electrode and electrolyte phases is at the interface and therefore each particle can only be linked to the particle immediately adjacent to it across the boundary. The average number of links per particle is hence 1.

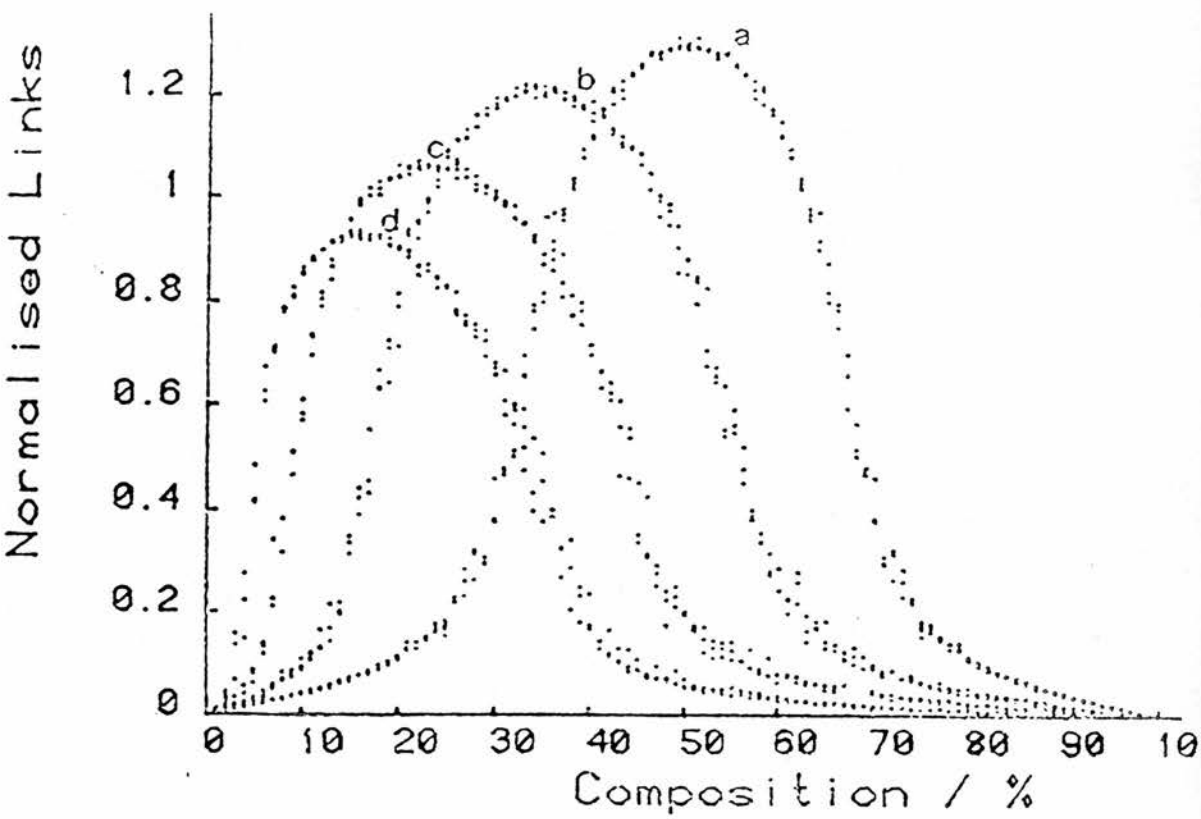

Figure 2.
Effect of particle size ratio on normalised link number versus composition curves (a) 1:1, (b) 2:1, (c) 4:1, (d) 8:1.

Using this model Nairn concluded that the normalised link number reached a maximum value of approximately 1.34, representing a 34 % increase in the average link number and thus in contact area, for a 50:50 composition ratio of equally sized particles of the two components. This value of

N_L is essentially independent of the size and shape of the array, except for very small arrays, and, in particular, does not decrease as the array thickness increases. (There is actually a very gradual increase in the maximum value as will be described below.)

Variation of the composition of the two constituents resulted in a bell-shaped curve symmetrical about the maximum value at the 50:50 component ratio (Figure 2a). Significantly, N_L is greater than one over a large composition range from 35 % to 65 %. (The percentages quoted here and below refer to the component which is at 0 % composition at the left hand side of the composition curves given. Since in the earlier models the particles are symmetrical in all respects, they are interchangeable and so the described results are equally applicable to the other component.) If the particle size of one component relative to the other is increased Nairn found that N_L decreases slightly and the curve becomes skewed towards lower compositions of the larger particles, this trend becoming more pronounced as the size disparity is increased (Figure 2 b - 2 d). This effect was examined further, as outlined in Section 7, and is actually not as extreme as illustrated here. The number of isolated particles was found to be negligible for arrays of moderate size and composition ratio.

3 THE PERCOLATION COMPUTER MODEL

The electronic conduction of mixtures of conducting and insulating particles has been successfully described using site percolation theory as outlined in Appendix 2. In terms of the computer model such a system can be simulated using an array as before and considering only chains of particles extending between ***both*** bases as contributing to the normalised link number (Figure 3). Particles on such pathways are 'doubly connected'. (Note: all doubly connected particles are, by definition, also singly connected.)

Harris reformulated the basic model to enable it to simulate such percolation conditions. [3] This was achieved by processing the array to distinguish singly connected particles as before. Then each singly connected particle is examined to determine whether the chain of which it is part is also connected to the opposite base of the array, thus making it doubly connected. Links between doubly connected particles only were then counted. Intermediate situations considering links from singly connected particles of one type to doubly connected particles of the opposite type were also examined.

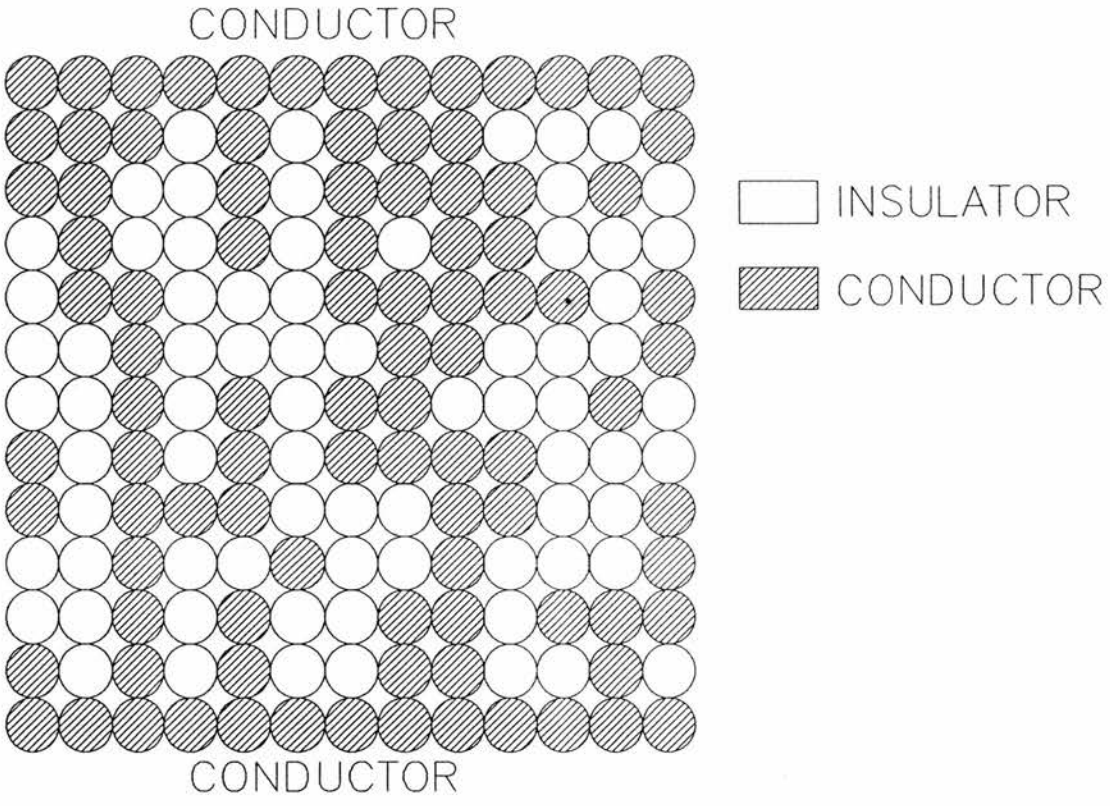

Figure 3.
Representation in two dimensions of an ideal percolation situation showing doubly connected particles.

The programs were also modified to improve the randomness of the array filling and to reduce edge effects attributable to the use of a finite lattice. The latter was accomplished by considering each face perpendicular to the array bases to be connected into the opposite face of the array, as is frequently done in Monte Carlo simulations [5, 6] thus giving each facial site the same coordination as the interior sites and creating an essentially infinite lattice.

4 COMPARISON BETWEEN MIXED PHASE ELECTRODE AND PERCOLATION MODELS

Three fundamental situations were considered as described above :-

a) The mixed phase electrode model i.e. links were counted between singly connected particles of the two types.

b) The percolation situation where the normalised link number was calculated from consideration of links between doubly connected particles of the two types.

c) The intermediate situations counting links from singly connected particles of one type to doubly connected particles of the other.

Note however that in a real percolation situation conduction occurs between two bases of the same type along chains of particles of that type, whereas in a mixed phase electrode conduction occurs as a result of conduction from one base via chains of one type of particle, then mass and charge transfer at the interface between the two different materials and finally conduction to the second base via chains of the other type. Despite this fundamental difference in conduction mechanism a great deal of similarity is observed between the two computer simulations.

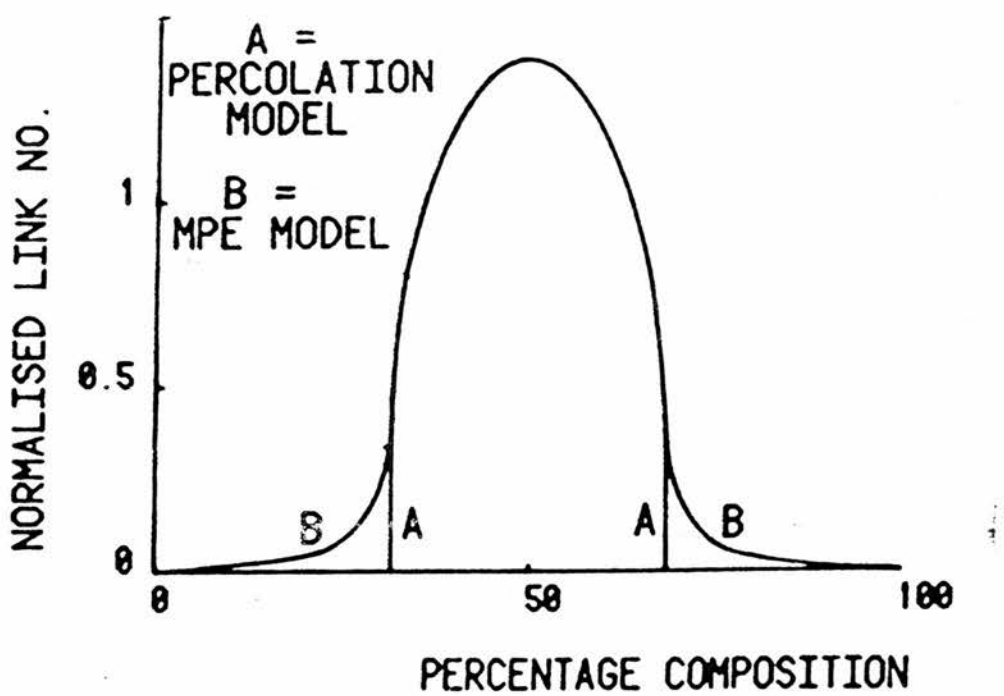

Figure 4.
Normalised link number versus lattice composition curves for a) Mixed phase electrode and b) Percolation models (35 x 35 x 35 lattice).

The variation of N_L with the percentage composition of the lattice was examined for both the MPE and percolation models. As illustrated in Figure 4 N_L tends towards a maximum of 1.36 for both simulations for the lattice size considered. The slightly higher maximum value here, compared with that observed by Nairn, can be attributed to the elimination of edge effects. The maximum occurs at a 50:50 composition ratio, with the plots being symmetrical about this ratio. (Note however that

under true percolation conditions no such symmetry would exist for the conductivity, which increases monotonically as the percentage of conducting material is increased.) There are virtually no differences between the models when the percentage of the minor component is between 30 % and 50 %, insignificant variations being attributable to a small fraction of singly connected particles which are not doubly connected which contribute to N_L only in the MPE model. These result in a reduction of only 1.5 % in the value of N_L for the percolation model compared with the MPE model.

Another interesting feature to emerge in this comparison is that the computer time necessary to process the array (i.e. the number of iterations through the lattice required to distinguish singly and doubly connected particles) maximises at or around the percolation threshold. [3] This reflects the degree of tortuosity of the particle chains present near this composition and is similarly found in other percolation simulations. [6] Below 30 % compositions, corresponding to the percolation threshold for the simple cubic lattice packing under examination, major variations do exist between the models. The percolation model exhibits a zero N_L below this threshold indicating that, as expected, there are no doubly connected chains of particles of the minor component. However singly connected chains still contribute to N_L in the MPE model and thus N_L drops off less rapidly as the composition falls.

This is confirmed on examination of the fractions of singly and doubly connected particles as a function of the lattice composition. A significant fraction of singly connected particles exists at compositions below 30 % for the MPE model while there are no doubly connected ones. Above 30 % the fraction of singly connected particles is approximately equal to that of the doubly connected particles confirming that the majority of singly connected particles are also doubly connected. These differences in behaviour between the MPE and percolation models are evident whenever any of the properties reported below are changed. There is always a sharp well-defined threshold for the percolation model, while the MPE model exhibits a more gradual change in properties owing to the existence of singly connected chains.

The intermediate models show both of these forms of behaviour: the slow reduction in N_L associated with the MPE model being observed at the end of the composition range corresponding to the region where singly connected chains of particles contribute to the N_L, and the sharp percolation cutoff at the other end where links to doubly connected particles are necessary.

The effect of different lattice thicknesses with a constant base area, on the N_L versus percentage composition curves was considered next, predominantly for the MPE model. As shown pictorially (Figure 5) for mixtures containing more than 35 % of the minor component, neither the efficiency maximum (of 1.36) nor the N_L values are significantly affected by the change from very thin to very thick lattices. As the lattice thickness is increased there is the expected slight increase in N_L as described above. However below this composition marked variation of N_L with lattice thickness is observed for the MPE model. The thicker the lattice becomes the more N_L is reduced, approaching, in the limit, the percolation result of zero N_L below the percolation threshold. No similar trend is observed for the percolation model, there always being a sharp cutoff at the percolation threshold, slight differences around this value being associated with the random filling of the array. The maximum value of N_L still increases slightly with thickness.

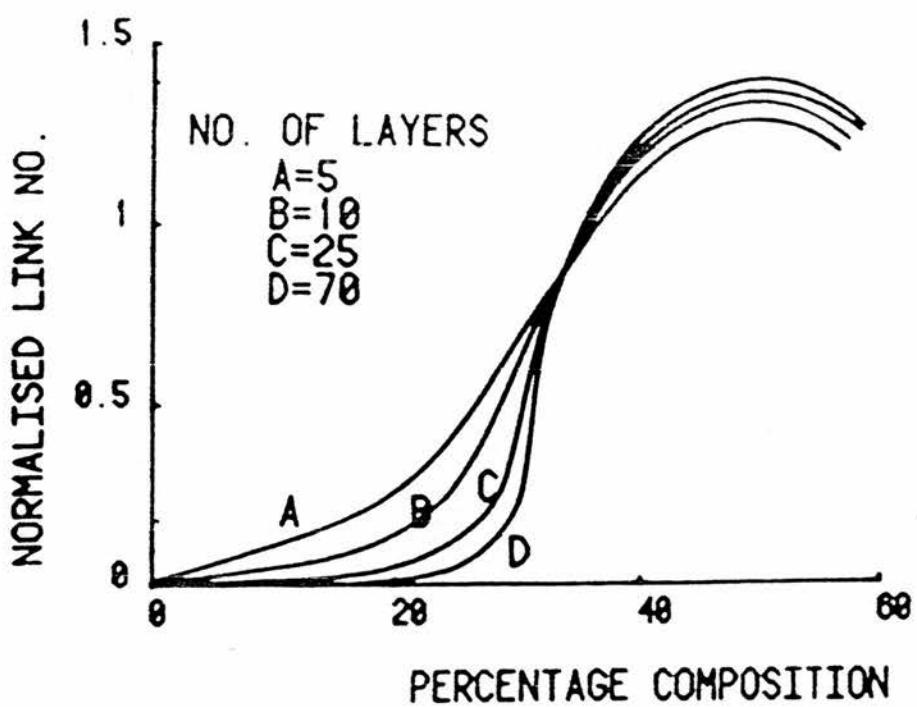

Figure 5.
Variation of normalised link number/lattice composition curves for MPE model as a function of lattice thickness. a) 5, b) 10, c) 25, d) 70 layers (25 x 25 base size)

For the MPE model Figure 6 illustrates the effect on N_L of changing the lattice thickness, while maintaining a constant base area, at various fixed lattice compositions around the percolation threshold. As expected from the preceding experiment two distinct behaviours are observed either side of the percolation threshold. At low lattice compositions (< 30 % of the minor component) the N_L decreases rapidly with increasing lattice thickness, rapidly approaching zero in the limit as the thickness approaches infinity. At larger compositions (> 35 %) there is initially a very rapid increase of N_L with the thickness and then the rate of increase reduces and the trend becomes linear. For this coordination the gradient of the linear portion is $2x10^{-4}$ $layer^{-1}$. Intermediate between these extremes a gradual transition from one behaviour to the other is observed. This is indicated by the more diffuse nature of the graphs and is caused by a greater susceptibility to the random filling of the array at compositions close to the percolation threshold. As expected the drop off below the percolation threshold is much more marked for the percolation model.

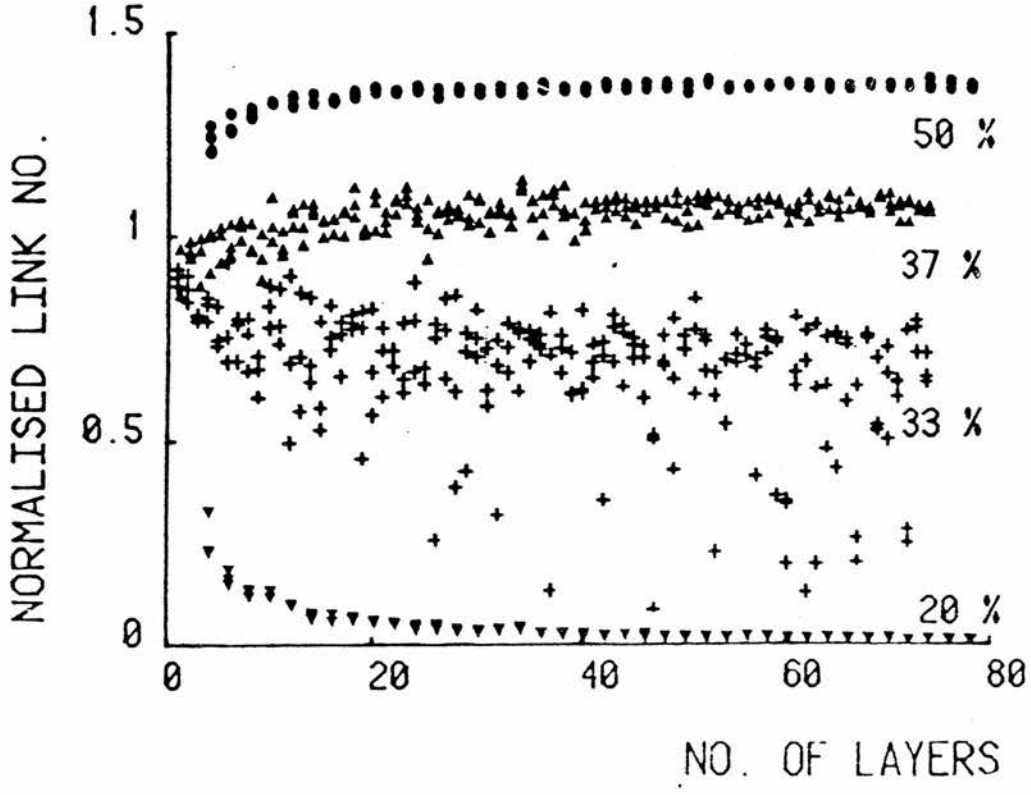

Figure 6.
Variation of normalised link number/lattice thickness curves for MPE model at defined compositions. a) 50 %, b) 37 %, c) 33 % d) 20 % (25 x 25 x 25 lattice)

An 'efficiency threshold' is defined where N_L is roughly unity. This corresponds to the actual transition point where the MPE becomes an effective method of increasing the interfacial contact area and here occurs at approximately 35 % of the minor component.

4.1 EXPLANATION OF RESULTS USING PERCOLATION THEORY

The above results can be explained using some concepts from percolation theory. Consider a lattice of a certain thickness. At lattice compositions below the percolation threshold for the system there will exist, by definition, no complete connecting pathways of the minor component between the two bases. Thus, in the MPE model, only singly connected particles close to their own base will contribute to the N_L calculated. The subsequent addition of further layers to the lattice remote from this base will result in no further contacts with these chains and thus N_L will decrease with thickness.

However, above the percolation threshold the lattice will contain complete connecting pathways of both components between the two bases. Consequently particles in any additional layers will contact with these doubly connected chains, extending them further and resulting in an increase of N_L with lattice thickness. At compositions close to the percolation threshold the intermediate behaviour is explained by the transition between these extremes.

The validity of this explanation was examined by consideration of the fraction of particles of one type linked to any number of the other type. (The fraction of particles linked to x particles was defined as the number of particles linked to x particles divided by the total number of particles in the lattice.) In the simple cubic lattice configuration any connected particle of a particular type can form links to 0,1,2,3,4 or 5 of the opposite component. A graph of the fraction of particles linked to three of the other type versus the lattice thickness is given in Figure 7 for various fixed lattice compositions. Similar graphs result for the other possible numbers of links.

Below the efficiency threshold the fraction of such particles decreases with lattice thickness for the reason given above. As the efficiency threshold is approached and passed the fraction of particles remains constant with increasing thickness confirming that in each additional layer particles are connecting with doubly connected chains in the previous layers to further increase N_L. This increase is an approximately constant value per layer. The fraction of particles concerned increases with the percentage composition since there is a higher proportion of particles in each subsequent layer which can form connections with the chains in the preceding layers.

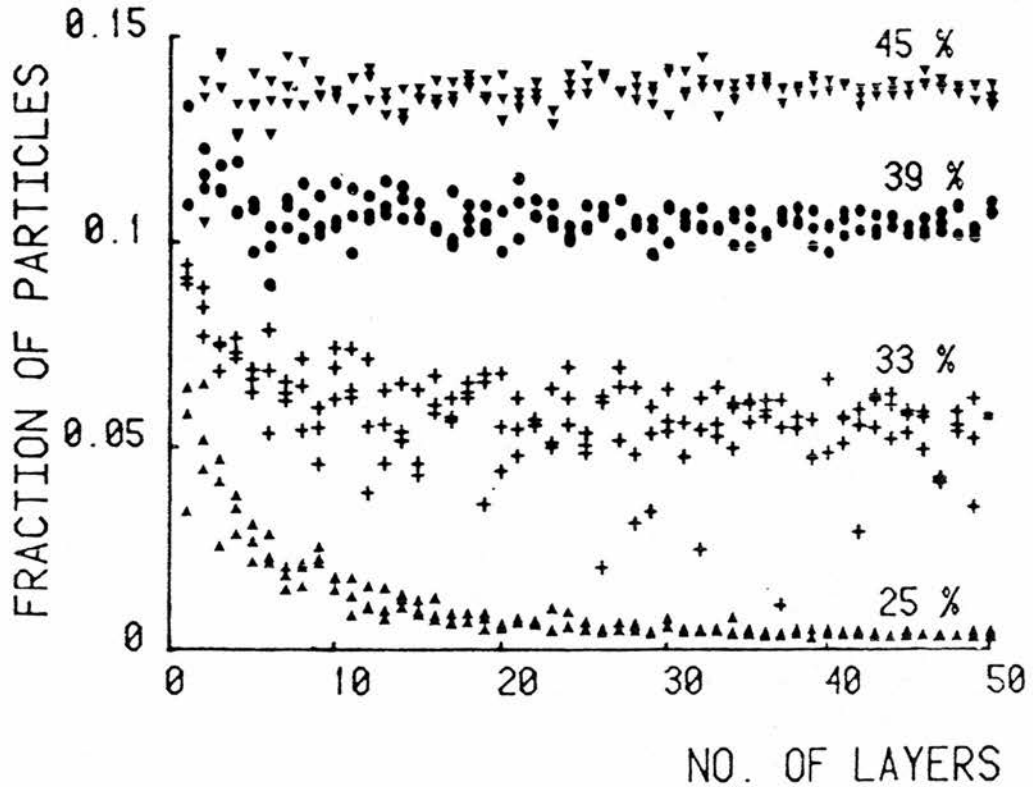

Figure 7.
Fraction of particles linked to three others versus the number of layers in the lattice. (MPE model, 25 x 25 base size, 50 %)

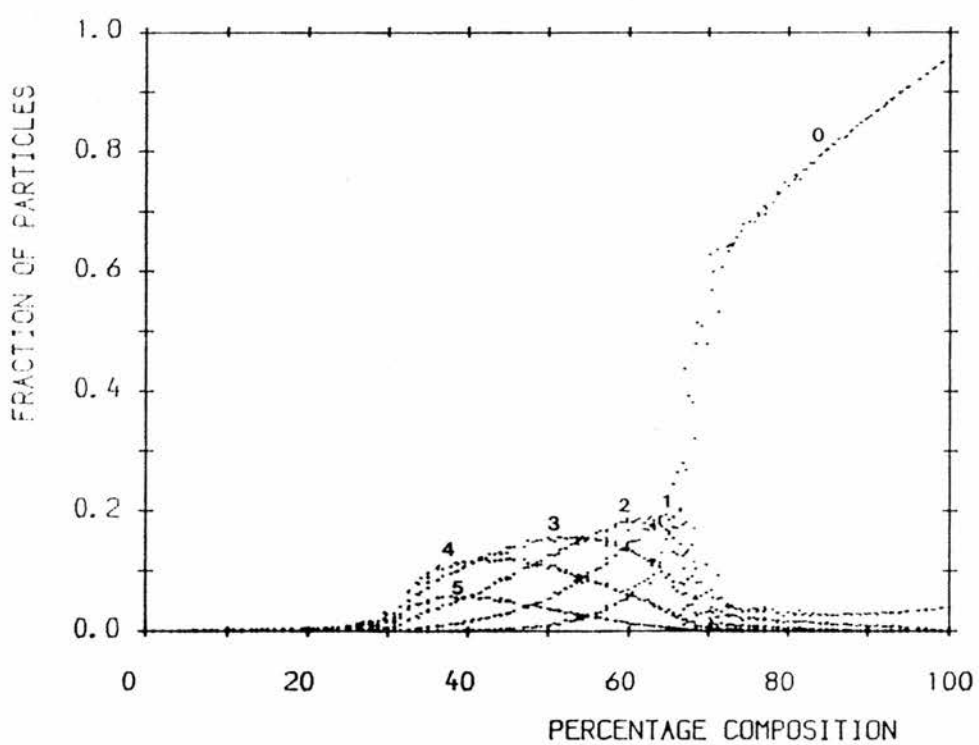

Figure 8.
Fraction of particles of component 1 linked to each of 0,1,2,3,4 and 5 of component 2 versus percentage composition. (MPE model, 25x25x25 lattice)

Interesting results are also obtained when the fraction of particles linked to each of the possible numbers of the other component is plotted versus the percentage composition. Figure 8 shows all six possible graphs for the MPE model where particles of component 1 are linked to 0,1,2,3,4 and 5 of component 2. The graph for component 2 linked to component 1 is simply the mirror image of this one, as expected from the symmetry. The curve featuring links to zero other particles predominates over the remaining curves at high percentage compositions. This is to be expected from purely statistical grounds, since at these compositions there are very few particles of component 2 available for linking. The graph initially rises very slowly from 0 % until the upper percolation threshold (at 70 %) is approached, where it rises abruptly, rapidly overshadowing the other curves, before linea-rising as the composition tends to 100 %.

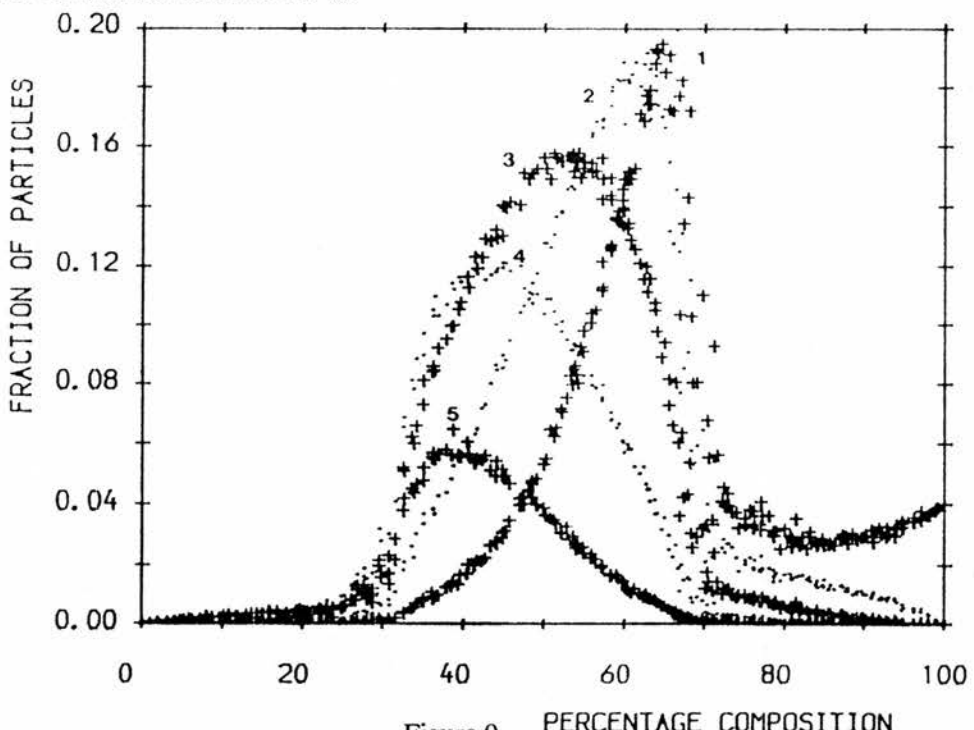

Figure 9. Fraction of particles of component 1 linked to each of 1,2,3,4 and 5 of component 2 versus percentage composition. (MPE model, 25x25x25 lattice)

In contrast all the other graphs exhibit distinct maxima, as illustrated more clearly in Figure 9. The percentage composition at which the maximum occurs is reduced with an increase in the number of links considered, as tabulated in Table 1. This is explainable from statistical factors. At low percentages of component 1 each particle is more likely to be surrounded by a larger number of the other type and so the fraction of particles linked to 4 or 5 others is predominant. As the percentage of component 1 is increased this changes until, at 50 % compositions, the most statistically likely

number of links predominates. For the simple cubic lattice this is three links, since any particle is equally likely to have a particle of component 1 or of component 2 in any of the six positions surrounding it.

Links from component 1	Position of Maximum	Fraction of particles at 50 % composition
0	100 %	0.01
1	65 %	0.06
2	60 %	0.12
3	50 %	0.16
4	45 %	0.11
5	40 %	0.04

Table 1.
Percentage at which maximum fraction occurs and the fraction of particles of component 1 linked to component 2 at 50% compositions.

The relative fractions of particles linked to each of the possible numbers of the other component at this 50 % composition are also listed in Table 1. Figure 10 shows that an approximately normal distribution of the relative fractions arises, as expected from probability considerations. Beyond 50 % compositions the situation is reversed and the particles with lower numbers of links become increasingly more significant. All the curves fall rapidly to zero at the upper percolation threshold. The only exception is the fraction of particles linked to one other which, because of effects at the base of the array, remains significant. This transition in properties at the percolation threshold is even more abrupt for the percolation model.

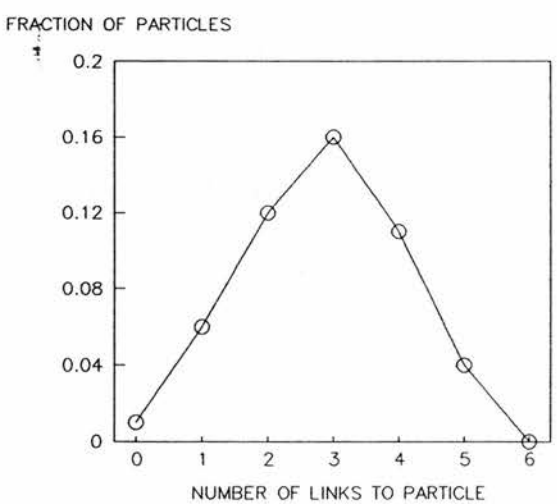

Figure 10.
Fraction of particles of component 1 versus the number of links to that particle at 50 % composition. (MPE model, 25x25x25 lattice)

5 HIGHER COORDINATION LATTICES

Within percolation models parameters such as the percolation threshold are dependent on the type and coordination of the lattice. [7] In a randomly packed mixed phase electrode coordinations greater than the 6 coordination of the simple cubic lattice are likely to be formed, even when sphericity of particles is assumed. [8] In particular if the particles of the two components are of different sizes then higher coordination systems akin to crystal structures are likely to result. The computer simulation was therefore remodelled to generate 8 and 12 coordination lattices, these being relatively straightforward to envisage using modifications to the three-dimensional array considered for the simple cubic situation.

5.1 12 COORDINATION LATTICE

The simple cubic lattice consists essentially of square planar layers, in which each particle is in contact with four other particle at each of its edges, stacked vertically above one another. (Figure 11a) If three such layers are considered (z-1, z and z+1 layers) and the uppermost and lowermost layers are displaced half a unit horizontally and half a unit vertically in the plane of the page then the configuration illustrated in Figure 11b results. The shaded particle in the z layer is now in contact with four others in the z+1 layer and four in the z-1 layer as well as the four in its own layer, thus giving it twelve coordination overall.

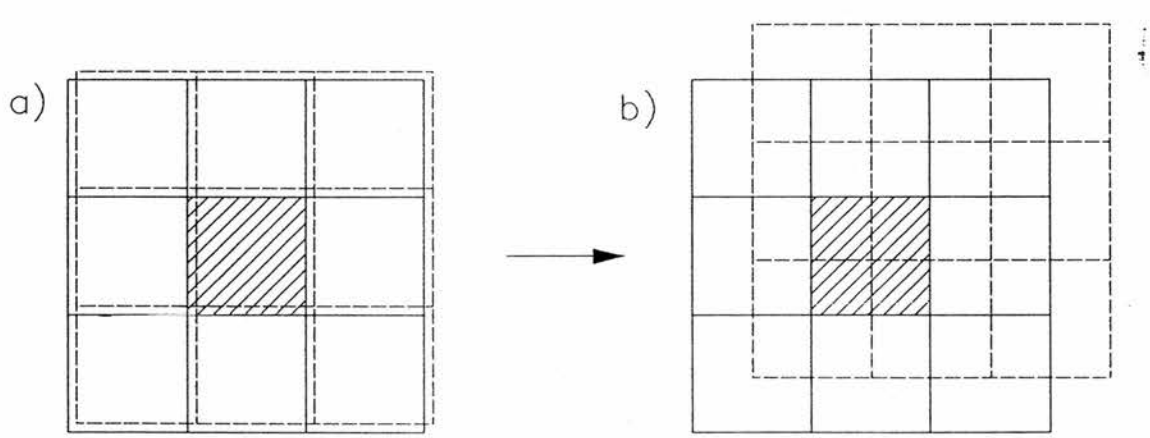

Figure 11.
Production of 12 coordination lattice from 6 coordination lattice.

As depicted however, the contact area between the central particles and the four surrounding particles in its own layer is different than between it and those in the layers above and below. In a true 12 coordination close packed structure this is not the case, but it is irrelevant here since, in terms of the simulation, an average contact area (represented by the link) is assumed between particles.

Thus a general particle (x,y,z) in the lattice is surrounded by the twelve particles in positions:-

(x+1, y, z)	(x+½, y+½, z+1)	(x+½, y+½, z-1)
(x-1, y, z)	(x+½, y-½, z+1)	(x+½, y-½, z-1)
(x, y+1, z)	(x-½, y+½, z+1)	(x-½, y+½, z-1)
(x, y-1, z)	(x-½, y-½, z+1)	(x-½, y-½, z-1)

These half units cannot easily be modelled in the existing array. However, displacing the layers above and below back to their original positions requires that links be counted from (x,y,z) to the particles in positions:-

(x+1, y, z)	(x, y, z+1)	(x, y, z-1)
(x-1, y, z)	(x, y-1, z+1)	(x, y-1, z-1)
(x, y+1, z)	(x-1, y, z+1)	(x-1, y, z-1)
(x, y-1, z)	(x-1, y-1, z+1)	(x-1, y-1, z-1)

Thus although the particles are no longer 12 coordinate physically, they ***are*** in terms of the lattice processing and counting.

5.2 8 COORDINATION LATTICE

Similarly an 8 coordinate lattice can be modelled. Such a body centred cubic configuration consists essentially of two simple cubic lattices intermeshed with each other, alternate layers being displaced half a unit horizontally, half a unit vertically and half a unit perpendicularly to the plane of the previous layer. A particle (x,y,z) is therefore linked to others at positions:-

(x+½, y+½, z+½)	(x-½, y+½, z+½)
(x+½, y-½, z+½)	(x+½, y+½, z-½)
(x-½, y+½, z-½)	(x-½, y-½, z+½)
(x+½, y-½, z-½)	(x-½, y-½, z-½)

The simplest way to simulate this in the normal simple cubic array is to multiply all the displacements by two, yielding the coordinating particles as being in positions:-

(x+1, y+1, z+1)	(x+1, y-1, z+1)
(x-1, y+1, z+1)	(x-1, y-1, z+1)
(x+1, y+1, z-1)	(x+1, y-1, z-1)
(x-1, y+1, z-1)	(x-1, y-1, z-1)

Again these are not physically touching the central unit but they do provide a true 8 coordinate lattice in terms of the processing procedure.

5.3 RESULTS FROM HIGHER COORDINATION MODELS

In general the same type and shape of graphs result from the higher coordination systems as obtained for the simple cubic system, and therefore the same conclusions may be drawn concerning the effect of composition and thickness variation, and the similarities of the MPE and percolation models. Major differences are evident however in the magnitude of N_L and the breadth of the N_L versus composition curves (Figure 12).

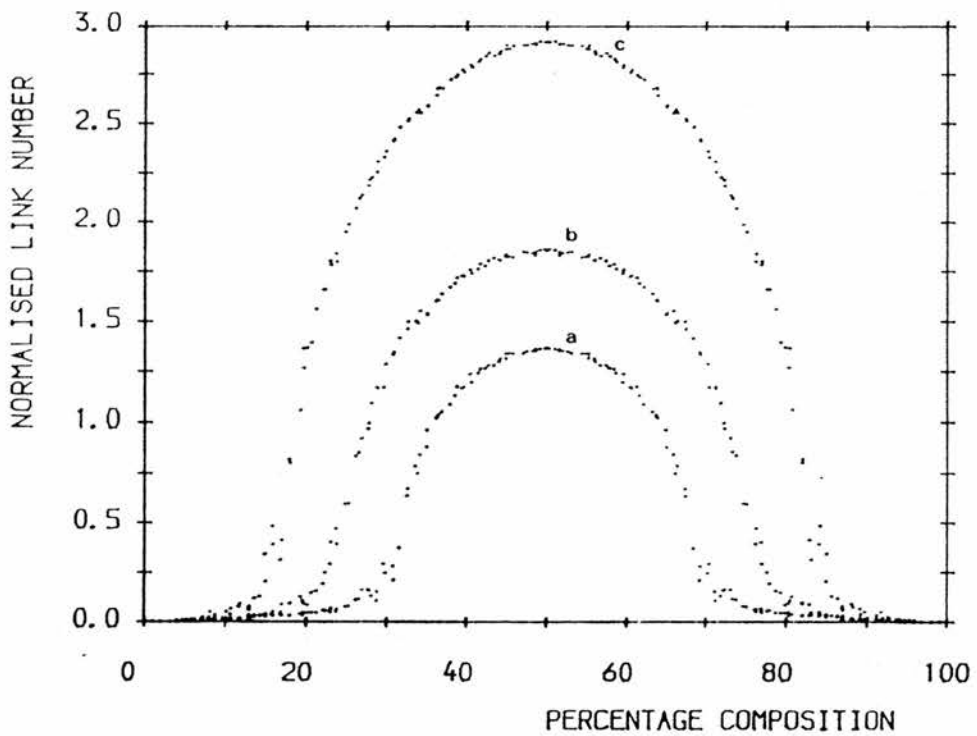

Figure 12.
Effect of coordination on the normalised link number/ composition curves for a) 6, b) 8, c) 12 coordination lattices. (MPE model, 30 x 30 x 30 lattice)

For the lattice thickness selected increasing the coordination increases the value of N_L to approximately 1.9 for the 8 coordinate system and to 3.0 for the 12 coordinate system, suggesting area enhancements of 90 % and 200 % respectively (compared to the 36 % for the 6 coordinate situation). The composition range over which the MPE provides such an area enhancement (i.e. $N_L > 1$) also increases with the coordination (approximately 35-65 % for 6 coordination, 30-70 % for 8 coordination and 20-80 % for 12 coordination) i.e. the efficiency threshold is reduced as the coordination is increased. The tendency of the MPE model to approach the percolation model in

the limit of very thick lattices is still evident with both 8 and 12 coordination systems. The gradient of the increase in N_L with thickness is now approximately $1x10^{-3}$ layer^{-1} for both these models. This value is four times as great as that for the 6 coordination model and probably reflects the fact that, for both the higher coordinations, a particle in an additional layer can be linked to 4 others in the layer below.

The percolation threshold for the 8 and 12 coordination systems used in the simulation is again in good agreement with the expected values of approximately 20 % and 25 % [7] for these face centred and body centred cubic configurations. Below the percolation threshold differences between the MPE and percolation models are still well defined with these coordinations, and the threshold is in evidence in the same situations as discovered for the simple cubic lattice.

6 CONCENTRATION GRADIENT ACROSS THE LATTICE

As determined above the lattice composition is of fundamental importance in determining the normalised link number and hence the contact area in the mixed phase electrode representation. It was now decided to investigate the effect of having a steady gradation of composition across the thickness of the lattice used in the simulation.

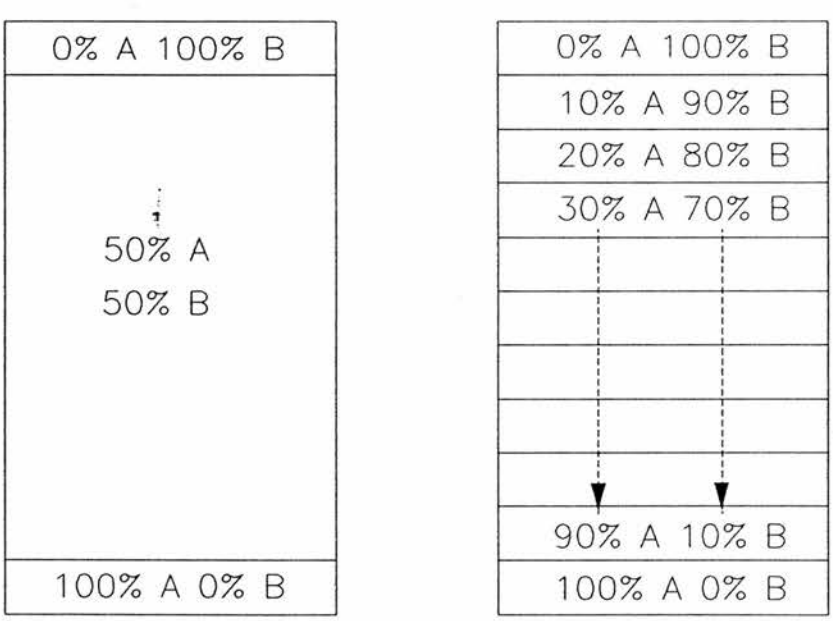

Figure 13.
Representation of a concentration gradient across the thickness of a lattice.

This was achieved by considering the lattice to be divided into a series of sections each consisting of an equal number of layers. The composition of each section was constant, but was different from the other sections in such a way that there was a gradual change from 0 % of one component at the bottom of the lattice to 100 % at the top. This is illustrated schematically in Figure 13 which, for comparison, also shows a cross-section of a normal lattice with the same overall composition. Only the simple cubic lattice was examined because the processing method which simulates the higher coordination lattices complicates this visualisation of distinct sections.

A number of parameters were therefore available for alteration, namely the number of sections across the lattice and the composition and thickness of each section. The reported results consider the effect of changing all of these variables, the only proviso being that all the sections were a uniform thickness in each case. All the experiments were carried out on cubic lattices of approximately the same size, there being some variation to allow the subdivision of the lattice into equally thick sections. Each experiment was repeated a number of times to yield an average normalised link number.

6.1 RESULTS AND DISCUSSION

Firstly lattices were considered which had a percentage variation of 0 - 100 % across their thickness. Various levels of subdivision were utilised and the results are summarised in Table 2 for both the mixed phase electrode and percolation models. For reference the results for a single section at the same average value of 50 % is shown. The figures in parentheses in the second column represent the minimum and maximum percentage compositions used in each experiment, there being a steady increment in the composition from section to section between these limits.

Lattice Size	Number of Sections	Thickness of section	Average Composition	Average N_L MPE	Percolation
27 x 27 x 27	1 (50)	27	50.17	1.362	1.350
27 x 27 x 27	3 (25,75)	9	50.02	0.554	0.055
28 x 28 x 28	4 (20,80)	7	49.89	0.622	0.000
27 x 27 x 27	9 (10,90)	3	50.01	0.532	0.000
18 x 18 x 18	9 (10,90)	2	50.02	0.566	0.000
19 x 19 x 19	19 (5,95)	1	49.94	0.510	0.000

Table 2.
Variation of normalised link number for mixed phase electrode and percolation models in a concentration gradient of 0-100 %.

The results demonstrate that in all cases the normalised link number is very much reduced for the mixed phase electrode model, when compared with the situation where there is one section of the same average 50 % composition. The normalised link number for the percolation model is

essentially zero in all cases. The only exception, where the N_L is non-zero for this model, occurred when one of the 10 results averaged was non-zero. The upper and lower composition limits in this case (25 % and 75 %) are very close to the percolation threshold so obviously there is a slight probability of doubly connected chains forming, yielding the finite N_L observed.

A striking comparison can again be made with percolation theory to explain these results, this time considering the case of percolation in a concentration gradient introduced by Sapoval [9, 10] to model diffusion fronts. Results from this model show that in a concentration gradient the two particle types are only connected along a frontier (as illustrated in Figure 14 for a two dimensional lattice), thus restricting the contact area to singly connected chains meeting at this interface. The length of the frontier can be related to the fractal dimension [11] thus giving an indication of contact points along the frontier. No doubly connected chains exist in the concentration gradient so the normalised link number is zero for the percolation model. No obvious trends are evident when the number of sections is adjusted though it seems that N_L is larger when the fraction of the lattice above the percolation threshold is greater.

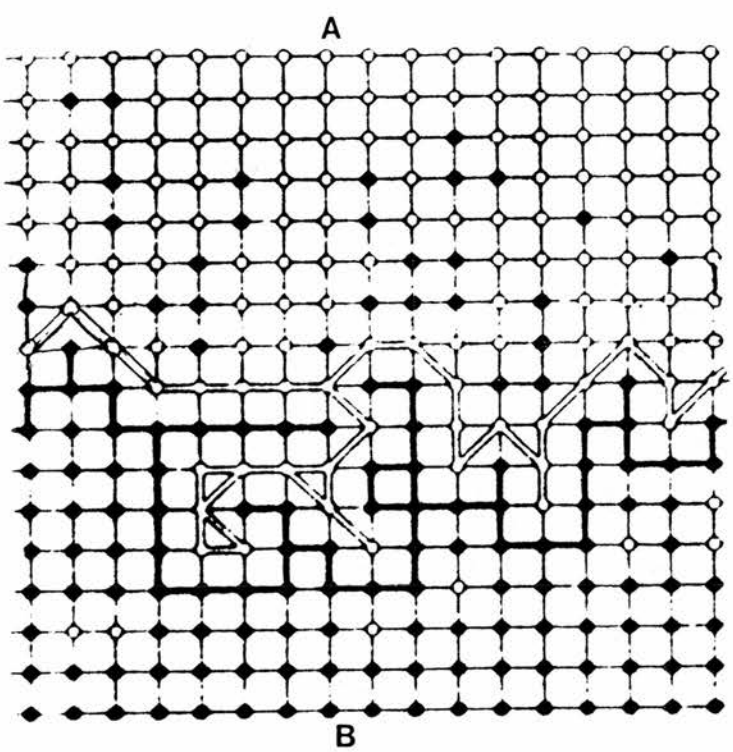

Figure 14.
Percolation in a concentration gradient (after Sapoval)
showing interaction fronts for both particles.

After this a series of lattices were considered where the compositions of each section were maintained within the percolation thresholds of the simple cubic lattice, i.e. all sections had a composition greater than 35 % and less than 65 %. A variety of lattices were examined and the results are summarised in Table 3.

Lattice Size	Number of Sections	Thickness of section	Average Composition	Average N_L MPE	Average N_L Percolation
30 x 30 x 30	3 (35,65)	10	50.00	1.029	1.028
32 x 32 x 32	4 (35,65)	8	49.88	1.100	1.100
35 x 35 x 35	7 (35,65)	5	50.00	1.155	1.154
33 x 33 x 33	11 (35,65)	3	49.97	1.173	1.172
32 x 32 x 32	16 (35,65)	2	50.00	1.182	1.181
31 x 31 x 31	31 (35,65)	1	50.11	1.197	1.196
30 x 30 x 30	3 (40,60)	10	49.89	1.241	1.239
30 x 30 x 30	5 (40,60)	6	49.91	1.266	1.264
30 x 30 x 30	6 (40,60)	5	49.98	1.270	1.268
33 x 33 x 33	11 (40,60)	3	50.04	1.284	1.283
30 x 30 x 30	3 (45,55)	10	49.95	1.328	1.325
30 x 30 x 30	6 (45,55)	5	50.09	1.335	1.331
33 x 33 x 33	11 (45,55)	3	50.00	1.338	1.333
33 x 33 x 33	1 (50)	33	50.01	1.365	1.358
30 x 30 x 30	2 (35,50)	15	42.30	1.126	1.122
33 x 33 x 33	3 (35,51)	11	42.87	1.173	1.170
32 x 32 x 32	4 (35,50)	8	42.62	1.183	1.179
30 x 30 x 30	5 (35,51)	6	43.00	1.195	1.192
30 x 30 x 30	6 (35,50)	5	42.41	1.196	1.191
27 x 27 x 27	9 (35,51)	3	43.22	1.212	1.207
32 x 32 x 32	16 (35,50)	2	42.53	1.215	1.214
25 x 25 x 25	1 (42)	25	42.45	1.274	1.250

Table 3.
Variation of normalised link number for mixed phase electrode and percolation models in a concentration gradient confined above the percolation threshold.

The first three sets of results all have an average percentage of 50 % but the three different sets illustrated represent three different ranges of composition, gradually becoming more centralised around the 50 % average composition. Again a single section is included for comparison. It can be concluded from these results that, in all cases, the average N_L for the sectioned lattice is less than that for the unsectioned one. The differences become less significant as the composition range is narrowed towards 50 %. The percolation model now has normalised link numbers only slightly less than the MPE values, as is expected. For all three composition ranges there is now an obvious enhancement of the N_L on increasing the number of sections in the lattice, but it never exceeds the optimum value attainable for a single section. The effect is more significant for the larger composition ranges, decreasing as the range is shortened.

The above results can all be rationalised by considering the relative contributions of each individual section to the overall N_L. Since the N_L increases monotonically towards 50 % composition from either direction then any layers not at 50 % compositions will contribute a smaller amount to the overall value. The further the composition is remote from 50 % the smaller the contribution will be. Thus as the composition range narrows each individual section has a higher N_L and the overall value is greater. Similarly as the number of layers is increased there are more sections with relatively higher individual normalised link numbers, and so once more the overall N_L is enhanced. The effect is reduced for a narrower composition range because there are not such great differences between individual sections.

Lastly a series of results were obtained where the average percentage was less than 50 % (Table 3). Experiments were carried out on lattices with subdivisions lying between 35 % and 50 %. An average value of 42.5 % is again given for reference for a single section. The results demonstrate that increasing the number of layers enhances the N_L but never to the extent that it improves on the average value and thus reaffirm the conclusions drawn.

7 PARTICLE SIZE VARIATION

All the above models consider that the particles of the mixed phase electrode are equally sized and that each occupies a single site of the lattice in the computer simulation. The effect of altering the relative sizes of the particles was now considered. Three separate situations were examined. Firstly the particles of each component were considered to be identical in size to each other, but to be a different size relative to those of the other component. Effectively therefore the components had different uniform distributions of particle sizes. Next each component was considered to have a geometric distribution of particle sizes. Latterly all the particles of both constituents were taken to be of equal size once more, but larger particle sizes were considered. Lastly the direction in which the larger particles were fitted into the lattice was altered to see whether the particle orientation changed anything.

In all the aforementioned cases a particle of size x occupies x consecutive lattice sites ***during the filling procedure***. The method of filling will break up some particles at the edges of the lattice, but this will generally be negligible, particularly for larger lattices and smaller particles.

7.1 DIFFERENT UNIFORM DISTRIBUTIONS OF PARTICLE SIZES

Experiments were carried out on both the 6 and 12 coordination lattices though in the latter the processing technique did not really consider links between different particles. However the results are interesting and Figures 15 and 16 illustrate the trend observed for the lower coordination lattice when the particle size ratio is successively doubled from 1:1 to 1:2 and so on up to 1:16. The percentage composition quoted on these graphs and in all succeeding situations with some form of particle size variation refers to the percentage of the smaller particles. The variation illustrated here corresponds to that mentioned in Section 2 where, as Nairn demonstrated [1], a consistent reduction in normalised link number is observed as the size disparity increases. The maximum N_L in each case here corresponds to that found by Nairn. The curves become slightly asymmetric around the 50 % composition value as the relative sizes increase, but the degree of skewing commented upon by Nairn (Figure 2) is not present here. The asymmetry that does occur seems to involve a shift in the percolation thresholds and will be discussed further below.

On consideration of Nairn's results it is obvious that he plotted N_L versus a composition corresponding to the percentage of one type of particle relative to the total number of particles in the lattice. Here the composition represents the volume percentage of one type of particle in the lattice. In a true MPE the latter is a more realistic parameter to consider since in general the properties depend on the volume fraction of each component and not on the number of particles of each type. [12, 13, 14] Indeed in the experimental studies described later it is the volume fraction of materials which is considered when constructing cells. Table 4 lists the maximum normalised link number as a function of the size difference used for both 6 and 12 coordination models. When the maximum N_L is plotted versus the logarithm (to the base 2 here) of the particle size Figure 17 results. The reduction in N_L is observed to be linear for both coordinations, the magnitude of the reduction being larger for the higher coordination system. This bears obvious similarities to the experimentally verified decrease in conductivity with increasing particle size discussed in Chapter 2 and reaffirms the suggestion that the contact area is the primary feature involved in the enhancement.

The decrease in N_L can be accounted for by a decrease in the randomness of the array. Some ordering is imposed in the filling procedure which changes the probabilities of a particular unit in the array being linked to an adjacent unit, since if the unit forms part of a large particle the units on either side of it are more likely to be of the same type.

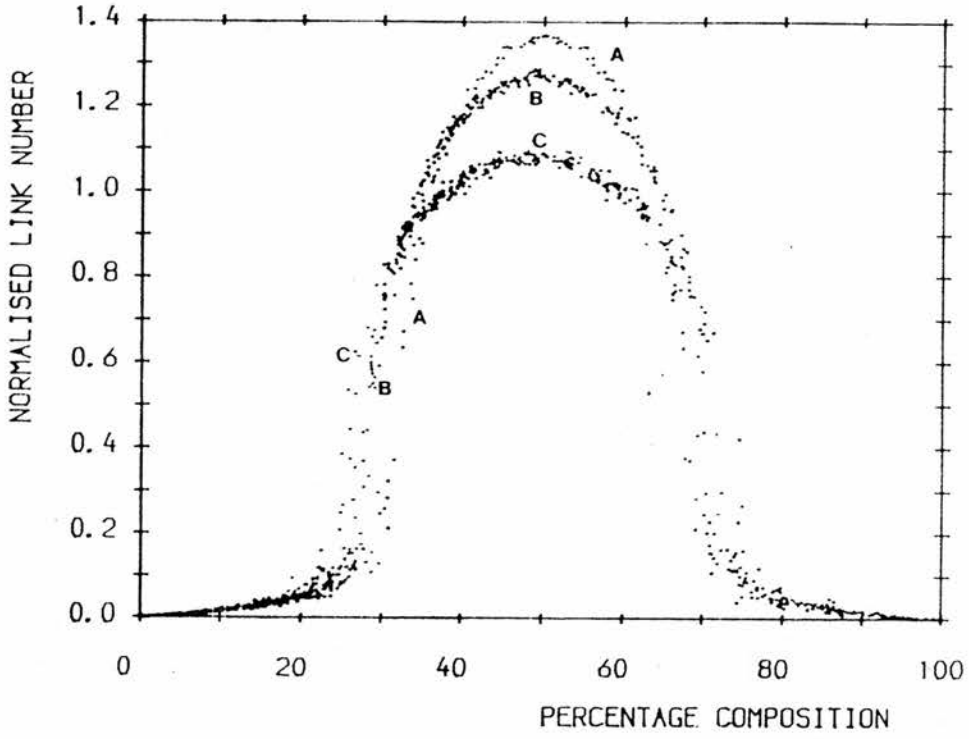

Figure 15.
Effect of particle size ratio on normalised link number/ composition curves (a) 1:1, (b) 2:1, (c) 8:1 (MPE model, 25 x 25 x 25 lattice)

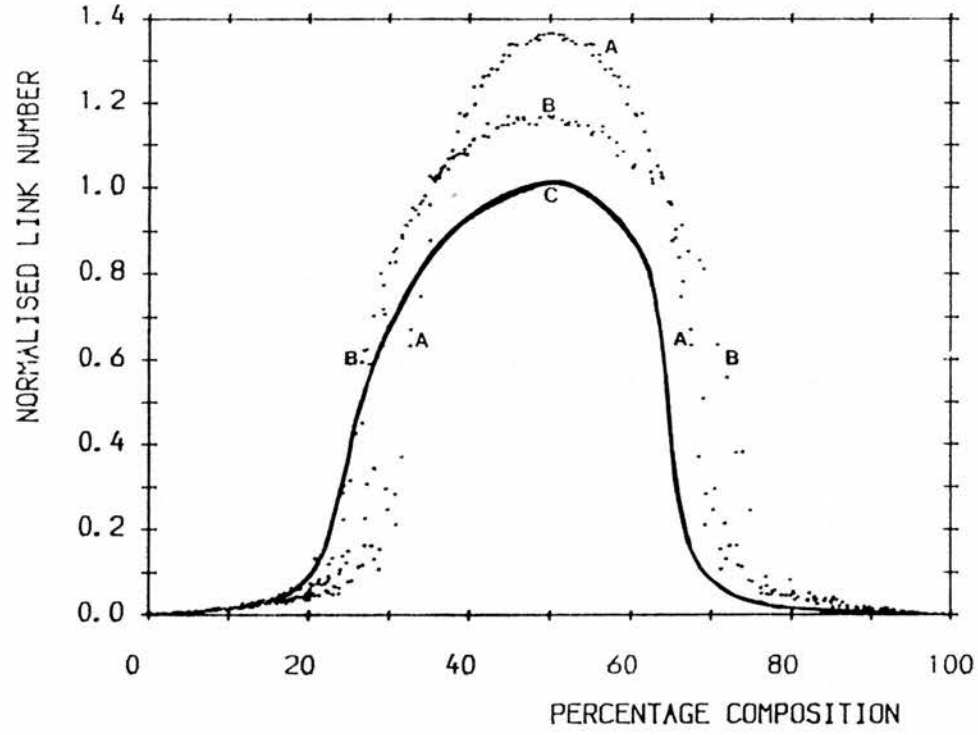

Figure 16.
Effect of particle size ratio on normalised link number/ composition curves (a) 1:1, (b) 4:1, (c) 16:1 (MPE model, 25 x 25 x 25 lattice)

6 Coordination Lattice		12 Coordination Lattice	
Size Ratio	N_L	Size Ratio	N_L
1:1	1.35	1:1	2.92
1:2	1.29	1:2	2.77
1:4	1.16	1:4	2.65
1:8	1.08	1:8	2.58
1:16	1.02	1:16	2.50

Table 4.
Maximum normalised link number as the relative particle size increases for 6 and 12 coordination lattices.

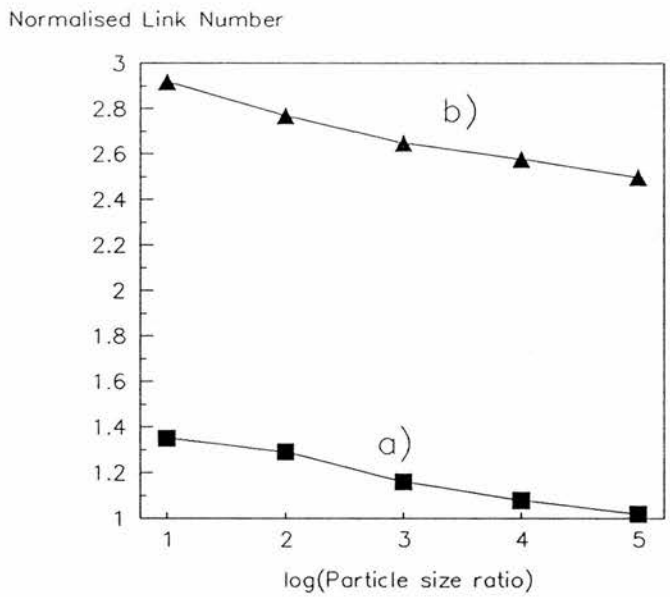

Figure 17.
Normalised link number versus logarithm of the particle size for a) 6 and b) 12 coordination lattices.

7.2 GEOMETRIC DISTRIBUTION OF PARTICLE SIZES

In the models described above the particles of each type have always been of uniform size, although in the most recently outlined case the two components had different sized particles relative to each other. The next obvious development was to consider a model where each component consisted of particles with a distribution of sizes. In real situations particles are frequently found to have a geometric or a log normal distribution of sizes. [15] The former distribution is defined in terms of one variable and was reasonably easy to convert to terms applicable to the computer model and so was considered first.

Figure 18 illustrates a discrete geometric distribution and compares it with a uniform distribution with the same mean. For the geometric distribution [16] the proportion of points $p(x)$ in an interval x is given by the expression:-

$$p(x) = qp^{(x-1)}$$

where $p = (1 - q)$ and the mean of the distribution is $1/q$ and the variance p/q^2. The breadth of the distribution is determined by the mean and thus the bias towards small (low mean) or large particles can be preselected. The method for translating this into the computer model is described fully in Chapter 4.

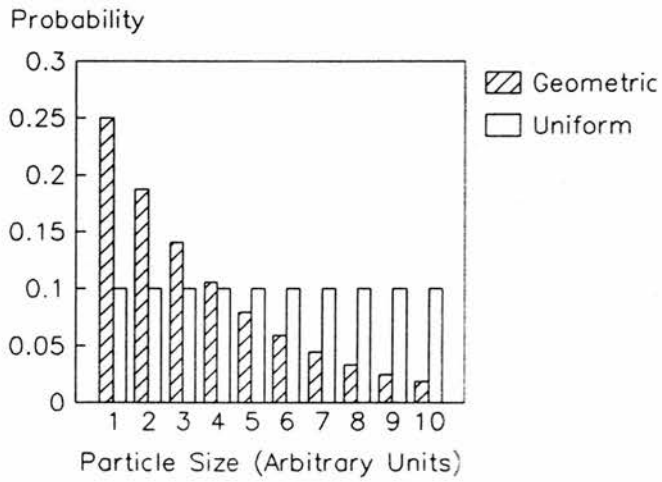

Figure 18.
Comparison of discrete uniform and geometric distributions.

7.2.1 RESULTS FROM GEOMETRIC DISTRIBUTION MODELS

Three distinct sets of experiments were carried out with this model. Firstly each component was considered to have an identically defined distribution of particle sizes. This allowed direct comparison with the simplest model in order to determine whether the presence of a distribution of sizes affected the N_L versus composition curves. The maximum array size of 35x35x35 was used and the distributions were chosen to have a mean particle size of 5 units and a maximum size of 25 units. This yields predominantly relatively small particles, but with a significant number of larger ones. It also gives a reasonable total number of particles in the lattice.

The next experiment altered the mean of the distribution to increase the number of larger particles. The distributions chosen maintained the same maximum particle size of 25 units, but defined the means to be 10 and 15 in turn. Because of the imposition of a maximum particle size the resultant distributions had means of 8 and 10 respectively.

Lastly the two components were considered to have very different geometric distributions. The distributions chosen for the two components had means of 2 and 16 units, and maximum particle sizes of 5 and 50 respectively, yielding approximately a 1:8 relative size difference.

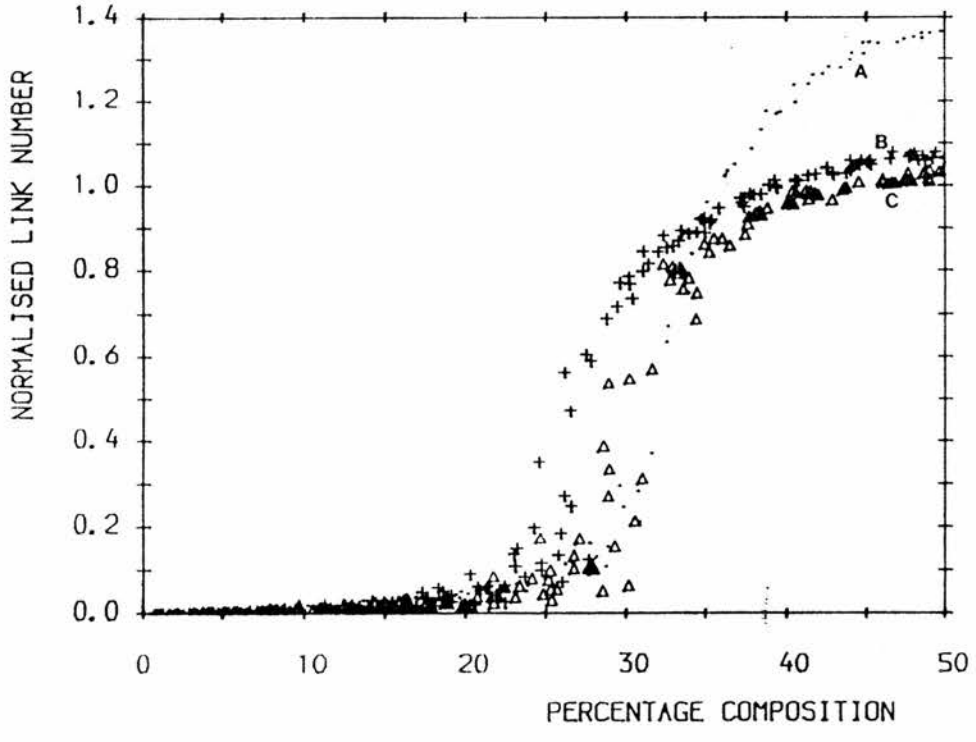

Figure 19.
The effect of a geometric distribution of particle sizes. a) Standard model, b) Mean 5 units, Maximum size 25 units, c) Mean 10 units, Maximum size 25 units. (MPE model, 35 x 35 x 35 lattice)

Figure 19 compares the presence of a geometric distribution of particle sizes with the standard MPE model and also illustrates the effect of increasing the mean of the geometric distribution (i.e. the first two experiments outlined above). Only half the composition range is shown since the situation is once more symmetrical. The general shape of the curves remains unchanged but the maximum attained value of N_L is drastically reduced. Indeed N_L becomes approximately unity indicating that, for this array size, the mixed phase electrode no longer appreciably enhances the contact area between

the two components i.e. the average number of links to each particle is approximately the same as if no mixed phase electrode existed. However increasing the lattice size should improve this value and increase the average number of links per particle.

Increasing the mean particle size does not change this much, the maximum value decreasing only slightly as the proportion of larger particles is increased. There are no visible alterations in the breadth of the curves. Figure 20 shows what occurs when the two substituents have significantly different geometric distributions. Once again the peak N_L value is reduced almost to one, but now there is also obvious asymmetry in the curve. The percolation threshold moves to a lower composition of the minor component. This is immediately comparable to the effect observed above when there was a similar difference in mean particle size but no distribution of sizes.

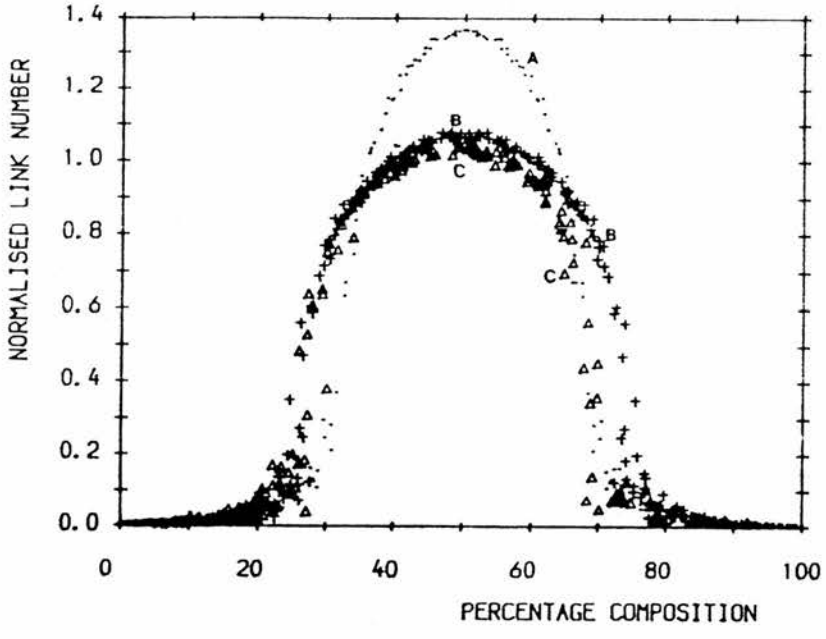

Figure 20.
Different geometric size distributions for each component. a) Standard Model, b) Component 1 - mean 2, maximum size 5, c) Component 2 - mean 16, maximum size 50. (MPE model, 35 x 35 x 35 lattice)

7.3 LARGER PARTICLE SIZES

The effect of proportionally increasing the particle sizes of both components is depicted in Figure 21. The sizes of both substituents were progressively doubled from one to sixteen. The curves obtained are once more symmetrical and the maximum value of N_L decreases with increasing particle size. As can be seen in Table 5 the drop off is more pronounced when particles of both components are increased in size than when the size of only one was altered. This reflects a more prominent

reduction in the randomness of the array filling. The reduction is no longer linear when plotted versus the logarithm of the particle size (Figure 22), although deviations from linearity are only present for very large particles (Table 5).

Particle Sizes (A:B)	Threshold Upper	Threshold Lower	Maximum N_L
1:1 H	30 %	70 %	1.36
1:2 H	28 %	72 %	1.28
1:4 H	24 %	76 %	1.17
1:8 H	19 %	70 %	1.09
1:16 H	25 %	67 %	1.03
1:1 H	30 %	70 %	1.36
2:2 H	22 %	78 %	1.24
4:4 H	26 %	74 %	1.12
8:8 H	32 %	68 %	1.05
16:16 H	38 %	62 %	1.01
1:1 V	30 %	70 %	1.36
2:2 V	20 %	80 %	1.25
4:4 V	13 %	87 %	1.12
8:8 V	5 %	95 %	1.06
16:16 V	1 %	99 %	1.03
1:8 V	18 %	92 %	1.10

Table 5.
Estimated percolation thresholds and maximum normalised link number for all particle size variation experiments. (MPE model 25 x 25 x 25 lattice, H = horizontal, V = vertical filling.)

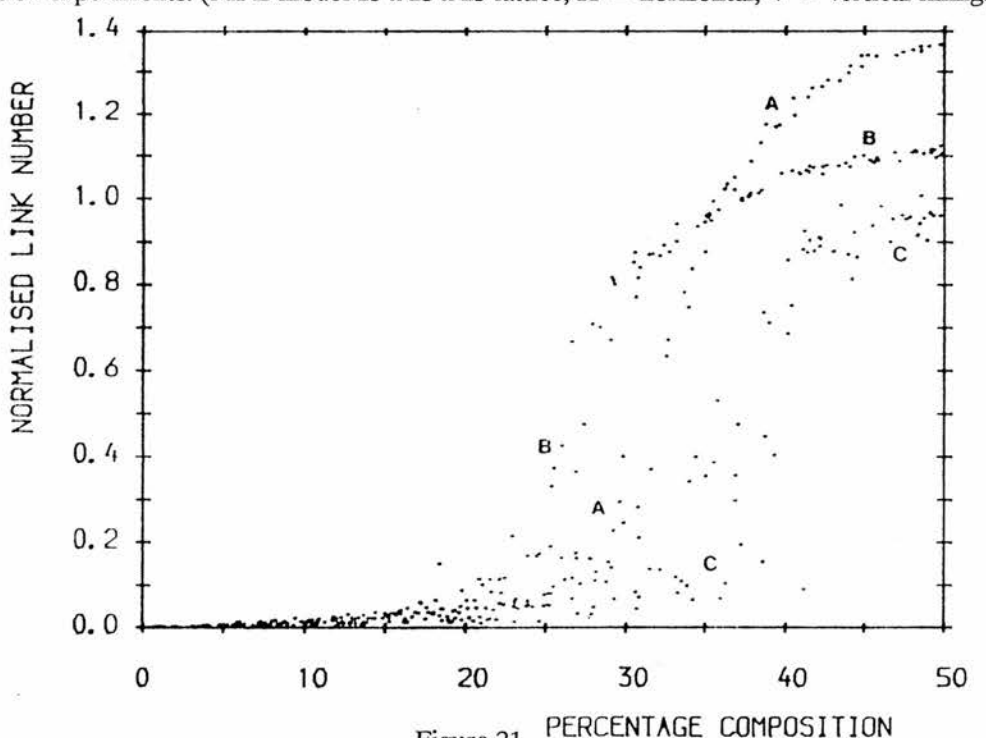

Figure 21.
The effect of increasing the particle size of both components. a) 1:1, b) 4:4, c) 16:16 (MPE model, 25 x 25 x 25 lattice)

Very significant differences in the breadths of the curves are now evident, but there is no distinguishable trend. The threshold where the curves rise abruptly moves to lower percentages of the minor component at first, and then to higher percentages as the particle sizes are further increased. This is discussed in more detail below.

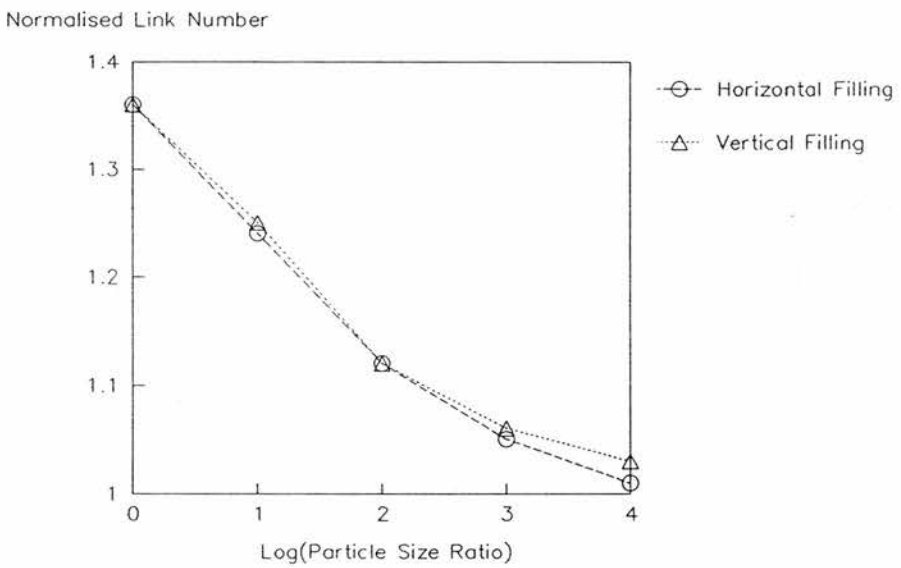

Figure 22.
Normalised link number versus the logarithm of particle size when both components are increased in size. a) Horizontal filling, b) Vertical filling. (MPE model, 25 x 25 x 25 lattice)

8 EFFECT OF PARTICLE ORIENTATION

The increasing asymmetry of the particles in the above examples prompted an investigation of the effect of particle orientation on the results obtained with larger particle sizes. For long thin particles in particular this is likely to be a crucial aspect. Such effects have been examined experimentally for electronic conduction in percolation situations [17] and it was shown that the percolation threshold in systems with asymmetric insulating spots on a conductive surface was dependent on the aspect ratio (i.e. length to width ratio) of the spots. In the situations described above all particles were aligned perpendicularly to the proposed direction of current flow in the mixed phase electrode, i.e. parallel to the bases of the array. Reconstruction of the model gave particles aligned perpendicularly to the bases, parallel to the proposed direction of current flow.

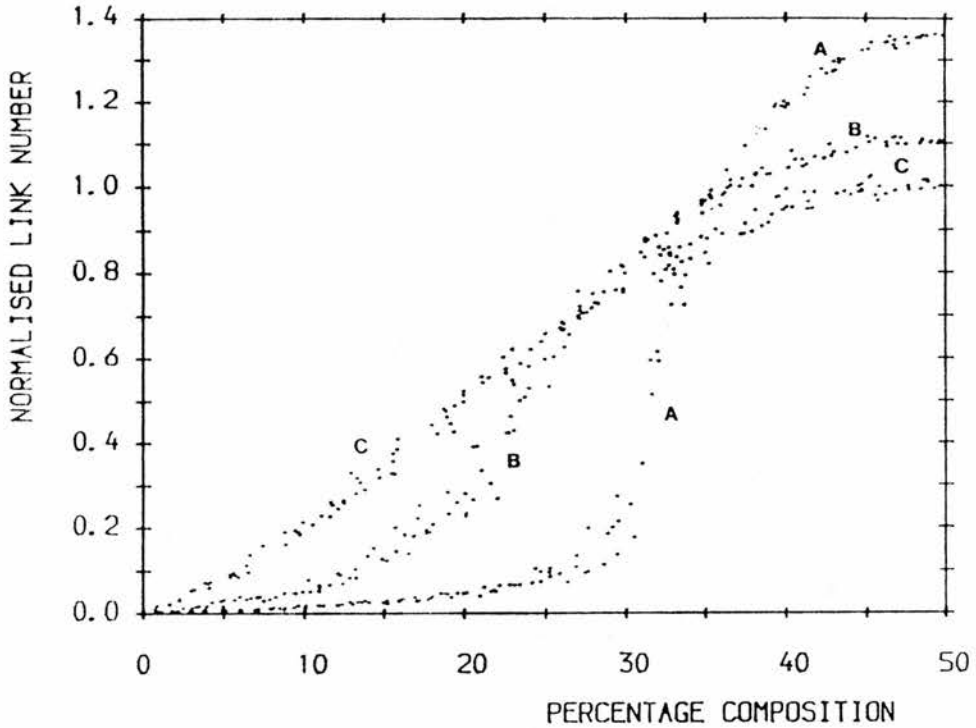

Figure 23.
The effect of increasing the particle size of both components. Vertical alignment. a) 1:1, b) 4:4, c) 16:16. (MPE model, 25 x 25 x 25 lattice)

Figure 23 illustrates the results obtained when the particle size of both components is increased with this new orientation. The particle sizes were again successively doubled from one to sixteen. The normal situation where each particle is of unit size is given for comparison and, as expected, the resultant graph is identical with the standard horizontally filled array. The remaining graphs are similarly symmetric about the 50 % composition point but now as the particle size is increased the shape of the graphs alters dramatically. The abrupt rise usually observed around the percolation threshold becomes more and more indistinct with increasing particle size until, for the largest particles there is an essentially linear decline in N_L towards low compositions. So, overall the percolation threshold is considerably lessened and the curves are broadened.

The reason behind this is clear. As the particle size becomes longer the particle stretches across a greater fraction of the distance between the array bases. So only a few particles need to be alongside one another to connect the bases. Thus the percolation threshold is moved to lower compositions with increasing particle size. The peak value of N_L still declines steadily with increased particle size. The magnitude of the value of N_L is virtually indistinguishable from that of the horizontally filled lattice at compositions above the efficiency threshold. However below the efficiency threshold N_L is

much larger for the vertically orientated particles. This is explainable by considering the change in chain length of particles in contact with their own base. Even at low compositions (of the longer particles) chains the length of the particle extend from the appropriate array base contributing to the contact area. Obviously the longer the particles the greater is this contribution.

Figure 24 compares horizontal and vertical filling when the two substituents of the array have different sized particles. The standard curve is also included for reference. Above the efficiency threshold there is still little difference between horizontal and vertical particles. At low and high composition ranges the curves are markedly different from each other. As above the vertically filled lattice is much broader and the percolation threshold is lower. The curve is also much more asymmetric than the horizontal case, there being greater differences between the two at low compositions of the larger particle size (70 - 100 % on the graph). This occurs for the same reasons as above.

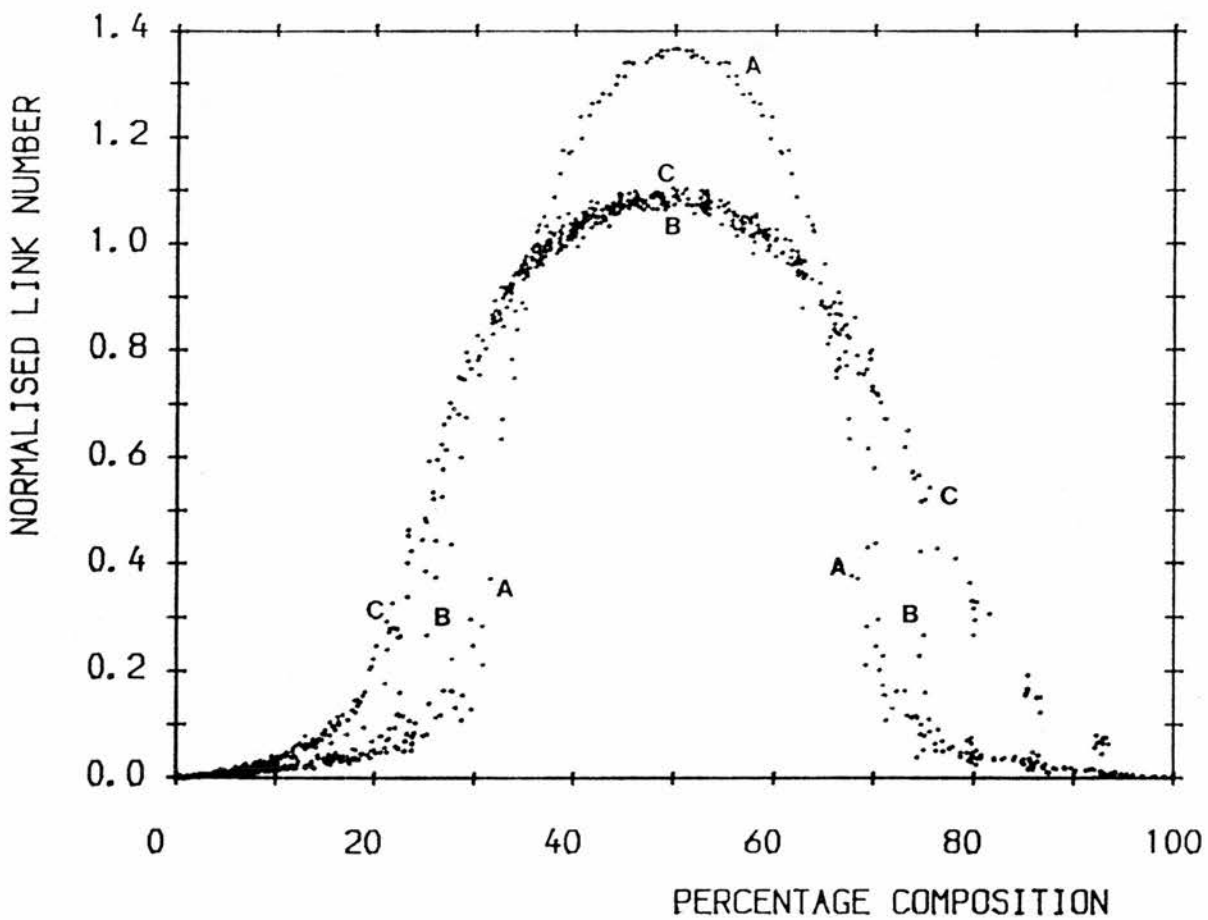

Figure 24.
Comparison of horizontal and vertical filling for particles of different sizes. a) 1:1, b) 1:8 H, c) 1:8 V. (MPE model, 25 x 25 x 25 lattice)

8.1 CHANGES IN PERCOLATION THRESHOLDS AND N_L MAXIMA

As mentioned above most of the situations examined with different particle sizes exhibit some form of alteration in the percolation threshold, and in the maximum value of N_L obtained. This concluding section discusses some of the changes which occur and attempts to rationalise them in terms of percolation theory.

In each case the percolation threshold was approximated as the average value of the last three consecutive percentage compositions at which a zero value of N_L is evident for the percolation model. (This is similar to the iterative determination of the threshold in other percolation systems [6], although many more lattices should be considered to yield an accurate value.)

Table 5 lists the percolation thresholds obtained by this method along with the maximum N_L observed for all the cases with uniformly sized particles. The major conclusion concerns the vertically orientated particles in which there is an obvious decrease in the percolation threshold with the particle size. In the preceding section this was explained in terms of the fraction of the lattice traversed by a single particle. These results agree well with the conclusions drawn by Smith and Lobb [17] where significant reductions in the percolation threshold are evident for long thin "particles".

The horizontally aligned particles pose more problems. Initially there seems to be a slight broadening of the curves, but as the particle size is increased further there is a definite narrowing. This can also be explained in terms of the likelihood of a particle connecting with like particles in adjacent layers. The ordering introduced into the lattice increases the probabilities initially and only when the particle size approaches dimensions of the same order as the lattice size do complications arise. Of course, the requirement of an infinite lattice is breaking down in the latter cases. One other feature worth mentioning is that there is only asymmetry when the components have different particle sizes. (This is also true for the geometrically distributed cases.)

In retrospect these situations represent not a change in particle size, but an alteration in the particle shape, the particles becoming progressively elongated. The changes in coordination described earlier probably reflect changes in particle size more realistically.

9 FURTHER WORK

Considerable scope for expansion still exists within the computer simulation described above, to yield still more refined and interesting results. Of the results discussed the application of a distribution of particle sizes offers many opportunities for extension, both in the distributions considered

and also in the coordination of lattice to which they are applied. The examination of the properties of the models with differing particle sizes under conditions where the lattice thickness is altered will probably provide interesting information concerning the percolation threshold variation observed. Also it will almost certainly re-emphasise the unlimited increase in contact area available by increasing the size of the mixed phase electrode.

Many other modifications can also be envisaged. In particular work has begun on the development of a lattice which considers not only a distribution of particle sizes, but also irregularity in the shape of the particles and in the manner in which the lattice is filled. All the above models fill the lattice regularly from top to bottom, leaving no voids. By producing randomness in the filling procedure voids will result, yielding a more realistic simulation. The application of such a random filling procedure to the above models is likely to provide interesting deviations from the reported results, particularly where non-uniform sizes are considered.

Another reasonable modification is to consider situations where the contact area is effective only at some of the faces of a particle, thus simulating diffusion in one or two dimensions rather than three. This is probably realistic considering the two-dimensional nature of diffusion in the transition metal dichalcogenides compared with three-dimensional diffusion in metal oxide systems. Similarly the introduction of random orientation of larger particle would be more realistic.

Ultimately the model could be tailored to simulate, as far as possible, the known parameters for individual materials, in terms of the particle size, shape, lattice coordination etc.

10 CONCLUSIONS

The statistical computer model formulated by Nairn [1] to simulate a mixed phase electrode and improved and extended by Harris [3] to treat percolation situations has, in this work, been considerably modified to consider a variety of further conditions. Notably the effect of higher coordination lattices, distributions of particle sizes, particle orientation and changes in concentration across the thickness of the MPE have been considered. Some important and interesting new results have emerged from these extensions.

The initial results, on comparing the mixed phase electrode and percolation situations, confirmed that increasing the thickness of a composite electrode proportionally increases the operative contact area, assuming that the percentage of both components exceeds an efficiency threshold of 35 % for the simple cubic lattice considered. Above this threshold the mixed phase electrode

conditions coincide with standard percolation conditions and indeed some of the results obtained from the MPE model have been explained using aspects of percolation theory. Conductivity equations applicable in such percolation situations may therefore prove useful in predicting MPE behaviour.

This is only a first approximation since other contributing factors, such as iR drop and problems of particle size distributions and lattice voids exert an increasingly important influence on the properties of thicker regions. However, because of the relatively broad composition range in which the area is increased by the introduction of a mixed phase region it is possible to increase the volume percentage of the lower resistance component to minimise problems of iR drop without drastically affecting the interfacial contact area.

Results from higher coordination models demonstrate that, as the coordination is increased, the efficiency threshold moves towards lower compositions thus increasing the range over which the mixed phase region provides a means of improving the contact area. The normalised link number is also greatly enhanced with the move to higher coordinations, suggesting an improvement in the contact area of 80 % for 8 coordination and 200 % for 12 coordination for the array size used. Note however that in real systems this enhancement may not be so significant since the average contact area between particles may be reduced as the coordination increase due to the greater packing density around each particle. Again as an initial estimation it should be possible to improve the effective interfacial contact area in a composite region by selecting particles sizes or material properties which yield high coordination packing.

Introducing a gradient of composition across the MPE does not improve the contact area between the two components beyond that obtainable for a single section of an identical average composition. However, for a defined average increasing the number of layers present increases the N_L towards the optimum value, providing that the composition of each is greater than the percolation threshold composition. This suggests that for real systems a property such as the conductivity may be enhanced by the introduction of a series of layers of gradually changing composition.

The relative size (or, on reconsideration, the shape) of particles can also have a detrimental effect on the contact area as it was shown that the normalised link number decreased linearly with the logarithm of the particle size ratio. This has also been related to experimental evidence which demonstrates a similar effect with the conductivity of glassy silver iodotungstate electrolyte. Similar response has been observed in situations where a geometric size distribution of either or both components is introduced, or where the particle size of both components has been altered. The

particle orientation was also shown to be a significant factor in determining the breadth of the region where significant gains in area could be achieved and changes in the percolation thresholds observed in such situations can be related to the aspect ratio of the particles bearing comparison with reported percolation results of such effects. In real battery systems such effects can be important as smaller quantities of one of the components could be used to yield a good interfacial area. This would be useful if one of the components was considerably more expensive or had a relatively large resistance.

In summary a variety of features may need to be considered in the optimisation of the performance of a composite region in a solid-state battery, but the potential gains, from area enhancement at least, are extremely significant. The computer model suggests answers to some of the problems within such an optimisation of contact area between the electrode and electrolyte materials, but does not explore the problems of iR drop, voids in the lattice etc. Further advances in the simulation may overcome some of these to a limited extent.

11 REFERENCES

1 Nairn I.A. "The Study Of Mixed Phase Electrodes In Solid State Cells", Ph.D. Thesis University Of St. Andrews (1984)

2 Nairn I.A., Smith M.J., Vincent C.A. "Mixed-Phase Electrodes In Solid State Cells", Solid State Ionics 9 & 10 (1983) 383

3 Harris K.D.M. "A Computer Study Of Mixed Phase Electrodes", Unpublished Work for a Carnegie Trust Report (1984)

4 Harris K.D.M., Rogers M.D., Vincent C.A. "A Comparison Between 'Mixed Phase Electrode' And Percolation Models For Composite Electrodes In Solid State Cells", Solid State Ionics 18 & 19 (1986) 833

5 Atkins P.W. "Physical Chemistry" (3rd Edition), Publ.Oxford University Press (1986)

6 Stauffer D. "Introduction To Percolation Theory", Publ.Taylor & Francis Ltd. (1985)

7 Shante V.K.S., Kirkpatrick S. "An Introduction To Percolation Theory", Advances In Physics 20 (1971) 325

8 Finney J.L. "Modelling The Structure Of Amorphous Metals And Alloys", Nature 266 (1977) 309

9 Rosso M., Gouyet J-F., Sapoval B. "Determination Of Percolation Probability From The Use Of A Concentration Gradient", Physical Review B 32 (1985) 6053

10 Gouyet J-F., Rosso M., Sapoval B. "Percolation In A Concentration Gradient", Fractals In Physics, Eds. Pietronero L., Tosatti E., Publ. Elsevier Science Publishers (1986)

11 Bunde A., Gouyet J.F. "On Scaling Relations In Growth Models For Percolating Clusters And Diffusion Fronts", J. Phys. A 18 (1985) L285

12 Atlung S., Zachau-Christiansen B., West K., Jacobsen T. "The Composite Insertion Electrode Theoretical Part. Equilibrium In The Insertion Compound And Linear Potential Dependence", J. Electrochem. Soc. 131 (1984) 1200

13 Landauer R. "The Electrical Resistance Of Binary Metallic Mixtures", Journal Of Applied Physics 23 (1952) 779

14 Meredith R.E., Tobias C.W. "Conduction In Heterogeneous Systems", Adv. In Electrochem. And Electrochem. Engineering 2 (1962) 18

15 Green H.L., Lane W.R. "Particulate Clouds: Dusts Smokes And Mists", Publ. E. & F. N. Spon Ltd. (1957)

16 Kreyszig E. "Introductory Mathematical Statistics", Publ. John Wiley and Sons

17 Smith L.N., Lobb C.J. "Percolation In Two-Dimensional Conductor-Insulator Networks With Controllable Anisotropy", Physical Review B 20 (1979) 3653

1 INTRODUCTION

This chapter describes in detail the construction and operation of the computer programs which simulate the mixed phase electrode and percolation models, and their subsequent extension to consider more advanced simulations.

In general four different programs were required to allow the computer simulations to operate. Each modification to the simplest MPE representation required variation of one or more of these basic programs and, in addition, other programs were occasionally necessary. The four fundamental programs were:-

a) The main command file which consisted of a series of Digital Command Language instructions. This file controlled and ran the other programs and handled data input, output and storage from the appropriate files and directories.

b) Another command file RAND.GLM which contained commands for the statistical package GLIM which was used as a random number generator.

c) An S-Algol program SEED.S which generated the input required for RAND.GLM in order to improve the selection of random numbers.

d) The main S-Algol program PAC6.S which created and processed the random array which represented the mixed phase electrode.

The operation of RAND.GLM and SEED.S have been described in detail by Nairn. [1] RAND.GLM was used without further alteration but SEED.S incorporated the modification of Harris [2] to improve the randomness of its output. A sample of one of the main command files and the main program PAC6.S are listed below, in partially truncated form, and their operation is discussed in detail. The variations in these two main programs and the other programs used in the more advanced simulations are described thereafter with reference to each individual change in the formulation of the model.

2 THE MAIN COMMAND FILE (THICKCH.COM)

The outline of one of the main command programs, THICKCH.COM, is listed as Program 1 and exemplifies the method used to control the different programs contributing to the simulation. For clarity and brevity various lines have been deleted, these, in general, being comments or lines controlling the changing of directories etc., which are unimportant to the discussion of the operation of the program but which facilitate data handling and storage. The program is submitted with

appropriate parameters to the queue slow$batch which is available on the VAX. There it is run non-interactively, resubmitting itself when the one hour CPU time limit is approached or with different parameters when it is finished.

Programme 1 - THICKCH.COM.
Example of VAX command programme.

```
1 - $!Main command file THICKCH.COM
4 - $ on error then goto ABORT
5 - $START:
7 - $ tstart = 'f$getjpi("","CPUTIM")'
8 - $ tlimit = 'f$getjpi("","CPULIM")'
9 - $ P2 = 'P2'
10 - $ P3 = 'P3'
11 - $ P1 = 'P1' + 1
12 - $ if P1.GE.3 then goto CHANGE
13 - $CONT:
14 - $ if P2.GT.100 then goto LEAVE
15 - $ if P3.GT.70 then goto LEAVE
16 - $ row = 25
17 - $ col = 25
18 - $ lay = 'P3'
19 - $ perc = 'P2'
21 - $ n = row * col * lay / 2000
23 - $ open/write out perc.dat
24 - $ write out perc
25 - $ write out n
26 - $ close out
27 - $ sr seed.out
28 - $ delete perc.dat;*
29 - $ assign RAND.GLM FOR005
30 - $ assign SEED.GLM FOR011
31 - $ assign RANDOMARY.DAT FOR008
32 - $ run sys$user:glim3a
33 - $ delete seed.glm;*
35 - $ open/write outfile dim.dat
36 - $ write outfile row
37 - $ write outfile col
38 - $ write outfile lay
39 - $ write outfile perc
40 - $ close outfile
41 - $ run pac6.exe
43 - $ append adata2.dat anumbnorm.dat
46 - $ append btempdata.dat bmainout.dat
47 - $ append bdata2.dat bnumbnorm.dat
51 - $ append bdataa3.dat blinka3.dat
55 - $ delete *tempdata.dat;*
56 - $ delete *data*.dat;*
57 - $ delete randomary.dat;*
58 - $ purge dim.dat
59 - $ purge thickch.log
62 - $ trun = 'f$getjpi("","CPUTIM")' - 'tstart'
63 - $ if(f$getjpi("","CPUTIM") + trun).
      - LT.(tlimit-500) then goto START
64 - $SUBSLOW:
66 - $ submit/queue = slow$batch/log_file = user1:[chrmr] -
      /priority = 4/cputime = 01:00:00 -
        user1:[chrmr.com]thickch.com -
```

```
        /parameters=('P1','P2','P3')
67 - $ exit
68 - $CHANGE:
69 - $ P3 = P3 + 1
70 - $ P1 = 0
71 - $ goto CONT
72 - $ABORT:
73 - $ P1 = P1 - 1
74 - $ n = P1 + 1
75 - $ t = f$getjpi("","CPUTIM")/100
76 - $ if(f$getjpi("","CPUTIM")).GE.(tlimit-100) then goto SUBSLOW
77 - $ open/write out mail.dat
78 - $ write out "An error has occurred in thickch.com"
79 - $ write out "and the values of P1 = "n' & P2 = "P2""
80 - $ write out "with cputime = "t' secs."
81 - $ close out
82 - $ mail/subject="error" mail.dat chrmr
83 - $ delete mail.dat;*
84 - $ goto LEAVE
85 - $ exit
86 - $LEAVE:
90 - $ send me end
    The job using the program thickch.com is now finished.
91 - $stop
```

The program itself can be considered as being subdivided into separate groups of commands (or procedures), to each of which program control can be directed during its execution. Line 4 instructs the program to transfer control to the command group ABORT: (lines 72 to 85) if an error arises during any stage of program operation. Lines 5 to 11 represent the procedure START: which initialises the time monitoring facility used within the program and reads the parameters required by it (from the command which submitted the program to the slow$batch queue). This program changes the lattice thickness at a predetermined composition and P1 is the number of runs at each thickness, P2 the percentage composition of the lattice and P3 the number of layers in the lattice. The program (PERCCH.COM) which changed the percentage composition of the lattice required only the parameters P1 and P2, the number of layers being a predefined constant. The lattice size most commonly considered had a square base of size 25 by 25 units, this giving lattices large enough to negate problems caused by very small numbers of particles [1] but small enough to allow the processing to be carried out within the limitations imposed by the storage space and CPU time available. The maximum number of units permitted by these restrictions was of the order of 45000, giving a maximum lattice thickness of 70 layers in the thickness variation experiments and suggesting a cubic lattice of a maximum 35 layers thick when composition variation was examined.

The next command transfers the program control to the command group CHANGE: (lines 68 to 71) if three executions of the program have been made at the current thickness. Generally, in order to allow for the randomness of the filling procedure, three runs were carried out at each thickness (or composition) and so P1 is never greater than 3. CHANGE: adjusts the parameters P1 and P3 to allow further runs to be made at this thickness or increases the thickness.

Lines 13 to 62 represent the main command section CONT: which calls each of the other programs as necessary and creates and handles the necessary data files. Since the particles are equivalent in this basic model, they are interchangeable as a group and therefore a lattice consisting of x % of component 1 and (100-x) % of component 2 yields the same result as a lattice composed of (100-x) % of component 1 and x % of component 2. Thus the percentage composition P2 has only to be varied from 1 to 50 % during the execution of the program, the remaining results arising from symmetry. Lines 14 and 15 therefore check that P2 and P3 are within the required limits (P2 < 50 and P3 < 70), exiting from the program if these conditions are not fulfilled. The next four lines set up the parameters which determine the array size and it is these lines which are edited to produce different shapes and sizes of the lattice.

Lines 21 to 28 calculate the input required for SEED.S and run that program. Lines 29 to 40 run RAND.GLM creating a data file RANDOMARY.DAT and filling it with the random data generated by it, and also creating the file DIM.DAT which contains the array size and composition parameters for input to PAC6.S.

Lines 41 to 50 run the main program PAC6.S and store the calculated data from it in appropriate files. The lines given here illustrate some of the data which can be obtained including, for example, all the written output from the program (line 46), normalised link number versus the number of layers in the lattice (line 43) and the number of particles of one type linked to 3 of the other type (line 51). Lines 55 to 59 tidy up the filespace, deleting any files no longer required. If more than one program was to be run on the same lattice lines similar to 41 to 59 were inserted here to execute the programs required. This allowed results to be compared directly for identical random lattices. Lines 60 to 67 calculate the CPU time left, reverting control to START: if there is enough time left for another run. Otherwise the program resubmits itself to slow$batch via the command group SUB-SLOW: (lines 64 to 67) and execution is halted. The parameters necessary for the next execution are

passed on from the current one. The remainder of the program (procedures ABORT: and LEAVE:) notifies the user of any error which has occurred during execution and stops the program running when there has been an error or when the program has finished.

3 THE MAIN PROGRAM (PAC6.S)

The four programs discussed by Harris [2] simulating respectively a mixed phase electrode (Model 1), a percolation situation (Model 2) and the two possible intermediate situations (Models 3 and 4), were inefficient in the respect that, when more than one was employed, there was a significant overlap in the variables used and the operations undertaken. The program listed as Program 2 represents a combination of these programs eliminating most of the repetition and improving overall execution. The same iterative procedures for lattice processing were employed. Again a degree of truncation has been used when listing to remove comments and repetitive segments of program where this does not affect the description of the operation of the program.

In combining the programs into one all variables were reformulated as vectors (or matrices) with the first parameter of each vector corresponding to the model used. The main sections of the individual programs were reconstructed as procedures, again with parameters representing the model being employed. This made the programs easier to understand logically, reduced the amount of repetition and also simplified the rewriting of the program to consider different coordinations and methods of filling the array. The model numbers were read in from a new file SORT.DAT which held any combination of the model numbers 1 to 4 terminating with a zero. Various new program segments were written to handle the different model numbers and to produce the parameters required by the new variables and procedures.

The main written output from the original programs was also drastically reduced in size, and program sections were written to perform all cross-checking internally during the execution of the program rather than in the output as previously. The capacity for output of data to graphics files was extended to allow plotting of the number of links of one type of particle linked to any number of the other type versus either the lattice thickness or the percentage composition, as appropriate. Any or all of the available data sets could be used as requested by the main command file. Lastly a main program section was written which simply calls up the appropriate procedures required for the running of each model, inputting the required parameters to these procedures.

Programme 2 - PAC6.S.
The main Array modelling and sorting programme.

```
 1 - ! ********************************
 2 - ! COMBINED SORTING PROGRAMME
17 - ! ********************************


19 - ! ***************************
20 -   procedure cputime(-> real )
21 - ! ***************************
26 - begin
27 -   let time.str := time
28 -   let min.str := time.str(4|2)
29 -   let sec.str := time.str(7|2)
30 -   let temp := decode(min.str(1|1)) - 48
31 -   let mins := 10*temp + decode(min.str(2|1)) - 48
32 -   temp := decode(sec.str(1|1)) - 48
33 -   let secs := 10*temp + decode(sec.str(2|1)) - 48
34 -   mins*1.0 + secs/60
35 - end


36 - ! ******************
37 - ! DECLARATION SECTION
38 - ! ******************
39 - ! In declaring any vector names the first parameter
40 - ! is the model number under consideration.
41 - let first.time = cputime
42 - let number = vector 1::6 of 0
43 - let no.of.scans = vector 1::4 of 0
44 - let no.of.set.faces = vector 0::4 of 0
45 - let old.1 := 0
46 - let old.2 := 0
47 - let new.1 := 0
48 - let new.2 := 0
49 - let j := 0
50 - let m := 0
51 - let k := -1
52 - let total.sites.test := 0
53 - let prefix := ""
54 - let no.of.particles = vector 1::4,0::8 of 0
      ! Number of 1's, 2's to 6's after lattice processing.
55 - let flag = vector 1::4 of 0
56 - let no.of.links = vector 1::4 of 0
      ! Total number of links counted.
57 - let links.to.particles = vector 1::4,1::6,0::6 of 0
      ! Second parameter is the particle around which links
      ! are being counted, third parameter is the number of
      ! links to that particle.
58 - let norm.link.no = vector 1::4 of 0.0
      ! Normalised link number.
59 - let fract.conn1 = vector 1::4 of 0.0
      ! Fraction of connected particles of type 1.
60 - let fract.conn2 = vector 1::4 of 0.0
      ! Fraction of connected particles of type 2.
61 - s.w := 1
62 - i.w := 5
63 - r.w := 5
      ! Read the array dimensions from file dim.dat
68 - let Name = "dim.dat"
69 - let Inp = open(Name,"a",0)
```

```
70 - if Inp = nullfile do{write"'n",Name,
                    " cannot be opened."; abort}
71 - let R = readi(Inp) + 2   !Number of rows in lattice
72 - write "'nThe number of rows    =",R-2
73 - let C = readi(Inp) + 2   !Number of columns in lattice
74 - write "'nThe number of columns =",C-2
75 - let L = readi(Inp) + 2   !Number of layers in lattice
76 - write "'nThe number of layers  =",L-2
77 - let perc = readi(Inp)    !Percentage of 1's in lattice
78 - write"'nThe % of 1's to total  =",perc
79 - close(Inp)
    ! Read array from file randomary.dat.
    ! There must be at least (R-2)*(C-2)*(L-2)
    ! random 0's and 1's in randomary.dat
83 - let name = "randomary.dat"
84 - let inp = open(name,"a",0)
85 - if inp = nullfile do{write"The opening of",
                name," was unsuccessful.";abort}
86 - let count.1 := 0
    ! Counts no. of 1's input to lattice.
87 - let count.2 := 0
    ! Counts no. of 2's input to lattice.
88 - let Array = vector 1::R,1::C,1::L of 0
    !The array is declared.
    ! The array is filled by reading 0.0 or 1.0
    ! and converting to an integer one higher than itself.
91 - for iL = 2 to L-1 do
92 -    begin
93 -    for iR = 2 to R-1 do
94 -       begin
95 -       for iC = 2 to C-1 do
96 -          begin
97 -          let numb = readr(inp)
98 -          case numb of
99 -           0.0 : count.1 := count.1 + 1
100 -           1.0 : count.2 := count.2 + 1
101 -          default : {write"'nOne of the data points in ",
102 -                        name,". = ",numb,"'n" ; abort}
103 -          Array(iR,iC,iL) := truncate( numb + 1 )
104 -          end
105 -       end
106 -    end
107 - close(inp)
109 - number(1) := count.1
110 - number(2) := count.2
111 - write"'n",count.1+count.2,"points
                    have been read in to the Array"
112 - write"'nand it took ",cputime-first.time," mins."
113 - let base.area    = (R-2)*(C-2)
114 - let total.sites  = (L-2)*base.area
115 - let fract.1      = count.1/total.sites
      ! Fraction of 1's in lattice.
116 - let fract.2      = count.2/total.sites
      ! Fraction of 2's in lattice.
117 - let p1           = 100*fract.1
     ! Percentage of 1's.
118 - let p2           = 100*fract.2
      ! Percentage of 2's.
```

```
120 - ! ************************
121 -   procedure scan.down(int t)
122 - ! ************************
123 - begin
134 - old.1 := -10
135 - new.1 := number(t+2)
136 - while (new.1~ =old.1) do
137 - begin
138 - no.of.scans(t) := no.of.scans(t) + 1
139 - for iL = 2 to (L-1) do
140 - begin
141 -    for iR = 2 to (R-1) do
142 -    begin
143 -  for iC = 2 to (C-1) do
144 -  begin
145 -  if Array(iR,iC,iL) = t do
146 -  begin
147 -  if (Array(iR,iC,(iL-1)) = t+2 or
                    Array(iR,iC,(iL+1)) = t+2 or
148 -     Array((iR-1),iC,iL) = t+2 or
                    Array((iR+1),iC,iL) = t+2 or
149 -     Array(iR,(iC-1),iL) = t+2 or
                    Array(iR,(iC+1),iL) = t+2 ) do
150 -  {Array(iR,iC,iL) := t + 2
151 -   number(t+2) := number(t+2) + 1
152 -   number(t) := number(t) - 1}
153 -  end
154 -  end
155 -    end
156 - end
157 - old.1 := new.1
158 - new.1 := number(t+2)
159 - end
160 - end


162 - ! ************************
163 -   procedure scan.up(int t)
164 - ! ************************
165 - begin
176 - old.1 := -10
177 - new.1 := number(t+2)
178 - while (new.1~ =old.1) do
179 - begin
180 - no.of.scans(t) := no.of.scans(t) + 1
181 - for iL = (L-1) to 2 by -1 do
182 - begin
183 -    for iR = 2 to (R-1) do
184 -    begin
185 -  for iC = 2 to (C-1) do
186 -  begin
187 -  if Array(iR,iC,iL) = t do
188 -  begin
189 -  if (Array(iR,iC,(iL+1)) = t+2 or
                    Array(iR,iC,(iL-1)) = t+2 or
190 -     Array((iR+1),iC,iL) = t+2 or
                    Array((iR-1),iC,iL) = t+2 or
191 -     Array(iR,(iC+1),iL) = t+2 or
                    Array(iR,(iC-1),iL) = t+2 ) do
192 -  {Array(iR,iC,iL) := t + 2
193 -   number(t+2) := number(t+2) + 1
194 -   number(t) := number(t) - 1}
```

```
195 -  end
196 -  end
197 -     end
198 - end
199 - old.1 := new.1
200 - new.1 := number(t+2)
201 - end
202 - end


204 - ! ****************************
205 -   procedure set.top.base(int x)
206 - ! ****************************
      ! This procedure sets the TOP base (ie. iL=1) to x
207 - begin
209 - for iR = 2 to (R-1) do
210 - begin
211 -     for iC = 2 to (C-1) do
212 -     begin
213 -     Array(iR,iC,1) := x
214 -     end
215 - end
216 - end


218 - ! ********************************
219 -   procedure set.bottom.base(int x)
220 - ! ********************************
      ! This procedure sets the TOP base (ie. iL=1) to x
221 - begin
223 - for iR = 2 to (R-1) do
224 - begin
225 -     for iC = 2 to (C-1) do
226 -     begin
227 -     Array(iR,iC,L) := x
228 -     end
229 - end
230 - end


232 - ! ********************************
233 -   procedure set.outer.faces(int t)
234 - ! ********************************
      ! Set the iR=1,iR=R,iC=1 and iC=C planes of the array
      ! to be the same as the iR=(R-1),iR=2,iC=(C-1) and iC=2
      ! planes of the array respectively.
235 - begin
239 - no.of.set.faces(t) := no.of.set.faces(t) + 1
240 - for iR = 2 to (R-1) do
241 - begin
242 -     for iL = 2 to (L-1) do
243 -     begin
244 -     Array(iR,1,iL) := Array(iR,(C-1),iL)
245 -     Array(iR,C,iL) := Array(iR,2,iL)
246 -     end
247 - end
248 - for iC = 2 to (C-1) do
249 - begin
250 -     for iL = 2 to (L-1) do
251 -     begin
252 -     Array(1,iC,iL) := Array((R-1),iC,iL)
253 -     Array(R,iC,iL) := Array(2,iC,iL)
```

```
254 -     end
255 - end
256 - end


258 - ! ****************************
259 -   procedure convert.down(int t)
260 - ! ****************************
261 - begin
272 - let x1 : = t+2
272 - set.top.base(x1)
274 - set.bottom.base(0)
275 - scan.down(t)
276 - old.2 : = -10
277 - new.2 : = number(x1)
278 - while (new.2 ~ = old.2) do
279 - begin
280 -     set.outer.faces(t)
281 -     scan.down(t)
282 -     old.2 : = new.2
283 -     new.2 : = number(x1)
284 - end
285 - end


287 - ! ***************************
288 -   procedure convert.up(int t)
289 - ! ***************************
290 - begin
301 - let x1 : = t+2
302 - set.top.base(0)
303 - set.bottom.base(x1)
304 - scan.up(t)
305 - old.2 : = -10
306 - new.2 : = number(x1)
307 - while (new.2 ~ = old.2) do
308 - begin
309 -     set.outer.faces(t)
310 -     scan.up(t)
311 -     old.2 : = new.2
312 -     new.2 : = number(x1)
313 - end
316 - end


318 - ! ***************************************
319 -   procedure base.contribution(int t -> int)
320 - ! ***************************************
321 - begin
324 - let base.no.of.links : = 0
325 - for iR  = 2 to (R-1) do
326 -  begin
327 -     for iC = 2 to (C-1) do
328 -        begin
329 -          if Array(iR,iC,2) = t do
330 -             begin
331 -             base.no.of.links
                        : = base.no.of.links + 1
332 -             end
333 -        end
```

```
334 -  end
335 - base.no.of.links
336 - end


338 - ! *************************
339 -  procedure reconvert(int t)
340 - ! *************************
341 - begin
346 - for iL = 2 to (L-1) do
347 -  begin
348 -     for iR = 2 to (R-1) do
349 -        begin
350 -           for iC = 2 to (C-1) do
351 -           begin
352 -              if Array(iR,iC,iL) = t do
353 -              begin
354 -                 Array(iR,iC,iL) := t-2
355 -              end
356 -           end
357 -        end
358 -  end
359 - set.outer.faces(0)
360 - number(t-2) := number(t-2) + number(t)
361 - number(t) := 0
362 - end


364 - ! ***********************************
365 -  procedure change.parameters(int v)
366 - ! ***********************************
367 - begin
371 - case v of
372 -  1 : begin
373 -        j := v+2       ! 3's
374 -        m := v+3       ! 4's
375 -        prefix := "a"
376 -     end
377 -  2 : begin
378 -        j := v+3       ! 5's
379 -        m := v+4       ! 6's
380 -        prefix := "b"
381 -        end
382 -  3 : begin
383 -        j := v+2       ! 5's
384 -        m := v+1       ! 4's
385 -        prefix := "c"
386 -     end
387 - 4 : begin
388 -        j := v-1       ! 3's
389 -        m := v+2       ! 6's
390 -        prefix := "d"
391 -     end
392 -  default : write "'nIncorrect input from sort.dat"
393 - end


395 - ! ****************************************
396 -  procedure count.particles.and.links(int v)
397 - ! ****************************************
398 - begin
411 - for i = 0 to 6 do
```

```
412 - begin
413 -    links.to.particles(v,j,i) := 0
414 -    links.to.particles(v,m,i) := 0
415 -    no.of.particles(v,i) := 0
416 - end
417 - no.of.links(v) := 0
418 - flag(v) := 0
419 - for iL = 2 to (L-1) do
420 -   begin
421 -   for iR = 2 to (R-1) do
422 -     begin
423 -     for iC = 2 to (C-1) do
424 -       begin
425 -       case Array(iR,iC,iL)  of
426 -       1 : no.of.particles(v,1) :=
                  no.of.particles(v,1) + 1
427 -       2 : no.of.particles(v,2) :=
                  no.of.particles(v,2) + 1
428 -       3 : no.of.particles(v,3) :=
                  no.of.particles(v,3) + 1
429 -       4 : no.of.particles(v,4) :=
                  no.of.particles(v,4) + 1
430 -       5 : no.of.particles(v,5) :=
                  no.of.particles(v,5) + 1
431 -       6 : no.of.particles(v,6) :=
                  no.of.particles(v,6) + 1
432 -      default : {write"'nAn element is
                     not 1,2,3,4,5 or 6."
433 -               write "'nIt is ",Array(iR,iC,iL)
434 -                no.of.particles(v,7):=
                      no.of.particles(v,7)+1}
437 -          case Array(iR,iC,iL) of
438 -           j : begin
439 -               flag(v) := 0
440 -               if Array(iR-1,iC,iL) = m do
                    {flag(v) := flag(v) + 1
441 -                no.of.links(v) := no.of.links(v) + 1}
442 -               if Array(iR+1,iC,iL) = m do
                    {flag(v) := flag(v) + 1
443 -                no.of.links(v) := no.of.links(v) + 1}
444 -               if Array(iR,iC-1,iL) = m do
                    {flag(v) := flag(v) + 1
445 -                no.of.links(v) := no.of.links(v) + 1}
446 -               if Array(iR,iC+1,iL) = m do
                    {flag(v) := flag(v) + 1
447 -                no.of.links(v) := no.of.links(v) + 1}
448 -               if Array(iR,iC,iL-1) = m do
                    {flag(v) := flag(v) + 1
449 -                no.of.links(v) := no.of.links(v) + 1}
450 -               if Array(iR,iC,iL+1) = m do
                    {flag(v) := flag(v) + 1
451 -                no.of.links(v) := no.of.links(v) + 1}
452 -               case flag(v) of
453 -               0:  links.to.particles(v,j,0)
                        := links.to.particles(v,j,0) + 1
454 -               1 : links.to.particles(v,j,1)
                        := links.to.particles(v,j,1) + 1
455 -               2 : links.to.particles(v,j,2)
                        := links.to.particles(v,j,2) + 1
456 -               3 : links.to.particles(v,j,3)
                        := links.to.particles(v,j,3) + 1
457 -               4 : links.to.particles(v,j,4)
```

```
                    := links.to.particles(v,j,4) + 1
458 -             5 : links.to.particles(v,j,5)
                    := links.to.particles(v,j,5) + 1
459 -
460 -         default : {write "'nAn element",j," of
                        the array has too many links."
461 -                   links.to.particles(v,j,6)
                    := links.to.particles(v,j,6) + 1}
465 -             end
466 -          m : begin
467 -             flag(v) := 0
468 -             if Array(iR-1,iC,iL) = j do
                        flag(v) := flag(v) + 1
469 -             if Array(iR+1,iC,iL) = j do
                        flag(v) := flag(v) + 1
470 -             if Array(iR,iC-1,iL) = j do
                      flag(v) := flag(v) + 1
471 -             if Array(iR,iC+1,iL) = j do
                        flag(v) := flag(v) + 1
472 -             if Array(iR,iC,iL-1) = j do
                        flag(v) := flag(v) + 1
473 -             if Array(iR,iC,iL+1) = j do
                        flag(v) := flag(v) + 1
474 -             case flag(v) of
475 -             0 : links.to.particles(v,m,0)
                      := links.to.particles(v,m,0) + 1
476 -             1 : links.to.particles(v,m,1)
                      := links.to.particles(v,m,1) + 1
477 -             2 : links.to.particles(v,m,2)
                      := links.to.particles(v,m,2) + 1
478 -             3 : links.to.particles(v,m,3)
                      := links.to.particles(v,m,3) + 1
479 -             4 : links.to.particles(v,m,4)
                      := links.to.particles(v,m,4) + 1
480 -             5 : links.to.particles(v,m,5)
                      := links.to.particles(v,m,5) + 1
481 -
482 -         default : write "'nAn element",m," of the
                        array has too many links."
483 -              links.to.particles(v,m,6)
                    := links.to.particles(v,m,6) + 1
486 -             end
487 -       default : no.of.particles(v,8)
                      := no.of.particles(v,8)+1
488 -       end
489 -    end
490 - end
491 - write"'nThe array has been processed"
492 - write"'nand it took ",cputime-first.time," mins"
494 - end


496 - ! ***************************
497 -   procedure main.output(int v)
498 - ! ***************************
499 - begin
508 - i.w := 7
509 - s.w := 1
510 - norm.link.no(v) := (no.of.links(v)-base.area)/total.sites
511 - if norm.link.no(v) < 0.0 do norm.link.no(v) := 0.0
512 -
513 - fract.conn1(v) := no.of.particles(v,j)/total.sites
```

```
514 - fract.conn2(v) := no.of.particles(v,m)/total.sites
515 - let file.name = prefix + + "tempdata.dat"
516 - let total.time = cputime-first.time
517 - let out = create(file.name,"s","a","v",256 )
518 - output out,"'n**************************
519 - case v of
520 -  1 : output out,"'nRESULTS FROM SORTA2E.S
521 -  2 : output out,"'nRESULTS FROM SORTB2E.S
522 -  3 : output out,"'nRESULTS FROM SORTC2E.S
523 -  4 : output out,"'nRESULTS FROM SORTD2E.S
524 -  default : output out,"'nIncorrect input from sort.dat"
525 - output out,"'nNo. of rows     = ",R-2
526 - output out,"'nNo. of columns  = ",C-2
527 - output out,"'nNo. of layers   = ",L-2
528 - output out,"'nApprox. % of 1"s in lattice = ",perc
529 - let total.sites.test := 0
530 - for i = 1 to 6 do
531 -  begin
532 -  total.sites.test := total.sites.test +
                          no.of.particles(v,i)
533 -  end
534 - if total.sites ~ =total.sites.test do
535 -  begin
536 -  output out,"'nNo. of sites does
                  not equal the no. of test sites"
537 -  end
538 - output out,"'nNo. of 1"s before analysis  =",count.1
539 - output out,"'nNo. of 2"s before analysis  =",count.2
540 - if total.sites ~ = count.1 + count.2 do
541 -  begin
542 -  output out,"'nNo. of 1"s + No. of 2"s
                  does not equal no. of lattice sites"
543 -  end
544 - output out,"'nFRACTION OF 1"s IN LATTICE = ",fract.1
545 - output out,"'nFRACTION OF 2"s IN LATTICE = ",fract.2
546 - output out,"'n'nAfter analysis of the lattice -->'n"
547 - for i=1 to 6 do
548 -  begin
549 -  if no.of.particles(v,i) ~ = number(i) do
550 -  begin
551 -  output out,"'nThere is an error in the
                  comparison of counting of the particle types"
552 -  end
553 -  end
554 - if no.of.particles(v,7) ~ = 0 do
555 - begin
556 -    output out,"'nThere are unexpected particles in lattice."
557 - end
558 - case v of
559 -  1 : begin
560 -  output out,"'nNo. links 3"s to 4"s =",no.of.links(v)
561 -  output out,"'nNorm. link number     =",norm.link.no(v)
562 -  output out,"'nFraction 3"s in lattice =",fract.conn1(v)
563 -  output out,"'nFraction 4"s in lattice =",fract.conn2(v)
564 -     end
565 -  2 : begin
566 -  output out,"'nNo. links 5"s to 6"s  =",no.of.links(v)
567 -  output out,"'nNorm. link number      =",norm.link.no(v)
568 -  output out,"'nFraction 5"s in lattice =",fract.conn1(v)
569 -  output out,"'nFraction 6"s in lattice =",fract.conn2(v)
570 -     end
571 -  3 : begin
```

```
572 - output out,"'nNo. links 5"s to 4"s  =",no.of.links(v)
573 - output out,"'nNorm. link number      =",norm.link.no(v)
574 - output out,"'nFraction 4"s in lattice =",fract.conn1(v)
575 - output out,"'nFraction 5"s in lattice =",fract.conn2(v)
576 -    end
577 - 4 : begin
578 - output out,"'nNo. links 3"s to 6"s  =",no.of.links(v)
579 - output out,"'nNorm. link number      =",norm.link.no(v)
580 - output out,"'nFraction 3"s in lattice =",fract.conn1(v)
581 - output out,"'nFraction 6"s in lattice =",fract.conn2(v)
582 -    end
583 -  default : write "'nThere is an error in sort.dat"
584 - output out,"'nTotal CPU time used = ",total.time," mins"
585 - close(out)
586 - end


588 - ! ****************************
589 -  procedure graph.output(int v)
590 - ! ****************************
591 - begin
594 - let total.time := cputime-first.time
595 - let no.of.layers = total.sites/base.area
596 - let fraction.of.particles = vector 1::4,1::6,0::6 of 0.0
597 - for i = 0 to 5 do
598 - begin
599 -    fraction.of.particles(v,j,i) :=
          links.to.particles(v,j,i)/total.sites
600 -    fraction.of.particles(v,m,i) :=
          links.to.particles(v,m,i)/total.sites
601 - end
602 - !This outputs the percentage composition and the normalised
603 - !link number for plotting.
604 - let file.name0 = prefix + + "data0.dat"
605 - let filout0 = create(file.name0,"s","a","v",256)
606 - output filout0,p1:15,norm.link.no(v):15
607 - close (filout0)
609 - !This outputs the normalised link no. vs. the no. of
610 - !layers in the lattice.
611 - let file.name2 = prefix + + "data2.dat"
612 - let filout2 = create(file.name2,"s","a","v",256)
613 - output filout2,no.of.layers:15,norm.link.no(v):15
614 - close (filout2)
616 - !This outputs the fraction of 1's initially vs. the fraction
617 - !of the first connected particles of interest in the lattice.
618 - let file.name3 = prefix + + "data3.dat"
619 - let filout3 = create(file.name3,"s","a","v",256)
620 - output filout3,fract.1:15,fract.conn1(v):15
621 - close (filout3)
637 - for i=0 to 5 do
638 - begin
639 - !This outputs the fraction of particles of type a linked
640 - !to i particles vs. the no. of layers in the lattice.
641 - let file.name = prefix + + "dataa" + + code(i+48) + + ".dat"
642 - let filout = create(file.name,"s","a","v",256)
643 - output filout,no.of.layers:15,fraction.of.particles(v,j,i):15
644 - close (filout)
645 - end
647 - for i=0 to 5 do
648 - begin
649 - !This outputs the fraction of particles of type b linked
650 - !to i particles vs. the percentage composition of the lattice.
```

```
651 - let file.name = prefix + + "datad" + + code(i+48) + + ".dat"
652 - let filout = create(file.name,"s","a","v",256)
653 - output filout,p1:15,fraction.of.particles(v,m,i):15
654 - close (filout)
655 - end


694 - ! ***********
695 - ! MAIN PROGRAM
696 - ! ***********
697 - convert.down(1)
698 - convert.up(2)
709 - let input = "sort.dat"
710 - let in.file = open(input,"a",0)
711 - repeat k := readi(in.file)
712 - while k ~ = 0 do
713 - begin
714 -    case k of
715 - 1 : begin
716 -        set.top.base(3)
717 -        set.bottom.base(4)
718 -        change.parameters(k)
719 -        count.particles.and.links(k)
720 -        no.of.links(k) := no.of.links(k)
                    + base.contribution(4)
721 -        main.output(k)
722 -        graph.output(k)
723 -    end
724 - 2 : begin
725 -        convert.up(3)
726 -        convert.down(4)
727 -        set.top.base(5)
728 -        set.bottom.base(6)
729 -        change.parameters(k)
730 -        count.particles.and.links(k)
731 -        no.of.links(k) := no.of.links(k)
                    + base.contribution(6)
732 -        main.output(k)
733 -        graph.output(k)
734 -        reconvert(5)
735 -        reconvert(6)
736 -    end
737 - 3 : begin
738 -        convert.up(3)
739 -        set.top.base(5); set.bottom.base(4)
741 -        change.parameters(k)
742 -        count.particles.and.links(k)
743 -        no.of.links(k) := no.of.links(k)
                    + base.contribution(4)
744 -        main.output(k); graph.output(k)
746 -        reconvert(5)
748 -    end
749 - 4 : begin
750 -        convert.down(k)
751 -        set.top.base(3); set.bottom.base(6)
753 -        change.parameters(k)
754 -        count.particles.and.links(k)
755 -        no.of.links(k) := no.of.links(k)
                    + base.contribution(6)
756 -        main.output(k); graph.output(k)
758 -        reconvert(6)
760 -    end
```

```
761 -  default : {write "There is an error in sort.dat"}
762 - end
765 - ?
```

Once the combined program was complete it was thoroughly tested against the original programs, both singly and when used in any possible combination. A large range of lattice sizes were used and percentage and thickness variation situations were examined. In all cases the results from the original program and the appropriate section of the combined program were identical.

The procedure CPUTIME is used to calculate the amount of CPU time used during the execution of the program. Lines 36 to 118 declare all the necessary constants, variables and vectors required for execution of the program. The names of the variables correspond to their function or to the data which they are to store. The array modelling the mixed phase electrode is created after reading its dimensions from DIM.DAT and then filled from the appropriate data file RANDOMARY.DAT (lines 91 to 112). This consists of 0's and 1's, randomly generated by RAND.GLM which are changed to 1's and 2's representing the two particle types as they are read into the array.

Procedure SCAN.DOWN (SCAN.UP) works its way down (up) through the lattice layer by layer changing any particles of type t to type t + 2 if any of the particles connected to it in the previous layer are already of type t + 2. This is repeated iteratively until there are no further changes whereupon all particles of type t + 2 are singly connected to the base of the lattice from which processing is initiated. This layer by layer approach is comparable with standard Monte Carlo processing techniques and is generally used in computer simulations of percolation conditions. [3]

The array under consideration as the mixed phase electrode region has an extra plane at each of its faces, the ones at the top and bottom representing the regions of pure materials and those at the sides enabling edge effects to be eliminated. The next three procedures adjust these layers. SET.TOP.BASE (SET.BOTTOM.BASE) changes all the values of the top (bottom) layers of the array to the value read into the procedure. SET.OUTER.FACES changes each of the extra planes at the sides of the lattice to match the opposite outside face of the lattice, thus, in terms of the processing, effectively connecting the array back into itself on the opposite side.

The procedure CONVERT.DOWN (CONVERT.UP) processes the array downwards (upwards) layer by layer using the above procedures. Firstly the top (bottom) base is set to the value t + 2 and the array is processed using SCAN.DOWN (SCAN.UP) until all particles of type t in the bulk of the array have been altered to t + 2 if they are singly connected. The outer faces are then

changed by SET.OUTER.FACES as described above. Consequently a particle t may now be singly connected via these altered outer faces and so the above is repeated iteratively until there are no further changes in the lattice.

The procedure BASE.CONTRIBUTION calculates the number of links caused by the base of the array. Procedure RECONVERT changes particles t + 2 back to t throughout the lattice, while CHANGE.PARAMETERS reads in the model number and calculates the required parameters for this model. The counting procedure (lines 395 to 495) considers each element of the array in turn and counts the number of links from each element (iR,iC,iL) in the lattice to the surrounding six particles and also counts the number of each type of particle.

The remaining two procedures (MAIN.OUTPUT and GRAPH.OUTPUT) respectively output all the written data and all the data to be plotted in graph form to temporary files. The former also carries out all the internal testing of variables within the program for inconsistencies in the calculations, there being a degree of duplication built into the processing method.

The main program section (lines 694 to 765) calls the required procedures for each of the simulations it is asked to undertake. As an example of the operation consider the most complicated case of the percolation model which counts the number of links between doubly connected particles of each type. Only the mixed phase electrode model and the percolation model were used regularly in the experiments described previously, these representing real physical situations while the intermediate models do not. The array is filled initially with 1's and 2's representing the two particle types. The 1's are then converted to 3's by line 697 if they are singly connected to the top layer of 3's in the array, and similarly all 2's that are singly connected to the bottom layer of the array are converted to 4's (line 698). This part is common to all four simulations and represents the mixed phase electrode model. (Lattice processing would commence at this juncture for the MPE model, counting links between 3's and 4's in the array.) The variable 2 is then read in representing the percolation simulation and execution continues from lines 724 to 735. Line 725 converts all 3's to 5's if they are now singly connected to the bottom base (and thus doubly connected overall) and the subsequent line converts 4's to 6's if they too are doubly connected. Lines 727 and 728 set the top and bottom of the array to 5's and 6's respectively, and line 729 sets up the parameters appropriate to the percolation model ready for the counting procedure. Lines 730 and 731 carry out the counting of the numbers of particles of each type (1's to 6's) and calculates the total number of links from 5's to 6's. The number of particles

of type 5 linked to 0,1,2,3,4 or 5 of type 6 (and vice versa) are also counted at this point. The next two lines output the data to the appropriate files and lastly (lines 734 and 735) all 5's are reconverted to 3's and 6's to 4's to allow further processing using one of the other models if desired.

4 HIGHER COORDINATION VARIATIONS (PAC8.S AND PAC12.S)

In the two programs PAC8.S and PAC12.S, which simulate 8 and 12 coordination lattices as described in Chapter 3, the major changes necessary to PAC6.S involved changing the counting procedures to allow for the greater coordination. However, in these and all subsequent programs the section of program which declares the variables and vectors was separated from the segment which fills the array. The latter section was reconstructed as a procedure FILL.ARRAY called at the beginning of the main program section. This further facilitated the writing of the programs described below which, in general, required no changes to the counting procedures but only different methods of filling the array. Several of the vectors in the declaration section were extended in size at this point to enable them to cope with the possibility of particles being linked with up to 7 (or 11) others in the higher coordination systems.

The procedures BASE.CONTRIBUTION and COUNT.PARTICLES.AND.LINKS were altered only to cope with the different particles surrounding a central particle (iR,iC,iL). This involved changing the array positions to be checked and extending the program segments to include the extra positions. The counting sections also had to be extended to allow for the possibility of extra numbers of links. Similarly the MAIN.OUTPUT and GRAPH.OUTPUT procedures were extended to allow handling of this additional information. A summary of the array positions to be checked for each of the described situations is given in Table 1.

The programs were run identically to the 6 coordination program but more data files were created to store the extra output resulting from their execution. The only necessary changes to the command program were therefore to allow for this extra data collection. All three coordination programs were run on the same lattices for direct comparison.

A) 6 Coordination	8 Coordination	12 Coordination
(iR-1 , iC , iL) (iR+1 , iC , iL) (iR , iC-1 , iL) (iR , iC+1 , iL) (iR , iC , iL-1) (iR , iC , iL+1)	(iR+1 , iC+1 , iL+1) (iR-1 , iC+1 , iL+1) (iR+1 , iC-1 , iL+1) (iR-1 , iC-1 , iL+1) (iR+1 , iC+1 , iL-1) (iR-1 , iC+1 , iL-1) (iR+1 , iC-1 , iL-1) (iR-1 , iC-1 , iL-1)	(iR+1 , iC , iL) (iR , iC , iL+1) (iR , iC , iL-1) (iR-1 , iC , iL) (iR , iC-1 , iL+1) (iR , iC-1 , iL-1) (iR , iC+1 , iL) (iR-1 , iC , iL+1) (iR-1 , iC , iL-1) (iR , iC-1 , iL) (iR-1 , iC-1 , iL+1) (iR-1 , iC-1 , iL-1)
B) 6 Coordination	8 Coordination	12 Coordination
(iR , iC , 2)	(iR+1 , iC+1 , 2) (iR-1 , iC+1 , 2) (iR+1 , iC-1 , 2) (iR-1 , iC-1 , 2)	(iR , iC , 2) (iR , iC-1 , 2) (iR-1 , iC , 2) (iR-1 , iC-1 , 2)

Table 1
Particles surrounding A) a central particle (iR , iC , iL) and B) a base particle (iR , iC , 1) for each coordination.

5 CONCENTRATION GRADIENT OF PARTICLES

The major problem in reproducing the lattice type shown in Chapter 3, Figure 13 where a concentration gradient of particles is represented by a series of individual sections each of different compositions, was in the filling of the array which simulated this. Rather than use the approach of altering the procedure FILL.ARRAY in the main program, it was decided to rewrite the main command file so that the data file RANDOMARY.DAT was filled with data in the required format. This also necessitated writing another brief S-Algol program (TRUNCATE.S) to manipulate the data.

5.1 TRUNCATE.S

TRUNCATE.S is reproduced as Program 3 in slightly abbreviated form. Its operation is very straightforward. Randomly produced 0's and 1's are read one by one from the file RANDOM.DAT, which contains an excess of data. Exactly enough points are output to the file RANDOM2.DAT to fill one section of the subdivided array. This number is determined by input of the array dimensions and also the number of layers in each section of the lattice from the usual file DIM.DAT. The percentage composition of each section is also calculated and output to PERCCHANGE.DAT.

Program 3 - TRUNCATE.S.
Programme to restrict the number of data points.

```
1 - ! **********
2 - ! TRUNCATE.S
3 - ! **********
7 -
8 - let numb := 0.0
9 - let Name="dim.dat"
10 - let Inp= open(Name,"a",0)
11 - if Inp = nullfile do{write"'n",Name,"cannot be opened.";abort }
13 - let R = readi(Inp)
14 - let C = readi(Inp)
15 - let L = readi(Inp)
16 - let P = readi(Inp)
17 - let L2 = readi(Inp)
18 - close(Inp)
19 -
20 - let filename = "random.dat"
21 - let input = open(filename,"a",0)
22 - if input = nullfile do{ write"The opening of ",
23 -                 filename," was unsuccessful.";abort}
25 - let file.name = "random2.dat"
26 - let out = create(file.name,"s","a","v",256 )
28 - let count.1 := 0    ! No. of 0's
29 - let count.2 := 0    ! No. of 1's
30 - let count.3 := 0    ! No. of data points per line.
31 -
32 - for i = 1 to R*C*L2 do
33 - begin
34 -    numb := readr(input)
35 -    output out, numb:2
36 -    case numb of
37 -       0.0 : count.1 := count.1 + 1
38 -       1.0 : count.2 := count.2 + 1
39 -    default : abort
40 -    count.3 := count.3 + 1
41 -    if count.3 = 10 do
42 -    begin
43 -       output out, "'n"
44 -       count.3 := 0
45 -    end
46 - end
48 - close(input)
49 - close(out)
50 -
51 - write "'n", count.1, " 0"'s have been read into random2.dat"
52 - write "'n", count.2, " 1"'s have been read into random2.dat"
53 -
54 - let perc1 = (count.1/(count.1 + count.2))*100
55 - let perc2 = (count.2/(count.1 + count.2))*100
57 - let file.name2 = "perchange.dat"
58 - let out2 = create(file.name2,"s","a","v",256 )
59 - output out2, perc1, perc2, "'n"
60 - close(out)
62 - ?
```

5.2 GRADDIST.COM

The new command file GRADDIST.COM was used in combination with TRUNCATE.S to produce RANDOMARY.DAT such that it held only sufficient random 0's and 1's to exactly fill the array and these were already ordered into a composition gradient. The main differences between it and the command file previously described are outlined in Program 4. It has been further segmented into command groups and control is switched between them more often to allow repetition of the random number generating section at different percentages. The parameter P3 is no longer required and P2 is unchanged between different submissions of the program.

On entering the program command is immediately transferred to the section CHANGE: (lines 69 to 76) which creates the files DIM2.DAT and RANDOMARY.DAT. The former file stores the compositions of the individual sections which form the concentration gradient thus allowing the actual concentrations of each section to be compared with the specified values. P1 still represents the number of executions of the program under the defined conditions and is augmented by one. P2, the percentage composition of one of the sections is initially set to its required starting value (100 here). The variable P2 now defines the percentage of 1's in the section under construction and since the procedure to fill the array works from the base representing 100% 1's then the percentage of 1's is consecutively reduced for each section across the lattice. Control is then transferred to CONT: (lines 12 to 58).

CONT: decreases P2 by the desired percentage increment and the next two lines again check that P1 and P2 are within their delimited values. In this example 10 executions of the program are carried out under each set of conditions to yield an average result. An extra parameter lay2 is defined to give the thickness of each section of the lattice. The next few lines are omitted but are identical to the already described command file, running SEED.S and RAND.GLM to produce the initial random data. This data is output to the file RANDOM.DAT required as input for TRUNCATE.S.

Program 4 - GRADDIST.COM.
Command programme to produce and analyse an array with a concentration gradient of particles.

```
 5 - $START:
 9 - $ P2 = 'P2'
10 - $ P1 = 'P1'
11 - $ if P1.LE.10 then goto CHANGE
12 - $CONT:
13 - $ P2 = P2 - 10
14 - $ if P2.LE.0 then goto ANALYSE
15 - $ if P1.EQ.10 then goto LEAVE
16 - $ row = 27
17 - $ col = 27
```

```
18 - $ lay = 27
19 - $ lay2 = 3
20 - $ perc = 'P2'

    22 lines omitted

43 - $ sr truncate
44 - $ append random2.dat randomary.dat
45 - $ append perchange.dat dim2.dat
46 - $ delete random.dat;*
47 - $ delete random2.dat;*
48 - $ goto CONT
50 - $ANALYSE:
51 - $ run pac6.exe
52 - $ append adata0.dat apercnorm.dat
55 - $ delete *data*.dat;*
56 - $ purge dim.dat
57 - $ purge perchange.dat

    11 lines omitted

69 - $CHANGE:
70 - $ create dim2.dat
71 - $ create randomary.dat
73 - $ purge randomary.dat
74 - $ P1 = P1 + 1
75 - $ P2 = 100
76 - $ goto CONT

    18 lines omitted

85 - $stop
```

The next five listed lines run the program TRUNCATE.S, append its output (RANDOM2.DAT) to RANDOMARY.DAT and delete unwanted files. Control is now looped back to the beginning of CONT: where the percentage is again decreased and the above set of commands is repeated until P2 attains its defined minimum value (0% here) whereupon the command group ANALYSE: is summoned. Thus the file RANDOMARY.DAT is filled consecutively with groups of data of different compositions from the successively produced RANDOM2.DAT files. Each set of data consist of the exact number of points required to fill one section of the array and thus overall RANDOMARY.DAT contains only enough data to exactly fill the array.

The command group ANALYSE: now runs PAC6.S as normal. However the only data output is the normalised link number versus percentage composition so this section is considerably shortened. Lastly, in the omitted section, the data files are tidied up and the program restarted or resubmitted as usual.

6 UNIFORM SIZE DISTRIBUTION OF PARTICLE (UNIFSIZE.S)

The production of a model which considered the two types of particles as having different sizes involved making minor changes to the main command file and rewriting the procedure FILL.ARRAY in the main simulation program, along with a few other minor changes. The sizes are considered to be the number of consecutive lattice sites occupied by a particle.

To produce UNIFSIZE.S from PAC6.S involved the addition of four more variables, size1, size2, count.3 and count.4. Size1 and size2 are the sizes of the two particle types and the remaining variables are simply counters used in the new version of the filling procedure. FILL.ARRAY now works by reading, as before, a random selection of 0's and 1's from the file RANDOMARY.DAT. If a 0 is read then size1 0's are output to a new file RANDOM.DAT and if a 1 is read then size2 1's are output to RANDOM.DAT. Thus RANDOM.DAT consists of a series of 0's and 1's in the size ratio size1:size2. Count.3 is used in formatting the data output and count.4 gives the total number of data items read to this file. The array is subsequently read from RANDOM.DAT and processed in the normal manner.

The changes in the main command file consisted of introducing two new parameters P4 and P5 representing the sizes of the two types of particle. These remained constant throughout the running of the command file and were included in the output to the file DIM.DAT as data for the simulation program (UNIFSIZE.S).

Also the percentage change now had to be carried out over the full composition range as there is no longer equivalence of particles. For the larger relative particle sizes the command file caused the program to be run more frequently over the upper percentage range. This was necessary as the method used to produce the different sizes caused a very significant bias towards the lower percentage region of the curve. (A nominal 50 % proportion of particles in RANDOMARY.DAT initially yields a composition of approximately 33 %, 25 %, 12.5 % and 6 % in the file RANDOM.DAT for the size ratios 1:2, 1:4, 1:8 and 1:16 respectively.)

Similar changes were made to PAC12.S yielding UNIFSIZE12.S which carried out the same function on the 12 coordination lattice.

7 GEOMETRIC SIZE DISTRIBUTION OF PARTICLES

The simulation of a mixed phase electrode in which both particles had a geometric distribution of sizes, as described in Chapter 3 was much more complex. A new program to produce random

data in the required distributions had to be written, and PAC6.S had to be altered considerably to produce the new main program GEOMSIZE.S. A new command file GEOMSIZE.COM was also necessary.

7.1 GEOM.MTB

This new random data program is listed below as Program 5. It consists of a series of commands for the statistical package MINITAB, which is available on the VAX mainframe computer. MINITAB was used in preference to GLIM since it was easier to generate the required output and the programs are more accessible to the unfamiliar user. GEOM.MTB produces three sets of random numbers, the first two being geometrically distributed numbers with means and maxima corresponding to the defined means and maximum particle sizes for the two components in the MPE. The third set consists of randomly distributed 1's and 2's in proportions corresponding to the defined percentage composition of the array. (i.e. This set of data is equivalent to the data formerly produced by GLIM, but it is used somewhat differently.)

Program 5 - GEOM.MTB.
Minitab programme to produce a geometric distribution of data

```
1 - READ data from 'SIZE.DAT' into C100
2 - LET K1 = C100(1)
3 - LET K2 = C100(2)
4 - LET K3 = C100(3)
5 - LET K4 = C100(4)
6 - LET K5 = 1/K2
7 - LET K6 = 1/K4
8 - READ data from 'DIM.DAT' into C101
9 - LET K7 = C101(1)
10 - LET K8 = C101(2)
11 - LET K9 = C101(3)
12 - LET K10 = C101(4)/100
13 - LET K11 = 1-K10
14 - NOTE - K1 is max size type 1. K2 = mean type 1.
15 - NOTE - K3 is max size type 2. K2 = mean type 2.
16 - NOTE - K5 is q for type 1, K6 = q for type 2
19 - SET the following data into C11
20 - 1:K1
21 - END
22 - SET the following data into C12
23 - 1:K3
24 - END
25 - SET the following data into C21
26 - 1:2
27 - END
28 - SET the following data into C22
29 - K10 K11
30 - END
36 - LET C13 = K5*(1-K5)**(C11-1)
37 - LET K13 = SUM(C13)
```

```
38 - LET C14 = C13/K13
39 - LET C15 = K6*(1-K6)**(C12-1)
40 - LET K15 = SUM(C15)
41 - LET C16 = C15/K15
42 - NOTE - C14 and C16 hold the normalised probabilities to
43 - NOTE - generate the geometric distribution for 1s and 2s.
44 - RANDOM 10000 points into C1;
45 - DISCRETE C11 C14.
46 - NOTE - Generation of geometric distribution for 1s.
47 - RANDOM 10000 points into C2;
48 - DISCRETE C12 C16.
49 - NOTE - Generation of geometric distribution for 2s.
50 - RANDOM 50000 points into C3;
51 - DISCRETE C21 C22.
52 - NOTE - Generation of distribution of particle types.
53 - WRITE to 'RAND.DAT' the data in C3
54 - WRITE to 'RAND1.DAT' the data in C1
55 - WRITE to 'RAND2.DAT' the data in C2
56 - HISTOGRAM of C1
57 - HISTOGRAM of C2
58 - HISTOGRAM of C3
59 - END
```

Lines 1 to 7 read the mean and maximum size for each of the two particle types from a new data file SIZE.DAT, and the parameter q (= 1/mean), which defines the geometric distribution, is calculated for each and stored in an appropriate variable (K5 and K6 respectively). Lines 8 to 17 read the array dimensions from the data file DIM.DAT (also used by the main program) and the proportions of 1's and 2's required for the array are calculated and stored in K10 and K11. Lines 19 to 30 create four columns of data necessary for the production of random numbers in a discretely distributed form. C11 and C12 hold the number of intervals (i.e. the number of different particle sizes) for the types 1 and 2 respectively. C21 and C22 store the particle types and the probabilities of them occurring in the lattice. Lines 36 to 38 calculate the probabilities required to simulate a discrete geometric distribution for component 1. Firstly $q\,p^{i} - 1$ is calculated (line 36) for each of the intervals i stored in C11, where $p = 1 - q$. Then the result is normalised (line 38) to allow for the restriction of the imposed maximum particle size. Lines 39 to 41 do the same for component 2.

The subsequent lines (44 to 52) actually generate the random numbers. The command RANDOM x Cy generates x random numbers and stores them in the data column Cy. The sub-command DISCRETE Ca Cb instructs the former command to use the intervals stored in column Ca with the probabilities stored in Cb to form the random output.

The remaining lines output the random data to the appropriate files and produces histograms of each data set to allow visual inspection of the shape of the three random distributions formed.

7.2 GEOMSIZE.S

The altered main program GEOMSIZE.S differed from the original PAC6.S in a variety of ways. The major changes are listed below in Program 6. In the declaration section (not shown) a selection of new vector variables were created to store the means and maximum particle sizes of each distribution, and also the number of particles of each type and size which were input into the array. The three files, RAND.DAT, RAND1.DAT and RAND2.DAT, which stored the three sets of random data produced by GEOM.MTB, were also opened to allow access to the data.

Three new procedures were written to allow selection of the particle type and size in the filling procedure. The first of these (RESET) is not listed and is simply a precautionary procedure which reopens a data file at the beginning should the end be reached during program execution. For larger arrays this can reduce the storage space required for the random data. The remaining two procedures are outlined below along with a truncated version of the modified filling procedure (FILL.ARRAY).

Program 6 - extracts from GEOMSIZE.S

```
1 - ! ************************************
2 -   procedure choose.particle.type( -> int)
3 - ! ************************************
4 - begin
5 -
6 - if eof(input0) do {input0 := reset(input1,"rand.dat")}
7 - let temp := readi(input0)
8 - let temp1 := read(input0)
9 - if (temp ~ = 1 and temp ~ = 2) do
10 -      {write "'nIncorrect type entered."; abort}
11 - let type := temp
12 - type
13 - end
14 -
15 - ! ******************************************
16 -   procedure choose.particle.size(int type -> int)
17 - ! ******************************************
18 - begin
19 - let temp := 0
20 - case type of
21 -      1 : begin
22 -          temp := readi(input1)
23 -          let temp2 := read(input1)
24 -          if eof(input1) do
25 -            {input1 := reset(input1,"rand1.dat")}
26 -          end
27 -      2 : begin
28 -          temp := readi(input2)
29 -          let temp2 := read(input2)
30 -          if eof(input2) do
31 -            {input2 := reset(input2,"rand2.dat")}
32 -          end
33 - default : begin
34 -          write "'nWrong type entered."; abort
```

```
35 -          end
36 -
37 - if temp < 0 or temp > max.particle.size(type) do
38 -        {write "'nIncorrect particle size."; abort}
39 -
40 - let particle.size := temp
41 - particle.size
42 - end
43 -
44 - ! ********************
45 -   procedure fill.array
46 - ! ********************
47 - begin
48 -
49 - let name = "randomary.dat"
50 - let out = create(name,"s","a","v",256)
51 - let name1 = "partdist1.dat"
52 - let out1 = create(name1,"s","a","v",256)
53 - let name2 = "partdist2.dat"
54 - let out2 = create(name2,"s","a","v",256)
55 -
56 - let counter := 0
57 - while counter < (L-2)*(C-2)*(R-2) do
58 - begin
59 -     let type := choose.particle.type
60 -     let size := choose.particle.size(type)
61 -     for k = 1 to size do
62 -     begin
63 -      output out, type:3
64 -      count.3 := count.3 + 1
65 -      if count.3 = 15 do {output out, "'n"; count.3 := 0}
66 -      counter := counter + 1
67 -     end
68 -     no.of.particles.in.interval(type,size) :=
69 -             no.of.particles.in.interval(type,size) + 1
70 -     total.no.of.particles(type)
71 -                     := total.no.of.particles(type) + 1
72 - end
73 - close(out)
74 -
75 - write "'nMax particle size type 1", max.particle.size(1)
76 - write "'nMean particle size type 1", mean(1)
77 - write "'nNo. particles type 1", total.no.of.particles(1)
78 - write "'nMax particle size type 2", max.particle.size(2)
79 - write "'nMean particle size type 2", mean(2)
80 - write "'nNo. particles type 2", total.no.of.particles(2)
81 -
82 - for i1 = 1 to max.particle.size(1) do
83 - begin
84 -  for i2 = 1 to no.of.particles.in.interval(1,i1) do
85 -   begin
86 -    output out1, i1:3
87 -    count.4 := count.4 + 1
88 -    if count.4 = 15 do
89 -       {output out1, "'n"; count.4 := 0}
90 -  end
91 - end
92 - close(out1)
93 - count.4 := 0
94 - for i1 = 1 to max.particle.size(2) do
95 - begin
96 -  for i2 = 1 to no.of.particles.in.interval(2,i1) do
```

```
97 - begin
98 -  output out2, i1:3
99 -  count.4 := count.4 + 1
100 -  if count.4 = 15 do {output out2, "'n"; count.4 := 0}
101 - end
102 - end
103 - close(out2)
105 - let name.2 = "randomary.dat"
106 - let inp2 = open(name.2,"a",0)
107 - if inp2 = nullfile do{ write"The opening of",
108 -                 name," was unsuccessful.";abort}
109 -
110 - for iL = 2 to L-1 do
111 -    begin
112 -    for iR = 2 to R-1 do
113 -       begin
114 -       for iC = 2 to C-1 do
115 -        begin
116 -        let numb = readi(inp2)
117 -        case numb of
118 -        1 : count.1 := count.1 + 1
119 -        2 : count.2 := count.2 + 1
120 -        default : { write"'nOne of the data points in ",
121 -                    name," = ",numb,"'n" ; abort }
122 -        Array(iR,iC,iL) := numb
123 -        end
124 -       end
125 -    end
126 - close(inp2)
127 - end
```

Procedure CHOOSE.PARTICLE.TYPE reads in a 1 or 2 from RAND.DAT and outputs this integer, representing the particle type, to the main program section. CHOOSE.PARTICLE.SIZE uses the type selected above, opens the appropriate data file for this type (RAND1.DAT or RAND2.DAT) and reads the particle size from the opened file, passing it to the main program section. FILL.ARRAY now operates quite differently. Initially three data files, RANDOMARY.DAT, PARTDIST1.DAT and PARTDIST2.DAT are created. The former stores the geometrically distributed data required to fill the array, and the remaining two retain information on the distribution of particle sizes which are actually input into the array. A particle type is then selected (line 59), and an appropriate size chosen (line 60) using the two new procedures. The value of the type (1 or 2) is output size times to RANDOMARY.DAT by lines 62 to 67, where size is the particle size selected. Effectively, therefore, a particle of the required size has been output to this file. The appropriate counters are incremented (lines 68 to 71) and the procedures repeated until there are sufficient particles in RANDOMARY.DAT to fill the array.

Now the data corresponding to the type and size of the particles read into RANDOMARY.DAT are output to PARTDIST1.DAT and PARTDIST2.DAT (lines 75 to 103). The array is filled by reading the 1's and 2's back from RANDOMARY.DAT. This is slightly inefficient but prevents too many points being read into the array. Not shown after this are the usual lines which count the number of particles of each type in the array and calculate some of the parameters associated with it.

7.3 GEOMSIZE.COM

A few alterations were also required to produce the new command file GEOMSIZE.COM and Program 7 illustrates these changes. Essentially it is identical with THICKCH.COM initially, until the section where GLIM is invoked. The lines to do this (23 to 40 in Program 1) are omitted and replaced by the listed lines 26 to 36. These create DIM.DAT and then enter into MINITAB (line 32). The following three MINITAB commands instruct the package to carry out a batch of instructions stored in the file GEOM.MTB and then to stop and exit back to the command file. The execution of GEOMSIZE.S is then initiated. After completion of this, MINITAB is entered once more and the instructions stored in PARTDIST.MTB are executed and output to the file PARTDIST.LOG.

Program 7 - GEOMSIZE.COM.
Command programme to fill and process an array with a geometric size distribution of particles.

```
 1 - $!Main Command file GEOMSIZE.COM
 2 - $ set process/name = geomsize
 5 - $ on error then goto ABORT
 6 - $START:

     20 lines omitted

26 - $ open/write outfile dim.dat
27 - $ write outfile row
28 - $ write outfile col
29 - $ write outfile lay
30 - $ write outfile perc
31 - $ close outfile
32 - $ MINITAB
33 - BATCH
34 - EXECUTE 'GEOM.MTB'
35 - STOP
36 - $ run geomsize.exe

     29 lines omitted

66 - $ MINITAB
67 - BATCH
68 - OUTFILE 'PARTDIST.LOG'
69 - EXECUTE 'PARTDIST.MTB'
70 - STOP
71 - $ delete *tempdata.dat;*
72 - $ delete *data*.dat;*
```

```
73 - $ delete rand*.dat;*
74 - $ delete partdist*.dat;*
75 - $ purge dim.dat
76 - $ purge geomsize.log

    28 lines omitted

105 - $LEAVE:
106 - $ send me end
107 -   The job using the program geomsize.com is now finished.
108 - $stop
```

```
EXECUTE 'PARTDIST.MTB'
SET data from 'PARTDIST1.DAT' into C1
SET data from 'PARTDIST2.DAT' into C2
MEAN of C1
MEAN   =     4.8931
MAXIMUM value of C1
MAXIMUM =     25.000
HISTOGRAM of C1
Histogram of C1  N = 2581  Each * represents 20 obs.
  Midpoint      Count
         2        974    **************************************************
         4        619    *******************************
         6        331    ****************
         8        223    ***********
        10        162    *********
        12         93    *****
        14         59    ***
        16         45    ***
        18         30    **
        20         15    *
        22         10    *
        24         11    *
        26          9    *

MEAN of C2
MEAN   =     4.8988
MAXIMUM of C2
MAXIMUM =     25.000
HISTOGRAM of C2  Histogram of C2  N = 6176  Each * represents 45 obs.
  Midpoint      Count
         2       2223    **************************************************
         4       1440    ********************************
         6        899    ********************
         8        574    *************
        10        412    *********
        12        233    *****
        14        153    ***
        16         91    **
        18         76    *
        20         36    *
        22         19    *
        24         14    *
        26          6    *
END
STOP
```

Table 2.
Sample output from PARTDIST2.MTB showing shape of particle size distributions

The latter program, PARTDIST.MTB, is not listed, but simply reads in the data describing the distribution of particle sizes stored in PARTDIST1.DAT and PARTDIST2.DAT. Then it produces histograms depicting the distributions and also outputs the actual mean and maximum particle sizes found for each. This enables comparison with the previously defined values. Table 2 lists the output for one run of the program, and illustrates that the particles input into the array do indeed follow the required geometric distribution with the specified parameters (30% of 1's, Mean 5 and maximum particle size 25 for each distribution here).

8 VERTICAL FILLING MODIFICATIONS (UNIFSIZEV.S, GEOMSIZEV.S)

The above programs all fill the array sequentially by layers from the top to the bottom. Individual particles thus lie in horizontal planes perpendicular to the direction of processing through the array. In order to alter the orientation of the particles so that they are aligned along the direction of processing a minor adjustment was made to the program UNIFSIZE.S yielding UNIFSIZEV.S. This simply involved interchanging the lines 91 and 95 listed in PAC6.S (PROGRAM 2) above. The filling then starts at the top of the array and units are sequentially placed into the array in the direction towards the bottom base.

A similar switch was made to yield GEOMSIZEV.S from the normal geometric size distribution model.

9 CONCLUSIONS AND FURTHER WORK

The set of computer programs which simulated MPE, percolation and intermediate situations have here been modified in a variety of different fashions to produce some important new programs. The construction and operation of these programs has been described above.

Initially the four programs of Harris [2] were reprogrammed as a single simpler and more efficient program PAC6.S, which could carry out all the functions of the originals. It also produced more concise written output and extended the facility for graphical output.

The manner in which this program processed the array simulating the MPE was then altered to allow simulation of 8 and 12 coordination lattices (PAC8.S and PAC12.S) by adjustment of the particles which were considered to surround a central particle. The output was further augmented to allow collection of the extra data now available.

The next modification considered the production of a concentration gradient across the thickness of the MPE. This was achieved by rewriting the main command file to a new form (GRADDIST.COM) which created a data file consisting of a series of sections of different overall percentage compositions. A new program, TRUNCATE.S, was used in conjunction with this to reduce the amount of data to the exact number of points necessary to fill an individual section.

The procedure which fills the array was then rewritten so that the relative sizes of the two components comprising the array could be varied. The main controlling program was extended to allow input of parameters defining the relative sizes and to permit operation evenly over the full composition range.

Next a further modification was made to produce a distribution of particle sizes for each component. This involved creating a new random number generating program (GEOM.MTB), using the MINITAB statistical package, to produce data in the required format. Considerable modifications were made to the array filling procedure to permit the data to be input into the array as particles forming the desired geometric distribution. A new command file (GEOMSIZE.COM) was altered to cope with the new filling program (GEOMSIZE.S) and the use of MINITAB.

Lastly the direction of lattice filling was altered in the uniform and geometric size distribution programs to simulate a vertical orientation of particles in the lattice.

The adaptions described above, in particular the geometric size distribution of particles, were consecutive improvements to the original model aiming ultimately towards the development of a more realistic model, in which the particles of the two components are of irregular shape and non-uniform size. The procedure to construct an array such as this is much more complicated than those already described, since it must fill the array non-sequentially unlike the above models. In the model envisaged a position in the array is selected at random, and checked to see if it is empty. If so the surrounding positions are tested to discover if a particle of a selected size can be fitted, and it is fitted if this is the case. If not another starting point is chosen and the process repeated. The procedure is still systematic to a limited extent, in that the larger particles are fitted first and there is a restriction placed on the number of attempts made to fit a particle. This reduces the CPU time necessary to a reasonable level. Most of the procedures are written to allow this to be achieved and their testing and expansion to a full program is underway. The usual processing and counting procedures will still be applicable but now the number of voids in the lattice must also be considered.

The other problems suggested in the concluding section of Chapter 3 are conceptually more accessible and the translation to workable programs is likely to be relatively straight forward.

10 REFERENCES

1 Nairn I.A. "The Study Of Mixed Phase Electrodes In Solid State Cells", Ph.D. Thesis University Of St. Andrews (1984)

2 Harris K.D.M. "A Computer Study Of Mixed Phase Electrodes", Unpublished Work for a Carnegie Trust Report (1984)

3 Stauffer D. "Introduction To Percolation Theory", Publ. Taylor & Francis Ltd. (1985)

1 INTRODUCTION

Various theoretical treatments of mixed phase electrodes or similar heterogeneous systems have been developed. The theory of porous electrodes is well characterised[1,2] and more recently Atlung's models of intercalation systems with liquid electrolytes[3,4] have helped in the understanding of the behaviour of more modern battery systems. The most important theory devoted to mixed phase electrodes is that developed by Atlung.[5,6] Based on Newman and Tobias' heterogeneous porous electrode theory[2] Atlung derived analytical expressions to describe the distribution of potential in a composite electrode and hence permitted the discharge curve to be calculated under certain simplifying conditions. In essence he demonstrated that a composite electrode behaves essentially as an electrode of the pure insertion material but with an enhanced apparent chemical diffusion coefficient (D_c) of metal ions in the bulk of the electrode. This diffusion coefficient is dependent on parameters of the mixed phase electrode as a whole. Assuming a high constant electronic conductivity of the material this dependence is given by:-

$$D_c = \frac{kS}{F\upsilon C_0} \quad \ldots\ldots 1$$

where k is related to the EMF versus composition curve of the insertion material, C_O is the saturation concentration of the inserted metal ions, V is the volume fraction of the electrode component and S is the effective ionic conductivity of the MPE region. (The effective ionic conductivity is the ionic conductivity of the pure electrolyte allowing for such factors as the tortuosity and the volume fraction when incorporated into the MPE.)

Potentially therefore a number of factors can affect the apparent chemical diffusion coefficient of metal ions within the MPE. Firstly from equation 1 altering the conductivity of the electrolyte should change S and consequently D_C. The effective conductivity could also be altered by changing the particle size of either component, the relative volume fractions or the manufacturing conditions of the cell since all of these alter the tortuosity.

This chapter reports the results of a study in which the electrochemical characteristics of a typical mixed phase electrode consisting of a silver ion-conducting glass electrolyte and niobium disulphide electrode material are systematically varied and the effect on the apparent chemical diffusion coefficient measured. Variations in intercalation level, glass conductivity, particle size, electrode thickness and composition are all considered.

2 EXPERIMENTAL ANALYSIS

Full details of the experimental techniques for applying galvanostatic pulses and measuring the associated potential changes have been described in Chapter 2. There is a number of ways of interpreting the potential transient response resulting from such constant current pulses.

For simple semi-infinite linear diffusion[7] a strict $t^{1/2}$ dependence is expected for the overpotential during current passage, where t is the time for which the current has been applied. More complex behaviour can be predicted under other diffusion conditions e.g. spherical or cylindrical diffusion. Nairn et al[8] have previously demonstrated that in similar systems consistent analysis of such pulse data is possible within a particular range of pulse durations (< 1 s). Nairn[7] however observed systematic trends in the fitted parameters as the pulse length is increased.

In contrast for much longer pulses (100 - 5000 s) excellent linearity is found for plots of the overpotential versus time for both forward and reverse pulses.

Anomalous behaviour at short times during a galvanostatic pulse has also been observed by Atlung[9] who ascribes the effect to contact problems between the pure electrolyte and the MPE electrode. If contact is not uniform, diffusion in the MPE will be non-linear near this boundary resulting in a higher gradient until the diffusion front has levelled out. As a consequence in the present study measurements of overpotential during the first 20 - 100 s have been discarded from the analysis.

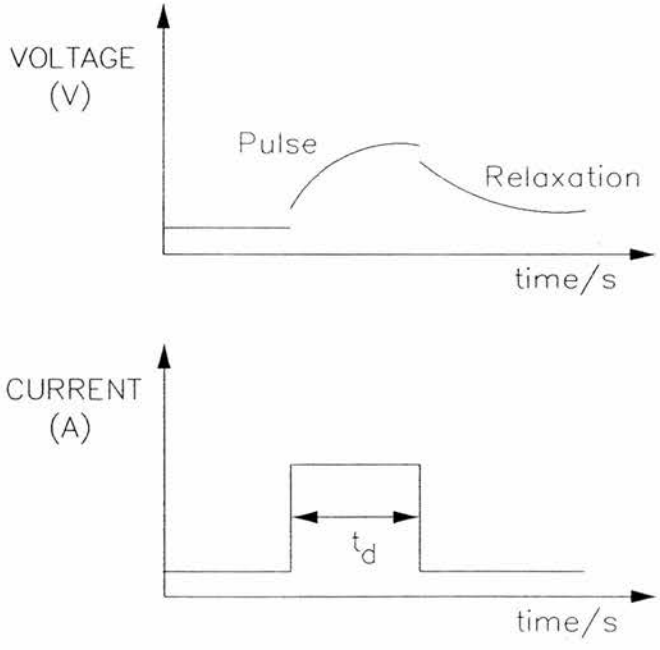

Figure 1. The effect on overpotential of applying a galvanostatic pulse.

On completion of a current pulse the voltage relaxes back towards its equilibrium value (see Figure 1) due to redistribution within the MPE without transport across the electrolyte/MPE boundary. This process is therefore independent of the uniformity of contact at this boundary. For such a relaxation Atlung has shown[9] that the gradient of the overpotential versus $\sqrt{t} - \sqrt{(t - t_d)}$ where t_d is the pulse length, should also be linear.

From Fick's laws it may be shown that for a constant current I flowing in an MPE :-

$$D_c = \frac{4I^2k^2d^2}{n^2a^2} \quad \ldots\ldots 2$$

where d is the thickness of the MPE region, a is the gradient of the overpotential versus time parameter curve ($t^{1/2}$ for the pulse, $\sqrt{t} - \sqrt{(t - t_d)}$ for the relaxation. $k = dE/dQ$ where dE is the change in overpotential associated with the passage of total charge dQ during the pulse.

For the pulse, classical semi-infinite diffusion theory yields the equation:-

$$D_c = \frac{4I^2V_m^2k^2}{n^2F^2A^2a^2} \quad \ldots\ldots 3$$

where I is the current passed, V_m is the molar volume of the solid solution electrode component of the MPE, F is Faraday's constant, A the interfacial area between electrode and electrolyte components of the MPE and a the gradient of the overpotential versus root time plot. k is now dE/dx where dx is the change in intercalation level caused by the galvanostatic pulse. In this equation however an estimate for the area A must be used. This is usually taken to be the geometric area of the cell. However the actual diffusion coefficient of the metal ion in the electrode structure is measured rather than the apparent value in the MPE.

There is a number of different ways of obtaining a value for k. When using the semi-infinite diffusion equation (3) previous workers[8] have used the gradient (dE/dx) of the discharge curve for the electrode material being studied. This is measured on a single sample cell. However this makes the assumption that all subsequent test cells are identical to the one used to measure dE/dx. Alternatively a possibility is to measure dE/dx for the cell under examination, for example during the long intercalation pulse, and use this value in all subsequent experiments on that cell only. In both these cases it is straightforward to convert the measured dE/dx value to dE/dQ when the composition of the composite electrode is known. Thus equation 2 can be used in any analysis as well as the semi-infinite diffusion case.

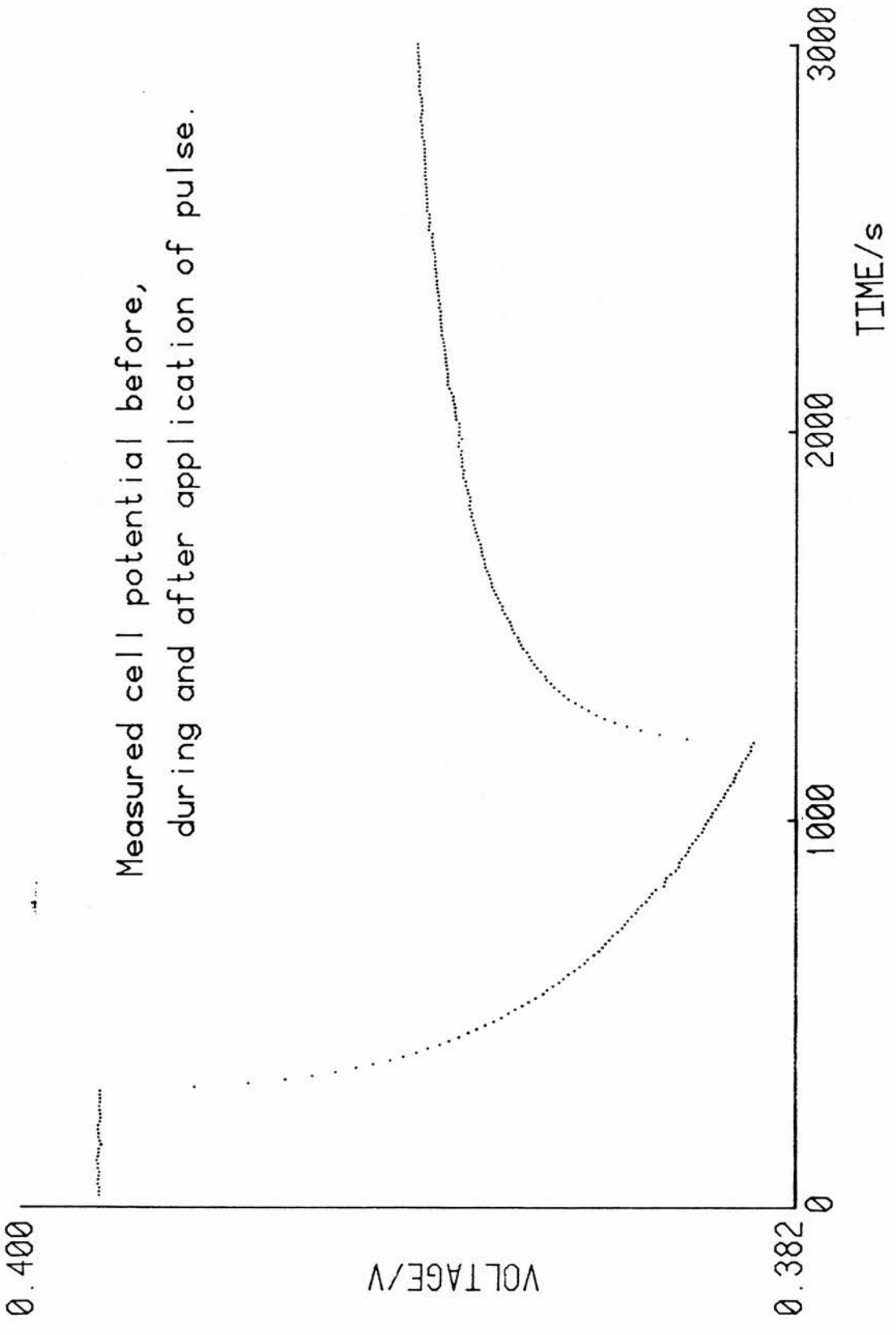

Figure 2.
Typical measured potential versus time behaviour.

In contrast Atlung recommends[9] that dE/dQ is measured for individual pulses. This eliminates any variations in tortuosity and surface area from cell to cell. In conjunction with measurement of the thickness of the MPE the apparent chemical diffusion coefficient (D_C) can be calculated from equation 2 with no assumptions as to the surface area.

In this examination the value of k was measured by all three different techniques and these were compared to ascertain which gave the most consistent results using both Atlung's analysis and the semi-infinite diffusion equation.

In this and subsequent data the following nomenclature has been used :-

a) $D_C(pulse)$ - the apparent diffusion coefficient measured for the pulse using Atlung's method of analysis,

b) $D_C(relax)$ - the apparent chemical diffusion coefficient measured for the relaxation using Atlung's analysis.

c) $D_C(semi)$ - the diffusion coefficient calculated using the semi-infinite diffusion equation 3.

If nothing else is indicated then the value of k (be it dE/dx or dE/dQ) has been calculated on the individual pulse. If k_C is given then k has been measured on the individual cell during the initial long intercalation pulse and if k_{ave} is mentioned then the gradient of the discharge curve of a sample cell (as in Chapter 2) has been used.

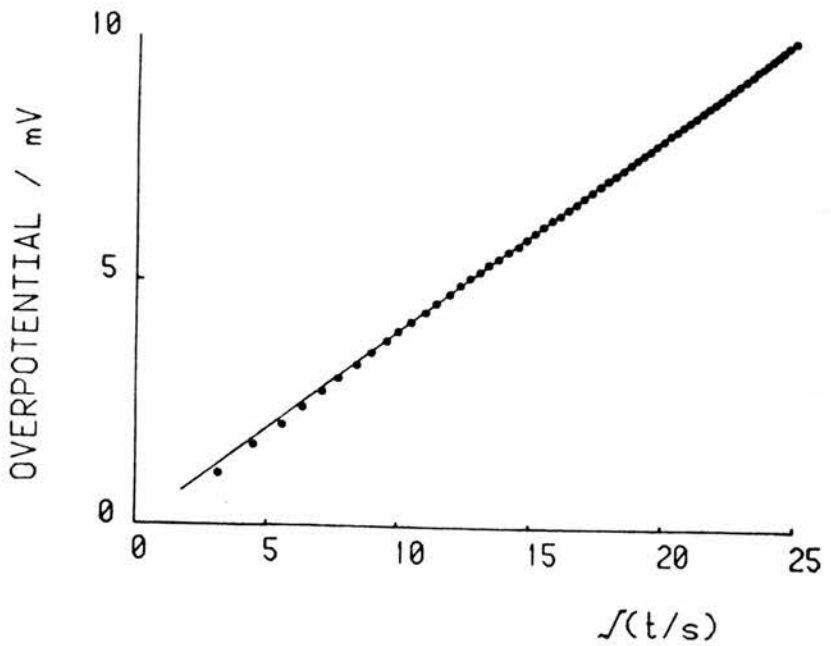

Figure 3.
Typical plot of overpotential versus $t^{1/2}$ during a current pulse.

Figure 2 illustrates the typical potential versus time response measured on a sample cell during and after the application of a 10 μA pulse for 900 s. Figures 3 and 4 show respectively the overpotential versus root time parameter plots for the pulse and relaxation obtained after analysis of the data recorded for the above pulse.

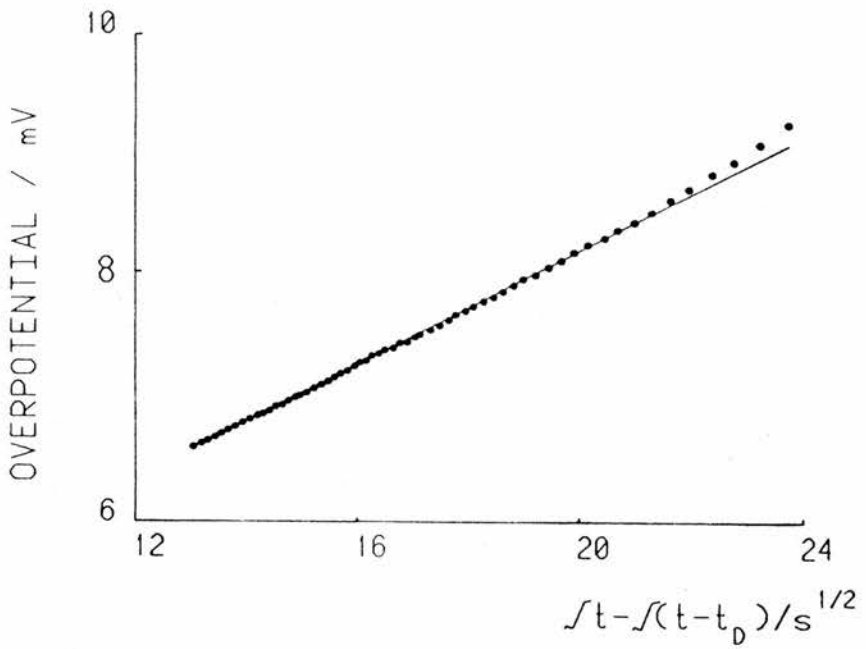

Figure 4.
Typical plot of overpotential versus $\sqrt{t}-\sqrt{(t-t_d)}$ following a constant current pulse.

Appendix 1 details how the results were analysed using various computer programmes to manipulate the data and calculate the required gradients . The values of D_C for pulse and relaxation using the different methods of measuring k were calculated using a computer spreadsheet package (Lotus 123). The spreadsheet set up is also described in Appendix 1.

3 THE EFFECT OF INTERCALATION LEVEL

During the measurement of the intercalation discharge curve for NbS_2 (as described in Chapter 2) a full analysis of the pulse data was performed. This allowed the effect on the apparent diffusion coefficient of the intercalation level to be examined. It also gave an insight into the consistency of the pulse technique and permitted a comparison of the different analysis methods described above. Table 1 details all the results obtained using Atlung's method of analysis (Equation 2) while Table 2 lists the equivalent results for the same pulses using the semi-infinite diffusion analysis.

	A		B		C	
Initial Silver level	$D_C(Pulse)$ (cm^2s^{-1})	$D_C(Relax)$ (cm^2s^{-1})	$D_C(Pulse)$ k_C (cm^2s^{-1})	$D_C(Relax)$ k_C (cm^2s^{-1})	$D_C(Pulse)$ k_{ave} (cm^2s^{-1})	$D_C(Relax)$ k_{ave} (cm^2s^{-1})
0%	3.2×10^{-8}	3.0×10^{-8}	1.6×10^{-8}	1.5×10^{-8}	1.4×10^{-8}	1.3×10^{-8}
1%	1.2×10^{-8}	5.5×10^{-9}	2.2×10^{-8}	1.0×10^{-8}	1.9×10^{-8}	9.1×10^{-9}
2%	1.6×10^{-8}	3.3×10^{-9}	2.8×10^{-8}	6.1×10^{-9}	2.5×10^{-8}	5.3×10^{-9}
3%	1.5×10^{-8}	6.8×10^{-9}	1.5×10^{-8}	6.7×10^{-9}	1.3×10^{-8}	5.8×10^{-9}
4%	9.9×10^{-9}	3.6×10^{-9}	1.8×10^{-8}	6.7×10^{-9}	1.6×10^{-8}	5.8×10^{-9}
5%	2.0×10^{-8}	9.7×10^{-9}	1.8×10^{-8}	8.8×10^{-9}	1.6×10^{-8}	7.5×10^{-9}
6%	2.2×10^{-8}	1.4×10^{-8}	1.6×10^{-8}	1.0×10^{-8}	1.4×10^{-8}	8.7×10^{-9}
7%	3.7×10^{-8}	1.8×10^{-8}	2.2×10^{-8}	1.1×10^{-8}	2.0×10^{-8}	9.3×10^{-9}
8%	2.7×10^{-8}	9.3×10^{-9}	2.8×10^{-8}	1.0×10^{-8}	2.5×10^{-8}	8.7×10^{-9}
9%	3.3×10^{-8}	2.4×10^{-8}	2.8×10^{-8}	2.0×10^{-8}	2.5×10^{-8}	1.8×10^{-8}
10.5%	1.4×10^{-5}	4.8×10^{-5}	3.0×10^{-9}	1.0×10^{-8}	2.6×10^{-9}	8.7×10^{-9}
10.5%	4.9×10^{-7}	2.4×10^{-6}	2.0×10^{-9}	1.0×10^{-8}	1.8×10^{-9}	8.7×10^{-9}
Mean D_C	2.2×10^{-8}	1.2×10^{-8}	2.1×10^{-8}	8.7×10^{-9}	1.9×10^{-8}	9.1×10^{-9}
S.D.	9.5×10^{-9}	8.9×10^{-9}	5.4×10^{-9}	3.5×10^{-9}	4.7×10^{-9}	3.7×10^{-9}
S.D./Mean	0.42	0.72	0.26	0.40	0.25	0.41

Table 1.
Apparent chemical diffusion coefficients versus intercalation level calculated using equation 2. dE/dQ measured on A - pulse, B - cell during intercalation, C - sample cell.

Some interesting points emerge from examination of the data. Firstly for all the pulses used in producing the discharge curve (initial silver level 0 - 9 %) the data is remarkably consistent. These pulses all used the same current (10 μA) and lasted approximately 3600 s. There is some fluctuation in the results (a factor of 3-4 from the lowest D_C value to the highest) but no order of magnitude variation.

None of the analysis methods show any trend in diffusion coefficient as the intercalation level is increased. This is consistent with previous results where changes are observed only at very low intercalation levels[10] and at higher intercalation levels due to phase changes.[11]

	A	B	C
Initial Silver level	$D_C(semi)$ (cm^2s^{-1})	$D_C(semi)$ k_C (cm^2s^{-1})	$D_C(semi)$ k_{ave} (cm^2s^{-1})
0%	4.0×10^{-9}	2.1×10^{-9}	1.7×10^{-9}
1%	1.4×10^{-9}	2.9×10^{-9}	2.4×10^{-9}
2%	1.9×10^{-9}	3.7×10^{-9}	3.0×10^{-9}
3%	1.8×10^{-9}	1.9×10^{-9}	1.6×10^{-9}
4%	1.2×10^{-9}	2.3×10^{-9}	1.9×10^{-9}
5%	2.5×10^{-9}	2.3×10^{-9}	1.9×10^{-9}
6%	2.7×10^{-9}	2.1×10^{-9}	1.7×10^{-9}
7%	4.7×10^{-9}	2.9×10^{-9}	2.4×10^{-9}
8%	3.2×10^{-9}	3.7×10^{-9}	3.0×10^{-9}
9%	4.0×10^{-9}	3.7×10^{-9}	3.0×10^{-9}
10.5%	1.8×10^{-6}	3.9×10^{-9}	3.2×10^{-10}
10.5%	6.0×10^{-8}	2.6×10^{-10}	2.1×10^{-10}
Mean D_C	2.8×10^{-9}	2.8×10^{-9}	2.3×10^{-9}
S.D.	1.2×10^{-9}	7.0×10^{-10}	5.7×10^{-10}
S.D./Mean	0.44	0.25	0.25

Table 2.
Chemical diffusion coefficient versus intercalation level calculated using semi-infinite diffusion analysis.

There are clear differences however between the results obtained from the different analysis techniques. The apparent diffusion coefficients obtained from the relaxations are generally 2-3 times smaller than those measured for the pulse. Although this difference may not be significant with respect to the variations observed over a series of pulses and the possible experimental errors it was generally observed. The main reason for this discrepancy in diffusion coefficient between the pulse and the relaxation probably lies in the calculation of the gradient of the overpotential versus root time parameter curve. The gradient obtained for the overpotential/time parameter curves was generally lower for the relaxation than for the pulse. It was more difficult to analyse the data of overpotential

versus $t^{1/2}$ plotted for the pulse since the data frequently exhibited marked curvature. There was a longer time interval before linearity was achieved and the best fit straight line had larger confidence limits.

Means and standard deviations (S.D.) were calculated on each of the columns of diffusion coefficients. These are given at the end of Tables 1 and 2 together with the ratio of standard deviation to mean. To one significant figure each of the analysis using Atlung's method gave the average $D_C(pulse)$ to be 2×10^{-8} cm^2s^{-1} while $D_C(relax)$ was 1×10^{-8} cm^2s^{-1}.

In all cases the ratio of standard deviation to mean is smaller for the pulse than for the relaxation indicating less spread of results in the former case. When using the analysis based around measuring dE/dQ on the actual pulse the ratio of standard deviation to mean is larger than using either of the other methods based on a longer pulse performed on the individual cell or on the average value obtained for the NbS_2. There is generally very little difference in the results between using k_C or k_{ave}. The major source of errors in these measurements is in the value of dE/dQ where particularly for smaller pulses the overall potential change is often reasonably small compared with the errors in the measurement technique.

Using the semi-infinite diffusion equation for calculating D_C gives results consistently an order of magnitude lower than using Atlung's method. This presumably is attributable to the estimation of interfacial area used in the calculation. However the conclusions regarding the standard deviations for each of the analysis techniques are reaffirmed in this data. Longer pulses give more reproducible results.

This is illustrated in the last two results quoted in each table where shorter pulses (900 s) of the same current size were applied to the cell after intercalation to 10.5 % The dE values in either case were very small and the calculated diffusion coefficients are considerably larger than those measured before.

4 THE EFFECT OF CONDUCTIVITY

Initial results[12] of D_C measurements from cathodes consisting of either MPE systems composed of glasses with a range of conductivities or of pure $Ag_{0.05}NbS_2$ are reported in Table 3. Each value of D_C quoted is the average of several transients associated with both forward and reverse pulses. Most pulse are 10uA lasting for around 1000 s. All diffusion coefficients are calculated using Atlung's method of analysis and dE/dQ based on the individual pulse.

Glass Composition [x(AgI)]	Conductivity at 50°C (Scm^{-1})	$D_c(Pulse)$ (cm^2s^{-1})	$D_c(Relax)$ (cm^2s^{-1})
0.79	9.7×10^{-3}	2.5×10^{-8}	1.7×10^{-7}
0.79	9.7×10^{-3}	1.9×10^{-8}	4.0×10^{-8}
0.50	3.5×10^{-4}	3.0×10^{-8}	1.6×10^{-8}
0.30	3.5×10^{-5}	3.8×10^{-8}	6.6×10^{-8}
0.10	2.6×10^{-6}	4.2×10^{-8}	2.1×10^{-7}
0.10	2.6×10^{-6}	4.7×10^{-8}	2.1×10^{-7}
$Ag_{0.05}NbS_2$	-	1.6×10^{-9}	3.0×10^{-9}

Table 3.
Measured Apparent Chemical Diffusion Coefficients as a function of glass composition.

These results indicate that there is a clear increase in the apparent chemical diffusion coefficient by a factor of 20-30 for the MPE systems in comparison with the electrode of pure $Ag_{0.05}NbS_2$. However there is no discernible dependence on the conductivity of the glass as expected from the theoretical equation for D_c. If the results are considered using k_c (or similarly k_{ave}) then the results in Table 4 are obtained. These are the average values for the same pulses as before.

Glass Composition [x(AgI)]	Conductivity at 50°C (Scm^{-1})	$D_c(Pulse)$ k_c (cm^2s^{-1})	$D_c(Relax)$ k_c (cm^2s^{-1})
0.79	9.7×10^{-3}	2.8×10^{-9}	1.2×10^{-8}
0.79	9.7×10^{-3}	1.5×10^{-8}	5.5×10^{-9}
0.50	3.5×10^{-4}	4.4×10^{-9}	7.0×10^{-9}
0.30	3.5×10^{-5}	9.3×10^{-9}	1.1×10^{-8}
0.10	2.6×10^{-6}	8.3×10^{-10}	2.8×10^{-9}
0.10	2.6×10^{-6}	3.2×10^{-9}	7.9×10^{-9}
$Ag_{0.05}NbS_2$	-	1.1×10^{-8}	2.5×10^{-8}
Al_2O_3	-	5.9×10^{-11}	3.6×10^{-11}
B5 TOT	-	1.8×10^{-12}	1.3×10^{-12}

Table 4.
Measured apparent chemical diffusion coefficients as a function of conductivity using dE/dQ measured on the long intercalation pulse.

There is still no significant difference in diffusion coefficients due to the change in conductivity of the glasses but now there is no improvement seen when comparing the use of a composite electrode with the pure electrode of $Ag_{0.05}NbS_2$.

These results emphasize the necessity of using a consistent correct technique for analysing results. In Atlung's method the largest errors seem to be associated with the measurement of dE. this is particularly true for small intercalation changes (very small currents or short times) where changes in cell potential can be very close to the error associated with making such measurements.

The similarity between the apparent chemical diffusion coefficient values for the composite electrode and the pure $Ag_{0.05}NbS_2$ suggest that the diffusion mechanism is the same in each case. The predominant process in all cases must be the diffusion of metal ions within the individual NbS_2 crystals.

Two other experiments were attempted to investigate the effect of conductivity changes. In the first the glass electrolyte in the MPE was replaced by an electrical insulator (Al_2O_3) and secondly the three electrode cell was constructed entirely with the lowest conductivity glass (B5 TOT).

In neither case could even small currents ($< 1\ \mu A$) be sustained for even short times without unacceptably large overpotentials developing. Apparent diffusion coefficients were calculated of both cells (but on these very short, low current pulses) and yielded values 100 - 1000 times smaller than before (see Table 4). This demonstrates that the glassy component in the composite electrode is being efficient in transporting ions throughout the depth of the composite since when it is replaced by an insulating component (cell Al_2O_3) diffusion coefficients are significantly reduced. In the latter case (B5 TOT) the effectiveness of using high conductivity glasses in the electrolyte region of the three-electrode cell is demonstrated.

5 THE EFFECT OF PARTICLE SIZE

In the above experiments the NbS_2 and electrolyte in the composite electrode had particle sizes in the range 125 - 175μm taken form the middle of the seven sieves. In the next experiments glass and niobium disulphide particle sizes of $< 45\mu m$ (from the bottom sieve) were used to examine whether this had an effect on the diffusion coefficient measured. Atlung's earlier work on solid solution electrodes with liquid electrolyte[3] suggest that the particle size is crucial in determining the discharge

characteristics of the electrode. Deroo et al.[13] have also demonstrated a theoretical dependence of the discharge curve on the particle size and distribution with optimum particle sizes being certainly less than 10 μm for complete first cycle discharge.

The effect of conductivity was again measured with the smaller particle size electrode material, although this time only the lowest and highest conductivity glasses were employed. Table 5 reports the results obtained. These are again the average of a number of pulses all resulting in a change of intercalation level of at least 1%.

Conductivity at 50°C (Scm^{-1})	Particle size (μm)	$D_C(Pulse)$ k_C (cm^2s^{-1})	$D_C(Relax)$ k_C (cm^2s^{-1})
9.7×10^{-3}	< 45	4.6×10^{-8}	4.0×10^{-8}
2.6×10^{-6}	< 45	3.5×10^{-10}	2.5×10^{-10}
9.7×10^{-3}	125 - 175	8.5×10^{-9}	8.9×10^{-9}
2.6×10^{-6}	125 - 175	3.2×10^{-9}	7.8×10^{-9}

Table 5.
Apparent Chemical Diffusion Coefficients as a function of particle size and conductivity

With the smaller particle size there is now an obvious two orders of magnitude difference in the apparent chemical diffusion coefficient between the low and high conductivity glasses. This *is* now in agreement with the predictions made by Atlung.[5,6]

The low conductivity glass with small particle size has an apparent chemical diffusion coefficient an order of magnitude lower than that observed with the larger particles. The diffusion process is obviously now dependent on the passage of ions through the electrolyte particles in the MPE and not just through the NbS_2 crystals.

The apparent diffusion coefficient measured for the high conductivity glass shows a five times increase using the smaller particles. Although possibly within experimental error this value is higher than those measured on the cells containing the larger particles. Again this increase in apparent chemical diffusion coefficient provides some indication of the benefits which can be obtained by optimising the mixed phase electrode not only in terms of the conductivity of the electrolyte but also in terms of the particle size of the electrode material.

These results, together with the above examination of the effect of conductivity, demonstrate a number of features. Firstly, as Atlung predicts there is a dependence of apparent diffusion coefficient on the effective ionic conductivity of the mixed phase electrode. However, this is dependent on utilising a small electrode particle size. As with previous work[3,13] this particle size allows full benefits and utilisation to be achieved from an electrode system. In the previous example where all particle sizes were large the measured apparent diffusion coefficient is obviously dominated by the diffusion coefficient of silver ions into the large niobium disulphide crystals. Any effects due to the increased surface area in the MPE are negligible by comparison. Secondly it re-emphasises the necessity for consistent preparation and experimental conditions in order to give reproducible measurements of the apparent chemical diffusion coefficients.

6 THE EFFECT OF ELECTRODE THICKNESS

In the next set of experiments cells were constructed with a composite electrode ca. five times the thickness used in the other experiments. (ca. 1 mm rather than 0.2 - 0.3 mm). Low and high conductivity glasses were used with particle sizes being 125 - 175 μm once more. The results are detailed in Table 6.

Conductivity at 50°C (Scm^{-1})	Thickness (mm)	$D_C(Pulse)$ k_C cm^2s^{-1}	$D_C(Relax)$ k_C cm^2s^{-1}	$D_C(Pulse)$ (k_{ave}) cm^2s^{-1}	$D_C(Relax)$ (k_{ave}) cm^2s^{-1}
9.7×10^{-3}	0.2	1.8×10^{-8}	6.7×10^{-9}	1.6×10^{-8}	5.8×10^{-9}
9.7×10^{-3}	1.0	2.0×10^{-6}	7.5×10^{-6}	2.9×10^{-8}	1.0×10^{-7}
2.6×10^{-6}	0.2	1.1×10^{-8}	1.6×10^{-9}	7.2×10^{-9}	1.1×10^{-9}
2.6×10^{-6}	1.0	2.0×10^{-7}	6.3×10^{-7}	1.4×10^{-8}	4.5×10^{-8}

Table 6.
Apparent chemical diffusion coefficients as a function of thickness.

These results are anomalous in some ways but also reveal some interesting points. The major anomaly lies in the difference in calculated D_C values between the results using the measured (k_{ave}) for the reference NbS_2 cell and for that measured during the intercalation pulse on the individual cell (k_C). This is the only set of data where significant differences are noticed. One possible reason is that k_C may be considerably in error as the thick cell takes longer before reaching potential equilibrium.

Now there is some evidence once more of differences between the low and high conductivity electrolyte glasses. The diffusion coefficient measured for the high conductivity glass is in general an order of magnitude larger than for the low conductivity glass. It seems that the increase in electrode/electrolyte contact area bestowed by increasing the electrode thickness begins to override the domination of the large NbS_2 particles on the diffusion coefficient.

In addition the apparent diffusion coefficient measured for the thicker electrode is larger than for the thin electrode and also larger than the thin electrode of pure NbS_2. This suggests that, in this case, there is a beneficial effect of using a composite working electrode compared with an electrode of the pure NbS_2. This result also correlates with that obtained from the computer model (Chapter 3) where increasing the thickness of the MPE yields a proportionate increase in the area of contact between the electrode and electrolyte particles. Obviously the composite here is not thick enough for iR drop and tortuosity effects to be significant.

Another obvious effect highlighted on these thick cells is a dependence of D_C on the current applied during the pulse - the larger the current, the greater the measured D_C (as illustrated in Table 7). This was also observed with other cells though such a large range of currents was not used. Nairn[15] has previously reported a similar phenomenon on the same system.

Current	Time (s)	$D_C(Pulse)$ k_C cm^2s^{-1}	$D_C(Relax)$ k_C cm^2s^{-1}	$D_C(Pulse)$ k_{ave} cm^2s^{-1}	$D_C(Relax)$ k_{ave} cm^2s^{-1}
10	900	4.3×10^{-7}	3.9×10^{-7}	5.5×10^{-9}	5.46×10^{-9}
10	900	2.5×10^{-7}	2.7×10^{-7}	3.5×10^{-9}	3.74×10^{-9}
100	900	9.0×10^{-6}	4.6×10^{-6}	1.3×10^{-7}	6.41×10^{-8}
1000	900	3.6×10^{-5}	1.7×10^{-5}	5.0×10^{-7}	2.43×10^{-7}
10	900	2.0×10^{-7}	6.3×10^{-7}	1.4×10^{-8}	4.53×10^{-8}
100	900	1.0×10^{-7}	4.0×10^{-7}	7.2×10^{-9}	2.90×10^{-8}
1000	900	4.0×10^{-6}	4.0×10^{-6}	2.8×10^{-7}	2.83×10^{-7}

Table 7.
Measured diffusion coefficients at varying amplitudes of current.

The larger currents give rise to much greater overpotentials in the cell which may impose a different diffusion mechanism on the cell, e.g. grain boundary or surface diffusion may become significant. This again demonstrates a need for exact duplication of experimental conditions in order to achieve reproducible and comparable diffusion measurements.

7 THE EFFECT OF COMPOSITION

The last set of experiments undertaken investigated the effect on D_C of the composition of the MPE. All experiments were performed under similar conditions to Nairn[15] who has reported a variation in D_C with composition as illustrated in Figure 5. i.e. All pulses were 20 μA and of 2000 s duration. Preparation conditions were identical except for the restriction of particle size used here.

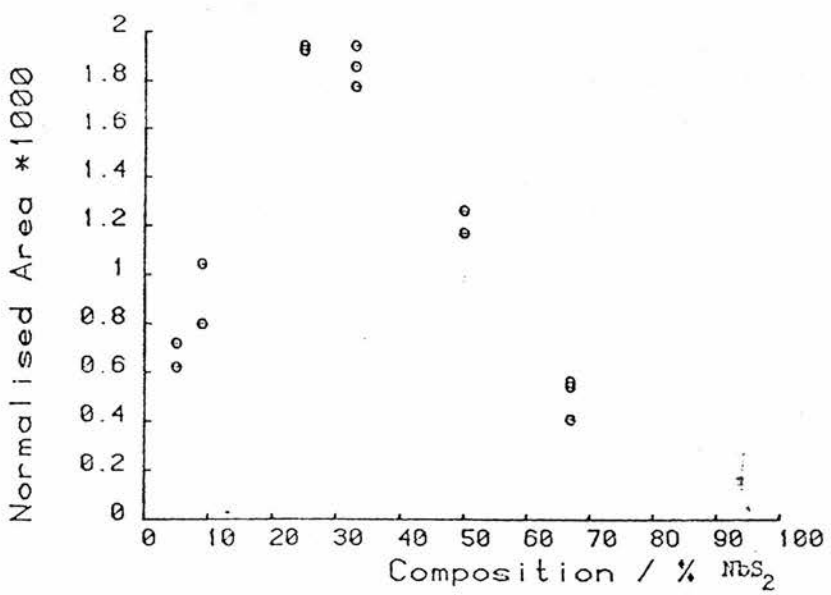

Figure 5.
Variation of diffusion $AD^{1/2}$ with MPE composition as observed by Nairn.[7]

The results are outlined in Table 8 (using the D_C values calculated with k_C) and depicted graphically in Figure 6. It was found to be very difficult to intercalate a cell with only 10 % NbS_2 present and four cells were made before a working cell was produced. This was thought to be because 10 % of niobium disulphide is well below the percolation threshold thus giving only very small conducting paths close to the pure electrolyte component in the cell.

Clearly from the results the composition of the working electrode has no effect on the apparent chemical diffusion coefficient observed, under the experimental conditions used here. This is in contradiction of the results observed by Nairn. Again the likeliest explanation is that the diffusion process is dominated by the diffusion within the NbS_2 component of the MPE.

Percentage of NbS_2	$D_C(Pulse)$ k_C cm^2s^{-1}	$D_C(Relax)$ k_C cm^2s^{-1}
10%	9.6×10^{-9}	1.8×10^{-8}
32%	3.3×10^{-8}	2.3×10^{-8}
35%	1.5×10^{-8}	5.5×10^{-9}
40%	8.7×10^{-8}	3.0×10^{-8}
50%	2.8×10^{-8}	5.9×10^{-8}
60%	3.1×10^{-8}	8.0×10^{-9}
70%	1.1×10^{-8}	1.6×10^{-8}
80%	3.6×10^{-8}	1.4×10^{-8}
100%	1.1×10^{-8}	2.5×10^{-8}

Table 8.
Apparent chemical diffusion coefficients as a function of NbS_2 fraction.

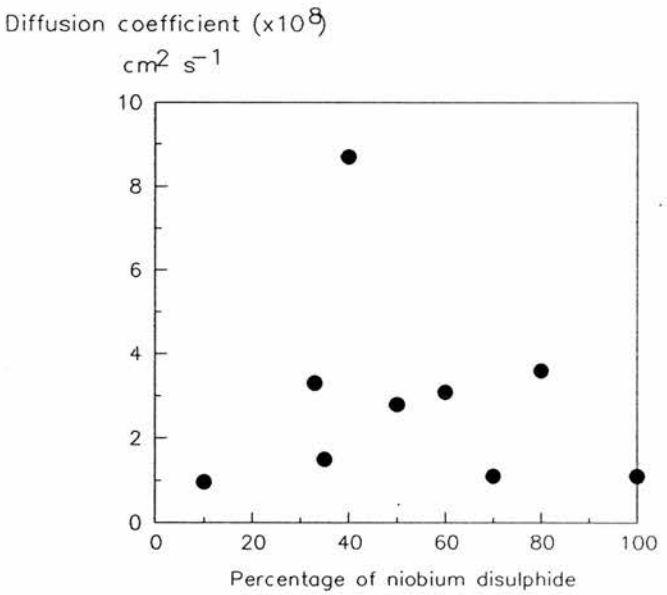

Figure 6.
Dependence of diffusion coefficient on composition of the MPE.

In addition any small effects may be masked by the errors involved in the measurement of the diffusion coefficients. The difference observed by Nairn was only of one order of magnitude, a figure of the same scale as potential errors in the measurements made in this investigation. In addition he quotes a parameter ($AD^{½}$) which contains an area term. As the percentage of NbS_2 increases the interfacial contact area between the electrode and the electrolyte will increase to a maximum and then decrease therefore the type of curve reported by Nairn is likely to occur if the diffusion coefficient is constant.

8 CONCLUSIONS AND FURTHER WORK

The work described in this Chapter has highlighted a number of interesting points associated with measuring apparent chemical diffusion coefficients of mixed phase electrodes and in the dependence of the measured diffusion coefficients on parameters of the mixed phase electrode.

Most importantly the necessity of clearly defining both experimental conditions (in terms of particle size, current and pulse length) and the analysis technique used for comparative evaluations has been demonstrated.

The analysis technique suggested by Atlung shows decided disadvantages in the inconsistency of dE/dQ measurements and also in the time taken for potential equilibrium between application of pulses. However using the same analysis and a dE/dQ measurement taken once on the cell, e.g. on the initial intercalation pulse (as in these experiments), yields more consistent results. This also enables the equilibrium period between pulse to be dispensed with since the reverse pulse to establish the original intercalation level can be applied immediately after the relaxation changes in overpotential are minimal. This usually occurs in a period of time equal to the original pulse length.

Most reproducible results are obtained where there is a reasonable change in the intercalation level (around 1 - 2 %) due to the passage of moderate currents (10 - 20 μA). Larger currents for shorter times cause more overpotential to develop and frequently yield plots of overpotential versus $t^{½}$ that exhibit marked curvature.

All the analysis techniques based on Atlung's method give values for the apparent chemical diffusion coefficient which are consistently an order of magnitude higher than those calculated using the classical semi-infinite diffusion equation. This may reflect the assumption made concerning contact area in the latter case.

A dependence of apparent diffusion coefficient on the effective ionic conductivity of the electrode has been demonstrated *but* only under conditions where the characteristics of the mixed phase electrode are not dominated by characteristics of the niobium disulphide particles i.e. when small particle sizes or large electrode thicknesses are utilised. This confirms the theory proposed by Atlung.[5]

The efficacy of using a composite electrode rather than one composed solely of niobium disulphide was not proven when large NbS_2 particles were used. In order to verify any improvement the experiment should be repeated with smaller particle sizes. However if the glass electrolyte in the MPE is replaced by an insulator then measured diffusion coefficient are significantly reduced thus verifying the importance of the electrolyte in transporting ions throughout the bulk of the composite electrode.

The composition of the composite had no effect on the apparent chemical diffusion coefficient measured but idealised condition using smaller particle sizes might yield more conclusive results.

Further work in a number of the areas investigated is indicated by the results discussed here. Firstly a more exhaustive examination of the effect of particle size on the diffusion coefficient would allow optimisation of the construction of the composite electrode. More meaningful results as to the effects of composition, conductivity and electrode thickness might then be ascertained. However niobium disulphide is a difficult material to grind so an optimum grinding technique to yield very small particle sizes must first be sought. The effect of the current passed should also be studied in more detail again to allow optimisation of the experimental technique. The order of magnitude errors considered likely here might then be reduced allowing smaller effects to be investigated.

9 REFERENCES

1 De Levie R. "Electrochemical Response of Porous and Rough Electrodes", Adv. In Electrochem. And Electrochem. Engineering 6 (1967) 329, Eds. Delahay P., Tobias C.W., Publ. John Wiley And Sons (1967)

2 Newman J.S., Tobias C.W. "Theoretical Analysis of Current Distribution In Porous Electrodes", J. Electrochem. Soc. 109 (1962) 1183

3 West K., Jacobsen T., Atlung S. "Modeling of Porous Insertion Electrodes With Liquid Electrolyte", J. Electrochem. Soc. 129 (1982) 1480

4 Atlung S., West K., Jacobsen T. "Dynamic Aspects of Solid Solution Cathodes For Electrochemical Power Sources" J. Electrochem. Soc. 126 (1979) 1311

5 Atlung S., Zachau-Christiansen B., West K., Jacobsen T. "The Composite Insertion Electrode. Theoretical Part. Equilibrium In The Insertion Compound And Linear Potential Dependence" J. Electrochem. Soc. 131 (1984) 1200

6 Atlung S. "Porous And Composite Electrodes For Solid State Batteries" from Solid State Batteries. Nato ASI Series. Series E: Applied Sciences No. 101, Eds. Sequeira C.A.C., Hooper A., Publ. Martinus Nijhoff Publishers (1985)

7 Nairn I.A., "The Study Of Mixed Phase Electrodes In Solid State Cells", Ph.D. Thesis, University Of St. Andrews (1984)

8 Nairn I.A., Smith M.J., Vincent C.A., "Mixed-Phase Electrodes In Solid State Cells", Solid State Ionics 9 & 10 (1983) 383

9 Atlung S. Personal communication to C.A. Vincent

10 Smith M.J., Vincent C.A., "Relative Diffusion Coefficients Of Silver In NbS_2 And TiS_2 Host Materials", Electrochim. Acta 30 (1985) 931

11 Bouwmeester H.J.M., "The Thermodynamic And Kinetic Properties Of Silver Intercalated Niobium Disulfide", Solid State Ionics 16 (1985) 163

12 Rogers M.D., Vincent C.A., "The Effect Of Ionic Conductivity On The Apparent Chemical Diffusion Coefficient Of A Composite Electrode", Solid State Ionics 28-30 (1988) 1138

13 Dalard F., Deroo D., Foscallo D., Merienne J.-L, "Theoretical Study Of A Composite Electrode Using An Intercalation Compound : Influence Of The Particle Size Distribution On The Depth Of Discharge", Journal Of Power Sources 14 (1985) 209

1 ELECTRON PROBE MICROANALYSIS STUDIES OF COMPOSITE ELECTRODES

Electron probe microanalysis (EPMA) is a powerful experimental technique and can provide important qualitative and quantitative information about a suitable sample. In particular it is often straightforward to relate quantitative information to structural features in a sample or to elucidate quantitative information on small distinct regions of a sample.

Previously a variety of EPMA experiments measurements have been carried out on insertion electrode materials. Frindt et al. performed EPMA measurements on single crystals of titanium disulphide insertion material [1, 2] in order to investigate the intercalation mechanism, and to confirm results of x-ray diffraction [3] and optical measurements [1] on the same system. Results confirmed the presence of staging caused by a moving island domain model [4] during the intercalation process. Experiments have also been undertaken on polycrystalline electrodes of tantalum disulphide in order to examine the silver distribution within the insertion cathode after intercalation. [5] The latter investigation showed that immediately after the passage of the intercalating current the highest concentration of silver in the host structure was at the boundary nearest to the source of the silver ions, and that this concentration decreased as the distance from this boundary increased. After leaving for a period of several weeks the concentration distribution evened out tending towards a uniform level throughout the electrode. This effect varied with particle size and orientation.

The related technique of scanning electron microscopy (S.E.M.) has also been used to study mixed phase electrodes and in particular to examine interfacial contact effects as a function of the pressure of preparation [5] and of annealing of the composite. [6] The latter study also correlated this effect with measurements of diffusion coefficient. More recently the insertion of lithium ions into FeS, TiS_2, and V_6O_{13} electrode materials has been investigated by S.E.M. [7] These materials are observed to undergo significant morphological changes as the insertion proceeds; the structure of FeS disintegrating, that of TiS_2 remaining comparatively unchanged while the crystals of V_6O_{13} crack and break up as the level of inserted lithium increases. (Similar cracking has also been observed with TiS_2 thin crystals using optical techniques. [8])

A transmission electron microscopy examination of lithium intercalation into titanium disulphide was also reported recently. [9] A comparison was made of the structures of Li_xTiS_2 when intercalated chemically and electrochemically using both liquid and solid electrolytes. The crystal microstructure was heavily dependent on the intercalation technique used. The use of a liquid electrolyte resulted in solvent co-intercalation and structural deformity. Solid electrolytes and

chemical intercalation yielded better structures, showing evidence of staging. The crystal dislocations were fewer in smaller crystals confirming the results of Atlung[10,11] which point to the use of smaller crystals to gain optimum efficiency in all-solid-state cells.

On the whole though very little use has been made of electron microscopy techniques, and in particular of EPMA, in studying the intercalation process. No quantitative results exist at all on mixed phase electrodes. This investigation therefore undertook an EPMA examination of the composite electrodes described above in an attempt to gain an insight into their efficiency of operation. The silver concentration distribution was examined within the MPE to ascertain whether the MPE functioned efficiently in transporting silver ions throughout its depth. Comparison was made between high and low conductivity glassy electrolytes to determine whether this efficiency was affected by the change in conductivity. The effect of particle size was also studied for these electrolytes. An electrode consisting of the pure insertion material was examined for comparison, and the electrochemically intercalated material was compared with the chemically synthesized $Ag_{0.05}NbS_2$. Individual crystals were also studied to look for unevenness in the silver distribution.

2 ELECTRON BEAM INTERACTION WITH A SAMPLE

When a high energy electron beam impinges on a sample it penetrates into it to a depth (typically of the order of 1 μm) dependent on the accelerating voltage, the probe diameter and the nature of the sample. [12] Interactions occur which are both electromagnetic and particulate in nature and Figure 1 illustrates the principal emissions which occur from the sample. After suitable detection and analysis these provide identification of the elements present along with their concentrations.

Electron interaction with the fields surrounding the atoms in the sample reduce the energy of the incident electrons and produce a broad spectral band of radiation from visible cathodoluminescence to background X-radiation. For imaging purposes however, it is the particulate interactions which are more important. Backscattered electrons are produced as a result of deflections of the incident electrons by the atoms in the sample and their intensity is dependent on the mean atomic number of the sample constituents. Their analysis thus leads to general qualitative information concerning compositional variation within the sample. [13] Secondary electrons are ejected from the atoms within the sample by the incident beam and their collection allows good imaging and focussing.

The most important interaction for determination of the composition of the sample is the production of the characteristic X-rays of each element present in the sample. These arise when an electron in an inner shell around an atom is dislodged by the impinging beam, and requires that the beam has an energy greater than the critical excitation potential necessary to eject the electron. The vacancy thus created is filled by one of the outer shell electrons, the energy difference resulting in the emission of an X-ray photon. Similarly the new vacancy can be filled by an electron from an even more remote shell. This results in a series of X-rays of different energies. The energies (and thus wavelengths) of the X-rays are dependent on the atomic number of the element concerned and thus are characteristic of that element.

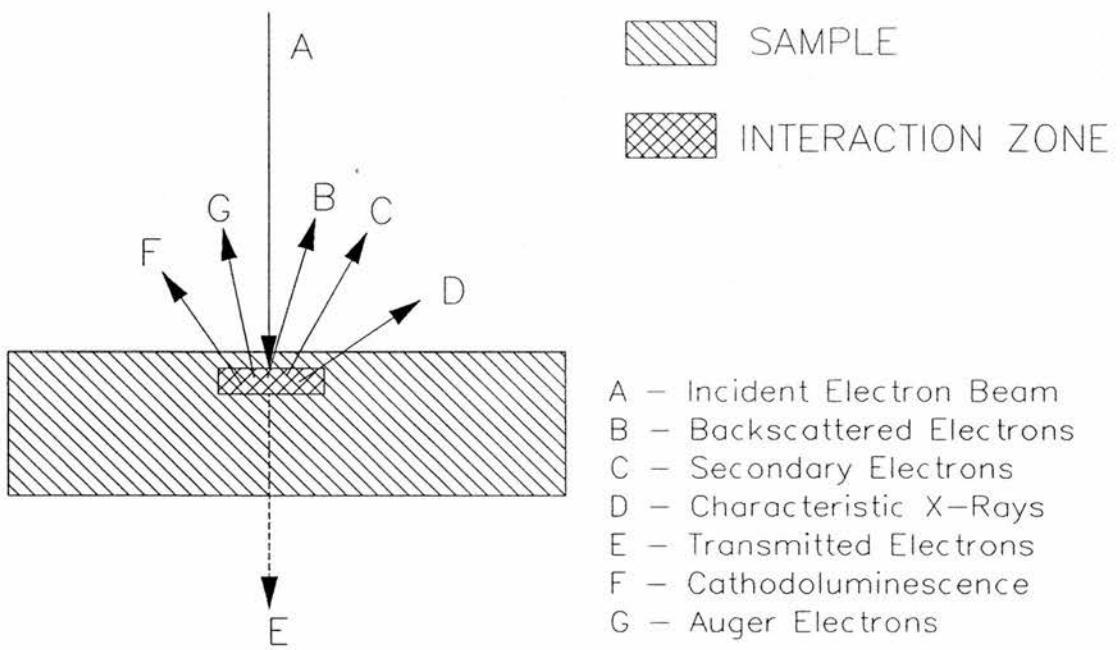

Figure 1.
Interactions of an electron beam with a sample.

Elucidation of quantitative information is complicated by a variety of factors. Firstly the rate of emission of X-rays is not an empirical property of an atom but is dependent on the operating conditions and the sample. To yield information concerning the concentration of a species the count rate of X-ray emission from a sample must be compared with that of a reference material (or standard) of well-defined and stable chemical composition, under the same operating conditions. Frequently

the standards used are the pure elements. In simplest terms the concentration (C) of an element in the sample is the ratio of the intensities of X-ray emission from the sample (I_S) compared with the reference (I_R) such that:-

$$C = I_S / I_R$$

Three important corrections are then generally made to allow for the influence of physical differences between the sample and the standard. Firstly allowances are made for the difference in atomic number (Z corrections) by using a correction factor which compensates for backscattering and stopping effects caused by density differences between the materials. Absorption (A) effects are caused by interaction of the emitted X-rays with surrounding atoms and their compensation requires knowledge of a number of factors such as the beam's penetration into the sample, the beam angle and the absorption coefficient of the sample. This is the most important of the three corrections made. Lastly fluorescence (F) effects must be compensated for. These are caused by the production of X-rays from surrounding atoms as the original X-ray passes out of the sample. The combination of these factors is known as ZAF analysis and when used allow very good quantitative results to be obtained for stable samples.

3 THE ELECTRON MICROPROBE

The electron microprobe combines the scanning electron microscope with spectroscopic techniques for analysis of the described X-rays, thus allowing the quantitative examination of composition and distribution of elements composing a sample.

The basic layout of an electron microprobe analyser is presented schematically in Figure 2. [12] In the microprobe a small region of the sample is bombarded by a finely focused electron beam (the probe ca. 1 μm in diameter). The electrons are produced by heating a tungsten filament and are accelerated through a voltage gradient to the required energy level (from 1 to 50 kV) before passing from the electron gun into a double electromagnetic lens system. The condenser lens is of variable focal length, allowing control of the direction, size and current density of the electron beam. The objective lens usually has a predefined focal length which is determined by the space necessary for the detectors etc. positioned between it and the sample. It is also equipped with scanning coils which permit rastering of the beam over an area of the sample thus facilitating examination of the sample, probe positioning and allowing distribution and composition maps to be obtained. Stigmators are also included to ensure the beam remains circular. Feedback loops are incorporated into all these

components to ensure the stability of the accelerating voltage and the focussing over the long times required for analysis. The whole section must also be maintained under high vacuum to retain the integrity of the beam.

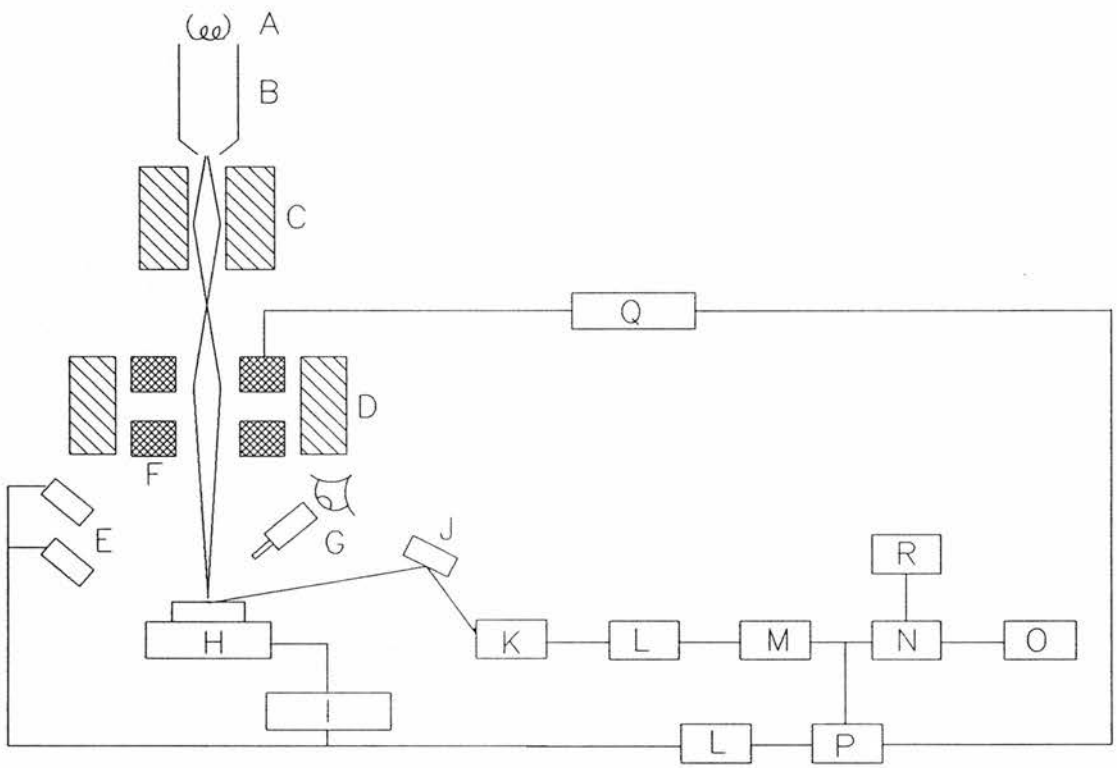

Figure 2.
Schematic representation of an electron microprobe analyser.
A - Tungsten Filament, B - Electron Gun, C - Condenser Lens, D - Objective Lens/Stigmator, E - Electron Detectors, F - Scanning Coils, G - Optical Microscope, H - Specimen Holder, I - Specimen Current Meter, J - Crystal Spectrometer, K - X-Ray Detector, L - Amplifier, M - Pulse Analyser, N - Rate Meter, O - Chart Recorder, P - Cathode Ray Tube, Q - Scan Generator, R - Microcomputer for Automatic Analysis

An optical microscope is directed at the sample to allow visual observation of the sample and to allow the beam to be seen when projected onto a suitably fluorescent sample. This enables the shape of the beam to be optimised. The sample itself is held in the specimen holder which also holds reference samples and monitors the probe current to the sample. It is capable of motion in three directions, the X and Y directions in the plane perpendicular to the electron beam giving control over the area of electron incidence and the Z direction along the beam permitting precise focussing.

The remainder of the microprobe is devoted to the collection and analysis of the information resulting from interaction of the electron beam with the sample. Detectors for backscattered and

secondary electrons and X-ray spectrometers are all mounted above the sample. The X-ray spectrometer is generally a crystal (or a diffraction grating) which diffracts the incident X-rays according to Bragg's law, leading to wavelength and thus energy separation. Crystals with different lattice parameters allow selective diffraction of X-rays of different energies, and usually 2 or 3 crystals can be used simultaneously thus speeding up data collection. The detector is usually an ionisation chamber and it differentiates between the X-rays of different energies permitting identification of those characteristic to a particular element.

Qualitative output is by means of chart recorder or photographically from the attached cathode ray tube. Quantitative results are calculated automatically, with ZAF corrections, by the controlling microcomputer and are output to a printer or the chart recorder.

Thus the electron microprobe can yield high speed qualitative analyses from photographs, compositional variation and topographical imaging from backscattered electrons, atomic distributions from mapping of characteristic X-rays and quantitative analysis also from these X-rays.

4 PREPARATION OF SAMPLES

The three-electrode cells used were prepared and intercalated as described in Chapter 2. On completion of the required intercalation the cell was sectioned into two halves and the cell constant measured if necessary. Now the sections were immersed in Epicure epoxy resin and impregnated with this resin by holding under vacuum for 20 minutes. The samples were then cured by sitting them on a hot-plate at 60 °C for 3-4 hours. The impregnation held the particulate materials together during the polishing procedure and improved the polish obtained. The quality of the polish is of primary importance in quantitative analysis, a good polish reducing X-ray scattering and changes in their path length.

Plastic moulds, comprising a flat base-plate and a cylindrical upper section (Figure 3a) were now used to mount the samples in a polyester resin. One half of the cell was placed flat onto the base of the mould, working electrode downwards and a little resin mixture was poured into the mould and allowed to partially set. The second half of the cell was now positioned vertically in the resin with the working electrode adjacent to the base. The mould was then filled with resin and allowed to set overnight in a cold water bath.

When firmly set the base was removed from the moulds and the cast samples pushed free. The rough cylindrical casting was reduced in thickness to 1.5 - 2 cm, the edges were smoothed down and a 4.7 mm diameter hole drilled centrally in the rear of the sample to a depth of 5 mm. This was required for the mechanical polishing. Figure 3b illustrates the final configuration.

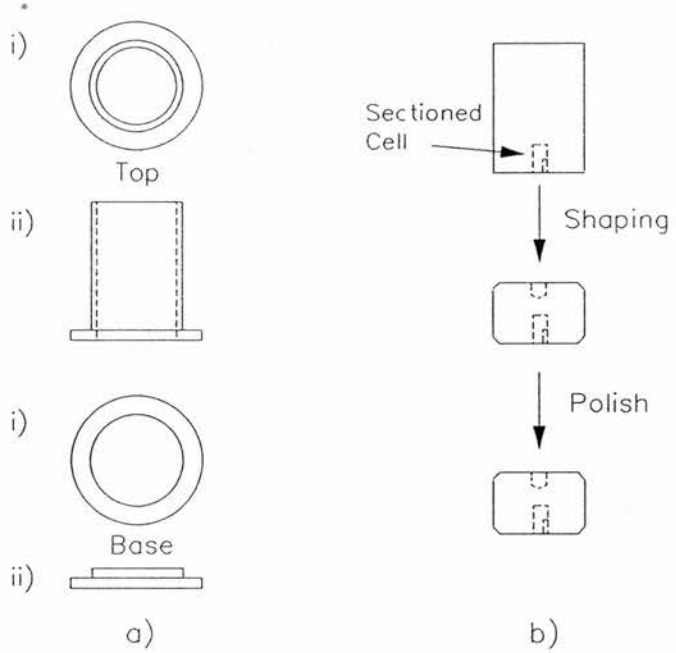

Figure 3.
Electron Microprobe Sample Preparation.
a) Details of mould used for sample preparation. i) Top View, ii) Side View, b) Preparation stages

Excess resin over the mounted samples was removed using a coarse rotating diamond lap and initial polishing carried out using three grades of Carborundum powder in succession until a sheen was evident on the surface of the sample. The polishing was completed using an Engis Ltd. Kent Mk. 2a polisher which rotates the sample while held face down on a counter-rotating lap covered with diamond paste. Three Hyprez diamond pastes, progressively of 6 μm, 1 μm and ¼ μm grades, were used for an hour or so each. The surface of the sample was examined under a microscope to ensure that it reflected an incident light beam evenly, thus indicating that the polishing was adequate, and further polishing carried out if required. After initial trials it was discovered that because of the softness of the materials in the working electrode the polish was not sufficiently good using the diamond pastes which broke up the surface. Final polishing was thereafter carried out using a lap coated with tin oxide. This was a much softer polishing agent and also had the advantage that the particle size decreased as the polishing was carried out, thus providing a more even finish.

A very thin (μm) layer of carbon was vacuum deposited onto the polished face of the sample using an Edwards vacuum carbon coater. This allowed electrical contact between the sample and the probe. Finally the sample was mounted in a holder which allowed insertion into the Jeol JCXA-733 Superprobe electron microprobe.

5 USE OF THE MICROPROBE

On first using the microprobe a protocol was initialised on the controlling DEC microcomputer which instructed the microprobe on how to carry out the analysis of the samples. Various parameters were chosen and input to the computer so that an internal program could calculate the necessary calculations for quantitative analysis.

An electron beam energy of 15 kV was selected, this being relatively low to prevent burning of the sample but high enough to excite the inner electrons of all elements present. The probe current was defined to be 200 nA. The X-rays generated from the four elements Nb (L line), S (K line), Ag (L line) and I (L line) were searched for, the lines indicated being the strongest emission line in each case. Next the sequence of analysis was defined, the measurement channel and diffracting crystal chosen. Here a crystal of polyethylene terephthalate (PET) had to be used for all four elements so each had to be analysed sequentially. Positions for background radiation measurement were also defined, usually 2 or 3 mm remote from the peak emission on either side of it and avoiding any secondary peaks from other elements.

The composition of the standards used for reference was now entered to allow for the ZAF corrections to be calculated for each element. The standards used were the pure elements for niobium and silver, FeS (53.4 % S, 46.6 % Fe) for sulphur and $Ag_7I_4AsO_4$ (36.22 % I, 53.87 % Ag, 35 % As, 4.57 % O) for iodine. Lastly the counting procedure for the unknown sample was outlined. For each element two peak searches were carried out. These measure the count rate at a series of steps through the approximate peak position for the desired element. Thus the exact peak position is pinpointed by the maximal count rate observed. The count rate was then measured at the optimum wavelength for 10 seconds and background counts for 5 seconds at their defined positions remote from the peak.

After the protocol was defined it was stored on the dedicated microcomputer and recalled when required for analysis.

The required operating conditions were now set up ready for use. The sample and standards were then mounted into sample holders and these were inserted into the microprobe and onto the specimen stage via the exchange airlock. The alignment of the beam was then checked and adjusted as necessary by focussing on a fluorescent sample of pyroxene (MgO). This was a complicated iterative process involving altering a number of parameters such as the beam position, the probe current, its concentricity and the astigmatism.

The protocol was then loaded and the appropriate section of the controlling program called up to allow counting of the standards. The standard block was positioned under the beam and the required standard located using the optical microscope and visual display. The beam was focussed onto a region of the sample and the counting procedure initiated, the computer automatically choosing the right wavelength and sequence for analysis. This was repeated at a number of different positions on the sample until a consistent maximum count rate was achieved. All standards were counted in an identical fashion.

The sample was now aligned underneath the beam ready for analysis. The general analysis procedure followed was to firstly perform a visual examination of the working electrode area, using both the optical and backscattered electron images. This distinguished regions of the sectioned cell where there were a series of niobium disulphide crystals across the thickness of the working electrode. Obviously in most cases where a mixed phase electrode was examined such crystals were separated from each other by particles of electrolyte (in two dimensions at least).

The silver distribution was examined qualitatively using the back scattered electron image to look at regions of different atomic number. The lightest coloured regions had the highest mean atomic number and corresponded to particles of the pure electrolyte. The darkest regions were pure unintercalated niobium disulphide crystals and the range of intermediate shades correspond to NbS_2 crystals with different intercalated levels of silver. Using this back scattered electron image a series of photographs were taken from the top of the working electrode to the bottom (as viewed on the cathode ray screen).

Quantitative results were then measured. These were performed at a number of different levels within the cell, at positions where there were a few NbS_2 particles across the thickness. At each of these levels a series of point analyses were taken across the working electrode from the side adjacent to the counter electrode to the external edge of the electrode. All measurements were performed on the electrode material rather than the electrolyte. This is illustrated schematically in Figure 4.

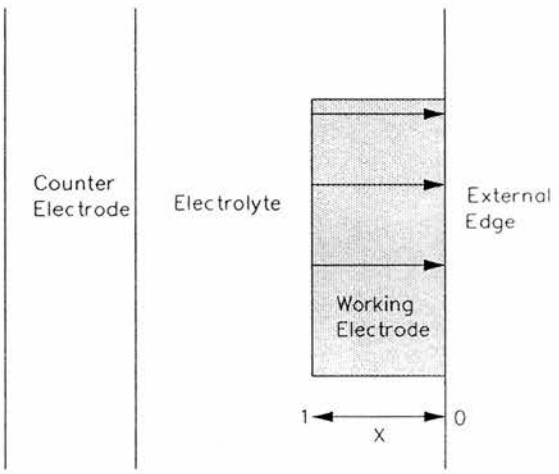

Figure 4.
Schematic representation of the quantitative analysis performed on each working electrode. Point analyses were made on niobium disulphide particles at different heights in the working electrode as shown by the arrows.

From the results calculated and output by the microcomputer the ratio of silver to niobium was determined. Using this ratio compensated for any discrepancies in the degree of polishing at a particular point, or any other inconsistencies in the technique. A normalised distance factor (X) was also calculated for each point which was simply the ratio of the distance to the point being measured to the total thickness of the working electrode, the latter parameter being the maximum x-coordinate measured minus the minimum x-coordinate measured during the analysis. In general, therefore, $X = 0$ at the external edge of the working electrode and $X = 1$ at the edge adjacent to the electrolyte.

6 RESULTS AND CONCLUSIONS

In all the experiments described below three electrode cells were constructed from each glass *under identical conditions,* then stripped, intercalated to the $Ag_{0.05}NbS_2$ level electrochemically and allowed to equilibrate using the procedures outlined in Chapter 2. Thus any differences observed should be a function of the properties of the composite electrode and not of the preparation conditions. In each case glasses from the ternary system $AgI:AgPO_3:B_2O_3$ were used with G1 denoting the highest conductivity glass and G5 the lowest conductivity glass. The particle sizes of all components were in the range 125 - 175 μm unless otherwise stated.

6.1 EFFECT OF CONDUCTIVITY

The first set of experiments examined the effect of the glass conductivity on the silver distribution within the composite electrode. The cells were analysed under the electron microprobe both

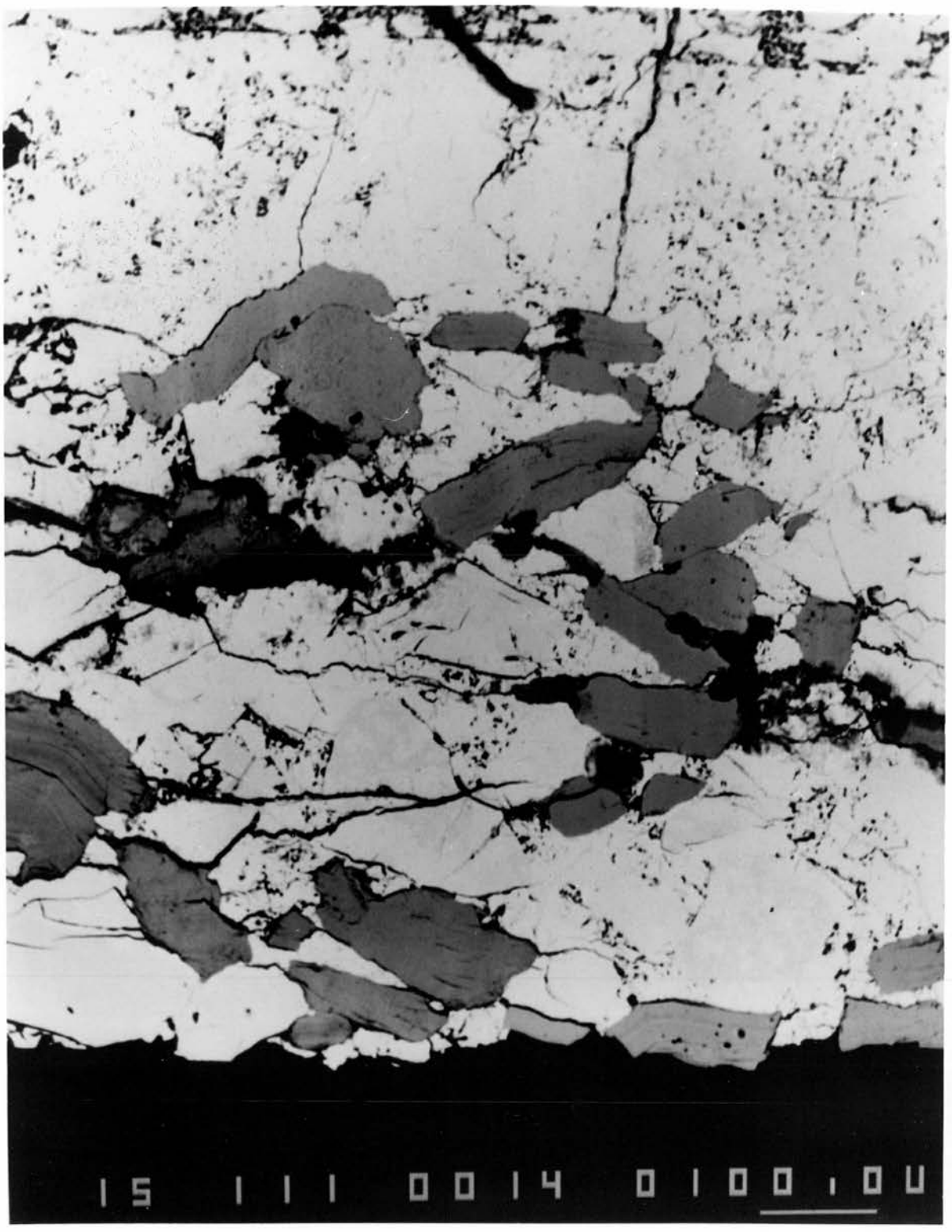

Plate 1.

Backscattered electron image of a composite electrode comprised of high conductivity glass G1 and niobium disulphide.

Plate 2.

Backscattered electron image of a composite electrode comprised of high conductivity glass G1 and niobium disulphide.

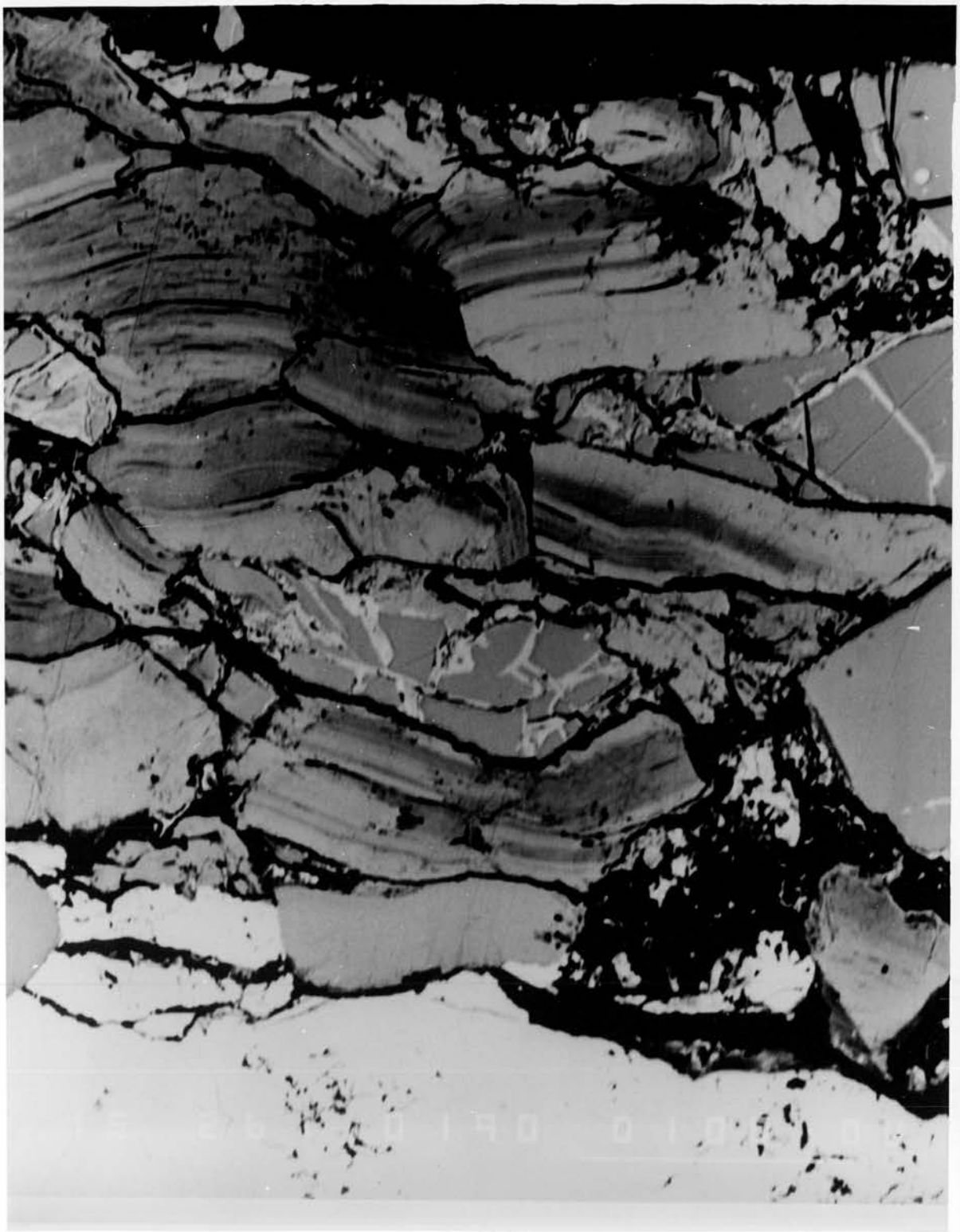

Plate 3.

Backscattered electron image of a composite electrode comprised of low conductivity glass G5 and niobium disulphide.

Plate 4.

Backscattered electron image of a composite electrode comprised of low conductivity glass G5 and niobium disulphide.

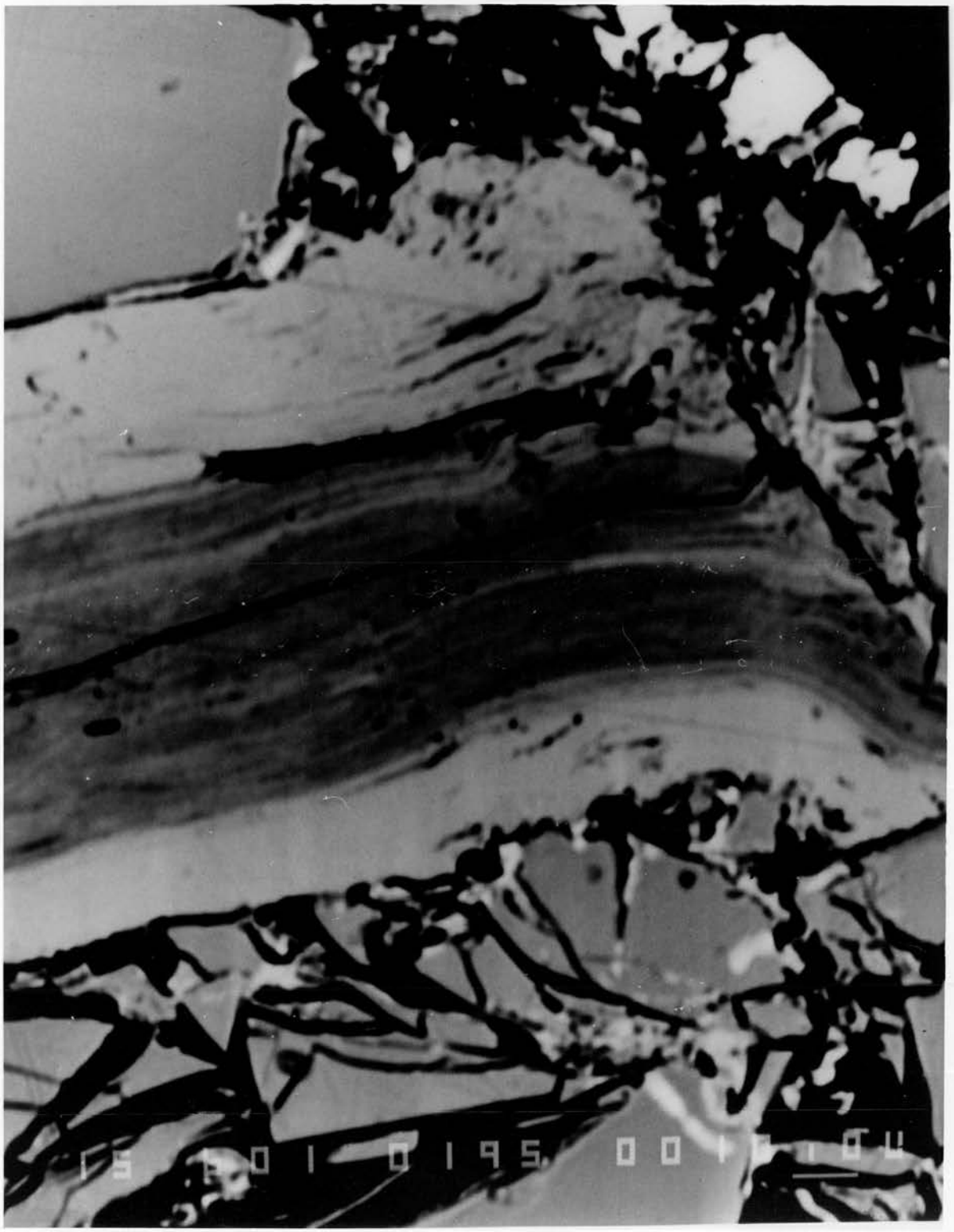

Plate 5.

High magnification back scattered electron image of a niobium disulphide particle showing areas of different silver concentration.

qualitatively and quantitatively as described above. Plates 1 to 5 are back scattered electron images from these two examples. Plates 1 and 2 show two different sections through the working electrode containing the high conductivity glass G1 and Plates 3 and 4 are similar pictures of regions within the cell prepared with the low conductivity glass G5.

Even at this qualitative level there are clear differences between the two cells. The first two plates clearly show that all the niobium disulphide crystals (the darker crystals) are approximately the same shade of grey, indicating that they have approximately the same average atomic weight. Thus they contain the same amount of silver. The overall distribution of silver within the working electrode and within individual crystals is even.

In contrast plates 3 and 4 demonstrate that when the electrolyte has a much lower conductivity it is not nearly as efficient in transporting the silver ions throughout the depth of the electrode. It is clearly seen that the colour, and hence mean atomic number, of the intercalated niobium crystals is very inhomogeneous. Towards the left of the working electrode (towards the source of the silver ions) there is a higher proportion of brightly coloured crystals indicating a high level of silver intercalation. Towards the other side the crystals are on average darker, though the effect is not an even progression. The latter reflects differences in the relative tortuosity and efficiency of the conducing paths leading to these crystals.

The above results were confirmed by looking at X-ray distribution maps over the electrode regions concerned. There was a fairly even concentration of Ag X-ray emissions from the niobium disulphide crystals in the former case, and considerable variation in the latter case.

There are also clear bands of different brightness within individual crystals particularly with the low conductivity glass suggesting that there is uneven distribution of the silver within them. Plate 5 illustrates a higher magnification example of this, and clearly shows a region where there is no intercalation in the centre of a NbS_2 crystal. This is possibly indicative of staging effects or blocking of the silver ions as they enter the middle of the niobium disulphide crystals. However the fine variations reflected in the different brightnesses in Plates 3 and 4 were not evident in the X-ray distribution maps.

One other interesting feature to emerge from the above photographs is that there are considerable differences in the interfacial regions between the electrode and electrolyte materials in the two cases. The higher conductivity glass appears to give very good contact with the electrode particles and it is quite difficult to distinguish different glass particles from each other in Plates 1 and 2. Indeed

they seem to form an amorphous mass. The harder, low conductivity glass in contrast seems to break up when compressed to form the mixed phase electrode. The glass particles in Plates 4 and 5 are much more clearly defined and often are cracked or broken. The boundaries with the electrode particles are much sharper and seem to be confined to smaller contact regions in general. This probably explains the banding of silver ion distribution observed, the point contacts restricting the silver ions to enter the electrode crystals over a much more limited region.

After this qualitative examination quantitative results were measured. Table 1 lists the normalised results of [Ag]/[Nb] for the high conductivity glass and these are plotted in Figure 5. The figures and the graph show that there is essentially no alteration in the silver concentration on travelling across the thickness of the working electrode. This indicates that the composite electrode is functioning efficiently in transporting ions through the electrolyte to most of the niobium disulphide crystals.

Point	X	[Ag]/[Nb]	Point	X	[Ag]/[Nb]
1	0.14	0.86	21	0.79	0.76
2	0.14	0.89	22	0.75	0.83
3	0.16	0.77	23	0.92	0.63
4	0.19	0.89	24	0.84	0.79
5	0.22	0.88	25	0.79	0.73
6	0.22	0.91	26	0.76	0.78
7	0.26	0.89	27	0.58	0.70
8	0.33	0.83	28	0.54	0.76
9	0.39	0.88	29	0.51	0.70
10	0.42	0.83	30	0.26	0.81
11	0.46	0.85	31	0.20	0.87
12	0.49	0.85	32	0.17	0.85
13	0.60	0.82	33	0.13	0.89
14	0.95	0.81	34	0.13	0.86
15	0.99	0.75	35	0.09	0.71
16	1.00	0.77	36	0.00	0.66
17	0.91	0.61	37	0.04	0.90
18	0.90	0.47	38	0.96	0.86
19	0.87	0.60	39	0.99	0.82
20	0.82	0.79	40	1.00	0.91

Table 1.
Silver concentration versus distance across an MPE with high conductivity glass as electrolyte.
Particle size 125 - 175 μm.
Points 1 - 16 are taken across the top of the electrode, while points 17 - 22, 24 - 34 and 35 - 40 are different sections through the middle.

Figures 6 and 7 show two slices through the same working electrode with Figure 6 depicting readings from the top of the working electrode and Figure 7 results from near the middle. Once more there is essentially no change in the intercalation level moving across the cell indicating that there is an almost even silver concentration at all points within the mixed phase electrode.

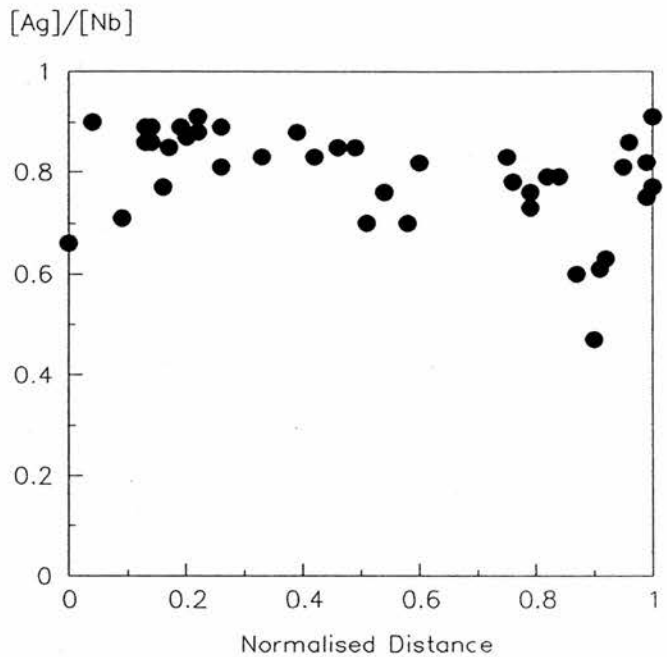

Figure 5.
Silver concentration in NbS_2 particles versus distance across a composite electrode of niobium disulphide and high conductivity glass.

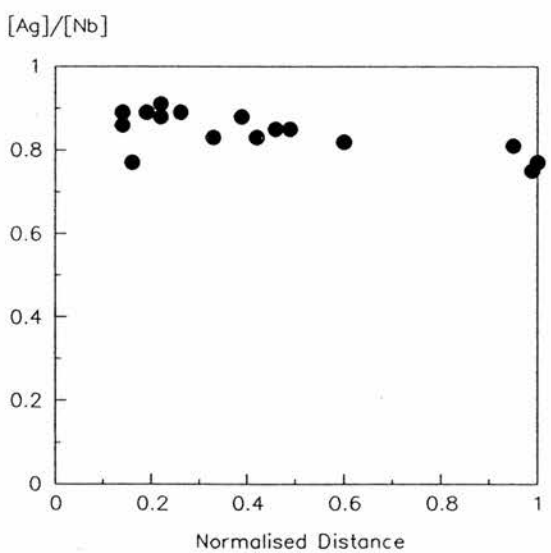

Figure 6.
Points 1 - 16 from above.

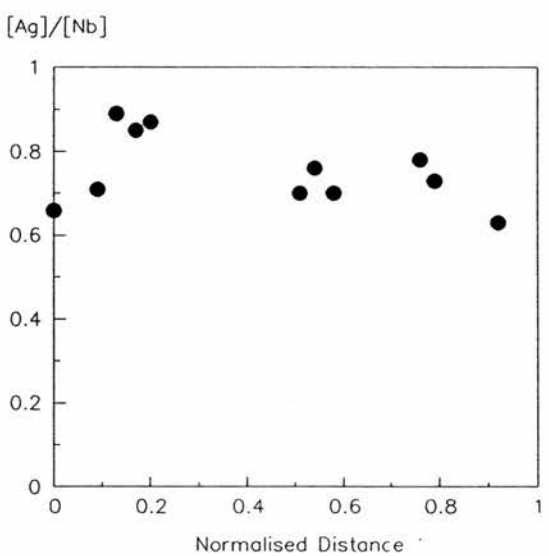

Figure 7.
Points 24 - 34 from above.

Table 2 and Figure 8 illustrate the same results for the lower conductivity electrolyte. Now in moving across the electrode from the external edge there is an apparent increase in the [Ag]:[Nb] ratio. However this trend is not totally clear and there is a lot of fluctuation in the results.

Point	x	[Ag]/[Nb]	Point	x	[Ag]/[Nb]
1	1.00	0.80	25	0.43	0.61
2	0.94	0.72	26	0.38	0.25
3	0.94	0.74	27	0.32	0.10
4	0.91	0.78	28	0.31	0.30
5	0.87	0.75	29	0.27	0.23
6	0.75	0.66	30	0.26	0.23
7	0.75	0.75	31	0.24	0.14
8	0.70	0.72	32	0.17	0.05
9	0.73	0.67	33	0.10	0.18
10	0.68	0.64	34	0.35	0.67
11	0.39	0.26	35	0.41	0.49
12	0.38	0.62	36	0.14	0.32
13	0.36	0.72	37	0.07	0.75
14	0.19	0.17	38	0.07	0.69
15	0.17	0.16	39	0.78	0.82
16	0.15	0.06	40	0.74	0.72
17	0.11	0.01	41	0.72	0.72
18	0.03	0.01	42	0.63	0.72
19	0.00	0.02	43	0.56	0.72
20	0.61	0.57	44	0.46	0.78
21	0.61	0.57	45	0.43	0.76
22	0.92	0.70	46	0.31	0.71
23	0.75	0.75	47	0.30	0.05
24	0.71	0.69			

Table 2.
Silver concentration versus distance across a MPE with low conductivity glass as electrolyte. Particle size 125 - 175 μm.
Points 1 - 19 and points 22 - 33 are taken from the middle of the electrode and points 34 - 38 and 39 - 47 from near the top and bottom respectively.

On closer examination of the data the reason for this becomes evident. Figures 9 and 10 show the points measured through two sections in the centre of the electrode. These pictures both demonstrate a reasonably steady increase in the silver level within the working electrode as the distance from the counter electrode is increased (X → 1) and thereby confirm the qualitative results. At the centre of the electrode the highest concentration of silver ions is found in the crystals immediately adjacent to the interface with the pure electrolyte region. There is a consistent drop off with distance from the interface and very little silver finds its way to the far side of the electrode. This parallels the results of Bonino et al[4] on a pure TaS_2 electrode and implies that the lower conductivity glass is not as efficient in transporting ions throughout the electrode.

However there are considerable differences if a slice near the top or bottom edge of the working electrode is considered as depicted in Figure 11. Here there is (apart from a slight fluctuation) a consistent silver level in all the NbS_2 across the electrode. This suggests that the electrolyte between the reference and working electrodes also acts as a source of silver ions into the composite electrode.

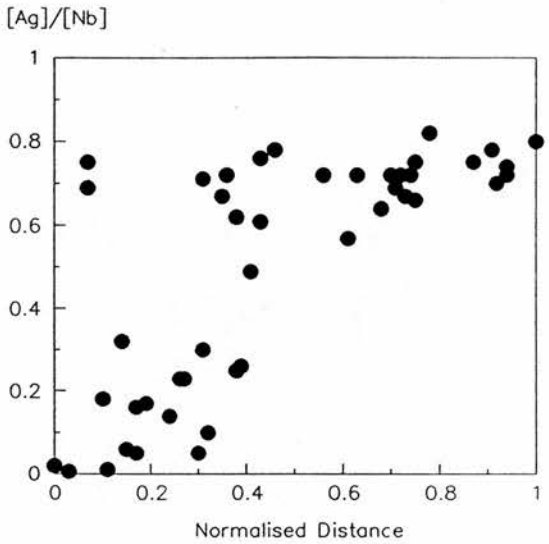

Figure 8.

Points 1 - 47 from Table 2.

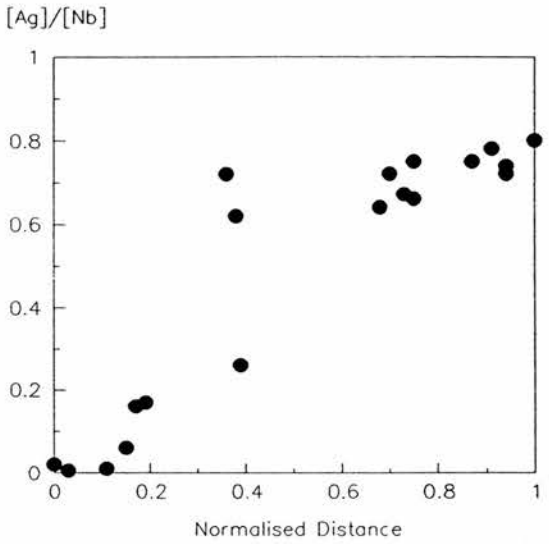

Figure 9.

Points 1 - 19 from Table 2.

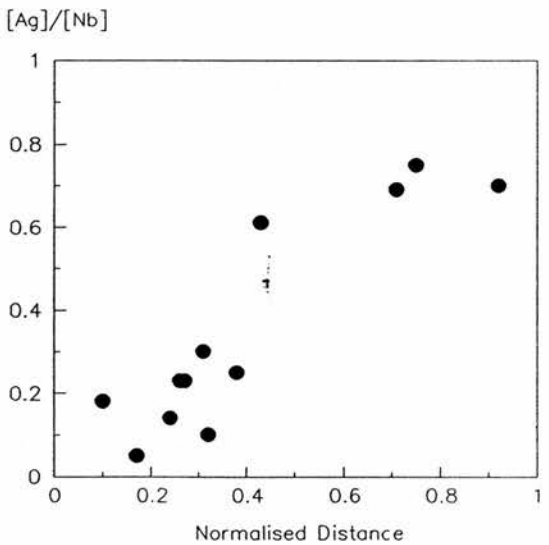

Figure 10.

Points 22 - 33 from Table 2.

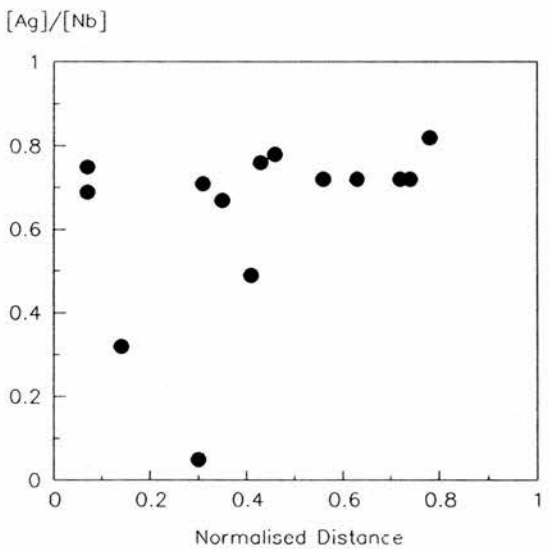

Figure 11.

Points 39 - 47 from Table 2.

The next experiment considered a cell with a working electrode composed solely of niobium disulphide. This yielded the results tabulated in Table 3. (Note that in this case the cell was reversed in the microprobe so that X = 1 is at the external edge of the cell.)

No photographs are shown for this case since it was impossible to adjust the contrast to allow reasonable resolution of the intercalated and vacant crystals.

Point	x	[Ag]/[Nb]	Point	x	[Ag]/[Nb]
1	0.13	0.59	28	1.00	0.57
2	0.20	0.28	29	0.35	0.15
3	0.27	0.20	30	0.36	0.16
4	0.35	0.00	31	0.41	0.08
5	0.36	0.00	32	0.44	0.00
6	0.46	0.00	33	0.49	0.00
7	0.54	0.00	34	0.53	0.00
8	0.57	0.00	35	0.62	0.00
9	0.60	0.00	36	0.64	0.00
10	0.65	0.00	37	0.67	0.00
11	0.74	0.03	38	0.69	0.35
12	0.85	0.00	39	0.72	0.00
13	0.00	0.67	40	0.76	0.00
14	0.10	0.51	41	0.36	0.29
15	0.16	0.32	42	0.40	0.33
16	0.18	0.31	43	0.45	0.54
17	0.22	0.55	44	0.49	0.56
18	0.28	0.61	45	0.54	0.58
19	0.31	0.58	46	0.60	0.27
20	0.40	0.60	47	0.66	0.10
21	0.54	0.56	48	0.69	0.32
22	0.60	0.55	49	0.72	0.03
23	0.60	0.59	50	0.74	0.52
24	0.69	0.57	51	0.78	0.55
25	0.75	0.65	52	0.83	0.33
26	0.80	0.60	53	0.90	0.33
27	0.90	0.58	54	0.97	0.02

Table 3.
Silver concentration versus distance across a MPE with a pure niobium disulphide electrode. Particle size 125 - 175 μm.
Points 1 - 12 across the centre of the electrode, points 13 - 28 at the bottom and the remainder between these two.

Once more if all the measurements are depicted graphically (Figure 12) there is no clear pattern in the silver concentration but again there is considerable fluctuation in the results. Splitting the results into measurements made in the centre of the working electrode and those made at the edge reveal that the trends observed with the low conductivity glass are also present here. In fact there is an even more abrupt drop off in the silver concentration at the centre of the electrode no doubt because orientation of the NbS_2 is also crucial in transporting silver from crystal to crystal since NbS_2 is only a two-dimensional intercalation material.

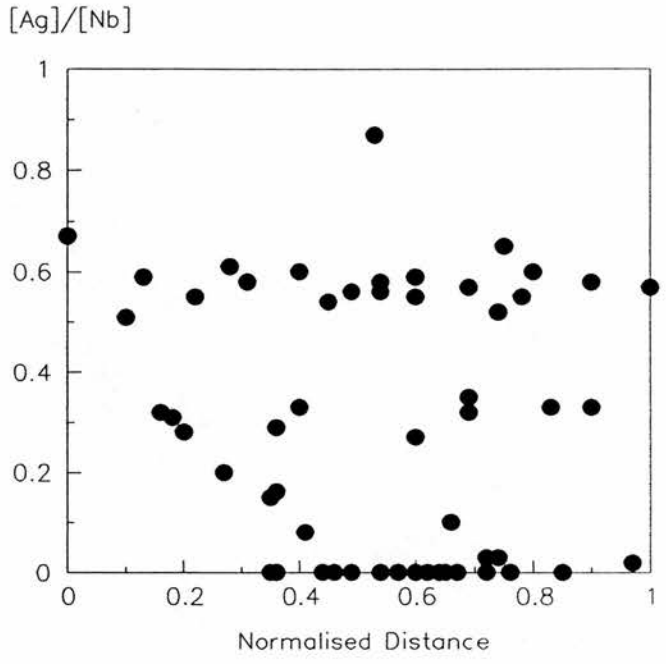

Figure 12.
Silver concentration versus distance across a pure niobium disulphide electrode.

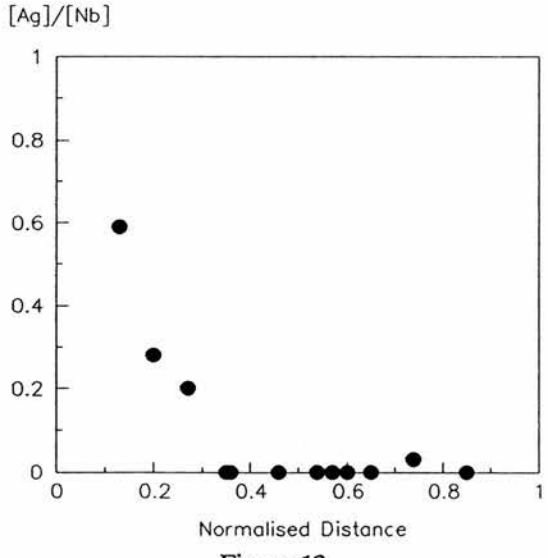

Figure 13.
Points 1 to 12 from Table 3.

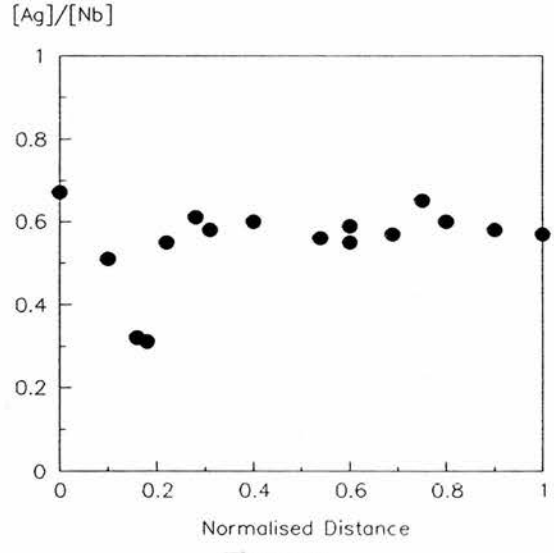

Figure 14.
Points 13 to 28 from Table 3.

The regions of high silver concentration found for the latter two cells are depicted schematically in Figure 15. The sides nearest the electrolyte obviously provide a low energy path for the silver ions

to enter the working electrode particularly when conduction through the working electrode is difficult due to the presence of a low conductivity component or when, as with the pure NbS_2 electrode, there is limited contact between crystals in an appropriate alignment for transport of ions.

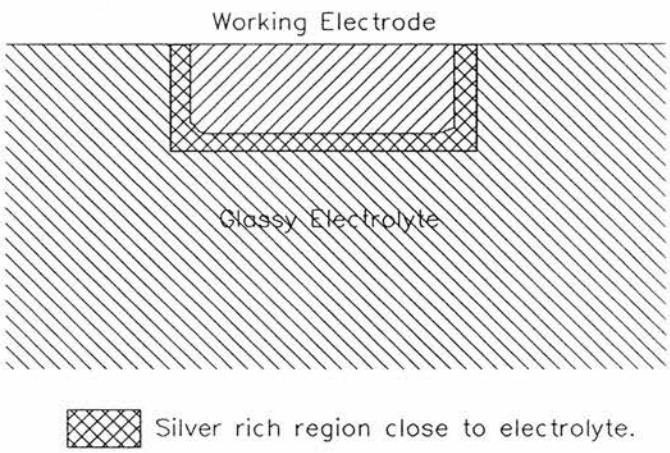

Figure 15.
Schematic representation of highest silver ion concentrations in low conductivity composite electrodes.

These results demonstrate that the efficiency of a composite electrode is dependent on the effective conductivity of the electrode as predicted by Atlung.[10] The high conductivity glass aids distribution of the silver ions throughout the mixed phase electrode and therefore should allow higher utilisation of the niobium disulphide particles within it. Even a mixed phase electrode with a low conductivity glass is more effective in transporting silver ions than an electrode composed purely of NbS_2 because it overcomes transport limitations associated with the boundaries between adjacent NbS_2 crystals in the latter case.

Similar experiments were also performed on chemically synthesized $Ag_{0.05}NbS_2$ as described in Chapter 2. Results are tabulated in Table 4 and show a series of measurements taken on a number of different crystals. The qualitative measurements showed that all the intercalated niobium disulphide crystals were approximately the same brightness suggesting the expected even distribution of silver ions. However the quantitative results shown reveal that there is still some inhomogeneity in the silver ion concentrations. Figure 16 demonstrates that there is no apparent dependence on position in the electrode as observed in the previous cases. This suggests that it is the synthesis route which produces some differences in the intercalation level, possibly owing to poor mixing of the original constituents.

Point	x	[Ag]/[Nb]	Point	x	[Ag]/[Nb]
1	0.00	0.27	14	0.75	0.19
2	0.04	0.10	15	0.76	0.20
3	0.04	0.30	16	0.80	0.07
4	0.32	0.27	17	0.86	0.22
5	0.35	0.30	18	0.88	0.18
6	0.43	0.31	19	0.88	0.16
7	0.50	0.25	20	0.96	0.02
8	0.50	0.31	21	0.93	0.17
9	0.53	0.33	22	0.94	0.04
10	0.63	0.12	23	0.95	0.07
11	0.63	0.07	24	1.00	0.17
12	0.63	0.10	25	1.00	0.25
13	0.63	0.09			

Table 4.
Silver concentration versus distance across a MPE with a chemically intercalated niobium disulphide electrode. Particle size 125 - 175 μm.

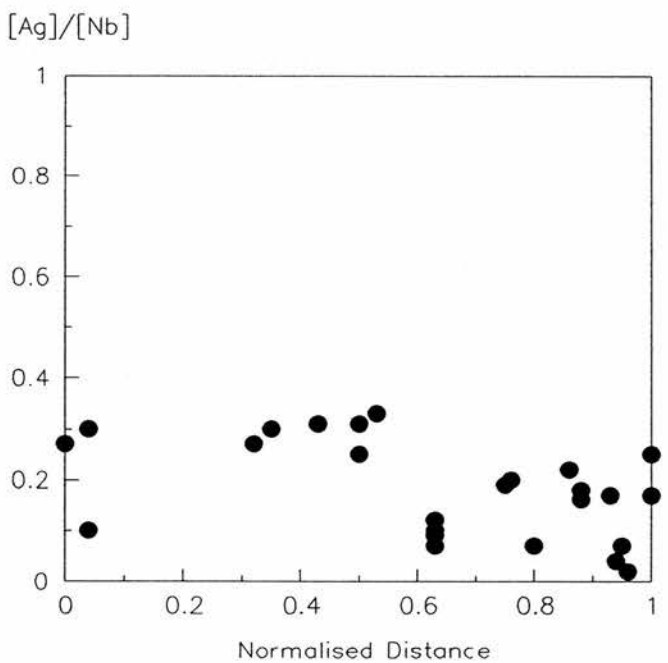

Figure 16.
Silver concentration versus distance for chemically synthesised $Ag_{0.05}NbS_2$.

Visual examination of the $Ag_{0.05}NbS_2$ crystals in this case showed them to be much less distinct from the surrounding glass particles. The crystalline shape was not so evident. This again reflects the difference in synthesis and correspond well with the broader peaks observed in the X-ray diffraction analysis which suggested a lower degree of crystallinity in this material.

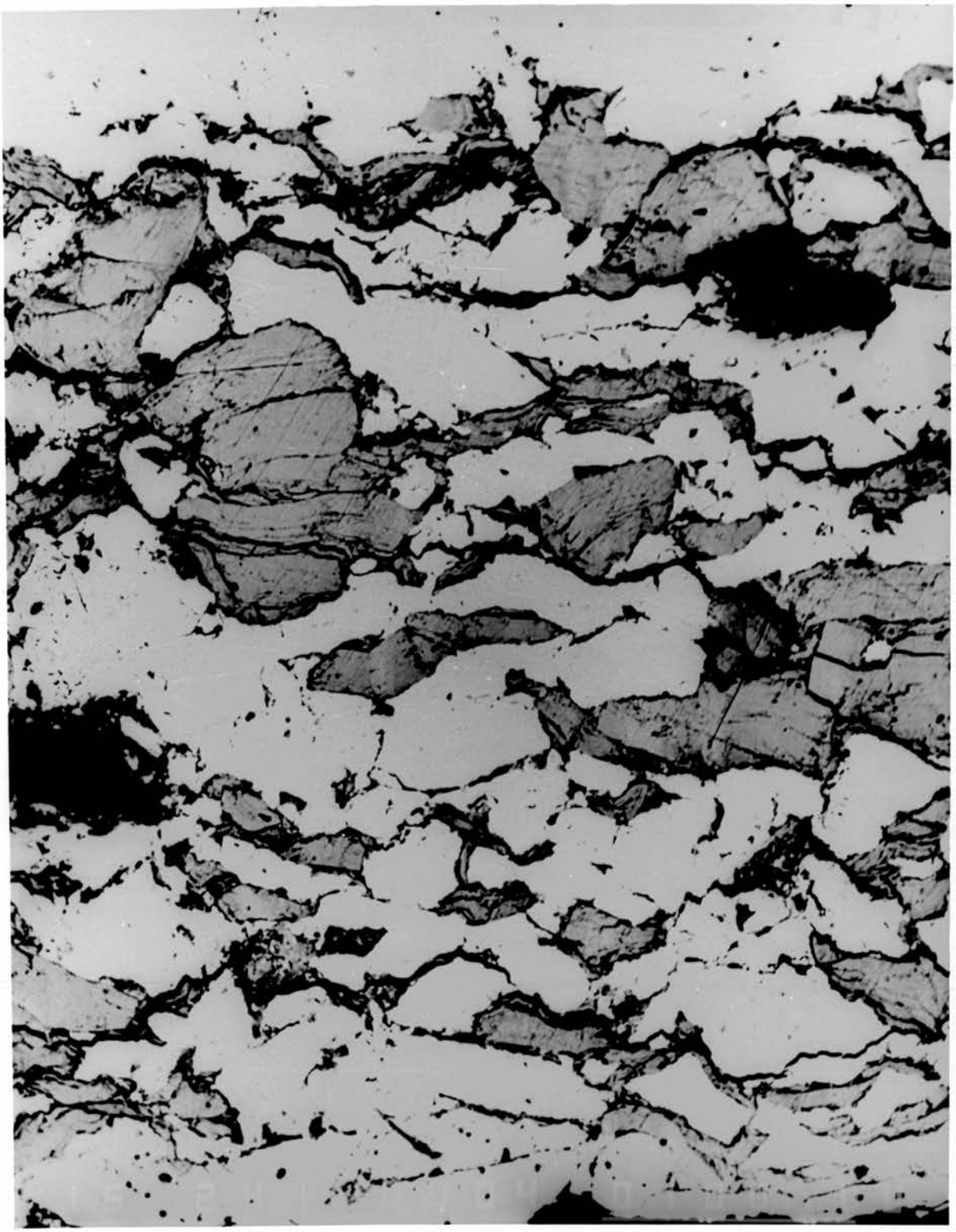

Plate 6.

Backscattered electron image of a composite electrode comprised of high conductivity glass G1 and niobium disulphide. Particle size $< 45\ \mu m$.

Plate 7.

Backscattered electron image of a composite electrode comprised of low conductivity glass G5 and niobium disulphide. Particle size < 45 μm.

6.2 EFFECT OF PARTICLE SIZE

The second set of experiments repeated the initial investigation but now the cells were constructed with glass and niobium disulphide particles of size < 45 μm taken from the bottom sieve.

Plates 6 and 7 depict typical back scattered electron images of sections through cells prepared with the high and low conductivity glasses respectively. On a qualitative level all the points made above for the differences between the two cells still hold. Plate 6 shows an even concentration of silver ions throughout the depth of the working electrode with the soft glass particles forming good boundaries with the niobium disulphide particles and meshing into each other. In contrast the NbS_2 particles in Plate 7 still show the uneven banded appearance mentioned earlier. The glass particles are again broken up into small fragments and have much sharper boundaries with the niobium disulphide particles.

Point	[Ag]/[Nb]	Point	[Ag]/[Nb]	Point	[Ag]/[Nb]
1	0.80	7	1.06	13	0.85
2	0.98	8	0.89	14	0.98
3	0.89	9	0.93	15	0.93
4	0.92	10	0.87	16	0.90
5	0.98	11	1.37	17	0.93
6	0.88	12	1.12	18	0.87

Table 5.
Silver concentration versus distance across a MPE with high conductivity glass as electrolyte. Particle size < 45 μm.
Points 1 - 6 across top edge of working electrode, points 7 - 12 and 13 - 18 across the centre.

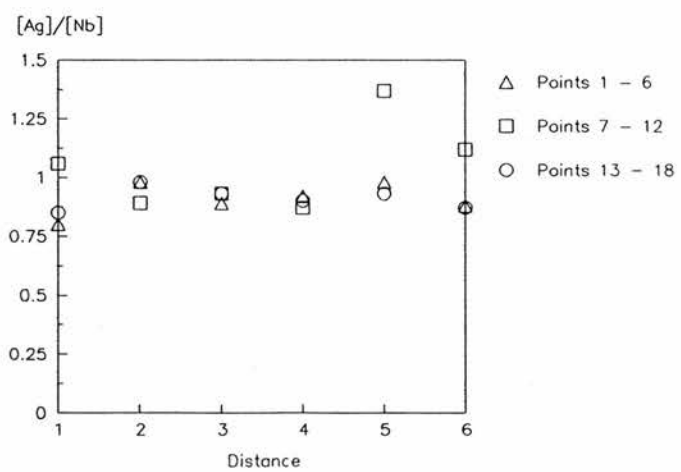

Figure 17.
Silver concentration versus distance - points from Table 5.

Three sets of quantitative measurements at different levels within the cell containing the high conductivity glass are given in Table 5 and depicted in Figure 17. The distance quoted now is not the normalised value but is simply shown as the number of the point being measured. In all cases the smallest numbered point is nearest to the electrolyte and the highest numbered point is at the external edge of the working electrode. Clearly, as with the larger particles reported earlier, there is no significant change in the silver concentration across the composite electrode. This is true at all heights within the cell.

Point	[Ag]/[Nb]	Point	[Ag]/[Nb]	Point	[Ag]/[Nb]
1	0.96	8	0.87	17	0.71
2	0.74	9	0.77	18	0.72
3	0.73	10	0.76	19	0.67
4	0.76	11	0.83	20	0.73
5	0.77	12	0.97	21	0.69
6	0.73	13	0.68	22	0.71
7	0.73	14	0.75	23	0.73
		15	0.74		
		16	0.74		

Table 6.
Silver concentration versus distance across a MPE with low conductivity glass as electrolyte. Particle size < 45 μm.
Points 1 - 7 across top edge of electrode, points 8 - 16 and 17 - 23 across the centre.

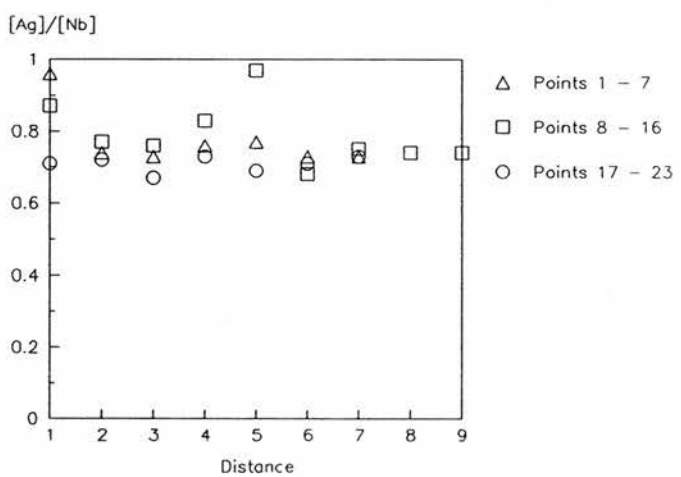

Figure 18.
Silver concentration versus distance - points from Table 5.

A similar set of results for the mixed phase electrode with the low conductivity glass is given in Table 6 and Figure 18. Now there is a significant difference between this cell and the cell with the larger particle sizes. Here the silver concentration is approximately level across the working electrode even when measurements are taken through the centre of the electrode.

These results tally with those reported in the previous chapter where differences in the apparent diffusion coefficient between composites containing G1 and G5 were only found when small particle sizes were used. This indicated that the cells were both functioning well as composites and that the diffusion process was dependent on ionic transport throughout the cell. The electron microprobe measurements made here confirm that the ions have indeed been transported throughout the bulk of the electrode.

6.3 OTHER COMMENTS

One disturbing aspect of all these results is that the ratio of silver to niobium concentrations is rarely close to the expected value of 0.05. In general the actual values are considerably higher. All possible checks were carried out and the results suggest that it is the samples themselves which may present a problem. The presence of iodine which dissociates under the beam currents used may cause some complications but should not affect those measurements restricted to the niobium disulphide crystals. The use of the [Ag]/[Nb] ratio should minimise any slight differences from measurement to measurement. However the trends in the results are still clear despite this disagreement with the expected ratio.

There are also considerable differences in the average [Ag]/[Nb] ratio observed in each experiment. The average values measured in each of the above experiments are reported in Table 7.

Table of Results	Average [Ag]/[Nb] Ratio	Standard Deviation
1	0.79	0.10
2	0.50	0.28
3	0.29	0.25
4	0.18	0.10
5	0.95	0.13
6	0.76	0.02

Table 7.
Average silver concentrations measured on each cell.

In theory these should all be identical since each cell was intercalated to the same 5 % level. Obviously not all particles were measured in a particular cell so this may account for the differences. One interesting feature is that those cells where the distribution is most even (Tables 1, 5 and 6) give the highest average silver concentration.

Only a very low proportion of non-intercalated particles of niobium disulphide were observed, even for the low conductivity electrolyte which illustrates the good mixing obtained during the cell construction procedure.

7 FURTHER WORK

The system investigated has proved very interesting and has clearly illustrated the effectiveness of using, and optimising, a mixed phase electrode. However the experiments performed have been very limited and there is considerable scope for further expansion and refinement. The protocol which has been defined and the experimental procedures used provide an easily accessible means of collecting data on the parameters crucial to the optimum operation of a mixed phase electrode.

The initial parameters worth investigating are those examined in the computer simulation and diffusion coefficient studies. That is the silver distribution could be examined as a function of the electrode thickness, the proportions of the two components and over a wider range of particle sizes. This should be reflected in the silver ion distributions.

It should also be possible to gain an estimate of the relative proportions of non-intercalated electrode particles by examination on a larger or more exhaustive scale than that performed here.

The time dependence of the distributions is also worth monitoring. All experiments performed here were done on cells sectioned and moulded immediately after passage of the intercalating current, although it was often a number of weeks before the full program of experiments was complete on the microprobe. The distribution at very short or very long times should prove interesting. It is surprising in the results reported here that there is still a distribution of concentration after such a long time and this may indicate that it is grain boundary contact problems that inhibit transport and not the effective ionic conductivity.

One initial impetus behind these experiments was to examine the cells at very low silver concentrations in an attempt to explain the unexpectedly fast diffusion coefficients observed for intercalation materials at such intercalant levels.[14] It has been suggested that this is due to enhanced transport along surfaces or edges of the crystal. If the accuracy of the technique could be improved

it might be possible to look at such effects. (Cells containing 1 % NbS_2, which were examined in initial experiments, had significantly more NbS_2 crystals with non-intercalated regions in their centres. This is possibly indicative of staging effects which may also explain the enhanced diffusion rates at low intercalation levels.)

Lastly the obvious extension is to related electrode materials such as titanium disulphide to see how the electrode material affects the results described. Such experiments must however be confined to model intercalants such as silver or copper since lithium has too low an atomic number for detection.

8 REFERENCES

1 Scholz G.A., Joensen P., Reyes J.M., Frindt R.F. "Intercalation of Ag in TaS_2 And TiS_2", Physica 105B (1981) 214

2 Kaluarachchi D., Frindt R.F. "Intercalation Islands And Stage Conversion In Ag-TiS_2", Physical Review B 28 (1983) 3663

3 Scholz G.A., Frindt R.F. "Structure And Staging Of Intercalated Ag_xTaS_2 And Ag_xTiS_2", Mat. Res. Bull. 15 (1980) 1703

4 Daumas N., Herold A. "Sur Les Relations Entre La Notion De Stade Et Les Mecanismes Reactionnels Dans Les Composes D'Insertion Du Graphite", C.R. Acad. Sci. Ser. C. 269 (1969) 373

5 Bonino F., Lazzari M., Mari C.M., Vincent C.A. "Interfacial Properties In Silver/Silver Glassy Electrolyte/Insertion Electrode Cells", Solid State Ionics 9 & 10 (1983) 677

6 Nairn I.A. "The Study Of Mixed Phase Electrodes In Solid State Cells", Ph.D. Thesis University Of St. Andrews (1984)

7 Baudry P., Armand M., Gauthier M., Masounave J. "In Situ Observation By S.E.M. Of Positive Composite Electrode During Discharge Of Polymer Lithium Batteries", Solid State Ionics 28 - 30 (1988) 1567

8 Chianelli R.R., Scanlon J.C., Rao B.M.L. "In Situ Studies Of Electrode Reactions :The Mechanism Of Lithium Intercalation In TiS_2", Journal Of Solid State Chemistry 28 (1979) 323

9 Johnson D.R., Hutchison J.L. "TEM Studies Of Lithium Intercalation In The Solid-State Battery Cathode, Titanium Disulphide", Inst. Phys. Conf. Ser. No. 78 (1985) Emag '85 325

10 Atlung S., Zachau-Christiansen B., West K., Jacobsen T. "The Composite Insertion Electrode Theoretical Part. Equilibrium In The Insertion Compound And Linear Potential Dependence", J. Electrochem. Soc. 131 (1984) 1200

11 Atlung S., West K., Jacobsen T. "Dynamic Aspects Of Solid Solution Cathodes For Electrochemical Power Sources", J. Electrochem. Soc. 126 (1979) 1311

12 Scott R.G., Mckee A.N. "Electron Microscopy", Physical Methods In Chemistry Part IIIa. Optical, Spectroscopic And Radioactivity Methods p291, Eds. Weissberger A., Rossiter B.W., Publ. Wiley-Interscience (1972)

13 Scott V.D., Love G. "Quantitative Electron-Probe Microanalysis", Ellis Horwood Ltd. (1983)

14 Smith M.J., Vincent C.A. "Relative Diffusion Coefficients Of Silver In NbS_2 And TiS_2 Host Materials", Electrochim. Acta 30 (1985) 931

1 AN INTRODUCTION TO PSEUDO-IONIC CONDUCTANCE (P.I.C.)

Many investigations have been made of the properties of two phase heterogeneous disordered mixtures of materials in an effort to improve the characteristics of one of the individual phases by the addition of the second phase, or to produce a material combining particular properties of both components. A wide variety of systems has been examined both experimentally and theoretically and some of the important theoretical results are outlined elsewhere in this thesis.

In particular the conductivity of mixtures of an electronic conductor with an insulator have been studied and explained using percolation theory.[1, 2, 3, 4] Prediction of the conductivity of mixtures of two conducting materials has been attempted as far back as Maxwell in 1881 and Meredith and Tobias reviewed this and other related theoretical developments.[5] More recently the resistance of metallic mixtures was predicted by Landauer[6] using his so called "effective medium theory".

In this chapter an attempt to enhance the ionic conductivity of a solid electrolyte (which transports metal ions M^+) by doping with particles of the metal (M) is described. This allows the possibility of pseudo-ionic conductance postulated by Nairn et al.[7] and illustrated in Figure 1.

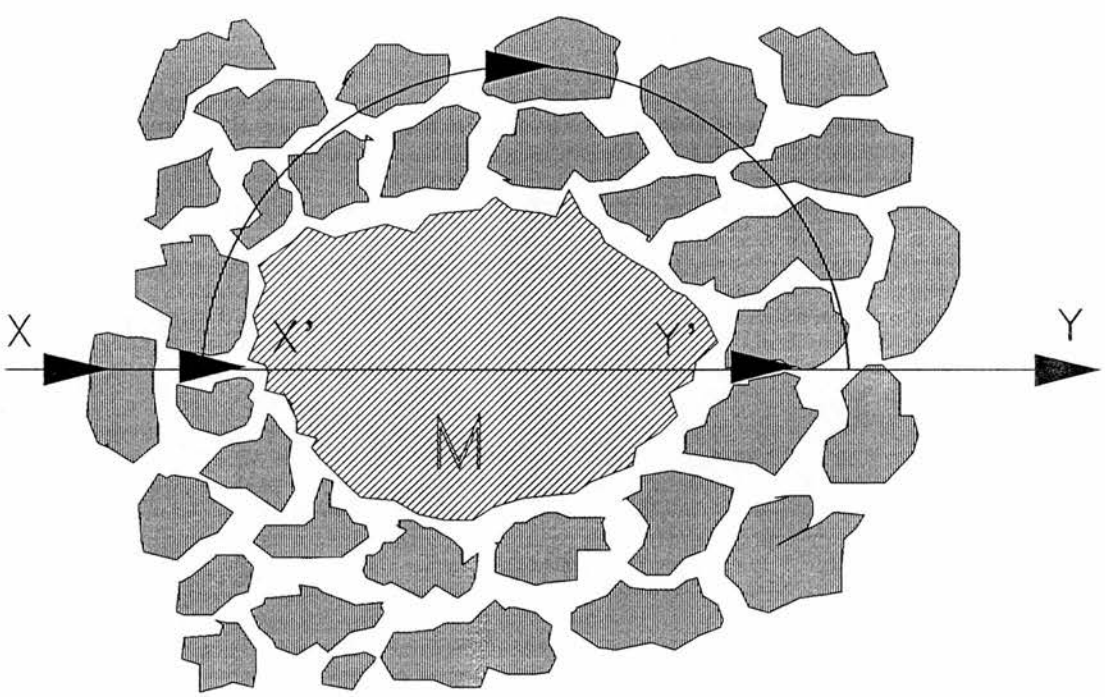

Figure 1.
A proposed mechanism for pseudo-ionic conductance

M is a metal particle surrounded by particles of solid electrolyte. When the process of a metal ion (M^+) moving from X to Y is considered two possible transport routes are possible. The first is the route shown on the diagram representing direct transport through the electrolyte around the metal particle :-

$$M^+(X) \quad \text{-----} > \quad M^+(Y) \qquad (1)$$

The alternative is a series of steps representing pseudo-ionic conductance and resulting in the same overall process as (1) :-

$$M^+(X) \quad \text{-----} > \quad M^+(X') \qquad (2)$$

$$M^+(X') + e^-(X') \quad \text{-----} > \quad M(X') \qquad (3)$$

$$e^-(Y') \quad \text{-----} > \quad e^-(X') \qquad (4)$$

$$M(Y') \quad \text{-----} > \quad M^+(Y') + e^-(Y') \qquad (5)$$

$$M^+(Y') \quad \text{-----} > \quad M^+(Y) \qquad (6)$$

Here the overall transport consists of ionic transport through the electrolyte from X to X' (2), deposition of a metal atom at the metal/electrolyte interface (3), electron transfer through the metal particle (4), the formation of a metal ion and an electron at Y' (5) and ionic transport from Y' to Y (6). This process can only occur if the charge transfer at the metal/electrolyte interface is fast. If this is the case then, because the electron transfer process is much more rapid than the ionic transfer process, the overall transport should be quicker resulting in an enhanced conductivity.

Previous experimental studies have undertaken modification of the ionic conductivities or other physical properties of solid electrolytes. Weston and Steele [8] demonstrated that the addition of up to 10 % alumina to lithium salt-PEO polymer electrolytes had a negligible effect on the ionic conductivity of the electrolyte but significantly improved the mechanical properties. More recently it has been shown [9] that the conductivity of NaSCN-PEO complexes can actually be enhanced by the addition of 30 mole per cent of very small particle size alumina, although at lower levels it is decreased.

This latter result agrees well with the well established concept of a composite electrolyte, as reviewed by Wagner [10] and Poulsen, [11] in which the conductivity of a poor (defect) ionic conductor can be enhanced, often by two or three orders of magnitude, by the addition of an inert insulating material. First reported for LiI-Al_2O_3 by Liang, [12] it has subsequently been shown that the conductivity enhancements arise for large volume fractions of the insulator and that the particle size is a critical parameter. [13] Submicron particles are generally required and the smaller the particle size

the greater is the enhancement suggesting that the surface area is a very important feature in the conduction mechanism. The physical properties of the composite electrolyte are also significantly improved relative to the original ionic conductor, the composite being considerably softer and more amenable to formation of good contacts in battery systems. As a consequence the addition of alumina to the glassy electrolytes used here has also been investigated.

Mixed phase electrolytes consisting of two ionically conducting components are now under investigation. $LiCF_3SO_3$ -PEO polymer electrolytes mixed with crystalline Li_3N exhibited conduction and physical properties intermediate between those of the two components [14] but the physical properties of the polymer were lost to some extent. More successful was the incorporation of Nasicon into NaI-PEO complexes where significant conductivity enhancement was achieved with no loss of processability of the polymer into films. There was seen to be considerable structural change of the PEO complex on the addition of the Nasicon, yielding a higher proportion of the higher conductivity amorphous PEO phase.

2 EXPERIMENTAL

As described in Chapter 2 all experimental measurements of conductivity were carried out using frequency response analysis on symmetrical two-electrode cells of the configuration:-

Ag, $Ag_6I_4WO_4$ / Glass + dopant / Ag, $Ag_6I_4WO_4$

The two glasses utilised in this series of experiments were glasses B4 and B5 from the ternary system AgI:$AgPO_3$:Ag_3AsO_4 (as described in Table 1, Chapter 2) with ternary mole fractions of AgI of 0.7 and 0.0 respectively. These electrolytes were selected for their extremely low conductivities which, it was hoped, would magnify any noticeable effect caused by pseudo-ionic conductance. Particles of silver and gold were added in a range of compositions from 0 to 10 weight per cent. Initially this was done at 2 % intervals but subsequently at smaller intervals. The particles of silver and gold additives were less than 50 microns in size. Two different particle sizes of alumina (< 250 μm and < 0.3 μm) were used in various cells when investigating the possibility of a composite electrolyte effect.

A variety of experimental problems were encountered during the measurement procedure and a number of interfering factors became evident as the work progressed.

Experiments on cells with no dopant particles showed that interfacial electrode effects were minimised by the use of mixed phase electrodes of silver and silver iodotungstate rather than pure compressed silver or thin film sputtered silver electrodes. A series of experiments determined that the optimum preparation conditions were those described in Chapter 2. In these experiments a variety of thicknesses of electrode and electrolyte regions were tried under differing pressures and the consistency and nature of the resultant conductivity spectra was examined. Measurements on a number of cells prepared under the ideal construction conditions yielded conductivities within 4-5 per cent of one another. This error is of the same order of magnitude as that possibly involved in the weighing of materials.

Further experiments immediately showed up the presence of problems when the electrolyte region contained particles of silver. A great deal of inconsistency crept into measurements done at different times. The most noticeable effects were changes in the cell resistance due to exposure of the cell to the atmosphere. Continual insertion, measurement, removal and immediate reinsertion of the cell into the cell holder showed a consistent alteration in the cell impedance as illustrated in Figure 2. This is probably attributable to water vapour or oxygen in the atmosphere, silver glasses being sensitive to the presence of these materials when not kept in darkness.[15, 16]

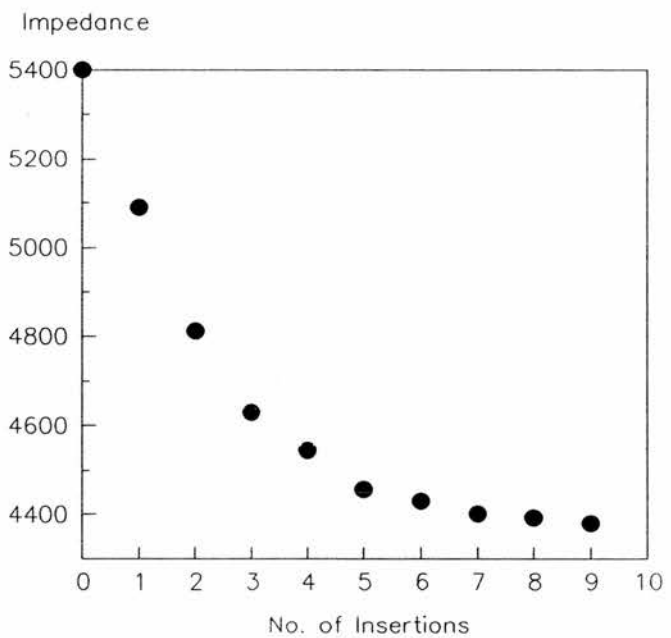

Figure 2.
Measured Cell Impedance (ohms) versus the number of times the cell was taken in and out of the holder (insertions).

The cells were therefore passed straight from the desiccator into the cell holder as rapidly as possible and then allowed to sit under the inert nitrogen atmosphere for at least half an hour before conductivity measurement. This was found, experimentally, to be long enough for the cell impedance to stabilise.

Other troubles emerged if a large number of measurements were performed on the same cell. Periodically the cells would undergo some form of failure at low frequencies during the analysis and the impedance of the cells fluctuated wildly at these frequencies, as illustrated in Figure 3. The sudden changes in impedance suggested the momentary short circuiting of the cell during the AC cycling, possibly due to the presence of dendrites joining adjacent silver particles. However, no evidence of such formations was evident when the cells were sectioned and the silver particles examined under the electron microprobe. The problem was overcome almost completely when the peak potential of the applied signal was reduced from 0.1 V to 0.01 V.

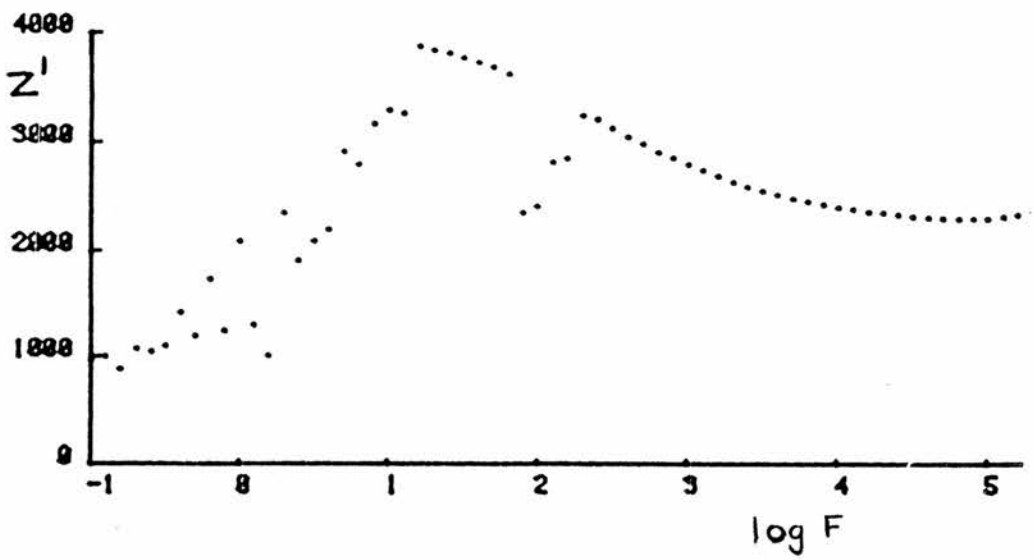

Figure 3.
Impedance plot for a cell with 6% silver dopant failing at low frequencies due to possible dendrite formation.

Thus in view of these problems, standard conditions were defined to ensure as much consistency as possible. All measurements were carried out under identical conditions of continuous dry nitrogen flow and constant temperature (25 °C). All cells were inserted into the cell holders, the holding screws

tightened to hand tight pressure, and left to equilibrate to constant temperature measured by the thermocouple adjacent to the cell. Electrical connections were made via shielded cabling and the standard resistor was sealed into its BNC socket with Araldite epoxy adhesive to ensure that even contact was maintained. A series of limited range frequency scans were then carried out to ensure that the cell impedance had stabilised, before the actual conductivity was actually measured using the reduced peak voltage and a frequency range of 1 Hz to 100000 Hz. The conductivities quoted below are the average of at least three consecutive measurements on each cell.

3 RESULTS

Figure 4 illustrates the type of plot obtained from the FRA analysis for a pure glass and Figure 5 for a glass doped with small particles of silver. Essentially under the almost ideal conditions used the pure glass acts as a resistor producing a linear non-frequency dependent value of impedance. (Slight deviations at lower frequencies are attributable to electrode effects.[17]) The impedance is generally taken from the totally linear region at higher frequencies as shown and this value is used to calculate the DC conductivity after allowing for the cell constant. On an Argand diagram of real versus imaginary impedance (not illustrated) an essentially vertical line is observed as expected for a pure resistor.

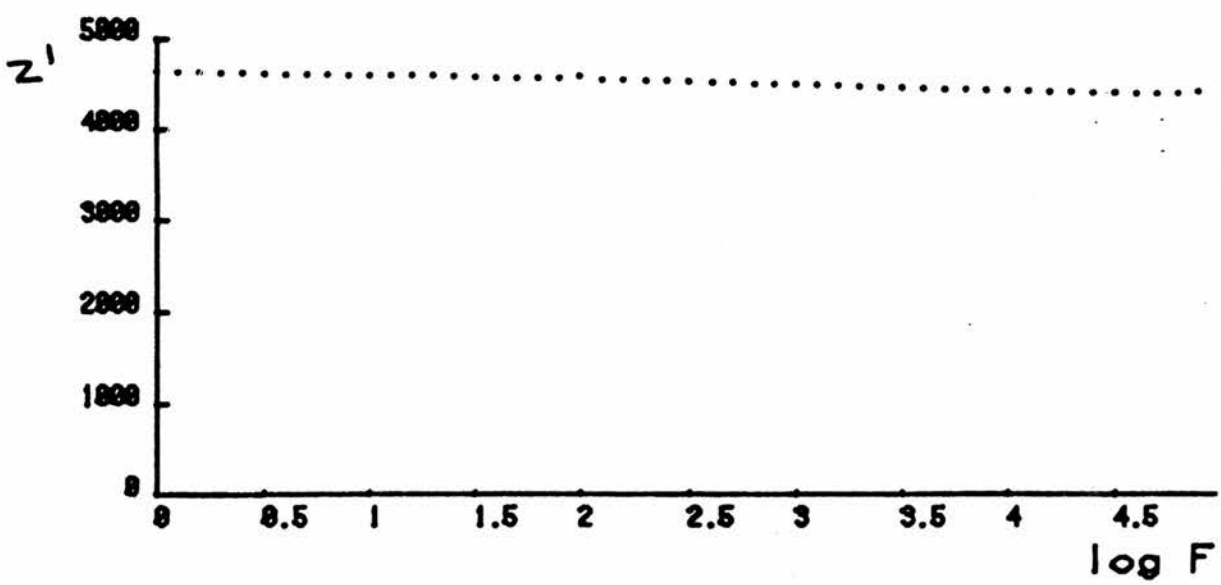

Figure 4.
Sample impedance plot for undoped cell showing linearity of Z' vs. frequency plot.

The doped glass represents a more complex picture, exhibiting a relaxation at moderate frequencies. This and the semi-circle found in the Argand diagram are typical of a circuit consisting of a resistor (representing the bulk impedance of the electrolyte) in series with a parallel combination of resistor and capacitor. This latter component arises from the effect of the silver particles, there being a double layer capacitance at the surface of the particles and a new resistance corresponding to the resistance of the silver particles themselves.

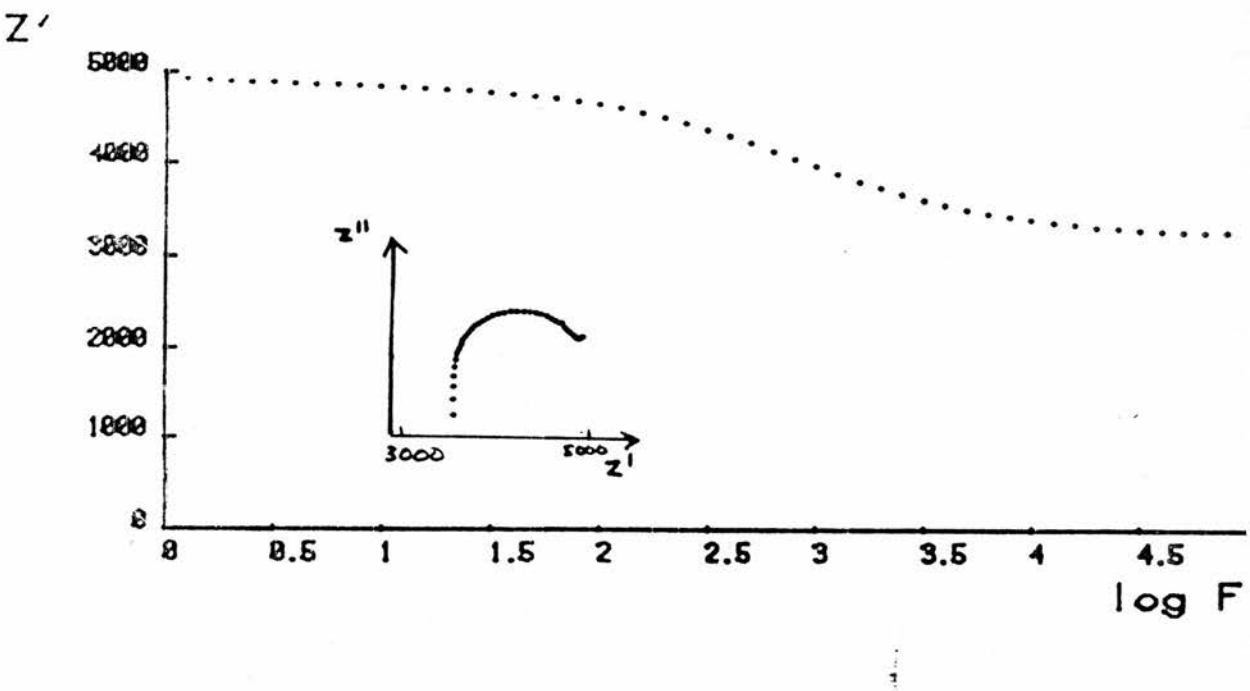

Figure 5.
Sample impedance plot for doped cell showing capacitative relaxation at moderate frequencies. Inset shows semi-circle found on an Argand diagram.

Both the high and low frequency plateau regions were extrapolated back to zero frequency (using a least squares fitting program - Appendix 1). The low frequency extrapolation was taken to be the DC conductivity and the difference between this and the high frequency extrapolation gives an indication of the capacitance. All the results quoted are the averaged values of a number of measurements on each cell and results from more than one cell are illustrated at some percentages.

For the lower conductivity glass (G5) Tables 1 and 2 display the calculated values of the high and low frequency conductivities (σ_{high} and σ_{low}) and the difference between them ($\Delta\sigma$) as extrapolated in the manner described above. The former table is for doping with silver and the latter for gold.

Percentage of silver	σ_{high} ($x10^7/Scm^{-1}$)	σ_{low} ($x10^7/Scm^{-1}$)	$\Delta\sigma$ ($x10^7/Scm^{-1}$)
0.0	3.58	3.94	0.36
0.0	2.65	2.76	0.11
0.5	1.94	2.05	0.11
1.0	4.91	6.12	1.21
1.0	2.00	2.13	0.13
1.5	2.78	3.19	0.41
2.4	2.73	3.11	0.38
1.9	2.20	2.45	0.25
2.5	2.47	2.90	0.43
3.0	3.12	3.90	0.77
3.0	2.55	3.03	0.48
4.2	1.71	2.02	0.31
5.4	1.89	2.44	0.55
6.2	2.69	3.80	1.11

Table 1.
Extrapolated conductivities for silver dopant in glass G5.

Percentage of gold	σ_{high} ($x10^7/Scm^{-1}$)	σ_{low} ($x10^7/Scm^{-1}$)	$\Delta\sigma$ ($x10^7/Scm^{-1}$)
1.0	2.15	2.35	0.2
2.9	2.10	2.43	0.33
4.0	1.80	2.07	0.27
5.0	1.78	2.10	0.32
5.3	1.60	1.86	0.26
6.0	1.71	2.02	0.31

Table 2.
Extrapolated conductivities for gold dopant in glass G5.

Figures 6 and 7 illustrate the change in conductivities with the percentage of each dopant, and Figures 8 and 9 the change in the relaxation measured. Error bars (not shown here) can be taken to be 5 % of the maximum conductivity on either side of the calculated point. This corresponds with the deviations in conductivity obtained in the experiments which checked the consistency of the cell manufacturing process. Even conservative estimates of all the possible errors are higher than this value and this is reflected in the scatter of the results.

For this glass it is apparent that there is no clear trend on adding silver to the electrolyte. On average the conductivities remain approximately the same as the silver level increases from 0 to 6 %. Some measurements at 10 % levels (not shown) also fitted this pattern. No higher levels were used because of the danger of approaching the percolation threshold, and also because the experimental difficulties involved with dendrite formation discussed above became more predominant as the silver concentration was increased. The considerable variation in results found even with nominally identical cells may reflect the hardness of this glass which could cause large differences in intergranular contacts.

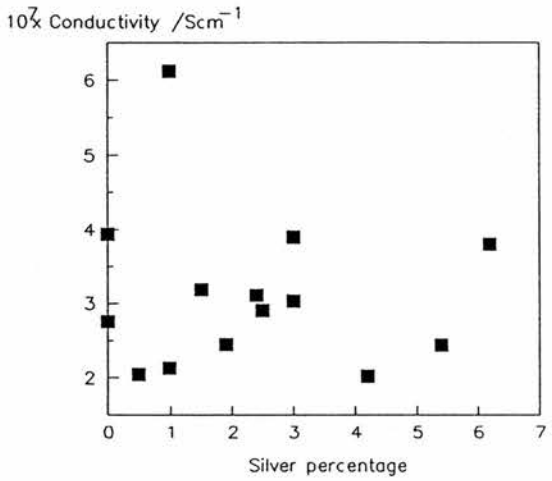

Figure 6.
Effect of silver concentration on conductivity of glass G5.

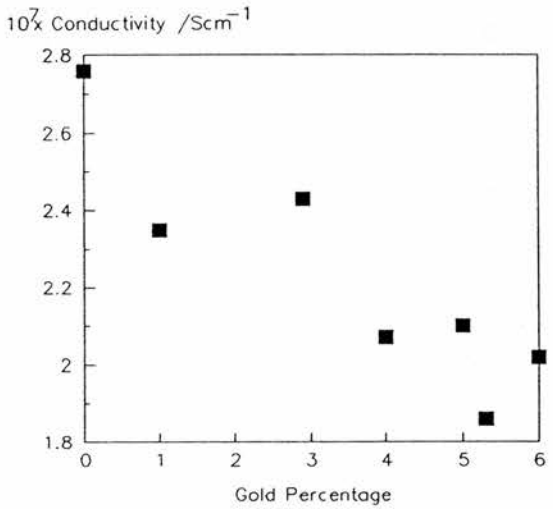

Figure 7.
Effect of gold concentration on conductivity of glass G5.

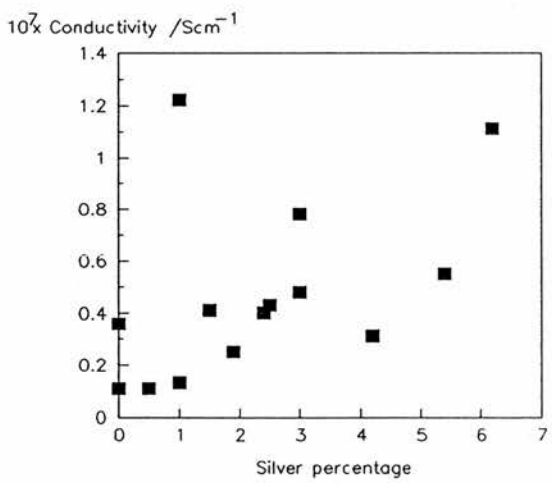

Figure 8.
Effect of silver concentration on conductivity relaxation of glass G5.

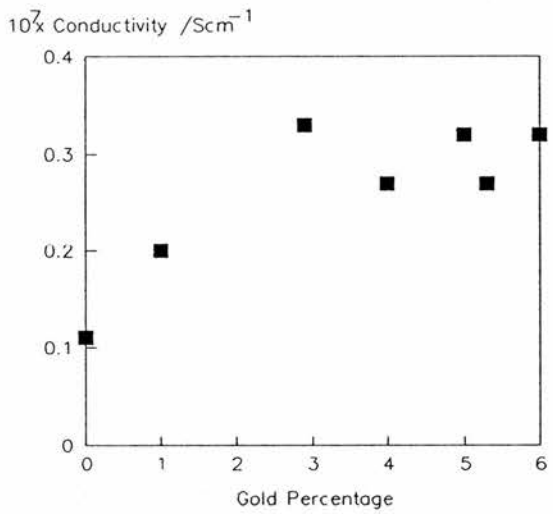

Figure 9.
Effect of silver concentration on conductivity relaxation of glass G5.

The results obtained for the addition of gold show a fairly clear decrease in the conductivity with increasing gold concentration. The conductivity is approximately 30 % lower when 5 % by weight of gold is added.

Both silver and gold dopants cause an increase in the value of $\Delta\sigma$ as the level of either metal is increased. The gradient of the increase for silver is approximately twice that for gold.

Tables 3 and 4 outline the results from experiments performed on cells with the glass G4 as electrolyte and with the same dopants. The results are plotted in Figures 10 - 13 where Figures 10 and 11 illustrate the change in conductivity on respectively increasing the amount of silver and gold particles. Figures 12 and 13 depict the change in σ for the same dopants.

Percentage of silver	σ_{high} ($x10^5/Scm^{-1}$)	σ_{low} ($x10^5/Scm^{-1}$)	$\Delta\sigma$ ($x10^5/Scm^{-1}$)
0.0	2.00	2.10	0.10
1.0	1.87	2.05	0.18
2.0	1.70	1.90	0.20
3.0	1.70	1.99	0.29
4.0	1.82	2.20	0.37
5.0	1.56	2.02	0.45

Table 3.
Extrapolated conductivities for silver dopant in glass G4.

Percentage of gold	σ_{high} ($x10^5/Scm^{-1}$)	σ_{low} ($x10^5/Scm^{-1}$)	$\Delta\sigma$ ($x10^5/Scm^{-1}$)
1.0	1.85	1.95	0.10
1.9	1.93	2.10	0.17
2.9	1.74	1.93	0.19
4.0	1.78	1.99	0.21
5.1	1.64	1.90	0.26
6.2	1.71	1.96	0.25

Table 4.
Extrapolated conductivities for gold dopant in glass G4.

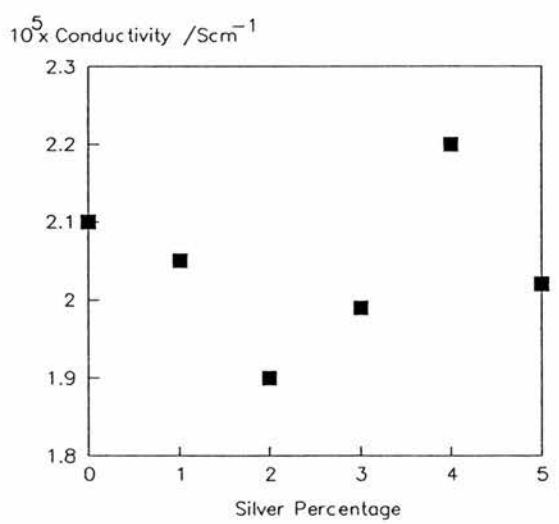

Figure 10.
Effect of silver concentration on conductivity of glass G4.

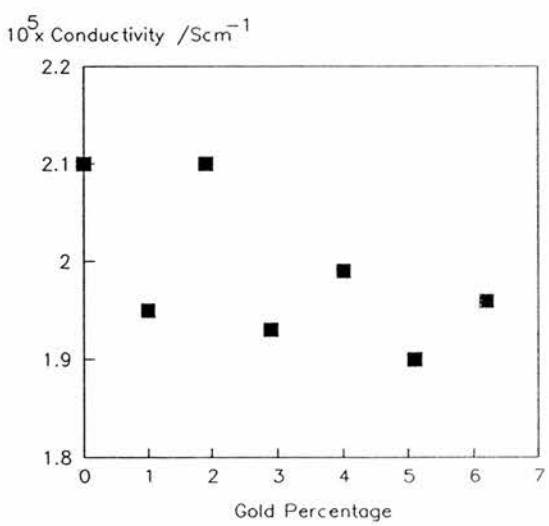

Figure 11.
Effect of gold concentration on conductivity of glass G4.

The results are still unclear and no distinct pattern emerges on the addition of either silver or gold. However there are indications that the conductivity tends to decrease rather than increase for silver addition. Gold also seems to reduce the conductivity as expected, though now only by about 15 % when introduced at 5 % levels by weight. Once again there is a clear increase in the double layer capacitance for either metal, the value for silver being approximately twice that of the gold.

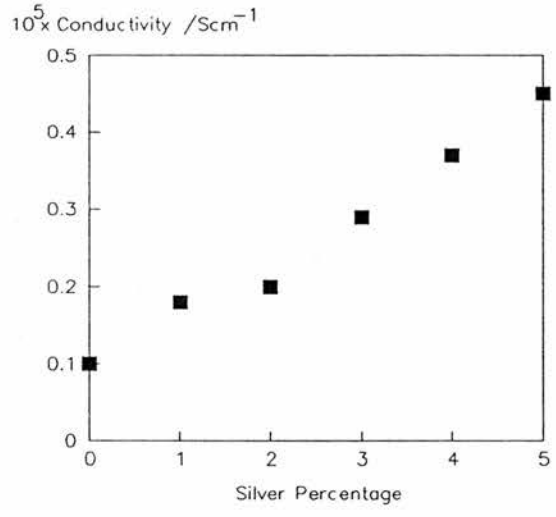

Figure 12.
Effect of silver concentration on conductivity relaxation of glass G4.

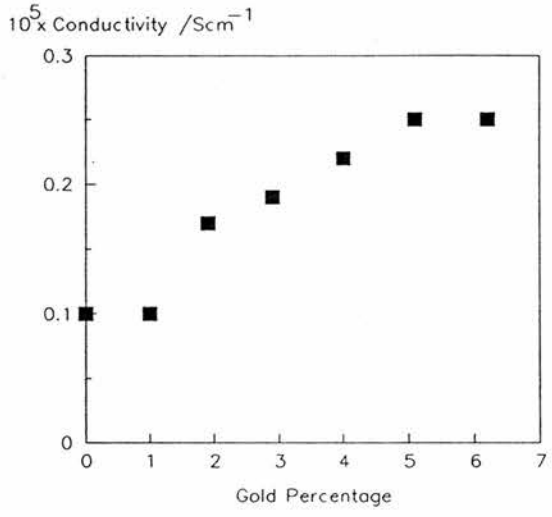

Figure 13.
Effect of silver concentration on conductivity relaxation of glass G4.

Any attempt at putting alumina into the electrolyte to produce a composite electrolyte enhancement of the conductivity had totally the opposite effect. The measured cell impedances for the introduction of both large and small alumina particles at various levels are tabulated in Table 5. All demonstrate a major increase in the electrolyte impedance giving no indication of any composite electrolyte effect.

Percentage of alumina	Impedance (Ohms)	Particle Size (microns)
0	4100	< 50
5	7900	< 50
30	21000	< 50
0	4100	< 0.3
2	4800	< 0.3
10	16000	< 0.3

Table 5.
Impedance of cells of glass G5 doped with various percentages of alumina.

4 CONCLUSIONS AND FURTHER WORK

The clearest factor to emerge from the results described is that there is no observable conductivity enhancement on the addition of silver dopant particles to the glasses considered. Thus it can be concluded that the suggested pseudo-ionic conductivity mechanism is not occurring in this system. Experimental errors and difficulties may shield a minor effect but the magnitude of such an enhancement is therefore negligible and unlikely to be of any practical use. This is particularly true since the use of metal dopant particles in the cell configuration described caused a variety of complications at low signal frequency. Considerable operational difficulties are likely to result in a practical system supplying or receiving a direct current.

Gold particles do seem to reduce the conductivity of the electrolyte to a minor extent but owing to the possibly large magnitude of the systematic errors this cannot be confirmed with any confidence. However such a reduction is to be expected in such situations since the gold particles block the ionic conduction, causing the silver particles to follow a more tortuous and thus higher impedance path.

For both silver and gold additives increasing the number of particles increases the $\Delta\sigma$ value observed. This is expected from the corresponding enhancement in the metal surface area associated with a larger number of particles. Any capacitative effect is proportional to the surface area and therefore will increase. That the enhancement is greater for silver than gold probably reflects that there is some form of surface process occurring at the silver particles that is limited at the gold particles. This is very likely to be a transfer mechanism akin to that postulated for pseudo-ionic conduction. However the rate for such a transfer compared with direct transport through the glass electrolyte must be of the same order of magnitude or lower as the conductivity is unaffected by the presence of such a mechanism.

The presence of alumina only serves to reduce the conductivity of the cells used, again presumably by increasing the tortuosity of the conduction paths. A composite electrolyte cannot entirely be ruled out as the fabrication of the electrolytes here is quite different from that generally used for composite electrolytes. [18]

A more recent investigation [19] into pseudo-ionic conductance examined the related system $AgI:Ag_2O:B_2O_3$ in a similar program of experiments. An added refinement was to use a complex analysis fitting program [20, 21] to calculate the best values for the model equivalent circuit given in Figure 14 :-

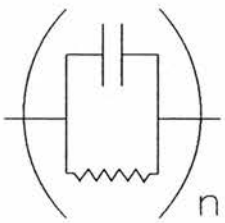

Figure 14.
Model equivalent circuit used in fitting programme.

Here n represents the number of repetitions of the basic parallel circuit. Good fits with experimental data were found for n = 6, and the resistance of the pure electrolyte was taken to be the value of R1, the capacitance C1 being negligible. (The equivalent circuit mentioned earlier corresponds to the one used by Anderson with n = 2 and C1 being negligible. The more complex results are likely to fit a similar equivalent circuit with larger values of n.)

The results showed that on the addition of silver particles there was again no evidence for pseudo-ionic conductance. The silver particles act solely as a block to the ionic conduction, the interfacial transfer energy obviously being higher than the energy required for transport around the particle. However on the addition of alumina some evidence of a composite electrolyte interfacial enhanced transport mechanism was noted at moderate (10%) alumina levels. However at lower levels a decrease in the cell conductivity was observed, confirming the results of the current work. No work was done on the inclusion of gold particles for a comparison with the results found for silver.

These results reaffirm that pseudo-ionic conductance is not a viable conduction mechanism under the conditions studied.

Possible further work could investigate changes of particle sizes and the addition of other conductors and insulators, particularly to confirm the work of Anderson. Possible benefits are likely to be extremely limited for pseudo-ionic conductance, but the indications of a composite electrolyte effect may be significant.

5 REFERENCES

1 Shante V.K.S., Kirkpatrick S. "An Introduction To Percolation Theory", Advances In Physics 20 (1971) 325

2 Stinchcombe R.B. "The Branching Model For Percolation Theory And Electrical Conductivity", J. Phys. C: Solid State Phys. 6 (1973) L1

3 Kirkpatrick S. "Classical Transport In Disordered Media : Scaling And Effective Medium Theories", Physical Review Letters 27 (1971) 1722

4 Kirkpatrick S. "Percolation And Conduction", Reviews Of Modern Phys. 45 (1973) 574

5 Meredith R.E., Tobias C.W. "Conduction In Heterogeneous Systems", Adv. In Electrochem. And Electrochem. Engineering 2 (1962) p18, Delahay P., Tobias C.W., Publ. John Wiley And Sons (1962)

6 Landauer R. "The Electrical Resistance Of Binary Metallic Mixtures", Journal Of Applied Physics 23 (1952) 779

7 Nairn I.A., Smith M.J., Vincent C.A. "Mixed-Phase Electrodes In Solid State Cells", Solid State Ionics 9 & 10 (1983) 383

8 Weston J.E., Steele B.C.H. "Effects Of Inert Fillers On The Mechanical And Electrochemical Properties Of Lithium Salt-Poly(Ethylene Oxide) Polymer Electrolytes", Solid State Ionics 7 (1982)

9 Yuankang H., Zhusheng C., Zhiyi Z., Chaoying W., Liquan C. "Effect Of Dispersed Phase Particles On Electrical Conduction Of PEO-NaSCN", Materials For Solid State Batteries p319, Eds. Chowdari B.V.R., Radhakrishna S., Publ. World Scientific Publ. Co. Singapore (1986)

10 Wagner J.B. "Composite Electrolytes", Solid State Batteries (Nato Asi Series. Series E: Applied Sciences No. 101) p47, Eds. Sequeira C.A.C., Hooper A., Publ. Martinus Nijhoff Publishers (1985)

11 Poulsen F.W. "Composite Electrolytes", Transport-Structure Relations In Fast Ion And Mixed Conductors, 6th Riso International Symposium p37, Eds. Poulsen F.W. Et Al., Publ. Riso International Laboratory

12 Liang C.C. "Conduction Characteristics Of The Lithium Iodide-Aluminium Oxide Solid Electrolytes", J. Electrochem. Soc. 120 (1973) 1289

13 Poulsen F.W., Moller P.J. "Conductivity Dependence Of Alumina Surface Area For LiI-Alumina Composites, Transport-Structure Relations In Fast Ion And Mixed Conductors, 6th Riso International Symposium p159, Eds. Poulsen F.W. Et Al., Publ. Riso International Laboratory

14 Skaarup S., West K., Zachau-Christiansen B. "Mixed Phase Solid Electrolytes", Solid State Ionics

15 Evans J. "The Anodic Electrolysis Products Of Silver Iodide Arsenate ($Ag_7I_4AsO_4$ Glass", Senior Honours Project Report, St. Andrews University (1984-5)

16 Magistris A., Chiodelli G., Schiraldi A. "Formation Of High Conductivity Glasses In The System AgI-Ag_2O-B_2O_3", Electrochim. Acta 24 (1979) 203

17 Boukamp B.A., Raistrick I.D., Huggins R.A. " Use Of Low Frequency Ac Measurements In Solid State Electrochemistry", Fast Ion Transport In Solids. Electrodes And Electrolytes p177, Eds. Vashista P., Mundy J.N., Shenoy G.K., Publ. North-Holland Publishing Company (1979)

18 "Solid State Batteries", Nato Asi Series. Series E: Applied Sciences No. 101, Eds. Sequeira C.A.C., Hooper A., Publ. Martinus Nijhoff Publishers (1985)

19 Anderson M.A." An Investigation Into Pseudo-Ionic Conductance", Senior Honours Project Report (1986) St. Andrews University

20 Boukamp B.A. " A Package For Impedance/Admittance Data Analysis", Solid State Ionics 18&19 (1986) 136

21 Boukamp B.A. "A Nonlinear Least Squares Fit Procedure For Analysis Of Immitance Data Of Electrochemical Systems", Solid State Ionics 20 (1986) 31

1 SUMMARY

The work in this thesis has given a considerable insight into the potential and actual properties of a mixed phase electrode. It has highlighted a number of interesting features concerning optimisation of composite electrodes for practical use in solid state battery systems. Experimental evidence has been obtained which confirms some of the predictions of the composite electrode behaviour made by Atlung.[1] The experimental work and results obtained from the statistical computer model have emphasised the necessity for consistency in preparation and technique in assessing properties such as the apparent chemical diffusion coefficient of mixed phase electrodes. Some pointers have been made as to better experimental procedures required to ensure such consistency.

The most important parameter found throughout this investigation was the particle size and shape, of both the electrolyte and electrode components, utilised in manufacturing a composite electrode.

The early work in Chapter 2 shows that the electrolyte conductivity increases with a reduction in particle size, even with a high conductivity glass electrolyte. Measurements of the apparent diffusion coefficient also showed a clear dependence on the size of the electrode particles when the electrolyte conductivity was good. Using smaller particles increased the apparent chemical diffusion coefficient measured on the cell if other parameters were the same. The efficiency of the composite, as measured by the degree of silver distribution found using electron probe microanalysis techniques, was also found to improve with a reduction in the particle size.

The use of large electrode particles resulted in a situation where, in terms of the apparent diffusion coefficient, the composite electrode is dominated by diffusion in the electrode particles and is not related to parameters of the composite as a whole. An electrode composed of the pure electrode material or using very low conductivity glass gives the same apparent diffusion coefficient as one with high conductivity glass. However in the latter two cases there is a much reduced utilisation of the electrode particles in the bulk of the mixed phase electrode presumably due to ion transportation problems. The majority of intercalated ions are found in particles close to the source of the ions.

The results from the computer model confirm that the optimal contact area between particles is obtained when the particles are of the same size. Increasing the particle size of one or both components resulted in a decrease in the overall contact area in all cases. Another way of considering this is that optimal contact area is gained when the particle size is small in relation to the total size of the composite. Increasing the particle size on lattices of the same size decreases the contact area.

However if the particle size is maintained constant and the thickness of the lattice is increased then the overall contact area increases. This can be considered as an effective reduction in the particle size relative to the composite thickness and demonstrates the benefits of moving to smaller particle sizes.

The computer model also predicts that the particles size distributions should be as narrow as possible. Changes such as size and shape away from the optimum values result in rapid reductions in the overall contact area.

The only other method of increasing the contact area that was predicted by the computer model was to increase the coordination between particles. This resulted in much more dramatic improvements in the contact area between the two components. This suggests using particles of the same shape but different sizes or of different shapes in order to change the coordination in a real system. The electron microprobe analysis suggests that, in the system investigated, the coordination and contact area is quite good but is also dependent on the physical properties of both components.

In a practical working system therefore great care should be taken in optimising the particle size of both components of the mixed phase electrode in order to give the best balance of electrolyte conductivity, electrode material utilisation and potential power output from the composite. All the work reported here points to the particle size being as small as possible to achieve this.

The second important parameter was found to be the thickness of the electrode. According to the computer model the thicker the electrode the larger the contact area per particle (as discussed above). This was confirmed by the measurements of apparent diffusion coefficient which were larger with thicker electrodes, despite the potentially adverse effects of higher overall resistance. However these results on thicker electrodes parallelled those on thinner electrodes but with smaller particles, emphasising that, even in experimental studies, it is the particle size relative to the thickness of the composite that is the important parameter.

All the above results emphasise the necessity for consistent construction techniques in manufacturing composite electrodes. Relatively small alterations in the particle size, shape and distribution can effect markedly the effective functioning of the composite.

This work has also emphasised the importance in using appropriate experimental conditions and analysis techniques when assessing the physical characteristics of the composites as a whole.

Experimentally it was shown that diffusion coefficients were considerably affected by the analysis technique used. Values measured during the application of current pulses were different from those calculated during the subsequent relaxation. Calculating the diffusion coefficient using the semi-infinite diffusion analysis yielded lower diffusion coefficients apparently because of assumptions made during the analysis. The method proposed by Atlung[2] is felt to be more realistic because all parameters used in calculating the apparent diffusion coefficient are measured on each cell for each applied pulse.

However errors in measuring the change in overpotential during short or small magnitude current pulses also considerably affected the diffusion coefficients calculated. Therefore in terms of ease and reliability it was concluded that the best method is to measure the gradient of overpotential versus the root time parameter once on the cell under investigation during a long pulse and to use this value in subsequent calculations on that cell only. This gives benefits in that shorter pulses can be used for many experiments so that possible phase changes are not encountered. In addition the equilibrium period between an intercalating and de-intercalating pulse is no longer necessary.

However when cells were manufactured under "optimum" conditions of particle size and analysed using the most appropriate technique the apparent diffusion coefficient was shown to be dependent on the effective ionic conductivity of the mixed phases electrode as predicted by theory.

2 REFERENCES

1 Atlung S., Zachau-Christiansen B., West K., Jacobsen T. "The Composite Insertion Electrode Theoretical Part. Equilibrium In The Insertion Compound And Linear Potential Dependence", J. Electrochem. Soc. 131 (1984) 1200

2 Atlung S. Personal Communication to C.A. Vincent

1 DATA ANALYSIS

This appendix details the procedures and programs used in calculations mentioned in this thesis. The two main areas where repetitive calculations were involved were:- a) conductivity calculations in the pseudo-ionic conductivity experiments. b) The calculation of apparent diffusion coefficients and analysis of the pulse data to obtain these as described in Chapter 5.

2 CONDUCTIVITY CALCULATIONS

As described in Chapter 2 frequency response analysis was used to measure conductivities of pure electrolytes and of electrolytes doped with various additives. Figure 1 illustrates schematically the impedance versus log frequency plots obtained for the pure and doped systems, and the extrapolations required to determine the zero frequency conductivity. In real situations both curves deviate from ideality at low frequencies due to the interference of electrode effects.

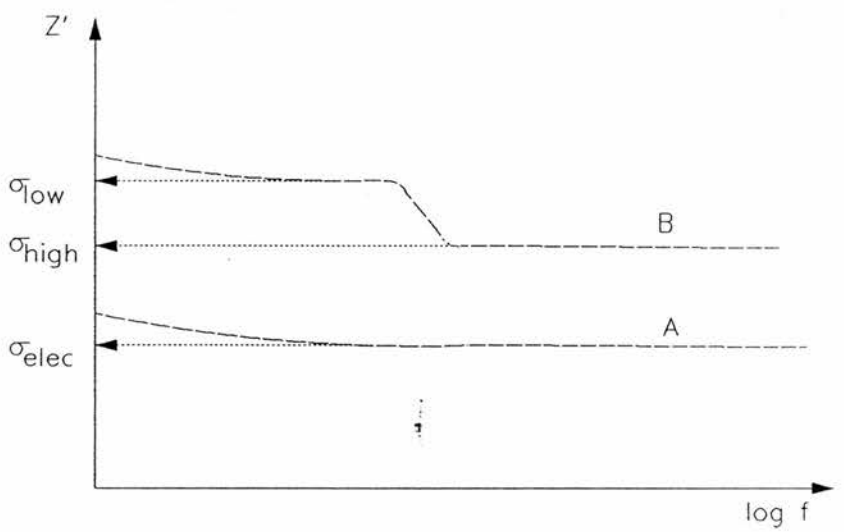

Figure 1.
Schematic representation of a) Extrapolation to electrolyte conductivity and b) low and high frequency conductivity extrapolations for doped cell.

In determining the conductivities of the pure electrolyte the impedance was calculated as the average of the values falling in the plateau region invariably observed at frequencies around 10^4 to 10^5 Hz. These values were displayed on the screen during the execution of the FRA control program and were taken direct from the screen for averaging. As usual the electrolyte conductivity is calculated by dividing by the cell constant as measured.

As outlined in Chapter 7 two extrapolations were made for the more complex pseudo-ionic conductance FRA spectrum, yielding estimations of the high and low frequency impedances. A program was written in Fortran 77 on the VAX 1170 mainframe computer to accomplish this. This programme (FRA.FOR) is listed below as programme 1.

The original data was examined graphically on the microcomputer to ensure that it was suitable for analysis by FRA.FOR i.e. there were no major deviations from plateaux in the appropriate high and low frequency regions.

Programme 1.
Analysis of frequency response data.

```
1 -- C FRA DATA ANALYSIS PROGRAM - MICHAEL ROGERS 8/4/86
 2 -- C DECLARATION SECTION
 3 -- C
 4 --      INTEGER FILENO, FIRST, LAST, COUNT
 5 --      CHARACTER*80 TITLE
 6 --      CHARACTER*9 INFILE, OUTFILE
 7 --      REAL CONST, STRES, TEMP, GRDNT, INTCPT,SDEVGR, SDEVIN
 8 --      DIMENSION F(100), A(100), B(100), Z1(100), Z2(100)
 9 -- C
10 -- C THE NUMBER OF FILES TO BE ANALYSED IS NOW DETERMINED
11 -- C
12 --      PRINT*, 'This program converts the F,a,b output form the FRA,
13 --      PRINT*, 'stored in the files FRAnnn.dat, to F,Z1,Z2, and'
14 --      PRINT*, 'outputs the data to file FZZnnn.dat'
15 --      PRINT*, 'The best straight line is also calculated'
16 --      PRINT*, 'and the relevant features output to the file LINE.DAT'
17 --      WRITE(6,5)
18 --    4 FORMAT(T2, ' What is the number of the first FRA file?')
19 --      READ(5,*) FIRST
20 --    5 FORMAT(T2, ' What is the number of the last FRA file?')
21 --      READ(5,*) LAST
22 -- C
23 -- C THE DATA IS NOW READ AND CONVERTED TO F,Z',Z"
24 -- C
25 --      DO FILENO = FIRST,LAST
26 --        INDEX=1
27 --        WRITE(INFILE,1) FILENO
28 --    1   FORMAT('FRA,I3.3)
29 --        WRITE(OUTFILE,2) FILENO
30 --    2   FORMAT('FZZ,I3.3)
31 --        OPEN(UNIT=16, READONLY, NAME=INFILE, STATUS='OLD')
32 --        OPEN(UNIT=17, NAME=OUTFILE, STATUS='NEW',
33 --     £                CARRIAGECONTROL='LIST')
34 --        READ(16,3) TITLE
35 --    3   FORMAT(A)
36 --        READ(16,*) CONST, STRES, TEMP
37 --        WRITE(17,3) TITLE
38 --   10   READ(16,*, END=20) F(INDEX), A(INDEX), B(INDEX),
39 --     £            F(INDEX+1), A(INDEX+1), B(INDEX+1)
40 --        Z1(INDEX) = STRES*(A(INDEX)-1)
41 --        Z2(INDEX) = -1*STRES*B(INDEX)
42 --        Z1(INDEX+1) = STRES*(A(INDEX+1)-1)
43 --        Z2(INDEX+1) = -1*STRES*B(INDEX+1)
44 --        WRITE(17,*) F(INDEX), Z1(INDEX), Z2(INDEX)
45 --        WRITE(17,*) F(INDEX+1), Z1(INDEX+1), Z2(INDEX+1)
```

```
46 --       INDEX = INDEX + 2
47 --       GOTO 10
48 --    20 CLOSE(UNIT = 16)
49 --       CLOSE(UNIT = 17)
50 -- C
51 -- C THE LEAST SQUARES ANALYSIS
            IS NOW CARRIED OUT BY THE SUBROUTINE LSTSQR
52 -- C
53 --       OPEN(UNIT = 19, NAME = 'LINE.DAT', STATUS = 'OLD',
54 --      £          CARRIAGE CONTROL = 'LIST')
55 --       IF (FILENO.EQ.FIRST) THEN
56 --          WRITE(19,*) '   FILE', '   GRADIENT', '   INTERCEPT',
57 --      £                '   ST.DEV GRD',   ST.DEV INT'
58 --       ELSE
59 --       GOTO 25
60 --       END IF
61 --    25 CALL LSTSQR(F,Z1,INDEX, GRDNT, INTCPT, SDEVGR, SDEVIN)
62 --       WRITE(19,*) INFILE, GRDNT, INTCPT, SDEVGR, SDEVIN
63 --       END DO
64 --       CLOSE(UNIT = 19)
65 --       STOP
66 --       END
67 -- C
68 -- C
69 -- C
70 --       SUBROUTINE LSTSQR(X,Y,I,GRAD,INTER,SDG,SDI)
71 -- C
72 --       REAL GRAD, INTER, SDG, SDI, N, DENOM
73 --       DIMENSION X(I), Y(I), YCALC(100), DIFF(100)
74 --       INTEGER COUNT
75 -- C
76 --       COUNT = 0
77 --       SUMX = 0.0
78 --       SUMY = 0.0
79 --       SUMXY = 0.0
80 --       SUMX2 = 0.0
81 --       SUMD2 = 0.0
82 --       N = I
83 -- C
84 --       DO 100 J = 1,I
85 --       IF ((X(J).LT.51).AND.(X(J).GT.0.90)) THEN
86 --          COUNT = COUNT + 1
87 --          SUMX = SUMX + X(J)
88 --          SUMY = SUMY + Y(J)
89 --          SUMXY = SUMXY + X(J)*Y(J)
90 --          SUMX2 = SUMX2 + X(J)*X(J)
91 --       ELSE
92 --          GOTO 100
93 --       END IF
94 --   100 CONTINUE
95 -- C
96 --       DENOM = COUNT*SUMX2-SUMX*SUMX
97 --       GRAD = (COUNT*SUMXY-SUMX*SUMY)/DENOM
98 --       INTER = (SUMY*SUMX2-SUMX*SUMXY)/DENOM
99 -- C
100 --      DO 101 K = 1,I
101 --      IF ((X(K).LT.51.AND.(X(K).GT.0.90)) THEN
102 --         YCALC(K) = GRAD*X(K) + INTER
103 --         DIFFK = YCALC(K) - Y(K)
104 --         SUMD2 = SUMD2 + DIFF(K)*DIFF(K)
105 --         ELSE
106 --         GOTO 101
```

```
107 --      END IF
108 --   101 CONTINUE
109 -- C
110 --      SDG = SQRT(SUMD2/(COUNT-2.0))*(N/DENOM)
111 --      SDI = SQRT(SUMD2/(COUNT-2.0))*(SUMX2/DENOM)
112 -- C
113 -- END
```

On completion of an FRA run (or sequence of runs) the data was transferred from tape on the Tektronix 4052 microcomputer to data files on the VAX mainframe. The data file consists of a title, then some data related to the experimental conditions (temperature, cell constant, standard resistance used etc.) utilised for the measurements. There then follows a number of data points of the format (f_i,a_i,b_i) where a_i and b_i are the complex parameters measured at the frequency f_i.

The programme FRA.FOR reads the appropriate titles and information. Then for each frequency f_i the values of a_i and b_i are read and converted to the real and imaginary impedance terms Z' and Z" using the formulae:-

$$Z' = R*(a-1)$$

$$Z'' = -R*b$$

This revised data is output to a new file for permanent storage.

The subroutine LSTSQR is called twice from the main programme section. The first time it is called it calculates the best least squares fit through the high conductivity plateau (from 10^4 Hz to 10^5 Hz in general) and extrapolates to the zero frequency value to give the high frequency impedance. The subroutine is then called again with different parameters and calculates the low frequency impedance in the same manner.

The gradients, intercepts and standard deviations are output to file line.dat. The high and low frequency impedances are subsequently used in conjunction with the cell constants to calculate the appropriate conductivities as used in Chapter 7.

3 ANALYSIS OF PULSE DATA AND CALCULATION OF DIFFUSION COEFFICIENTS

The general experimental procedures used to record pulse measurements were described in detail in Chapter 2. The programme which was run on the Tektronix to control the acquisition of the data recorded a file title and then pairs of points consisting of the elapsed time and the cell potential at that time. On completion of recording the data was transferred to the VAX mainframe computer using the standard file transfer programme.

A computer programme was written in S-Algol to manipulate this data into a number of forms suitable for both graphing and statistical analysis. It also separates the pulse and relaxation data and calculates the required overpotentials and square root of time parameters in each case. This is listed below as programme 2.

Programme 2.
Analysis of pulse data.

```
1 -- PROGRAMME PULSE.S
 2 --
 3 -- !All the variables are declared.
 4 --
 5 -- let voltage = vector 0::5000 of 0.0
 6 -- let time.in.seconds = vector 0::5000 of 0
 7 -- let pulse.time = vector 1::5000 of 0
 8 -- let pulse.voltage = vector 1::5000 of 0.0
 9 -- let recovery.time = vector 1::5000 of 0
10 -- let recovery.voltage = vector 1::5000 of 0.0
11 -- let file.title := ""
12 -- let temp := ""
13 -- let initial.voltage := 0.0
14 -- let current := 0.0
15 -- let start.time := 0
16 -- let current.start := 0
17 -- let current.stop := 0
18 -- let count.1 := 0
19 -- let count.2 := 0
20 --
21 -- let count.3 := 0
22 -- let total.time := 0
23 -- let interval := 0
24 -- let voltage.sum := 0.0
25 -- let irdrop := 0.0
26 -- let total.discharge.time := 0
27 -- let j := 0
28 -- let k := 0
29 -- let l := 0
30 --
31 --
32 --
33 -- ! The required files are declared and opened.
34 --
35 -- write "'nEnter name of file containing pulse data"
36 -- write "'n(No extension required - .dat assumed) - "
37 -- let name = read.a.line
38 -- filein = name + + ".dat"
39 -- let input = open(filein,"a",0)
40 --
41 -- let filout = name + + ".log"
42 -- let output = create(filout,"s","a","v",256)
43 --
44 -- let filout0 = name + + ".com"
45 -- let out0 = create(filout0,"s","a","v",256)
46 -- output out0, "$ sr pulse"
47 -- output out0, "'n", name
48 --
49 -- let filout1 = name + + "p.dat"
50 -- let out1 = create(filout1,"s","a","v",256)
51 --
```

```
52 -- let filout2 = name + + "r.dat"
53 -- let out2 = create(filout2,"s","a","v",256)
54 --
55 -- let filout3 = "d" + + name + + ".plt"
56 -- let out3 = create(filout3,"s","a","v",256)
57 --
58 -- let filout4 = "p" + + name + + ".plt"
59 -- let out4 = create(filout4,"s","a","v",256)
60 --
61 -- let filout5 = "r" + + name + + ".plt"
62 -- let out5 = create(filout5,"s","a","v",256)
63 --
64 --
65 -- !The pulse variables are requested and entered.
66 --
67 -- write "'nEnter time of first reading (s) - "
68 -- start.time := readi
69 -- write "'nEnter time interval between readings (s) - "
70 -- interval := readi
71 -- write "'nEnter current starting time in seconds - "
72 -- current.start := readi
73 -- write "'nEnter current stopping time in seconds - "
74 -- current.stop := readi
75 -- total.discharge.time := current.stop - current.start
76 -- write "'nEnter total time measurements taken for (s) - "
77 -- total.time := readi
78 -- write "'nEnter applied current (uA) - "
79 -- current := readr * 1e-6
80 -- write "'nEnter iR drop (mV) - "
81 -- iRdrop := readr * 1e-3
82 --
83 -- !The title of the file is read and output to the files where it is required.
84 --
85 -- file.title := read.a.line(input)
86 -- write "'n", file.title
87 -- output out, "'n", file.title
88 -- output out3, file.title
89 -- output out4, file.title
90 -- output out5, file.title
91 --
92 --
93 -- ! The first few voltages are read before the pulse is applied
94 -- ! and the initial constant voltage is calculated.
95 --
96 -- for i = (start.time div interval) to (current.start div interval) do
97 -- begin
98 -- count.1 := count.1 + 1
99 -- time.in.seconds(i) := readi(input)
100 -- temp := read(input)
101 -- voltage(i) := readr(input)
102 -- temp := read(input)
103 -- voltage.sum := voltage.sum + voltage(i)
104 -- end
105 --
106 -- initial.voltage := voltage.sum/count1
107 --
108 --
109 -- !The parameters which have been read and calculated are output
110 -- !to the terminal and to a log file.
111 --
112 -- write "'nInitial Voltage is - ", initial.voltage
113 -- write "'nTime of the first reading is - ", start.time
```

```
114 -- write "'nTime interval between readings is - ", interval
115 -- write "'nCurrent starting time is - ", current.start
116 -- write "'nCurrent stopping time is - ", current.stop
117 -- write "'nTotal discharge time is - ", current.stop - current.start
118 -- write "'nTotal.time measurements taken for is - ", total.time
119 -- write "'nApplied current is - ", current
120 -- write "'nIR drop is - ", irdrop
121 --
122 -- output out, "'nInitial Voltage - ":20, initial.voltage
123 -- output out, "'nTime of the first reading - ":20, start.time
124 -- output out, "'nTime interval between readings - ":20, interval
125 -- output out, "'nCurrent starting time - ":20, current.start
126 -- output out, "'nCurrent stopping time - ":20, current.stop
127 -- output out, "'nTotal discharge time - ":20, current.stop - current.start
128 -- output out, "'nTotal time measurements taken for - ":20, total.time
129 -- output out, "'nApplied current - ":20, current
130 -- output out, "'nIR drop - ":20, irdrop
131 --
132 --
133 -- ! The voltages during the pulse are read, converted to overpotentials
134 -- ! and output versus the square root of the time.
135 --
136 -- for i = ((current.start div interval) + 1) to
137 --             (current.stop div interval) do
138 -- begin
139 -- count2 := count2 + 1
140 -- time.in.seconds(i) := readi(input)
141 -- temp := read(input)
142 -- voltage(i) := readr(input)
143 -- temp := read(input)
144 -- pulse.time(count2) := time.in.seconds(i) - current.start
145 -- pulse.voltage(count2) := rabs((voltage(i) - irdrop -
146 -- initial.voltage)*1000)
147 -- end
148 --
149 -- write "'nEnter step interval for plotting pulse data."
150 -- write "'n(1 = every point, 2 = every 2nd point etc.) - "
151 -- j := readi
152 --
153 -- for i = 1 to count2 do
154 -- begin
155 -- output out1, sqrt(pulse.time(i)):10, pulse.voltage(i):10, "'n"
156 -- end
157 --
158 -- for i = 1 to count2 by j do
159 -- begin
160 -- output out4, "'n", sqrt(pulse.time(i)):10, pulse.voltage(i):10
161 -- end
162 --
163 --
164 --
165 -- !The voltages during the relaxation are read, converted to overpotentials
166-- !and output versus Atlung's time parameter.
167 --
168 -- for i = (current.stop div interval + 1) to
169 --             (total.time div interval) do
170 -- begin
171 -- count.3 := count.3 + 1
172 -- time.in.seconds(i) := readi(input)
173 -- temp := read(input)
174 -- voltage(i) := readr(input)
175 -- temp := read(input)
```

```
176 -- recovery.time(count3) := time.in.seconds(i) - current.start
177 -- recovery.voltage(count3) := rabs(voltage(i) - initial.voltage)*1000)
178 -- end
179 --
180 -- write "'nEnter step interval for plotting relaxation data. - "
181 -- k := readi
182 --
183 -- for i = 1 to count3 do
184 -- begin
185 -- output out2, sqrt(recovery.time(i)) -
186 --              sqrt(recovery.time(i) - total.discharge.time)):10,
187 --                  recovery.voltage(i):10, "'n"
188 -- end
189 --
190 -- for i = 1 to count3 by k do
191 -- begin
192 -- output out5, "'n", (sqrt(recovery.time(i)) -
193 --             sqrt(recovery.time(i) - total.discharge.time)):10,
194 --                  recovery voltage(i):10
195 -- end
196 --
197 --
198 --
199 -- !The entered data is output to a command file for future use.
200 -- output out0, "'n", start.time:8
201 -- output out0, "'n", interval:8
202 -- output out0, "'n", current.start:8
203 -- output out0, "'n", current.stop:8
204 -- output out0, "'n", total.time:8
205 -- output out0, "'n", current*1e6:8
206 -- output out0, "'n", irdrop*1e3:8
207 -- output out0, "'n", j:8
208 -- output out0, "'n", k:8
209 -- output out0, "'n", l:8
210 --
211 -- !The data files are closed.
212 -- close(input)
213 -- close(out)
214 -- close(out1)
215 -- close(out2)
216 -- close(out0)
217 --
218 -- end
219 --
220 -- ?
```

Lines 5 to 29 declare the variables required in the programme. The next few lines open up a series of files with appropriate names based on the original file names pulsexyz, where xyz is simply a unique numeric code for the pulse data. The data to be stored in these is as follows :-

Pulsexyz.log - records the output from the execution of pulse.s to allow future checking if necessary.

Pulsexyz.com - records the parameters input to pulse.s enabling it to be run quickly again without retyping all the appropriate data.

Pulsexyzp.dat - records all the pulse data as overpotential versus the square root of the time for analysis of the pulse data.

Pulsexyzr.dat - records all the relaxation data as overpotential versus the root time parameter required for the analysis of the relaxation data.

Pulsexyzd.dat - records all the relaxation data as potential versus time to allow inspection and plotting of the whole data.

The full data, pulse data and relaxation data were also recorded, with titles, in other files with a format suitable for the plotting programme available on the Tektronix microcomputer. These were transferred back to the Tektronix for plotting and examination before further analysis.

The next programme section (lines 65 to 90) read in the variables used within the programme for calculating the root time parameters and then output the title of the data set to those files where it is needed. All the data must be input as the programme is running.

Lines 93 to 106 read in all the potentials recorded before the pulse was applied to the cell and calculate the initial potential to be the average of all these readings. Lines 107 to 131 output all the data which has been input from the keyboard and some calculated parameters to the screen for immediate checking and to a log file to allow subsequent checking of the whole programme.

The next programme section (lines 133 to 164) reads from file all the potentials recorded during the pulse, converts these to overpotential and calculates the appropriate time associated with them. The overpotentials are output versus the square root of the time both to a file for data analysis (lines 153 to 156) and to a file for plotting. The latter file contains around 100 points usually rather than the whole data set. This is governed by the step interval entered at lines 149 to 151. Lines 165 to 195 perform a similar function but with the data recorded during the relaxation after the pulse. Data is now output versus the time parameter specified by Atlung (see Chapter 5).

Lastly the remaining lines output all the data which was input earlier to a command file to allow it to be used again if modifications are required without re-entering all the data. All files are then closed.

3.1 CALCULATION OF GRADIENTS

In order to calculate the gradients of overpotential versus the respective root time parameter for the pulse and the relaxation a statistical package called Minitab was used. This was available on the VAX mainframe computer and was able to be used interactively.

The general method was to input the data from the files output by the programme pulse.s. The data for the pulse (or relaxation) was plotted on the screen to allow visual examination of the linearity of the pulse and to ensure there had been no problems during the recording of the data. The best straight line through the data was then calculated using regression analysis on the xy data set. The gradient of the line and the correlation coefficient were noted.

Along with the equation of the straight line Minitab also lists all points deviating markedly from the line (outliers). The data set was then edited to remove any such outliers and also to remove any data points from the beginning of the recording time where there was evident curvature. The regression analysis was then repeated and the new gradient and correlation coefficient noted.

This process was repeated iteratively until consistent gradients with good correlation coefficients were obtained. At this stage a plot of the residuals (i.e. the deviations of the actual points from the best line) was examined to verify that they were randomly distributed.

In most cases linearity was reasonably good and correlation coefficients of greater than 95 % were obtained. However in some cases the gradients never quite reached a consistent value even when outliers were removed. In these cases an average gradient was taken from all the iterations in which good linearity was observed. The error in doing this was felt to be no more significant than other experimental errors.

3.2 CALCULATION OF DIFFUSION COEFFICIENTS

All the relevant diffusion coefficients were calculated using Lotus 123 - a computer spreadsheet package implemented on a Zenith portable computer. A selection of results were also checked by hand on a pocket calculator.

A spreadsheet is basically a matrix of cells (or positions in the matrix) each of which can store a numeric value, text or mathematical expressions resulting in the calculation of a numeric value. These mathematical expressions can use a variety of mathematical functions and can operate on data in that cell or in other cells by reference to a unique cell code indicating the position of the cell in the array. The cell code is simply a letter indicating the column in which the cell is followed by a number indicating the row (eg A5).

An example of the spreadsheet used here is shown in Figure 2.

CELL DISCHARGE

WEIGHT	1.95E-02	THICKNESS	3.20E-02	PERCENTAGE	3.33E-01

PULSE	INITIAL VOLTAGE	FINAL VOLTAGE	PULSE LENGTH	CURRENT	ALPHA PULSE	ALPHA RELAX
PULSE020	4.09E-01	4.04E-01	4.29E+03	1.00E-05	2.10E-01	2.20E-01
PULSE023	4.04E-01	4.02E-01	3.69E+03	1.00E-05	1.80E-01	2.64E-01
PULSE025	4.02E-01	4.00E-01	3.99E+03	1.00E-05	1.60E-01	3.46E-01
PULSE027	4.00E-01	3.97E-01	3.99E+03	1.00E-05	2.22E-01	3.30E-01
PULSE029	3.97E-01	3.95E-01	3.99E+03	1.00E-05	2.00E-01	3.30E-01
PULSE030	3.95E-01	3.92E-01	4.29E+03	1.00E-05	2.00E-01	2.90E-01
PULSE031	3.92E-01	3.88E-01	3.78E+03	1.00E-05	2.10E-01	
PULSE032	3.92E-01	3.88E-01	3.78E+03	1.00E-05		2.70E-01
PULSE033	3.88E-01	3.85E-01	3.78E+03	1.00E-05	1.80E-01	2.60E-01
PULSE034	3.85E-01	3.82E-01	3.60E+03	1.00E-05	1.60E-01	2.70E-01
PULSE035	3.82E-01	3.77E-01	5.94E+03	1.00E-05	1.60E-01	1.90E-01
PULSE036	3.78E-01	3.81E-01	6.00E+02	1.00E-06	4.90E-02	2.70E-02
PULSE037	3.81E-01	3.80E-01	6.00E+02	1.00E-06	6.00E-02	2.70E-02

NO. MOLES	4.14E-05	4D2/PI	1.30E-03

dE	dQ	dx	dE/dQ	dE/dx
-4.50E-03	4.29E-02	1.07E-02	-1.05E-01	-4.19E-01
-2.00E-03	3.69E-02	9.24E-03	-5.42E-02	-2.16E-01
-2.20E-03	3.99E-02	9.99E-03	-5.51E-02	-2.20E-01
-3.00E-03	3.99E-02	9.99E-03	-7.52E-02	-3.00E-01
-2.20E-03	3.99E-02	9.99E-03	-5.51E-02	-2.20E-01
-3.40E-03	4.29E-02	1.07E-02	-7.93E-02	-3.17E-01
-3.30E-03	3.78E-02	9.46E-03	-8.73E-02	-3.49E-01
-3.30E-03	3.78E-02	9.46E-03	-8.73E-02	-3.49E-01
-3.70E-03	3.78E-02	9.46E-03	-9.79E-02	-3.91E-01
-2.60E-03	3.60E-02	9.01E-03	-7.22E-02	-2.88E-01
-4.80E-03	5.94E-02	1.49E-02	-8.08E-02	-3.23E-01
3.10E-03	6.00E-04	1.50E-04	5.17E+00	2.06E+01
-7.00E-04	6.00E-04	1.50E-04	-1.17E+00	-4.66E+00

Kc	-7.46E-02	Kave	-6.96E-02

Dc PULSE	Dc relax	Dc semi inf	semiinf k	Dc semi inf ka	Dc Pulse Kc	Dc Relax Kc	Dc Pulse Kave	Dc Relax Kave
3.25E-08	2.96E-08	3.96E-09	2.13E-09	1.74E-09	1.65E-08	1.50E-08	1.43E-08	1.31E-08
1.18E-08	5.50E-09	1.44E-09	2.89E-09	2.37E-09	2.24E-08	1.04E-08	1.95E-08	9.06E-09
1.55E-08	3.31E-09	1.88E-09	3.66E-09	3.00E-09	2.84E-08	6.07E-09	2.47E-08	5.28E-09
1.50E-08	6.77E-09	1.82E-09	1.90E-09	1.56E-09	1.47E-08	6.67E-09	1.28E-08	5.80E-09
9.91E-09	3.64E-09	1.21E-09	2.34E-09	1.92E-09	1.82E-08	6.67E-09	1.58E-08	5.80E-09
2.05E-08	9.74E-09	2.49E-09	2.34E-09	1.92E-09	1.82E-08	8.63E-09	1.58E-08	7.51E-09
2.25E-08	ERR	2.74E-09	2.13E-09	1.74E-09	1.65E-08	ERR	1.43E-08	ERR
ERR	1.36E-08	ERR	ERR	ERR	ERR	9.96E-09	ERR	8.67E-09
3.86E-08	1.85E-08	4.69E-09	2.89E-09	2.37E-09	2.24E-08	1.07E-08	1.95E-08	9.34E-09
2.66E-08	9.33E-09	3.23E-09	3.66E-09	3.00E-09	2.84E-08	9.96E-09	2.47E-08	8.67E-09
3.33E-08	2.36E-08	4.04E-09	3.66E-09	3.00E-09	2.84E-08	2.01E-08	2.47E-08	1.75E-08
1.45E-05	4.77E-05	1.76E-06	3.90E-10	3.20E-10	3.02E-09	9.96E-09	2.63E-09	8.67E-09
4.93E-07	2.43E-06	6.00E-08	2.60E-10	2.13E-10	2.02E-09	9.96E-09	1.75E-09	8.67E-09

Figure 2.
Sample output from one of the spreadsheets employed.

In this spreadsheet the first column extends from the title ("CELL DISCHARGE") in cell A1 of the matrix to cell A19 ("PULSE037"). The spreadsheet is split into three parts for convenience at columns H (headed "dE" in cell position H5) and M (headed "Dc PULSE" in cells M5 and M6). All the cells with text in are present simply for convenience to map out the spreadsheet.

For calculating the diffusion coefficients in a particular mixed phase electrode a series of cells in the spreadsheet were defined into which were input all the relevant constant parameters associated with that MPE. These were weight (cell B3), thickness (cell D3) and percentage of NbS_2 (cell F3). From these measured values other constant values were calculated which were dependent on the input values. These were the number of moles of NbS_2 (J3) and the parameter $\frac{4a^2}{\pi}$ (cell L3) which is common to all the diffusion calculations. The gradients k_{ave} and k_c were also input as constants in cells S3 and U3 respectively.

For each individual pulse the pulse number and the parameters of initial voltage (V_1), final voltage (V_2), pulse length (t), current (I) and the gradients of the overpotential versus root time parameter for the pulse and relaxation (α_P and α_R) were also entered into row 7 in the spreadsheet. From these parameters the values *dE, dQ, dx, dE/dq* and *dE/dx* were calculated using suitable equations and added further along the same row. These calculated values are calculated by referring to the cells with the initial data in. For example in cell H7 is entered the command " + C7 - B7" indicating that the value in cell B7 (initial voltage) should be subtracted from the value in cell C7 (final voltage). The resultant value (dE) is output in H7.

All the necessary information was now present to calculate the diffusion coefficients using the appropriate equations given in Chapter 5. The following diffusion coefficients were calculated in the subsequent columns.

1) D_C*(Pulse)* - Apparent diffusion coefficient for the pulse using equation 2, Chapter 5 with $k = dE/dQ$ measured for that pulse.

2) D_C*(Relax)* - Apparent diffusion coefficient for the relaxation using equation 2, Chapter 5 with $k = dE/dQ$ measured for that pulse.

3) D_C*(Semi-inf)* - Chemical diffusion coefficient for the pulse using semi-infinite analysis (equation 3, Chapter 5) with $k = dE/dx$ measured for that pulse.

4) D_C*(Semi-inf* k_{ave}*)* - Chemical diffusion coefficient for the pulse using semi-infinite analysis (equation 3, Chapter 5) with $k = dE/dx$ measured for the standard cell.

5) $D_C(Semi\text{-}inf\ k_C)$ - Chemical diffusion coefficient for the pulse using semi-infinite analysis (equation 3, Chapter 5) with $k = dE/dx$ measured for the cell during the intercalation pulse.

6) $D_C(Pulse\ k_C)$ - Apparent diffusion coefficient for the pulse using equation 2, Chapter 5 with $k = dE/dQ$ measured for the cell during the intercalation pulse.

7) $D_C(Relax\ k_C)$ - Apparent diffusion coefficient for the relaxation using equation 2, Chapter 5 with $k = dE/dQ$ measured for the cell during the intercalation pulse.

8) $D_C(Pulse\ k_{ave})$ - Apparent diffusion coefficient for the pulse using equation 2, Chapter 5 with $k = dE/dQ$ measured for the standard cell.

9) $D_C(Relax\ k_{ave})$ - Apparent diffusion coefficient for the relaxation using equation 2, Chapter 5 with $k = dE/dQ$ measured for the standard cell.

Again the calculation entered into each of the cells was put in a general form referring to other cells. For example cell M7 contains the command "+ *L3 x E7 xE7 x K7 x K7 x 1 x 10⁶ / F7 / F7*".This yields the required diffusion coefficient since cell L3 contains the constant $\frac{4a^2}{\pi}$, cell E7 contains the current I, cell K7 the required value of dE/dQ and cell F7 the required gradient (α_P). The factor of one million is included since the gradient is calculated in units of millivolts rather than volts.

All the information in the above row could now be copied into subsequent rows for as many pulses as were performed on that cell. When this is done the cell values are translated to those in the new row i.e. in the above example all references to cell E7 are translated to references to cell E8 in row 8, E9 in row 9 and so forth. Thus only the parameters measured for each individual pulse needed to be entered in subsequent rows and all other parameters were calculated automatically. This allows repetitive calculations to be performed quickly, easily and accurately with a permanent record of the calculation.

For other cells the spreadsheet was simply copied and the new parameters relating only to the new cell and the pulses performed on it were changed.

1 PERCOLATION AND CONDUCTION

The process of percolation can generally be considered as the spreading of a "fluid" through a "medium" subject to random constraints associated with the medium. The most familiar example is the flow of liquid (e.g. water) through a porous medium (coffee granules) but the general principles can also be applied to the passage of fire through a forest,[1] the transport of electrons through a heterogeneous mixture of conducting and insulating particles[2] and many other similar situations.

The medium is generally defined to be an infinite set of points, usually known as sites or atoms. The fluid passes from the source atoms along paths to adjacent sites. These paths are known as bonds. The introduction of a random mechanism to control the flow can be achieved in two distinct ways leading to two different forms of percolation. In site percolation the sites can be filled or empty at random, while in bond percolation the bonds between sites are opened or closed at random.

It is the former model which is most closely related to the situation of the mixed phase electrode computer model which is described in the succeeding chapters, and therefore it is the conclusions and hypotheses of this model which will be concentrated on below.

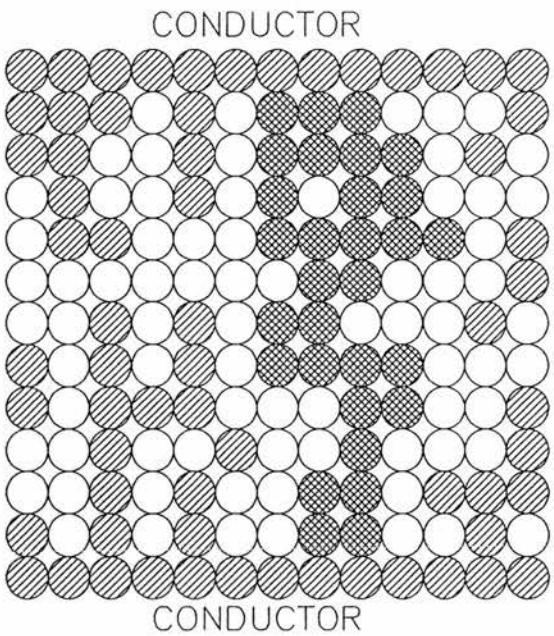

Figure 1.
Site percolation in a square lattice. All shaded particles are conducting, those cross hatched lie on the large cluster causing percolation.

The simplest site percolation situation is illustrated in Figure 1. A lattice of N sites (where strictly $N \to \infty$) has a fraction x of sites filled with conducting particles while the bulk of the medium *(1-x)* sites are insulating. When x is small the occupied sites appear singly or in small isolated clusters of adjacent occupied sites. As the proportion of occupied sites grows larger these clusters increase in size and become closer to one another. At a fraction $x > x_c$ of filled sites essentially the clusters merge and a complete pathway is formed across the medium. There are still a few small isolated clusters. For finite lattices the large cluster extends over the whole lattice and as a consequence a complete path exists from one side to the other.

The fraction x_c is known as the percolation threshold for the lattice and is dependent on the lattice coordination and structure, the particle size and aspect ratio and the type of percolation. Below the threshold percolation phenomena cannot occur throughout the lattice, while above it they can.

Lattice Type	Coordination	Percolation Threshold
Square	4	0.590
Diamond	4	0.425
s.c.	6	0.307
b.c.c.	8	0.243
f.c.c.	12	0.195
h.c.p.	12	0.204

Table 1.
Site percolation thresholds for various lattice types.

Table 1 gives the value of the site percolation threshold for a number of common lattice types, emphasising those used in the computer model described in Chapter 3. These can be determined exactly for simpler lattices but more commonly Monte Carlo techniques[3] or experimental work are used to give an approximation for this threshold. A full account of such methods is given by Stauffer[1] and Kirkpatrick[4] in their reviews. These approximation methods give quite a lot of scatter in the measurement of the percolation threshold, reflecting the random filling of sites in the lattice. From probability considerations it is possible to form a complete cluster across the lattice at compositions considerably below the percolation threshold (though unlikely in statistical terms) or not until compositions much greater than x_c. The results from the computer model relect this in that often there is considerable variation in the normalised link number measured at lattice compositions surrounding the percolation threshold.

The ratio of the number of occupied sites in the large cluster to the total number of sites in the lattice is known as the site percolation probability and is denoted $P^S(x)$. For the simplest situation considered in Chapter 3, namely that of a simple cubic lattice, $P^S(x)$ is dependent on x and x_c by an equation of the form :-

$$P^s(x)\alpha(x-x_c)^t$$

where $0.3 \leq t \leq 0.4$ when x is close to x_c. However as $x \rightarrow 100\%$, $P^s(x) \rightarrow x$ and at $x < x_c$, $P^s(x) \rightarrow 0$. This dependence is plotted in Figure 2. Note that this means there is an abrupt change of properties as x increases through the percolation threshold.

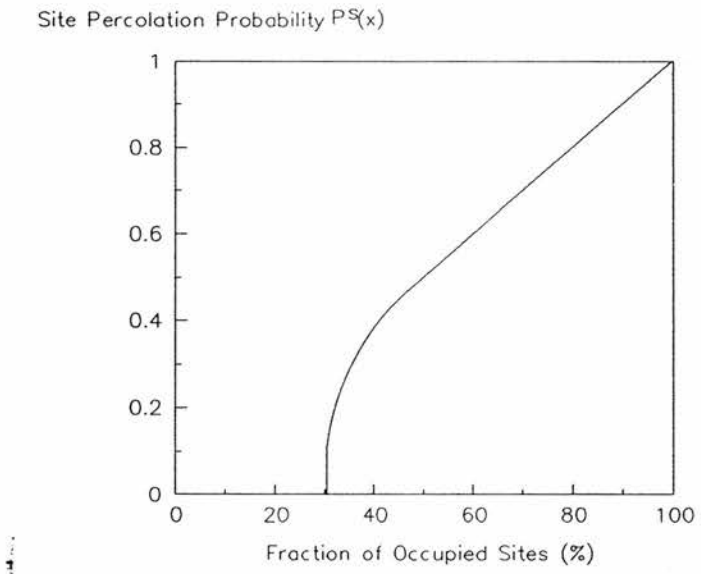

Figure 2.
Dependence of the site percolation probability on the composition of a simple cubic lattice.

In the situation where the fraction x is conducting particles in an insulating medium $P^S(x)$ can be considered as the fraction of sites in which conduction is possible. Below $x = x_c$ the conductivity must be zero since there is no path across the lattice. Above $x = x_c$ conduction is now possible along the complete path through the lattice. Theoretical and experimental studies have demonstrated a relationship between the conductance ($G(x)$) and x to be of the form :-

$$G(x)\alpha(x-x_c)^y$$

There is some dispute over the value of the superscript y. Kirkpatrick[5] suggests that $y = 1.5 \pm 0.2$ when $x_c \leq x \leq (x_c + 0.2)$ while Adler et al.[6] suggest that $y = 2$ when $x_c \leq x \leq 1$. A typical plot of the conductance versus x (for a simple cubic lattice) is given in Figure 3. $G(x)$ is normalised to give a value between zero and one. This again illustrates the importance of the percolation threshold.

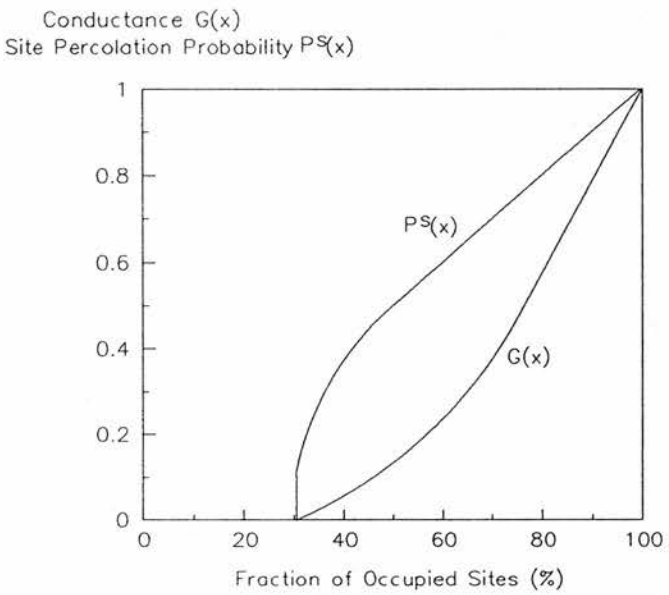

Figure 3.
Dependence of the site percolation probability and the conductance on the composition of a simple cubic lattice.

The foregoing description of some of the basic concepts of percolation theory demonstrates the fundamental difference between the percolation and mixed phase electrode situations considered in Chapter 3, that is in the importance of the percolation threshold and in the direct dependence of conductivity on the fraction of particles in the lattice.

2 REFERENCES

1 Stauffer D. "Introduction To Percolation Theory" Publ. Taylor & Francis Ltd. (1985)

2 Ottavi H., Clerc J., Roussenq J., Giraud G., Goyon E., Mitescu C.D. "Electrical Conductivity Of A Mixture Of Conducting And Insulating Spheres : An Application Of Some Percolation Concepts", J. Phys. C: Solid State Phys. 11 (1978) 1311

3 Frisch H.L., Hammersley J.M., Welsh D.J.A. "Monte Carlo Estimates Of Percolation Probabilities For Various Lattices", Physical Review 126 (1962) 949

4 Shante V.K.S., Kirkpatrick S. "An Introduction To Percolation Theory", Advances In Physics 20 (1971) 325

5 Kirkpatrick S. "Percolation And Conduction", Reviews Of Modern Phys. 45 (1973) 574

6 Adler D., Flora L.P., Senturia S.D. "Electrical Conductivity In Disordered Systems", Solid State Communications 12 (1973) 9